universität wien

DISSERTATION / DOCTORAL THESIS

Titel der Dissertation /Title of the Doctoral Thesis

„Ecophysiology and genomics of sulfate-reducers and other necromass-degrading microorganisms in arctic marine sediments“

verfasst von / submitted by

Claus Pelikan, BSc MSc

angestrebter akademischer Grad / in partial fulfilment of the requirements for the degree of

Doctor of Philosophy (PhD)

Wien, 2019 / Vienna, 2019

Studienkennzahl lt. Studienblatt / degree programme code as it appears on the student record sheet:	A 794 685 437
Dissertationsgebiet lt. Studienblatt / field of study as it appears on the student record sheet:	Biologie / Biology
Betreut von / Supervisor:	Univ.-Prof. Dipl.-Biol Dr. Alexander Loy

Acknowledgements

I want to express my sincere thanks to Alexander Loy for giving me the chance to write my PhD thesis in his research group. He has guided me through this sometimes quite difficult time of my life. Most of all I appreciate his accuracy and preciseness and his eye for details that often challenged me but eventually sharpened my scientific mind. I also want to thank Kenneth Wasmund, who has been my mentor and companion in the laboratory and during the field trip to Svalbard. He is an incredibly motivated scientist who inspired me and taught me the fun of focusing on the most interesting scientific endeavour. I also want to express my deep gratitude for Bela Hausmann and Craig Herbold, who introduced me to the world of bioinformatics, genome analyses and statistics. They always had an open ear for my questions and helped me when I was lost in my code or confused by complex metabolic pathways. Furthermore, I want to thank Marc Mußmann for employing me part-time for the last year of this thesis and for always supporting my graduation.

DOME is a wonderful work environment where one can easily learn new methods, seek advice and initiate exciting collaborations. In particular I want to thank the many past and current colleges at DOME for their help and fun times over the years: Albert, Allen, Alessandra, Alexander G, Alexander P, Alexander S, Andreas, Andrew, Anna, Astrid, Buck, Cecilia, Celine, Christiane, Christopher P, Christopher S, Christos, Clemens, Daniela, Daryl, David B, David S, Dimitri, Faris, Fátima, Florian S, Florian W, Hanna, Hannes, Huimin, Ilias, Isabella, Jan, Jasmin, Jay, Johanna, Julia P, Julia R, Julia V, Karin A, Katharina K, Lena, Mario, Markus, Marlies, Martin, Márton, Maximilian, Michael L, Michael P, Michaela, Nathalie, Orest, Paul, Patrick, Petra, Ping, Rebecca, Roey, Johanna, Sebastian, Stefan, Stefanie, Stephan, Stephanie, Tae Kwon, Thomas and Vincent.

I also want to thank my family for the continuous financial and more importantly emotional support they have given me. In particular I want to mention my mother, Gertrude Pelikan, who is incredibly attached to nature and inspired me with her love and fascination for all living organisms. Furthermore, I want to thank my father Bernhard Pelikan who is a scientist himself and thus provided me with a model for a scientific career. Finally, I wanted to thank my beloved partner Barbara Bayer. It was not always easy to go through this difficult time in life together but I am incredibly thankful that we are now better partners in life than ever.

Table of contents

Summary

Seafloor microorganisms mineralize vast quantities of organic matter from marine primary production and are considered key players of the global carbon cycle. Of prime importance are sulfate-reducing microorganism (SRM) that perform the respiratory reduction of sulfate to sulfide, which on a global scale facilitates the mineralization of 12-29% of the organic matter deposited to the seafloor. Rising temperatures in the Arctic will initially cause increased export of organic matter to the seafloor. Nevertheless, the identities and functions of organic matter degrading microorganisms in arctic marine sediments remain understudied.

This thesis aimed to reveal the identity, environmental distribution and genomic repertoire of key degraders of organic matter in arctic marine sediments. To assign specific functions to individual microbial species, arctic marine sediment microcosms were supplemented with ^{13}C-labelled substrates, e.g., spirulina bulk organic matter, macromolecules including protein, lipids and DNA, and the degradation intermediate acetate. The incorporation of ^{13}C-carbon into DNA and microbial biomass was monitored via DNA stable isotope probing (SIP) and catalyzed reporter deposition fluorescence *in situ* hybridization combined with Raman microspectroscopy, respectively. Microbial community dynamics and specific accumulations in ^{13}C-DNA-SIP fractions were investigated via next generation sequencing (NGS) of 16S rRNA amplicons. A novel NGS pipeline for reductive bacterial-type *dsrA* and *dsrB* sequences was established to investigate community dynamics of SRM. This novel pipeline was successfully tested on mock communities and environmental samples and was subsequently used to capture the diversity of SRM in the environment. The role of SRM during anaerobic organic matter degradation was investigated by selective inhibition of SRM with molybdate and measurements of sulfate-reduction rates, sulfate concentrations, and primary SRM substrate concentrations, including volatile fatty acids and lactate. Furthermore, metagenomes from several time points were sequenced and analyzed to obtain insights into the genomic potential of selected key degraders of organic matter. In addition, the influence of glacier run-off on the entire microbial community and the composition of SRM in arctic marine sediments was investigated.

Members of the *Psychrilyobacter* genus and various *Psychromonas* strains were identified as key protein and lipid degraders, respectively. Furthermore, a JTB215-related *Clostridia* population was able to hydrolyze both, proteins and lipids, whereas extracellular DNA was mainly hydrolyzed by diverse *Cand.* Izemoplasmatales. Genome analyses of these key hydrolyzers indicated the potential for extra-enzymatic macromolecule degradation and for the transport and intracellular catabolism of peptides, long-chain fatty acids, glycerol and nucleic acids. Volatile fatty acid and lactate concentrations were controlled by SRM during anaerobic incubations, but surprisingly no incorporation of

^{13}C-acetate was detected, potentially due to a decoupling of SRM activity from growth on acetate. Interestingly, *Desulfobacteraceae* incorporated ^{13}C-labelled lipids, which was corroborated by the presence of fatty acid transporters and a beta-oxidation pathway in the respective genomes. These findings indicate that SRM in arctic marine sediments might degrade butyrate and higher fatty acids in addition to volatile fatty acids and lactate. The anaerobic food chain investigated via microcosm experiments is most relevant in sediments with low sedimentation rates, in which comparably high amounts of organic matter are mineralized at or near the seafloor. In comparison, in glacier run-off influenced sediments, burial of labile organic matter and high concentrations of metals enabled active sulfur cycling in sediments several meters below sea floor.

In summary, this thesis identified key degraders of organic matter in arctic marine sediments and revealed their potential metabolic functions. Furthermore, a pipeline for the analyses of environmental SRM was developed and precisely tested and novel insights into the microbial sulfur cycle in glacier-influenced marine sediments were obtained.

Zusammenfassung

Mikroorganismen die im Meeresboden leben tragen in hohem Maße zum Abbau von Algenbiomasse aus der Wassersäule bei und spielen daher eine große Rolle im globalen Kohlenstoffkreislauf. Von entscheidender Bedeutung sind sulfatreduzierende Mikroorganismen (SRM), die für die Mineralisierung von etwa 12-29% des am Meeresboden abgelagerten organischen Materials verantwortlich sind. Steigende Temperaturen in der Arktis werden Prognosen zufolge dazu führen, dass sich mehr Phytoplanktonbiomasse in der Wassersäule bilden kann, was einen erhöhten Eintrag von organischem Material auf den Meeresboden zur Folge haben könnte. Obwohl Mikroorganismen in marinen Sedimenten eine großen Bedeutung für den globalen Kohlenstoffkreislauf haben, ist deren Identität und Funktion bisher jedoch fast unerforscht.

Der Fokus dieser Dissertation lag daher darauf wichtige mikrobielle Taxa zu identifizieren und deren Verbreitung und Funktion für das Ökosystem zu verstehen. Um die Funktion spezifischer Mikroorganismen zu erforschen, wurden anaerobe Sedimentinkubationen mit ^{13}C-markierten Substraten (Zell-, Protein- und Lipidextrakt von der Blaualge *Spirulina*, DNA und Acetat) versetzt und der Einbau dieser Substrate mittels DNA stable isotope probing und Fluoreszenz-in-situ-Hybridisierung in Kombination mit Raman Mikrospektroskopie untersucht. Die Veränderungen der mikrobiellen Gemeinschaft und die Abundanz spezifischer Mikroorganismen in der ^{13}C-angereicherten DNA wurde mittels Hochdurchsatzsequenzierung von 16S rRNA Genen untersucht. Um ähnliche Analysen mit SRM zu ermöglichen, wurde in dieser Dissertation eine Pipeline zur Hochdurchsatzsequenzierung von bakteriellen *dsrA* und *dsrB* Sequenzen etabliert. Diese Methode zur Hochdurchsatzsequenzierung von *dsrA* und *dsrB* wurde mit zwei künstlichen mikrobiellen Gemeinschaften und drei Umweltproben erfolgreich getestet. Um die Rolle von SRM während des Kohlenstoffabbaus zu untersuchen wurden Sulfatreduktionsraten und Sulfatkonzentrationen bestimmt und Kontrollinkubationen mit dem für SRM spezifischen Hemmstoff Molybdat angesetzt. Zusätzlich wurden Konzentrationsbestimmungen von kurzkettigen Fettsäuren und Laktat durchgeführt, da diese wichtige Substrate für SRM sind. Anhand von Metagenomen wurden mögliche Abbauwege für die zugegebenen Substrate postuliert. Weiters wurde der Einfluss von Gletschern auf die Mikroorganismen im Sediment untersucht.

Die Inkubationsexperimente zeigten, dass *Psychrilyobacter* auf Proteinabbau und einige Stämme von *Psychromonas* auf Lipidabbau spezialisiert waren. Weiters hat eine JTB215-affilierte *Clostridia* Population vermutlich Proteine und Lipide hydrolysiert. Für den Abbau von DNA waren vor allem Vertreter der neuen Bakteriengattung Izemoplasma verantwortlich. Genomanalysen ergaben, dass die Genome der meisten Hydrolysierer Enzyme für den extrazellulären Abbau von Makromolekülen sowie für eine Vielzahl von

Transportern und den intrazellulären Abbau von Peptiden, Fettsäuren, Glyzerin und Nukleinsäuren kodierten. Die Konzentrationen kurzkettiger Fettsäuren und Laktat in den anaeroben Inkubationen waren stark von der Aktivität sulfatreduzierender Mikroorganismen abhängig. Azetat, ein wichtiges Zwischenprodukt des anaeroben Abbaus von organischem Material, wurde jedoch nicht in SRM Zellen eingebaut, was womöglich auf eine Entkopplung von Aktivität und Wachstum zurückzuführen ist. Als *Desulfobacteraceae* klassifizierte SRM haben ^{13}C-Kohlenstoff in Lipidinkubationen aufgenommen und kodierten Enzyme für den Import und intrazellulären Abbau von Fettsäuren mittels ß-Oxidation. Zusammen deuten diese Beobachtungen darauf hin, dass SRM in den untersuchten Sedimenten neben kurzkettiger Fettsäuren und Laktat auch Butyrate und höhere Fettsäuren als Substrate verwenden konnten. Die Untersuchungen anaerober Abbauwege in dieser Dissertation sind vor allem für Sedimente mit geringen Sedimentationsraten relevant. In diesen Sedimenten findet ein Großteil der Mineralisierung von organischem Kohlenstoff in Oberflächennähe statt. Dem gegenüber stehen von Gletschern beeinflusste Sedimente, in denen die Sedimentation von anorganischem Material sehr hoch ist. In diesen bis zu mehreren Metern Tiefe vergelichsweise jungen Sedimenten, kann aufgrund hoher Metallkonzentrationen und geringen Mengen sehr reaktiven organischen Materials ein aktiver Schwefelkreislauf ablaufen.

Zusammenfassend wurde in dieser Dissertation die identität und Funktion von Mikroorganismen untersucht die für den Kohlenstoffkreislauf in arktischen marinen Sedimenten relevant sind. Weiters wurde eine Methode für die Analyse von SRM in der Umwelt entwickelt und umfassend getestet und die Verbreitung und Ökologie dieser wichtigen funktionellen Gruppe in Gletscher beeinflussten Sedimenten beschrieben.

Introduction

Sulfate-reducing microorganisms (SRM) are abundant inhabitants of marine sediments where they constitute main drivers of the carbon and sulfur cycles (Jørgensen, 1982). Furthermore, they act as antagonists of greenhouse gas-emitting methanogens in wetlands (Pester, 2012; Pester *et al.*, 2012), and play important roles in the animal intestine (Carbonero *et al.*, 2012). Considering the significance of SRM for the environment and the health of animals and humans, it is evident that the isolation and physiological characterization of novel SRM is of prime importance. However, only a fraction of microorganisms can be brought into culture (Kadnikov *et al.*, 2016), and thus cultivation-independent methods are required to study the diversity and ecology of SRM in the environment. Phylogenetic marker gene sequencing of 16S rRNA genes is broadly applied in the field of microbial ecology, but is not sufficient for studying SRM in the environment, as several SRM are closely related to groups of microorganisms that do not reduce sulfate (Wagner *et al.*, 2005). Instead, the two genes *dsrA* and *dsrB,* which encode for the dissimilatory sulfite reductase DsrAB, are frequently used as marker genes for SRM and other S-compound-dissimilating microorganisms (Müller *et al.*, 2015). The DsrAB catalyzes the two-electron reduction of sulfite to DsrC-trisulfide (Santos *et al.*, 2015), and is thus a key enzyme in the dissimilatory reduction of sulfate or sulfite to hydrogen sulfide (Figure 1).

In a pioneering study in which *dsrAB* genes of various SRM isolates were systematically sequenced and phylogenetically analyzed, the authors showed that microbial sulfite reduction most likely existed before the evolutionary split of *Bacteria* and *Archaea* (Wagner *et al.*, 1998). Later, studies successfully applied this functional gene sequencing approach to obtain insights into the diversity and the ecological roles of SRM in the environment such as in acidic fen soils (Steger *et al.*, 2011) and acid main drainage influenced salt marshes (Moreau *et al.*, 2010). A comprehensive phylogenetic analysis of all *dsrAB* sequences from isolates and environmental studies revealed a tremendous diversity of *dsrAB*-harbouring microorganisms, which were grouped into four main clusters, i.e., the reductive archaeal-type DsrAB, the oxidative bacterial-type DsrAB, the reductive bacterial-type DsrAB and the second *dsrAB* copy of *Moorella thermoacetica* (Müller *et al.*, 2015). The reductive archaeal-type DsrAB cluster was constituted by thermophilic *Archaea*, the reductive bacterial-type DsrAB cluster comprised most cultivated and environmentally relevant SRM, which included some *Archaea* that obtained their DsrAB enzyme from sulfate-reducing bacteria via horizontal gene transfer, and the oxidative bacterial-type DsrAB cluster, which was constituted by microorganisms that utilize their DsrAB in reverse for the oxidation of reduced sulfur compounds. The reductive-type DsrAB cluster also included many DsrAB sequences that were not affiliated with known taxa, i.e., 35 %, of which two thirds were grouped into so called uncultured DsrAB family-level

lineages (Müller *et al.*, 2015). Recent metagenomic studies revealed the phylogenetic affiliation of several uncultured DsrAB family-level lineages and also delineated novel DsrAB clades, including the three basal clades *Verrucomicrobia*, *Ca.* Rokubacteria and *Ca.* Hydrothermarchaeota (Anantharaman *et al.*, 2018; Hausmann *et al.*, 2018; Zecchin *et al.*, 2018). The majority of environmentally relevant SRM fall into previously described DsrAB families and uncultured DsrAB family-level lineages within the reductive bacterial-type DsrAB (Wasmund *et al.*, 2017). Therefore, the comprehensive DsrAB database introduced by Müller *et al.* 2015 still constitutes an important foundation to investigate the diversity, distribution and function of SRM in vastly different environments such as wetlands, engineered infrastructure, as well as freshwater and marine sediments (Jochum *et al.*, 2017; Liu and Conrad, 2017; Pavloudi *et al.*, 2017; St-Pierre and Wright, 2017; Liu *et al.*, 2018; Vigneron *et al.*, 2018).

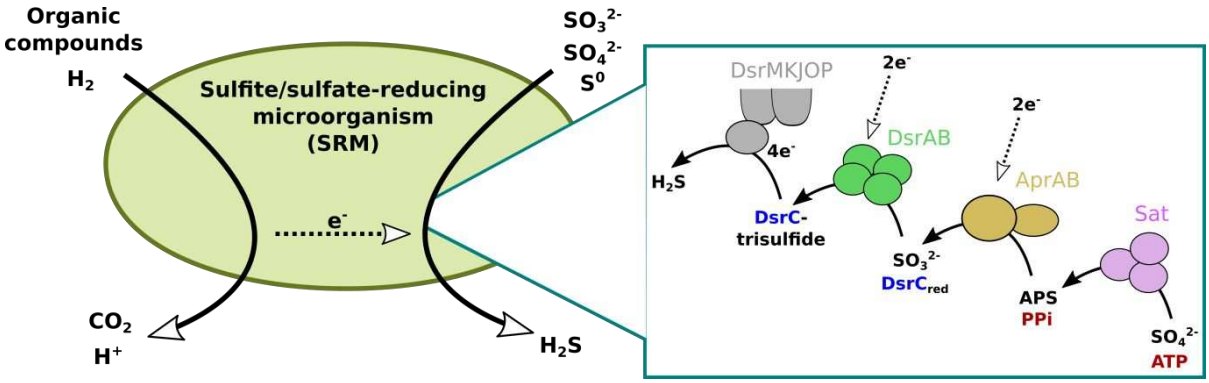

Figure 1. Microbial pathway of sulfate reduction. Modified from previous publications (Rabus *et al.*, 2013; Santos *et al.*, 2015). It depicts a model for a microorganism that anaerobically respires sulfate, sulfite or sulfur. Sulfate adenylyltransferase (Sat) catalyzes the ATP dependent activation of sulfate (SO_4^{2-}) to adenosine 5'-phosphosulfate (APS); adenylylsulfate reductase (AprAB) catalyzes the reduction of APS to sulfite (SO_3^{2-}); dissimilatory sulfate reductase subunits A and B (DsrAB) catalyze the reduction of SO_3^{2-} to sulfide (H_2S), which requires DsrC for shuttling the four electrons to the membrane complex DsrMKJOP.

Our planet's seafloor harbours as many microorganisms as the total overlying water column (Kallmeyer *et al.*, 2012). These sediment microbial communities depend on organic matter produced by photosynthetic organisms that thrive in surface waters and sink to the seafloor after death (Kędra *et al.*, 2012). Together with contributions of terrestrial organic matter, i.e., in areas close to land and rivers (Arndt *et al.*, 2013; Wehrmann *et al.*, 2014), this surface-derived phytodetritus constitutes the bulk of organic matter in marine sediments (Arndt *et al.*, 2013). All organic matter that settles to the seafloor is eventually oxidized by terminal mineralizers, which couple the anaerobic respiration of organic molecules to the reduction of diverse electron acceptors (Figure 2) (Arndt *et al.*, 2013). Sulfate is the second most abundant anion in seawater and diffuses into underlying sediments in high concentrations of up to 28 mM. Thus, in sediments with high organic matter contents, the more favorable electron acceptors O_2, Fe(III), Mn(IV), NO_3^- are quickly depleted, often within the top centimeters of the sediment, and sulfate

reduction becomes the dominant terminal mineralization process (Froelich *et al.*, 1979). Coastal sediments benefit from shallow water depth (up to 50 m) and receive up to 6–12% of the organic matter (OM) that is produced in the overlying water column (Dunne *et al.*, 2007). In these sediments, SRM account for up to 50% of the total organic matter mineralization (Jørgensen, 1982; Orcutt *et al.*, 2013). With increasing water depth, i.e., along a transect from coastal to deep sea regions, the proportion of organic matter from pelagic primary production that reaches the seafloor is dramatically reduced (Figure 2) (Dunne *et al.*, 2007), which is paralleled by a lower contribution of sulfate reduction, mainly caused by more extensive oxygen penetration deep into the sediment (Orcutt *et al.*, 2013). Nonetheless, it is estimated that SRM account for the oxidation of 12–29% of the global organic matter flux to the seafloor (Bowles *et al.*, 2014).

The importance of SRM during organic matter mineralization extends into arctic fjord sediments, where sulfate reduction accounts for up to 69 % of total organic matter mineralization (Sørensen *et al.*, 2015). Interestingly, sinking organic matter from pelagic primary production is only partially degraded in the water column due to low microbial activities in cold polar waters (Christian and Karl, 1995), and thus organic matter inputs into arctic marine sediments can be substantial (Fabiano and Pusceddu, 1998). Astonishingly, sulfate reduction rates (SRR) measured in arctic marine sediments with temperatures close to the freezing point of water are in the same range as SRR measured in temperate sediments (Sagemann *et al.*, 1998). These comparably high SRR in arctic marine sediments can only be explained by SRM that are well adapted to the cold (Robador *et al.*, 2016). Adaptations of psychrophilic microorganisms include an altered membrane lipid compositions, which maintains membrane fluidity at low temperatures, or adapted enzymes with enhanced local or overall structural flexibility that enable high catalytic activities (Deming, 2002; Cavicchioli, 2016). Interestingly, despite these psychrophilic adaptations, growth optima and highest growth yields of arctic SRM isolates were observed at 7–18°C (Knoblauch and Jørgensen, 1999).

The Arctic is disproportionately more impacted by climate change than temperate or tropical regions with severe consequences for life on our planet. Global change include a constant decline in the arctic sea ice cover (Vaughan *et al.*, 2014), which will lead to an extended phytoplankton growing season (Arrigo *et al.*, 2008) and might cause an initial increase of organic matter export to the seafloor (Figure 2) (Lalande *et al.*, 2009; Sørensen *et al.*, 2015). To date, no long-term studies on the development of organic matter export from pelagic primary production into arctic marine sediments are available. Global estimates indicate, however, enhanced rates of oxygen respiration and higher organic matter inputs into marine sediments (Hoegh-Guldberg and Bruno, 2010). Therefore, the importance of SRM for global carbon cycling is predicted to further increase (Vigneron *et al.*, 2018).

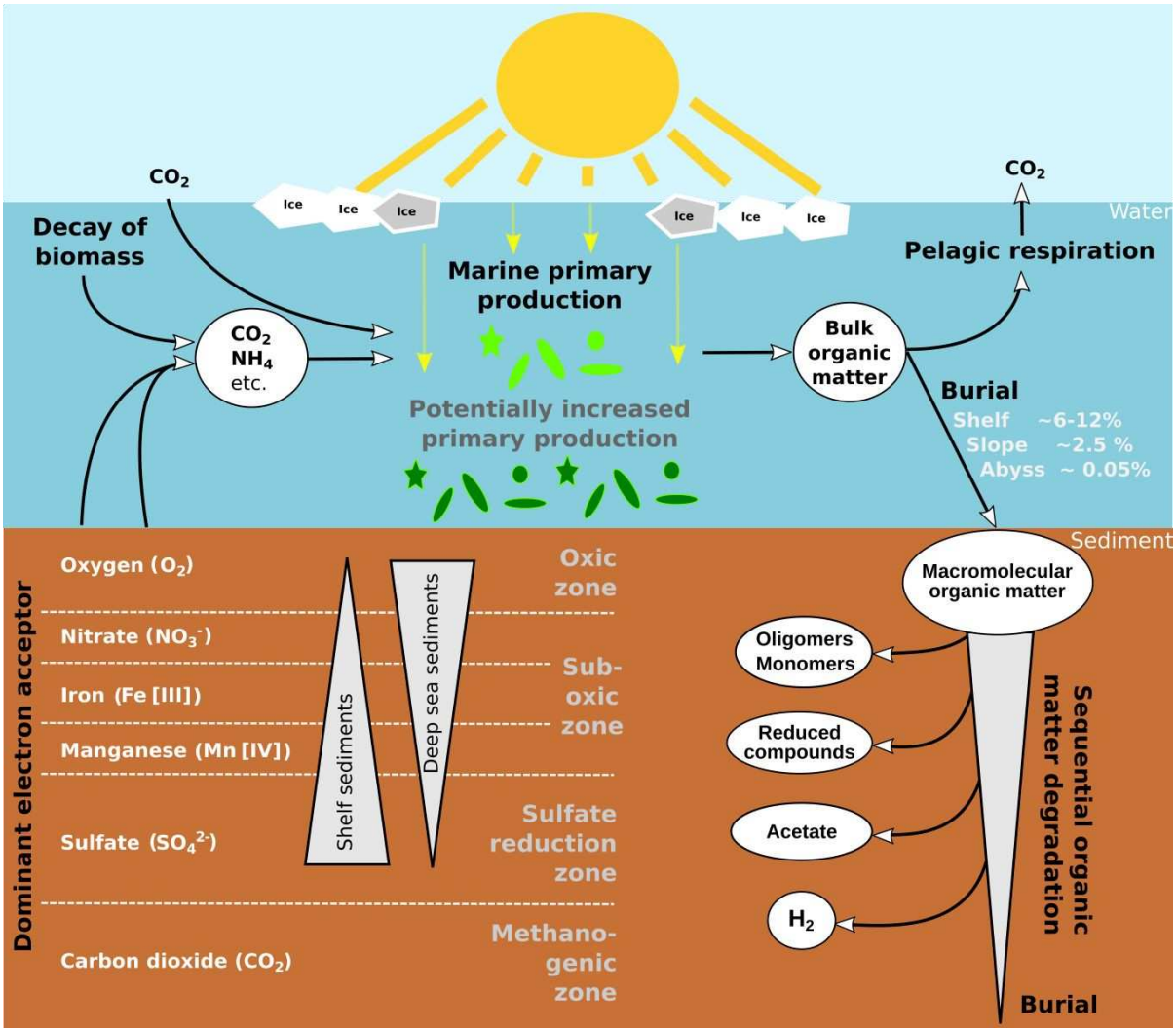

Figure 2. Schematic representation of the carbon cycle in arctic marine sediments. Organic matter from pelagic primary production is imported into the underlying sediments. The amount of organic matter that reaches the seafloor is highly dependent on water depth, but will potentially increase in the Arctic due to decreased extent of sea ice. Complex consortia of hydrolyzers and fermenters are responsible for the sequential degradation of sedimented organic matter. These provide electron donors for terminal mineralization, which also requires electron acceptors such as oxygen, nitrate, iron, manganese, sulfate, or carbon dioxide. The importance of these individual electron acceptors is highly dependent on the organic matter content and thus on the metabolic activity of the sediment microbial community.

SRM and other key organic matter-degrading microorganisms that thrive in arctic marine sediments are primarily affected by strong light and temperature fluctuations, which regulate organic matter supply and thus microbial activity (Hebbeln and Wefer, 1991). In comparison, the seafloor of fjords with water-terminating glaciers is exposed to much stronger environmental fluctuations with substantial consequences for animal and microbial communities in the adjacent sediments (Hop *et al.*, 2002; Park *et al.*, 2011; Bourgeois *et al.*, 2016). Glacier runoff transports significant amounts of inorganic particles to the fjord, which quickly settle to the seafloor where they accumulate and form vast deposits of terrestrial soil material (Zajaczkowski, 2008). The deposition of larger particles decreases exponentially with greater distance to the glacier (Svendsen *et al.*, 2002). Finer

particles, however, stay longer in the water column and cause extended areas of high water turbidity (Zajaczkowski, 2008), in which light availability for primary production is limited (Hop *et al.*, 2002). Glaciers are also a source of freshwater into the fjord, which causes upwelling of nutrients with overall positive effects on the productivity of glacier-influenced seawater (Meire *et al.*, 2017). Thus, the most favorable growth conditions for phytoplankton in arctic fjords are encountered in areas in which light and nutrient availability are high (Figure 3).

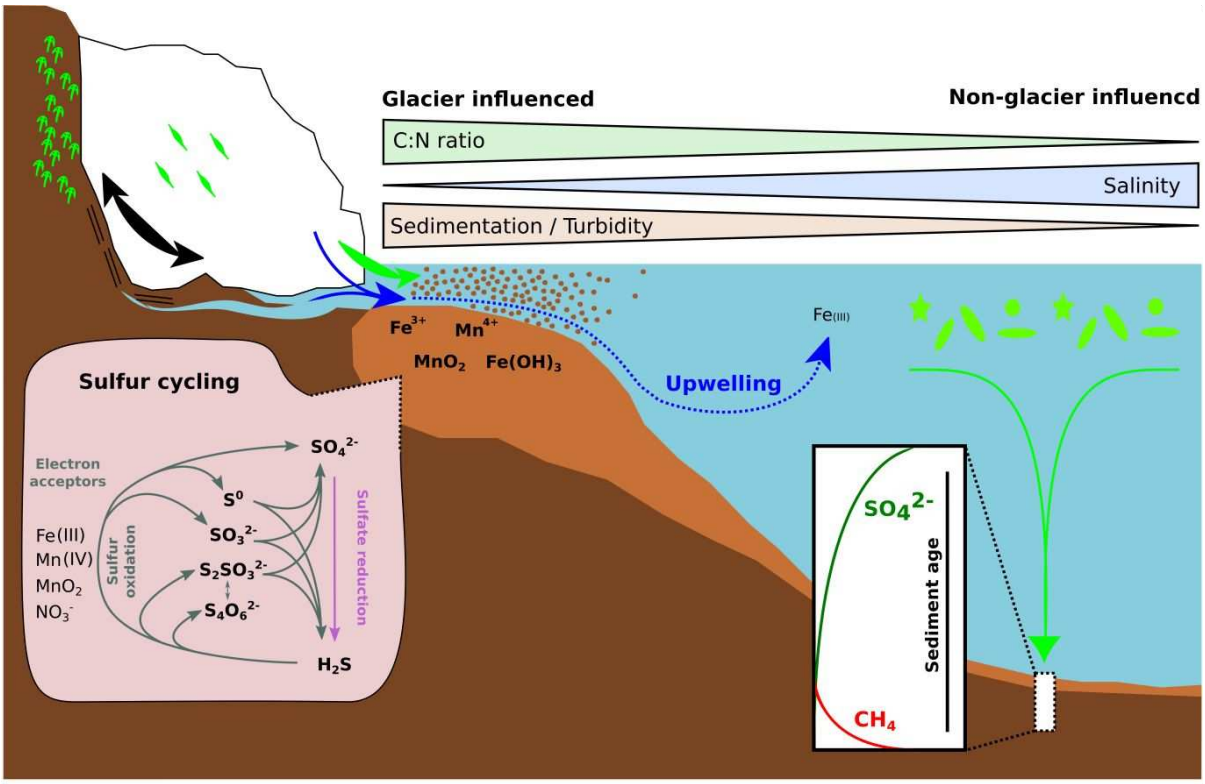

Figure 3. Major differences between glacier-influenced and non-glacier influenced sediments. Modified from Arndt *et al.*, 2013. At distance to the glacier, pelagic primary production prevails in the water column due to lower turbidity and increased nutrient availability. Upon sedimentation organic matter is mainly mineralized close to the surface, which causes a distinct depth zonation of electron acceptors. Glacier-influenced sediments are characterized by high sedimentation of inorganic material, high proportions of recalcitrant terrestrial organic matter, low salinity, and inputs of metals, which enables biotic and abiotic recycling of sulfide to sulfate.

In addition to organic matter from pelagic primary production, glaciated fjords with tremendous freshwater discharge also receive a substantial fraction of organic matter from terrestrial sources as indicated by high C:N ratios (Figure 3) (Wehrmann *et al.*, 2014). Terrestrial organic matter is highly altered by degradation processes in soil and freshwater habitats and its degradability is thus considered to be lower than the degradability of marine-derived organic matter (Burdige, 2007). Glacier run-off also contains several metals, in particular iron and manganese (Figure 3) (Bhatia *et al.*, 2013; Wehrmann *et al.*, 2014). These metals can serve as anaerobic electron acceptors

(Thamdrup, 2000), and are generally thought to preclude the use of sulfate due to thermodynamic constraints (Froelich *et al.*, 1979). In coastal sediments without glacial influence most organic matter is mineralized at or near the seafloor, which results in steep gradients of sulfate concentrations (Figure 3) (Røy *et al.*, 2012; Flury *et al.*, 2016). In glacier-proximal marine sediments high concentrations of iron and manganese can facilitate the oxidation of hydrogen sulfide to sulfate and sulfur cycle intermediates (Zopfi *et al.*, 2004). This enables a constant recycling of sulfate as an electron acceptor and sustains high activities of SRM in glacier-influenced sediments (Figure 3) (Wehrmann *et al.*, 2014, 2017).

All organic matter that settles to the seafloor is degraded by the sediment microbial community (Kędra et al., 2012). This bulk organic matter consists of cellular macromolecules such as proteins, carbohydrates, lipids and nucleic acids (Figure 4) (Dell'Anno, 2005; Burdige, 2007), which can be broken down by heterotrophic microorganisms and utilized as nutrient and energy sources (Arndt *et al.*, 2013). Proteins are often the principal organic constituent of phytoplankton species (Parsons *et al.*, 1961; Ciferri, 1983). Furthermore, subcomponents of proteins such as peptides and amino acids are important sources of organic nitrogen (McCarthy *et al.*, 1997), which become particularly important when organic matter content and hence inorganic nitrogen availability in the sediment are low (Vetter and Deming, 1994). Proteins that are enclosed in biological membranes can evade hydrolysis for prolonged times (Moore *et al.*, 2012), and might thus be available for deep subsurface microbiota (Zinke *et al.*, 2018). Lipids are primarily found in cellular membranes and are major components of phytoplankton biomass as well (Parsons *et al.*, 1961; Hudson and Karis, 1974). They consist of an alkyl chain, which is ester- or ether-bound to a polar head group such as phospho-glycerol or a glycerol that is glycosidically bound to a sugar moiety. The degradability of lipids is highly dependent on their chemical structure, e.g., glycolipids are considered more refractory than phospholipids (Schouten *et al.*, 2010). Accordingly, some lipids selectively survive degradation in the water column and are incorporated into the sediment in which they are available for microbial degradation (Wakeham *et al.*, 1984; Harvey *et al.*, 1986). Extracellular DNA constitutes only a small proportion of organic matter in marine sediments, but is, however, a crucial source of phosphorus for marine sediment microorganisms (Dell'Anno, 2005).

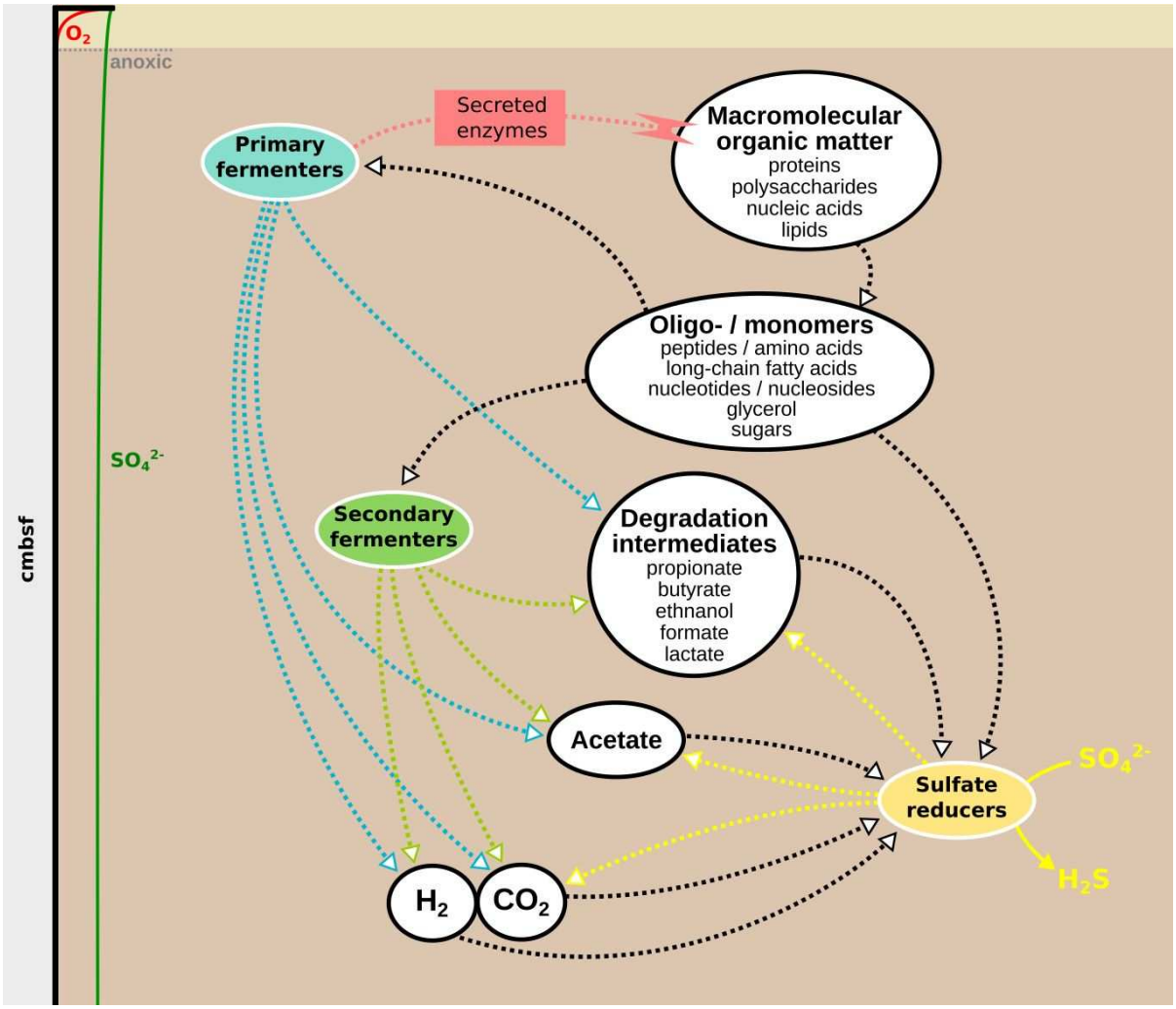

Figure 4. Sequential degradation of organic matter in anoxic marine sediments under sulfate reducing conditions. Macromolecules are initially hydrolyzed by secreted enzymes liberating oligomers and monomers that can be incorporated and fermented. Fermentation products are anaerobically respired by SRM, which couple the oxidation of organic molecules to the reduction of sulfate.

Macromolecules constitute important substrates for microbial degradation. However, they are too large to be directly transported into the peri- and/or cytoplasm (Meyer-Reil, 1991), and thus need to be degraded extracellularly. For this purpose, microorganisms release a diverse array of peptidases, lipases, and nucleases into the surrounding sediments for extracellular macromolecule hydrolysis (Vetter and Deming, 1994; Corinaldesi *et al.*, 2007; Orsi *et al.*, 2018; Zinke *et al.*, 2018). Secreted enzymes attack macromolecules and release oligomers and monomers such as peptides, amino acids, fatty acids, glycerol or other lipid headgroups, nucleotides, nucleosides and nucleobases (Figure 4). These can be imported into the cell via substrate-specific transporters. Released macromolecule subcomponents are also available for microorganisms which do not secrete costly extracellular enzymes themselves and are thus called ‘cheaters’ (Velicer, 2003). To circumvent diffusive loss of oligomers and monomers, some bacteria have developed a ‘selfish’ feeding strategy that involves

substrate binding to the outer membrane, partial hydrolysis and transport of larger oligomers into the periplasm (Reintjes *et al.*, 2017). Under anoxic conditions liberated oligomers and monomers are fermented to a range of volatile fatty acids (VFAs), i.e., butyrate, propionate, acetate, formate, as well as lactate, ethanol, H_2 and CO_2 (Figure 4) (Muyzer and Stams, 2008). In sulfate-bearing sediments, VFAs and other degradation intermediates are eventually oxidized to CO_2 via anaerobic respiration with sulfate as electron acceptor (Figure 4) (Arndt *et al.*, 2013). VFAs and lactate are considered to be very important substrates for SRM (Knoblauch *et al.*, 1999; Sahm *et al.*, 1999; Webster *et al.*, 2006; Na *et al.*, 2015; Müller *et al.*, 2018). However, up to 79 % of sulfate reduction is not fueled by VFAs (Finke *et al.*, 2007), and even complex substrates such as carbohydrates, higher fatty acids and aromatic compounds can be utilized by SRM (Rabus *et al.*, 2006; Musat *et al.*, 2009).

Research objectives

The overarching motivations of this thesis were to reveal the identity and metabolic capabilities of psychrophilic hydrolyzers, fermenters and SRM and to obtain novel insights into the diversity and environmental distribution of SRM in arctic marine sediments.

- The primary objective of Chapter 1 of this thesis was to develop a reliable next generation sequencing (NGS) and sequence analysis pipeline for reductive bacterial-type *dsrA* and *dsrB*. This pipeline was required to study SRM in the environment and under experimental conditions. At the time the work presented in Chapter 1 was initiated, a large part of the SRM diversity was not covered by the available *dsrAB* primers (Müller *et al.*, 2015). Besides, NGS of 16S rRNA gene amplicons has become routine in microbial ecology studies (Franzosa *et al.*, 2015; Tremblay *et al.*, 2015; Parada *et al.*, 2016), but applications of NGS of functional genes were still scarce and only one NGS-pipeline for *dsrB* was available (Zeleke *et al.*, 2013). Hence, the goals of Chapter 1 were to update and design *dsrA* and *dsrB*-specific primers and to benchmark the generation, bioinformatic processing, analysis and classification of *dsrA* and *dsrB* Illumina MiSeq sequencing reads.

- Fjord sediments in close proximity to water-terminating glaciers are characterized by massive sedimentation, as well as by high concentrations of metals and terrestrial organic matter. These habitat characteristics constitute strong influences on the microbial community and thus on the relevant biogeochemical processes. The composition and ecology of the microbial community that thrives in arctic fjord sediments is, however, poorly investigated. Therefore, the main goal of Chapter 2 was to understand the influence of glacier run-off on the assembly of the total microbial community and the community of sulfate reducers in fjord sediments.

- Hydrolyzers, fermenters and terminal mineralizers such as SRM are of key importance for global carbon and elemental cycles (Jørgensen, 1982; Bowles *et al.*, 2014). Nonetheless, the identities and physiological capabilities of the majority of the microorganisms that thrive in marine sediments are unknown (Lloyd *et al.*, 2018). In particular, the links between individual microbial species and specific functions, i.e., hydrolysis, fermentation or terminal mineralization, or the degradation of specific macromolecules, i.e., proteins, lipids, DNA and acetate, are largely unknown. Investigations of the identities and functions of organic matter-degrading microorganisms will, however, help to improve our understanding of the microbial carbon cycle in marine sediments and could indicate how these microorganisms will respond to ecosystem alterations. Thus, the main focus of Chapters 3-5 of this thesis was to investigate sediment microorganisms that are responsible for hydrolysis and fermentation of specific macromolecules, as well as to reveal the identities and ecosystem functions of SRM, which are considered to be key drivers of the terminal mineralization of organic matter.

References

Anantharaman, K., Hausmann, B., Jungbluth, S.P., Kantor, R.S., Lavy, A., Warren, L.A., *et al.* (2018) Expanded diversity of microbial groups that shape the dissimilatory sulfur cycle. *ISME J.* **12**: 1715–1728.

Arndt, S., Jørgensen, B.B., LaRowe, D.E., Middelburg, J.J., Pancost, R.D., and Regnier, P. (2013) Quantifying the degradation of organic matter in marine sediments: A review and synthesis. *Earth-Sci. Rev.* **123**: 53–86.

Arrigo, K.R., van Dijken, G., and Pabi, S. (2008) Impact of a shrinking Arctic ice cover on marine primary production. *Geophys. Res. Lett.* **35**: L19603.

Bhatia, M.P., Kujawinski, E.B., Das, S.B., Breier, C.F., Henderson, P.B., and Charette, M.A. (2013) Greenland meltwater as a significant and potentially bioavailable source of iron to the ocean. *Nat. Geosci.* **6**: 503–503.

Bourgeois, S., Kerhervé, P., Calleja, M.L., Many, G., and Morata, N. (2016) Glacier inputs influence organic matter composition and prokaryotic distribution in a high Arctic fjord (Kongsfjorden, Svalbard). *J. Mar. Syst.* **164**: 112–127.

Bowles, M.W., Mogollón, J.M., Kasten, S., Zabel, M., and Hinrichs, K.-U. (2014) Global rates of marine sulfate reduction and implications for sub-sea-floor metabolic activities. *Science* **344**: 889–891.

Burdige, D.J. (2007) Preservation of organic matter in marine sediments: controls, mechanisms, and an imbalance in sediment organic carbon budgets? *Chem. Rev.* **107**: 467–485.

Carbonero, F., Benefiel, A.C., Alizadeh-Ghamsari, A.H., and Gaskins, H.R. (2012) Microbial pathways in colonic sulfur metabolism and links with health and disease. *Front. Physiol.* **3**: 448.

Cavicchioli, R. (2016) On the concept of a psychrophile. *ISME J.* **10**: 793–795.

Christian, J.R. and Karl, D.M. (1995) Bacterial ectoenzymes in marine waters: Activity ratios and temperature responses in three oceanographic provinces. *Limnol. Oceanogr.* **40**: 1042–1049.

Ciferri, O. (1983) Spirulina, the edible microorganism. *Microbiol. Rev.* **47**: 551–578.

Corinaldesi, C., Dell'Anno, A., and Danovaro, R. (2007) Early diagenesis and trophic role of extracellular DNA in different benthic ecosystems. *Limnol. Oceanogr.* **52**: 1710–1717.

Dell'Anno, A. (2005) Extracellular DNA Plays a Key Role in Deep-Sea Ecosystem Functioning. *Science* **309**: 2179–2179.

Deming, J.W. (2002) Psychrophiles and polar regions. *Curr. Opin. Microbiol.* **5**: 301–309.

Dunne, J.P., Sarmiento, J.L., and Gnanadesikan, A. (2007) A synthesis of global particle export from the surface ocean and cycling through the ocean interior and on the seafloor. *Global Biogeochem. Cycles* **21**: 1–16.

Fabiano, M. and Pusceddu, A. (1998) Total and hydrolizable particulate organic matter (carbohydrates, proteins and lipids) at a coastal station in Terra Nova Bay (Ross Sea, Antarctica). *Polar Biol.* **19**: 125–132.

Finke, N., Vandieken, V., and Jørgensen, B.B. (2007) Acetate, lactate, propionate, and isobutyrate as electron donors for iron and sulfate reduction in Arctic marine sediments, Svalbard. *FEMS Microbiol. Ecol.* **59**: 10–22.

Flury, S., Røy, H., Dale, A.W., Fossing, H., Tóth, Z., Spiess, V., *et al.* (2016) Controls on subsurface methane fluxes and shallow gas formation in Baltic Sea sediment (Aarhus Bay, Denmark). *Geochim. Cosmochim. Acta* **188**: 297–309.

Franzosa, E.A., Hsu, T., Sirota-Madi, A., Shafquat, A., Abu-Ali, G., Morgan, X.C., and Huttenhower, C. (2015) Sequencing and beyond: integrating molecular “omics” for microbial community profiling. *Nat. Rev. Microbiol.* **13**: 360–372.

Froelich, P.N., Klinkhammer, G.P., Bender, M.L., Luedtke, N.A., Heath, G.R., Cullen, D., *et al.* (1979) Early oxidation of organic matter in pelagic sediments of the eastern equatorial Atlantic: suboxic diagenesis. *Geochim. Cosmochim. Acta* **43**: 1075–1090.

Harvey, H.R., Rodger Harvey, H., Fallon, R.D., and Patton, J.S. (1986) The effect of organic matter and oxygen on the degradation of bacterial membrane lipids in marine sediments. *Geochim. Cosmochim. Acta* **50**: 795–804.

Hausmann, B., Pelikan, C., Herbold, C.W., Köstlbacher, S., Albertsen, M., Eichorst, S.A., *et al.* (2018) Peatland Acidobacteria with a dissimilatory sulfur metabolism. *ISME J.* **12**: 1729–1742.

Hebbeln, D. and Wefer, G. (1991) Effects of ice coverage and ice-rafted material on sedimentation in the Fram Strait. *Nature* **350**: 409–411.

Hoegh-Guldberg, O. and Bruno, J.F. (2010) The Impact of Climate Change on the World’s Marine Ecosystems. *Science* **328**: 1523–1528.

Hop, H., Pearson, T., Hegseth, E.N., Kovacs, K.M., Wiencke, C., Kwasniewski, S., *et al.* (2002) The marine ecosystem of Kongsfjorden, Svalbard. *Polar Res.* **21**: 167–208.

Hudson, B.J. and Karis, I.G. (1974) The lipids of the alga Spirulina. *J. Sci. Food Agric.* **25**: 759–763.

Jochum, L.M., Chen, X., Lever, M.A., Loy, A., Jørgensen, B.B., Schramm, A., and Kjeldsen, K.U. (2017) Depth Distribution and Assembly of Sulfate-Reducing Microbial Communities in Marine Sediments of Aarhus Bay. *Appl. Environ. Microbiol.* **83**: e01547–17.

Jørgensen, B.B. (1982) Mineralization of organic matter in the sea bed—the role of sulphate reduction. *Nature* **296**: 643–645.

Kadnikov, V.V., Ivasenko, D.A., Beletsky, A.V., Mardanov, A.V., Danilova, E.V., Pimenov, N.V., *et al.* (2016) A Novel Uncultured Bacterium of the Family Gallionellaceae: Description and Genome Reconstruction Based on the Metagenomic Analysis of Microbial Community in Acid Mine Drainage. *Mikrobiologiia* **85**: 421–435.

Kallmeyer, J., Pockalny, R., Adhikari, R.R., Smith, D.C., and D’Hondt, S. (2012) Global distribution of microbial abundance and biomass in subseafloor sediment. *Proc. Natl. Acad. Sci. U. S. A.* **109**: 16213–16216.

Kędra, M., Kuliński, K., Walkusz, W., and Legeżyńska, J. (2012) The shallow benthic food web structure in the high Arctic does not follow seasonal changes in the surrounding environment. *Estuar. Coast. Shelf Sci.* **114**: 183–191.

Knoblauch, C. and Jørgensen, B.B. (1999) Effect of temperature on sulphate reduction, growth rate and growth yield in five psychrophilic sulphate-reducing bacteria from Arctic sediments. *Environ. Microbiol.* **1**: 457–467.

Knoblauch, C., Sahm, K., and Jørgensen, B.B. (1999) Psychrophilic sulfate-reducing bacteria isolated from permanently cold arctic marine sediments: description of Desulfofrigus oceanense gen. nov., sp. nov., Desulfofrigus fragile sp. nov., Desulfofaba gelida gen. nov., sp. nov., Desulfotalea psychrophila gen. nov., sp. nov. and Desulfotalea arctica sp. nov. *Int. J. Syst. Bacteriol.* **49**: 1631–1643.

Lalande, C., Bélanger, S., and Fortier, L. (2009) Impact of a decreasing sea ice cover on the vertical export of particulate organic carbon in the northern Laptev Sea, Siberian Arctic Ocean. *Geophys. Res. Lett.* **36**: 1–5.

Liu, P. and Conrad, R. (2017) Syntrophobacteraceae-affiliated species are major propionate-degrading sulfate reducers in paddy soil. *Environ. Microbiol.* **19**: 1669–1686.

Liu, P., Pommerenke, B., and Conrad, R. (2018) Identification of Syntrophobacteraceae as major acetate-degrading sulfate reducing bacteria in Italian paddy soil. *Environ. Microbiol.* **20**: 337–354.

Lloyd, K.G., Steen, A.D., Ladau, J., Yin, J., and Crosby, L. (2018) x^ *mSystems* **3**: e00055–18.

McCarthy, M., Pratum, T., Hedges, J., and Benner, R. (1997) Chemical composition of dissolved organic nitrogen in the ocean. *Nature* **390**: 150–154.

Meire, L., Mortensen, J., Meire, P., Juul-Pedersen, T., Sejr, M.K., Rysgaard, S., *et al.* (2017) Marine-terminating glaciers sustain high productivity in Greenland fjords. *Glob. Chang. Biol.* **23**: 5344–5357.

Meyer-Reil, L.-A. (1991) Ecological Aspects of Enzymatic Activity in Marine Sediments. In, *Brock/Springer Series in Contemporary Bioscience*., pp. 84–95.

Moore, E.K., Nunn, B.L., Goodlett, D.R., and Harvey, H.R. (2012) Identifying and tracking proteins through the marine water column: insights into the inputs and preservation mechanisms of protein in sediments. *Geochim. Cosmochim. Acta* **83**: 324–359.

Moreau, J.W., Zierenberg, R.A., and Banfield, J.F. (2010) Diversity of Dissimilatory Sulfite Reductase Genes (dsrAB) in a Salt Marsh Impacted by Long-Term Acid Mine Drainage. *Appl. Environ. Microbiol.* **76**: 4819–4828.

Müller, A.L., Kjeldsen, K.U., Rattei, T., Pester, M., and Loy, A. (2015) Phylogenetic and environmental diversity of DsrAB-type dissimilatory (bi)sulfite reductases. *ISME J.* **9**: 1152–1165.

Müller, A.L., Pelikan, C., de Rezende, J.R., Wasmund, K., Putz, M., Glombitza, C., *et al.* (2018) Bacterial interactions during sequential degradation of cyanobacterial necromass in a sulfidic arctic marine sediment. *Environ. Microbiol.* **20**: 2927–2940.

Musat, F., Galushko, A., Jacob, J., Widdel, F., Kube, M., Reinhardt, R., *et al.* (2009) Anaerobic degradation of naphthalene and 2-methylnaphthalene by strains of marine sulfate-reducing bacteria. *Environ. Microbiol.* **11**: 209–219.

Muyzer, G. and Stams, A.J.M. (2008) The ecology and biotechnology of sulphate-reducing bacteria. *Nat. Rev. Microbiol.* **6**: 441–454.

Na, H., Lever, M.A., Kjeldsen, K.U., Schulz, F., and Jørgensen, B.B. (2015) Uncultured Desulfobacteraceae and Crenarchaeotal group C3 incorporate 13C-acetate in coastal marine sediment. *Environ. Microbiol. Rep.* **7**: 614–622.

Orcutt, B.N., Larowe, D.E., Biddle, J.F., Colwell, F.S., Glazer, B.T., Reese, B.K., *et al.* (2013) Microbial activity in the marine deep biosphere: progress and prospects. *Front. Microbiol.* **4**: 189.

Orsi, W.D., Richards, T.A., and Francis, W.R. (2018) Predicted microbial secretomes and their target substrates in marine sediment. *Nat Microbiol* **3**: 32–37.

Parada, A.E., Needham, D.M., and Fuhrman, J.A. (2016) Every base matters: assessing small subunit rRNA primers for marine microbiomes with mock communities, time series and global field samples. *Environ. Microbiol.* **18**: 1403–1414.

Park, S.-J., Park, B.-J., Jung, M.-Y., Kim, S.-J., Chae, J.-C., Roh, Y., *et al.* (2011) Influence of deglaciation on microbial communities in marine sediments off the coast of Svalbard, Arctic Circle. *Microb. Ecol.* **62**: 537–548.

Parsons, T.R., Stephens, K., and Strickland, J.D.H. (1961) On the Chemical Composition of Eleven Species of Marine Phytoplankters. *J. Fish. Res. Bd. Can.* **18**: 1001–1016.

Pavloudi, C., Oulas, A., Vasileiadou, K., Kotoulas, G., De Troch, M., Friedrich, M.W., and Arvanitidis, C. (2017) Diversity and abundance of sulfate-reducing microorganisms in a Mediterranean lagoonal complex (Amvrakikos Gulf, Ionian Sea) derived from dsrB gene. *Aquat. Microb. Ecol.* **79**: 209–219.

Pester, M. (2012) Sulfate-reducing microorganisms in wetlands – fameless actors in carbon cycling and climate change. *Front. Microbiol.* **3**: 72.

Pester, M., Brambilla, E., Alazard, D., Rattei, T., Weinmaier, T., Han, J., *et al.* (2012) Complete Genome Sequences of Desulfosporosinus orientis DSM765T, Desulfosporosinus youngiae DSM17734T, Desulfosporosinus meridiei DSM13257T, and Desulfosporosinus acidiphilus DSM22704T. *J. Bacteriol.* **194**: 6300–6301.

Rabus, R., Hansen, T.A., and Widdel, F. (2013) Dissimilatory Sulfate- and Sulfur-Reducing Prokaryotes. In, *The Prokaryotes*., pp. 309–404.

Rabus, R., Hansen, T.A., and Widdel, F. (2006) Dissimilatory Sulfate- and Sulfur-Reducing Prokaryotes. In, *The Prokaryotes*., pp. 659–768.

Reintjes, G., Arnosti, C., Fuchs, B.M., and Amann, R. (2017) An alternative polysaccharide uptake mechanism of marine bacteria. *ISME J.* **11**: 1640–1650.

Robador, A., Müller, A.L., Sawicka, J.E., Berry, D., Hubert, C.R.J., Loy, A., *et al.* (2016) Activity and community structures of sulfate-reducing microorganisms in polar, temperate and tropical marine sediments. *ISME J.* **10**: 796–809.

Røy, H., Kallmeyer, J., Adhikari, R.R., Pockalny, R., Jørgensen, B.B., and D'Hondt, S. (2012) Aerobic microbial respiration in 86-million-year-old deep-sea red clay. *Science* **336**: 922–925.

Sagemann, J., Jørgensen, B.B., and Greeff, O. (1998) Temperature dependence and rates of sulfate reduction in cold sediments of svalbard, arctic ocean. *Geomicrobiol. J.* **15**: 85–100.

Sahm, K., Knoblauch, C., and Amann, R. (1999) Phylogenetic affiliation and quantification of psychrophilic sulfate-reducing isolates in marine Arctic sediments. *Appl. Environ. Microbiol.* **65**: 3976–3981.

Santos, A.A., Venceslau, S.S., Grein, F., Leavitt, W.D., Dahl, C., Johnston, D.T., and Pereira, I.A.C. (2015) A protein trisulfide couples dissimilatory sulfate reduction to energy conservation. *Science* **350**: 1541–1545.

Schouten, S., Middelburg, J.J., Hopmans, E.C., and Sinninghe Damsté, J.S. (2010) Fossilization and degradation of intact polar lipids in deep subsurface sediments: A theoretical approach. *Geochim. Cosmochim. Acta* **74**: 3806–3814.

Sørensen, H.L., Meire, L., Juul-Pedersen, T., de Stigter, H.C., Meysman, F., Rysgaard, S., *et al.* (2015) Seasonal carbon cycling in a Greenlandic fjord: an integrated pelagic and benthic study. *Mar. Ecol. Prog. Ser.* **539**: 1–17.

Steger, D., Wentrup, C., Braunegger, C., Deevong, P., Hofer, M., Richter, A., *et al.* (2011) Microorganisms with novel dissimilatory (bi)sulfite reductase genes are widespread and part of the core microbiota in low-sulfate peatlands. *Appl. Environ. Microbiol.* **77**: 1231–1242.

St-Pierre, B. and Wright, A.-D.G. (2017) Implications from distinct sulfate-reducing bacteria populations between cattle manure and digestate in the elucidation of HS production during anaerobic digestion of animal slurry. *Appl. Microbiol. Biotechnol.* **101**: 5543–5556.

Svendsen, H., Beszczynska-Møller, A., Hagen, J.O., Lefauconnier, B., Tverberg, V., Gerland, S., *et al.* (2002) The physical environment of Kongsfjorden–Krossfjorden, an Arctic fjord system in Svalbard. *Polar Res.* **21**: 133–166.

Thamdrup, B. (2000) Bacterial Manganese and Iron Reduction in Aquatic Sediments. In, *Advances in Microbial Ecology*., pp. 41–84.

Tremblay, J., Singh, K., Fern, A., Kirton, E.S., He, S., Woyke, T., *et al.* (2015) Primer and platform effects on 16S rRNA tag sequencing. *Front. Microbiol.* **6**: 771.

Vaughan, D.G., Comiso, J.C., Allison, I., Carrasco, J., Kaser, G., Kwok, R., *et al.* (2014) Observations: Cryosphere. In, Stocker,T.F., Qin,D., Plattner,G.-K., Tignor,M.M.B., Allen,S.K., Boschung,J., *et al.* (eds), *Climate Change 2013 - The Physical Science Basis. Contribution of Working Group I to the Fifth Assessment Report of the Intergovernmental Panel on Climate Change*. Cambridge University Press, Cambridge, United Kingdom and New York, NY, USA., Cambridge, pp. 317–382.

Velicer, G.J. (2003) Social strife in the microbial world. *Trends Microbiol.* **11**: 330–337.

Vetter, Y.A. and Deming, J.W. (1994) Extracellular enzyme activity in the Arctic Northeast Water polynya. *Mar. Ecol. Prog. Ser.* **114**: 23–34.

Vigneron, A., Cruaud, P., Alsop, E., de Rezende, J.R., Head, I.M., and Tsesmetzis, N. (2018) Beyond the tip of the iceberg; a new view of the diversity of sulfite- and sulfate-reducing microorganisms. *ISME J.* **12**: 2096–2099.

Wagner, M., Loy, A., Klein, M., Lee, N., Ramsing, N.B., Stahl, D.A., and Friedrich, M.W. (2005) Functional marker genes for identification of sulfate-reducing prokaryotes. *Methods Enzymol.* **397**: 469–489.

Wagner, M., Roger, A.J., Flax, J.L., Brusseau, G.A., and Stahl, D.A. (1998) Phylogeny of dissimilatory sulfite reductases supports an early origin of sulfate respiration. *J. Bacteriol.* **180**: 2975–2982.

Wakeham, S.G., Lee, C., Farrington, J.W., and Gagosian, R.B. (1984) Biogeochemistry of particulate organic matter in the oceans: results from sediment trap experiments. *Deep Sea Res. A* **31**: 509–528.

Wasmund, K., Mußmann, M., and Loy, A. (2017) The life sulfuric: microbial ecology of sulfur cycling in marine sediments. *Environ. Microbiol. Rep.* **9**: 323–344.

Webster, G., Watt, L.C., Rinna, J., Fry, J.C., Evershed, R.P., Parkes, R.J., and Weightman, A.J. (2006) A comparison of stable-isotope probing of DNA and phospholipid fatty acids to study prokaryotic functional diversity in sulfate-reducing marine sediment enrichment slurries. *Environ. Microbiol.* **8**: 1575–1589.

Wehrmann, L.M., Formolo, M.J., Owens, J.D., Raiswell, R., Ferdelman, T.G., Riedinger, N., and Lyons, T.W. (2014) Iron and manganese speciation and cycling in glacially influenced high-latitude fjord sediments (West Spitsbergen, Svalbard): Evidence for a benthic recycling-transport mechanism. *Geochim. Cosmochim. Acta* **141**: 628–655.

Wehrmann, L.M., Riedinger, N., Brunner, B., Kamyshny, A., Hubert, C.R.J., Herbert, L.C., *et al.* (2017) Iron-controlled oxidative sulfur cycling recorded in the distribution and isotopic composition of sulfur species in glacially influenced fjord sediments of west Svalbard. *Chem. Geol.* **466**: 678–695.

Zajaczkowski, M. (2008) Sediment supply and fluxes in glacial and outwash fjords, Kongsfjorden and Adventfjorden, Svalbard. *Pol. Polar Res.* **1**: 59–72.

Zecchin, S., Mueller, R.C., Seifert, J., Stingl, U., Anantharaman, K., von Bergen, M., *et al.* (2018) Rice Paddy Nitrospirae Carry and Express Genes Related to Sulfate Respiration: Proposal of the New Genus “Candidatus Sulfobium.” *Appl. Environ. Microbiol.* **84**: e02224–17.

Zeleke, J., Sheng, Q., Wang, J.-G., Huang, M.-Y., Xia, F., Wu, J.-H., and Quan, Z.-X. (2013) Effects of Spartina alterniflora invasion on the communities of methanogens and sulfate-reducing bacteria in estuarine marsh sediments. *Front. Microbiol.* **4**: 243.

Zinke, L.A., Glombitza, C., Bird, J.T., Røy, H., Jørgensen, B.B., Lloyd, K.G., *et al.* (2018) Microbial organic matter degradation potential in Baltic Sea sediments influenced by depositional conditions and in situ geochemistry. *Appl. Environ. Microbiol.* **84**: e02164–18.

Zopfi, J., Ferdelman, T.G., and Fossing, H. (2004) Distribution and fate of sulfur intermediates—sulfite, tetrathionate, thiosulfate, and elemental sulfur—in marine sediments. In, *Special Paper 379: Sulfur Biogeochemistry - Past and Present.*, pp. 97–116.

Chapter 1

Diversity analysis of sulfite- and sulfate-reducing microorganisms by multiplex *dsrA* and *dsrB* amplicon sequencing using new primers and mock community-optimized bioinformatics

Claus Pelikan, Craig W. Herbold, Bela Hausmann, Albert L. Müller, Michael Pester and Alexander Loy

Reference:

Environmental Microbiology (2016) 18(9), 2994–3009; doi:10.1111/1462-2920.13139

Supplementary information available at:
https://onlinelibrary.wiley.com/doi/abs/10.1111/1462-2920.13139

Author contributions:

CP, CWH and AL designed the experiments and the data analysis procedures with the help of all authors. CP performed experiments. CP, CWH and BH analysed data. CP and AL wrote the manuscript. CWH, BH, AM and MP revised the draft version and approved the final version of the manuscript.

environmental microbiology

Environmental Microbiology (2016) **18**(9), 2994–3009 doi:10.1111/1462-2920.13139

Diversity analysis of sulfite- and sulfate-reducing microorganisms by multiplex *dsrA* and *dsrB* amplicon sequencing using new primers and mock community-optimized bioinformatics

Claus Pelikan,[1,2] Craig W. Herbold,[1] Bela Hausmann,[1,3] Albert L. Müller,[1,2†] Michael Pester[3] and Alexander Loy[1,2*]

[1]*Division of Microbial Ecology, Department of Microbiology and Ecosystem Science, Research Network Chemistry Meets Microbiology, University of Vienna, Vienna, Austria.*

[2]*Austrian Polar Research Institute, Vienna, Austria.*

[3]*Department of Biology, University of Konstanz, Konstanz, Germany.*

Summary

Genes encoding dissimilatory sulfite reductase (DsrAB) are commonly used as diagnostic markers in ecological studies of sulfite- and sulfate-reducing microorganisms. Here, we developed new high-coverage primer sets for generation of reductive bacterial-type *dsrA* and *dsrB* polymerase chain reaction (PCR) products for highly parallel amplicon sequencing and a bioinformatics workflow for processing and taxonomic classification of short *dsrA* and *dsrB* reads. We employed two diverse mock communities that consisted of 45 or 90 known *dsrAB* sequences derived from environmental clones to precisely evaluate the performance of individual steps of our amplicon sequencing approach on the Illumina MiSeq platform. Although PCR cycle number, gene-specific primer mismatches and stringent filtering for high-quality sequences had notable effects on the observed *dsrA* and *dsrB* community structures, recovery of most mock community sequences was generally proportional to their relative input abundances. Successful *dsrA* and dsrB diversity analysis in selected environmental samples further proved that the multiplex amplicon sequencing approach is adequate for monitoring spatial distribution and temporal abundance dynamics of *dsrAB*-containing microorganisms. Although tested for reductive bacterial-type *dsrAB*, this method is readily applicable for oxidative-type *dsrAB* of sulfur-oxidizing bacteria and also provides guidance for processing short amplicon reads of other functional genes.

Received 7 August, 2015; accepted 18 November, 2015. *For correspondence. E-mail loy@microbial-ecology.net; Tel. (+43) 1 4277 76605; Fax (+43) 1 4277 876605. †Present address: Spormann Laboratory, Civil and Environmental Engineering, Stanford University, USA.

© 2015 Society for Applied Microbiology and John Wiley & Sons Ltd

Introduction

Microorganisms that anaerobically respire sulfate or other oxidized sulfur compounds engage in multi-member microbial communities that syntrophically degrade and mineralize organic molecules in various anoxic ecosystems such as wetlands, marine sediments and the gastrointestinal tract of humans and animals (Carbonero *et al*., 2012; Pester *et al*., 2012a,b; Rabus *et al*., 2015). They thereby hold prime positions in the global sulfur and carbon cycles and as intestinal symbionts that mediate substrate transfer to and from their host. All investigated isolates of sulfate-reducing microorganisms (SRM) depend on a DsrAB-type dissimilatory sulfite reductase as a crucial part of their enzymatic machinery for respiring sulfate (Venceslau *et al*., 2014). The evolutionary distribution of *dsrAB*, which is generally present in single copy in the genomes of extant microorganisms, is highly conserved and primarily driven by vertical descent (Zverlov *et al*., 2005; Müller *et al*., 2015). Genes encoding the DsrAB subunits alpha and beta are thus, with some limitations, suitable phylogenetic and functional markers for environmental studies of SRM. For interpretation of environmental *dsrAB* diversity data, it is important to know that *dsrAB* are also present in other microorganisms, including sulfite-reducing microorganisms (Simon *et al*., 2013), sulfur-disproportionating bacteria (Finster, 2008; Milucka *et al*., 2012), microorganisms that produce sulfite internally by degrading organosulfonates such as taurine or cysteate (Laue *et al*., 2001), and obligate secondary fermenters that apparently have lost the capability for respiring oxidized sulfur compounds (Brauman *et al*.,

1998; Imachi *et al*., 2006). A recent meta-analysis of all publicly available *dsrAB* sequences provided the necessary background for environmental *dsrAB* diversity studies by introducing a reference database and a hierarchical classification system, which integrates taxonomy of known isolates with phylogeny of environmentally retrieved *dsrAB* sequences. This reference phylogeny discerns three main DsrAB protein families. SRM and some sulfite/organosulfonate reducers have reductive bacterial-type or reductive archaeal-type DsrAB, whereas some sulfur-oxidizing bacteria have oxidative bacterial-type DsrAB that operates in reverse (Müller *et al*., 2015).

Classical *dsrAB* diversity surveys were performed via clone libraries and Sanger sequencing, which allowed the analysis of very few samples and produced maximally a few hundred clone sequences per study (Moreau *et al*., 2010; Steger *et al*., 2011). The recovered environmental *dsrAB* clone sequences were then generally identified by phylogenetic analysis and manual interpretation of the obtained tree (Wagner *et al*., 2005). Today, simultaneous comparative analysis of microbial community composition across many samples is possible because of the advent of next generation sequencing (NGS) technologies for highly multiplexed amplicon sequencing. Amplicon NGS surveys that use small-subunit rRNA genes as phylogenetic markers have become routine in microbial ecology studies (Franzosa *et al*., 2015; Parada *et al*., 2015; Tremblay *et al*., 2015), but are now also increasingly applied to target functional genes that are indicative of a particular microbial guild, such as *pmoA* for methanotrophs (Kip *et al*., 2011), *amoA* for ammonia-oxidizers (Pester *et al*., 2012a,b), *nxrB* for nitrite-oxidizers (Pester *et al*., 2013), *nifH* for diazotrophs (Collavino *et al*., 2014), *mcrA* for methanogens and *dsrB* for sulfite/sulfate reducers (Zeleke *et al*., 2013). However, efficient detection and identification of novel functional gene sequences in environmental samples are dependent on curated databases with taxonomically annotated reference sequences (Müller *et al*., 2015) and the use of primers with adequate coverage for the target group. Millions of short sequence reads can now be produced by NGS and are typically processed and classified by using semi-automated bioinformatics pipelines (Schloss *et al*., 2009; Caporaso *et al*., 2010; Edgar, 2013). These bioinformatics workflows are primarily tested and applied to 16S rRNA gene sequences, but still remain poorly, if at all, benchmarked for other marker genes such as *dsrAB*.

In the present study, we redesigned and newly developed primer sets to perfectly match almost all known sequences of reductive bacterial-type *dsrAB*. The new primer sets were used for generating barcoded amplicons for highly parallel sequencing on the ILLUMINA MISEQ platform. Barcoding polymerase chain reaction (PCR) at varying cycle numbers and bioinformatics sequence processing and analysis tools were evaluated using diverse *dsrAB* mock communities that consisted of 45 or 90 known sequences of differential abundance and similarity (Fig. S1). All steps in the sequence analysis pipeline, including removal of erroneous and chimeric sequences, sequence clustering into species-level operational taxonomic units (OTUs) and classification of OTUs using the hierarchical reference taxonomy (Müller *et al*., 2015), were individually optimized for *dsrA* and *dsrB* amplicon reads to yield final sequence data sets that are of high quality and best represent the *dsrAB* sequence composition of the original mock communities. The processing of selected environmental samples according to the final workflow demonstrated its applicability for large-scale *dsrAB* diversity studies in modern microbial ecology.

Results and discussion

New high-coverage primer sets for PCR amplification of reductive bacterial-type dsrAB

We initially modified existing and developed new primer sets to perfectly match ≥ 97% of all reductive bacterial-type *dsrAB* sequences in the reference database (Fig. 1, Table 1). Different combinations of these primer sets were tested with *dsrAB* mock community DNA and an environmental DNA sample for generation of *dsrA* and *dsrB* amplicons of sizes that are compatible with amplicon sequencing (approximately ≤ 0.8 kb) on most NGS platforms such as ILLUMINA MISEQ, 454-ROCHE GS FLX+ and IONTORRENT. Primers were used with and without the generic 5′-head sequence, which is needed for two-step barcoding of PCR products (Herbold *et al*., 2015), to compare their amplification efficiencies. A visible band of the expected size was obtained with most combinations of primers and DNA samples. Importantly, the barcoding approach always yielded a strong band of the correct size (Fig. S2). Primer pair sets DSR190Fmix/DSR916Rmix and DSR1762Fmix/DSR2107Rmix were subsequently used for generating barcoded *dsrA* and *dsrB* amplicons from two mock communities and three environmental samples for MiSeq sequencing (Tables S1 and S2).

Optimized sequence-processing produces high-quality data sets

MISEQ data obtained from *dsrA* and *dsrB* amplicons of the 90-sequence mock community (66 599 and 76 016 raw read pairs respectively) (Table S1) were used to optimize and evaluate the different steps in the bioinformatics sequence-processing pipeline (Fig. S3). Due to the initial differences in PCR amplicon size, paired-end MiSeq reads were either joined into incomplete *dsrA* scaffolds or assembled into continuous *dsrB* contigs, which required

© 2015 Society for Applied Microbiology and John Wiley & Sons Ltd,

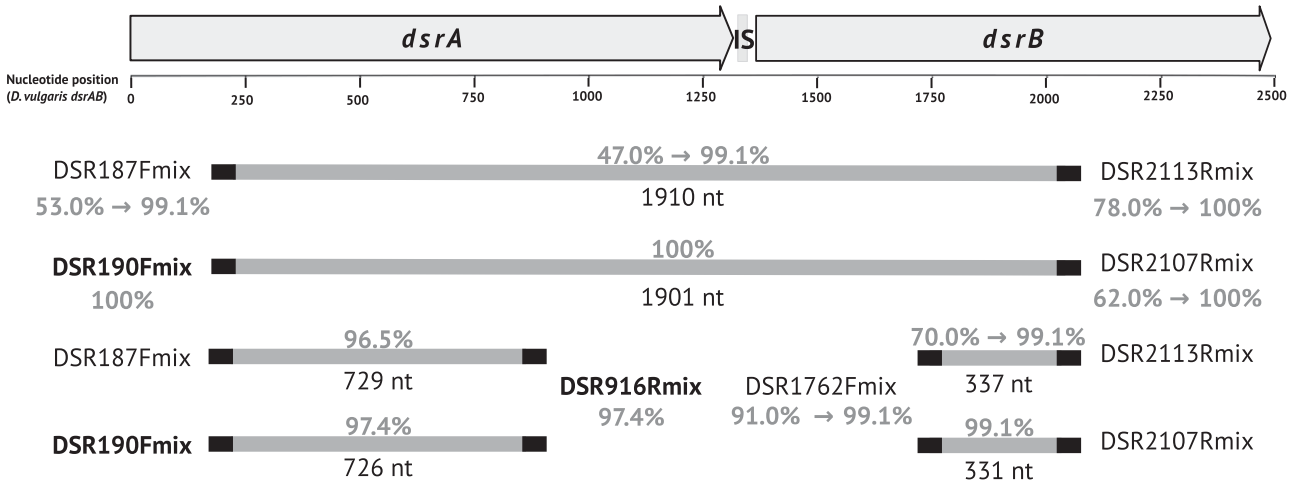

Fig. 1. Updated and newly designed primer sets for amplification of reductive bacterial-type *dsrAB*. Black and grey horizontal bars indicate the binding position of each primer and the lengths of the expected PCR amplicons relative to the complete *dsrAB* gene of the reference strain *Desulfovibrio vulgaris* str. Hildenborough respectively. The primer names refer to the primer-binding positions on the *dsrAB* sequence of *D. vulgaris*. Newly designed and updated primers are indicated in bold and regular type respectively. Percentages indicate the fraction of reductive bacterial-type *dsrAB* sequences in the reference database that have no mismatches to individual (pairs of) primer sets. The increase in coverage compared with the previous version of a primer set is indicated with an arrow. Sequences and coverages of the individual primer variants in each primer set are shown in Table 1. IS, intergenic spacer region between *dsrA* and *dsrB*.

the establishment of two slightly different sequence-processing pipelines (Fig. S3). The fraction of erroneous sequences gradually decreased after each processing step. Most erroneous sequences were accounted for by removal of singletons (i.e. sequences that were observed only once in the whole sequencing run) and pre-clustering into OTUs at 99% nucleic acid sequence identity (Fig. 2). The suggested 90% *dsrAB* identity threshold for approximate species-level OTUs (based on a ~1.9 kb fragment of the core reference sequences, Müller *et al.*, 2015) corresponds to 92% identity for the short *dsrA* scaffolds and 90% identity for the short *dsrB* contigs (Fig. S4). Many sequences that were not fully identical with mock community sequences, and likely derived from PCR and sequencing errors, are included into correct OTUs during pre-clustering and species-level clustering, which considerably increased the total number of used sequences (Fig. 2) and decreased the number of spurious OTUs (Table 2). This is in line with previous findings that sequential clustering at two identity thresholds can more accurately predict the number of expected OTUs (Huse *et al.*, 2010). Overall, our optimized sequence-processing pipeline produced *dsrA* and *dsrB* data sets of high quality (98.9% and 99.9% error-free or denoised *dsrA* and *dsrB* sequences respectively) (Fig. 2). The final *dsrA* data set contained a considerably lower total number of reads as compared with the *dsrB* data set, which is possibly due to the on average lower quality of raw *dsrA* reads from this MiSeq run (Fig. S5) and the generally lower quality of unassembled versus assembled read pairs (Masella *et al.*, 2012; Nelson *et al.*, 2014).

Besides optimizing sequence processing for a maximal number of error-free sequences, we also evaluated how well the established *dsrA* and *dsrB* amplicon sequencing approach preserves the expected richness (i.e. number of different mock community sequences) and evenness (i.e. relative abundances of mock community sequences) of the 90-sequence mock community in light of nine different cycle number combinations in the first and second PCR step. Out of 75 expected species-level OTUs, 50 were identified in the entire *dsrA* data set, which additionally contained 11 OTUs that did not match perfectly with any of the mock community sequences (Table 2). The identification rate was higher for the *dsrB* data set; 58 out of 70 expected mock community OTUs species-level OTUs were identified, whereas only 10 OTUs could not be assigned to a mock community sequence (Table 2). Most unidentified mock community OTUs were absent in the output data set because they (i) were removed during stringent sequence processing, (ii) had a very low input abundance of $\leq 0.01\%$ or (iii) contained mismatches in their primer-binding sites (Fig. 3, Table S3). Non-mock community OTUs were observed in the individual data sets at low relative abundances {*dsrA*: median = 0.074% [95% confidence interval (CI): 0.027%, 0.20%], *dsrB*: median = 0.026% [95% CI: 0.009%, 0.06%]}. The number of contaminant OTUs in the pre-clustered *dsrA* data set was correlated to the number of cycles in the first PCR ($R^2 = 0.71$, *P*-value = 0.002) and the number of total PCR cycles ($R^2 = 0.68$, *P*-value = 0.004). No such correlation was observed in the *dsrB* data set. Most contaminating OTUs in the *dsrB* data set were 100% identical to

Table 1. *dsrAB*-targeted primer sets that were modified and newly designed in this study.

Name	Previous name	Gene	Sequence (5′-3′)	Length (nt)	Deg.[a]	Coverage of full-length *dsrAB* (%)[b]	Coverage of core data-set *dsrAB* (%)[c]	Reference
DSR187Fmix	DSR1F	*dsrA*	–		45	–	99.1	–
DSR187F1	–	*dsrA*	ACHCACTGGAAGCACG	16	3	–	27	Modified from Wagner *et al.,* 1998
DSR187F2	–	*dsrA*	ACYCAYTGGAARCATG	16	8	–	12.2	Modified from Zverlov *et al.,* 2005
DSR187F3	DSR1Fa	*dsrA*	ACCCAYTGGAAACACG	16	2	–	11.3	Loy *et al.,* 2004
DSR187F4	–	*dsrA*	ACGCAYTGGAAGCACG	16	2	–	7.8	Modified from Wagner *et al.,* 1998
DSR187F5	–	*dsrA*	GGHCACTGGAAACATG	16	3	–	7.8	Modified from Pester *et al.,* 2010
DSR187F6	–	*dsrA*	ACTYACTGGAAACACG	16	2	–	7	Modified from Loy *et al.,* 2004
DSR187F7	–	*dsrA*	GGGCAYTGGAAACACG	16	2	–	3.5	Modified from Pester *et al.,* 2010
DSR187F8	–	*dsrA*	GGBCACTGGAAGCACG	16	3	–	3.5	Modified from Loy *et al.,* 2004
DSR187F9	–	*dsrA*	GGMCACTGGAAACACG	16	2	–	2.6	Modified from Pester *et al.* 2010
DSR187F10	–	*dsrA*	GCTCACTGGAARCACG	16	2	–	2.6	Modified from Pester *et al.*, 2010
DSR187F11	–	*dsrA*	GTYCACTGGAAACACG	16	2	–	1.7	Modified from Pester *et al.*, 2010
DSR187F12	–	*dsrA*	ACACACTGGAAACATG	16	1	–	1.7	Modified from Zverlov *et al.,* 2005
DSR187F13	–	*dsrA*	GGMCATTGGAAGCATG	16	2	–	1.7	Modified from Pester *et al.,* 2010
DSR187F14	–	*dsrA*	ACATACTGGAAGCAYG	16	2	–	0.9	This study
DSR187F15	–	*dsrA*	GGACACTGGAAGCATG	16	1	–	0.9	Modified from Pester *et al.,* 2010
DSR187F16	–	*dsrA*	ACCTACTGGAAGCATG	16	1	–	0.9	Modified from Zverlov *et al.,* 2005
DSR187F17	–	*dsrA*	GTGCACTGGAAGCACG	16	1	–	0.9	Modified from Pester *et al.,* 2010
DSR187F18	–	*dsrA*	GGTCATTGGAAACACG	16	1	–	0.9	Modified from Pester *et al.,* 2010
DSR187F19	–	*dsrA*	GGTTACTGGAAACACG	16	1	–	0.9	Modified from Pester *et al.,* 2010
DSR187F20	DSR1Fh	*dsrA*	GGCTATTGGAAGCACG	16	1	–	0.9	Pester *et al.,* 2010
DSR187F21	DSR1Ff	*dsrA*	AGCCACTGGAAACACG	16	1	–	0.9	Pester *et al.,* 2010
DSR187F22	–	*dsrA*	ACGCACTGGAAACACG	16	1	–	0.9	Modified from Wagner *et al.,* 1998
DSR187F23	–	*dsrA*	TACCACTGGAAACACG	16	1	–	0.9	Modified from Wagner *et al.,* 1998
DSR190Fmix	–	*dsrA*	–		27	–	100	–
DSR190F1	–	*dsrA*	CACTGGAARCAYGGYG	16	8	–	78.3	This study
DSR190F4	–	*dsrA*	CATTGGAAACAYGGYG	16	4	–	7.8	This study
DSR190F5	–	*dsrA*	YACTGGAAGCATGGAG	16	2	–	4.3	This study
DSR190F3	–	*dsrA*	CATTGGAAGCATGGWG	16	2	–	2.6	This study
DSR190F2	–	*dsrA*	CACTGGAAGCACGGAG	16	1	–	1.7	This study
DSR190F6	–	*dsrA*	CATTGGAAGCAYGGCG	16	2	–	1.7	This study
DSR190F7	–	*dsrA*	TACTGGAAACACGGCG	16	1	–	1.7	This study
DSR190F8	–	*dsrA*	TACTGGAAGCAYGGTG	16	2	–	0.9	This study
DSR190F10	–	*dsrA*	TATTGGAAGCACGGTG	16	1	–	0.9	This study
DSR190F11	–	*dsrA*	CAGTGGGGATTCGGTG	16	1	–	0[d]	This study
DSR916Rmix	–	*dsrA*	–		368	97.6	97	–
DSR916R1	–	*dsrA*	NNATRCARTGCATRCA	16	128	90.5	93	This study
DSR916R2	–	*dsrA*	NNAGACAGTRCATGCA	16	32	2.3	0.9	This study
DSR916R3	–	*dsrA*	NNAGGCAGYGCATGCA	16	32	1.3	0	This study
DSR916R4	–	*dsrA*	NNATRCAGTTCATGCA	16	16	1	1.7	This study
DSR916R5	–	*dsrA*	NNATGCAGTGKATGCA	16	16	0.8	0.9	This study
DSR916R6	–	*dsrA*	NNAGGCAATGCATGCA	16	32	0.6	0	This study
DSR916R7	–	*dsrA*	NNAGACAATGCATGCA	16	32	0.5	0.9	This study
DSR916R8	–	*dsrA*	NNATGCAGTGSGTGCA	16	32	0.3	0	This study
DSR916R9	–	*dsrA*	NNATRTAGTGCATGCA	16	32	0.2	0	This study
DSR916R10	–	*dsrA*	NNAGACATCTCATACA	16	16	0.1	0	This study
DSR1762Fmix	DSR1728Fmix	*dsrB*	–		98	97	99.1	–
DSR1762F1	DSR1728FmixA	*dsrB*	CAYACCCAGGGNTGG	15	8	64.1	43.5	Steger *et al.,* 2011
DSR1762F4	DSR1728FmixD	*dsrB*	CACACDCAGGGNTGG	15	12	10.1	12.2	Steger *et al.,* 2011
DSR1762F2	DSR1728FmixB	*dsrB*	CAYACBCAAGGNTGG	15	24	7	16.5	Steger *et al.,* 2011
DSR1762F3	DSR1728FmixC	*dsrB*	CATACDCAGGGHTGG	15	9	5.5	14.8	Steger *et al.,* 2011
DSR1762F5	DSR1728FmixE	*dsrB*	CATACHCAGGGNTAY	15	24	3.7	3.5	Steger *et al.,* 2011
DSR1762F6	–	*dsrB*	CACACSCAGGGKTAY	15	8	3	3.5	This study
DSR1762F7	–	*dsrB*	CACACBCAGGGMTAC	15	6	1.8	0.9	This study
DSR1762F8	–	*dsrB*	CACACHCAGGGCTAT	15	3	0.9	0.9	This study
DSR1762F9	–	*dsrB*	CACACCCAGGGWTTC	15	2	0.5	0.9	This study
DSR1762F10	–	*dsrB*	CAYACACAAGGATGG	15	2	0.5	2.6	This study
DSR2107Rmix	dsrB 4RSl1a–f	*dsrB*	–		29	–	100	–
DSR2107R1	–	*dsrB*	CAGTTDCCRCARTACAT	17	12	–	50.4	Modified from Lever *et al.,* 2013
DSR2107R2	–	*dsrB*	CAGTTACCRCAGAACAT	17	2	–	24.3	Modified from Lever *et al.,* 2013
DSR2107R3	–	*dsrB*	CAGTTGSCGCAGAACAT	17	2	–	17.4	Modified from Lever *et al.,* 2013
DSR2107R4	–	*dsrB*	CAGTTYCCGCAGAACAT	17	2	–	1.7	This study
DSR2107R5	–	*dsrB*	CAGTTKCCACAGAACAT	17	2	–	0 [d]	Modified from Lever *et al.,* 2013
DSR2107R6	–	*dsrB*	CAATTWCCACAGAACAT	17	2	–	0 [d]	This study

© 2015 Society for Applied Microbiology and John Wiley & Sons Ltd,

Table 1. *cont.*

Name	Previous name	Gene	Sequence (5′-3′)	Length (nt)	Deg.[a]	Coverage of full-length *dsrAB* (%)[b]	Coverage of core data-set *dsrAB* (%)[c]	Reference
DSR2107R7	–	*dsrB*	CAGTTGCCGCAAAACAT	17	1	–	0.9	This study
DSR2107R8	–	*dsrB*	CAGGCACCGCAGAACAT	17	1	–	0.9	This study
DSR2107R9	–	*dsrB*	CAGTTAGCGCACATCAT	17	1	–	0.9	This study
DSR2107R10	–	*dsrB*	CAATTGGCACAGTACAT	17	1	–	0.9	This study
DSR2107R11	–	*dsrB*	CAATTTCCGCAGTACAT	17	1	–	0.9	This study
DSR2107R12	–	*dsrB*	CAATTGCCGCAGAACAT	17	1	–	0.9	This study
DSR2107R13	–	*dsrB*	CAGTTGGCACAATACAT	17	1	–	0.9	This study
DSR2113Rmix	DSR4R	*dsrB*	–		37	–	100	–
DSR2113R1	–	*dsrB*	GTGTARCAGTTNCCGCA	17	8	–	59.1	Modified from Wagner *et al.,* 1998
DSR2113R2	–	*dsrB*	GTRTARCAGTTACCACA	17	4	–	18.3	Modified from Zverlov *et al.,* 2005
DSR2113R3	–	*dsrB*	GTATARCAGTTDCCGCA	17	6	–	10.4	Modified from Wagner *et al.,* 1998
DSR2113R4	–	*dsrB*	GTGAAGCAGTTKCCGCA	17	2	–	2.6	Modified from Pester *et al.,* 2010
DSR2113R5	–	*dsrB*	GTRTAGCAATTGCCGCA	17	2	–	0.9	Modified from Pester *et al.,* 2010
DSR2113R6	–	*dsrB*	GTGTAACARTTTCCACA	17	2	–	0.9	Modified from Loy *et al.,* 2004
DSR2113R7	–	*dsrB*	GTGTAGCAGTTKCCACA	17	2	–	0.9	Modified from Loy *et al.,* 2004
DSR2113R8	–	*dsrB*	GTGTAGCAGGCACCGCA	17	1	–	0.9	This study
DSR2113R9	–	*dsrB*	GAATAGCAGTTACCGCA	17	1	–	0 [d]	This study
DSR2113R10	–	*dsrB*	GTGAAACAATTTCCGCA	17	1	–	0.9	Modified from Pester *et al.,* 2010
DSR2113R11	–	*dsrB*	GAGAAGCAGTTGGCGCA	17	1	–	0 [d]	Modified from Pester *et al.,* 2010
DSR2113R12	–	*dsrB*	GAGAAACAGTTACCGCA	17	1	–	0.9	Modified from Pester *et al.,* 2010
DSR2113R13	–	*dsrB*	GTATAGCAGTTTCCACA	17	1	–	0.9	Modified from Loy *et al.,* 2004
DSR2113R14	–	*dsrB*	GAAAAGCAGTTACCACA	17	1	–	0.9	Modified from Zverlov *et al.,* 2005
DSR2113R15	–	*dsrB*	GTGTAGCAATTACCACA	17	1	–	0 [d]	Modified from Zverlov *et al.,* 2005
DSR2113R16	–	*dsrB*	GTAAAGCAATTGGCACA	17	1	–	0.9	This study
DSR2113R17	–	*dsrB*	GTAAAACAGTTGGCACA	17	1	–	0.9	This study
DSR2113R18	–	*dsrB*	ACGGTACAGTTAGCGCA	17	1	–	0.9	This study

a. Degeneracy is given as the number of oligonucleotides that comprise the primer.
b. Data indicate perfect-match primer coverage of all full length reductive bacterial type ($n = 115$) *dsrAB* sequences from genomes and metagenomes (Müller *et al*., 2015).
c. Data indicate perfect-match primer coverage of all reductive bacterial type ($n = 1110$) *dsrAB* sequences of the core dataset (Müller *et al*., 2015).
d. Primer with a coverage of 0% were designed based on sequences in a preliminary version of the reference database and were not included in the final version.

sequences from the environmental samples that were sequenced in the same MiSeq run (Fig. S6). Such minor levels of cross-contamination of samples are common and thus difficult to avoid during amplicon sequencing of unknown samples (Esling *et al*., 2015; Herbold *et al*., 2015) unless complex barcoding strategies are used (Seitz *et al*., 2015). OTUs with a very low abundance in a data set should thus always be interpreted cautiously (Reeder and Knight, 2009).

Despite the use of highly degenerate primer mixtures, the initial structure of mock communities was generally recovered in the processed amplicon data sets (Fig. 3, Fig. S7). A comparison of the regressions of observed : expected relative abundances across PCR cycle conditions showed that the coefficients were significantly decreasing with increasing number of total cycles in the first and second PCR step (*dsrA*: $R^2 = 0.59$, P-value = 0.009; *dsrB*: $R^2 = 0.77$, P-value = 0.001) (Fig. S8). This was mostly due to the number of PCR cycles in the first step (*dsrA*: $R^2 = 0.49$, P-value = 0.021; *dsrB*: $R^2 = 0.61$, P-value = 0.008), whereas the number of PCR cycles in the second step had no significant influence on observed : expected relative abundances correlations (*dsrA*: $R^2 = 0.04$, P-value > 0.1; *dsrB*: $R^2 = 0.05$, P-value > 0.1). This suggests that initial amplification with degenerate *dsrA* and *dsrB* primers is significantly more prone to quantitative PCR biases than the subsequent barcoding PCR with the non-degenerate head primer (Polz and Cavanaugh, 1998). The number of total PCR cycles, particularly in the first-step PCR, should thus be kept as low as possible (Suzuki and Giovannoni, 1996; Acinas *et al*., 2005; Wu *et al*., 2015). For both genes, we obtained the highest correlation of observed : expected relative abundances with 15:15 and 10:20 cycles in the first and second PCR steps (Fig. S7). Overall, our results show that the *dsrA*/*dsrB* amplicon sequencing approach is a suitable method for comparative SRM community analysis. It is also preferred over 16S rRNA gene amplicon sequencing because *dsrAB* typically occur only once (Müller *et al*., 2015), whereas 16S rRNA genes occur in variable copy numbers (1–11) in genomes of known SRM (Pester *et al*., 2012a,b). The use of *dsrAB* as

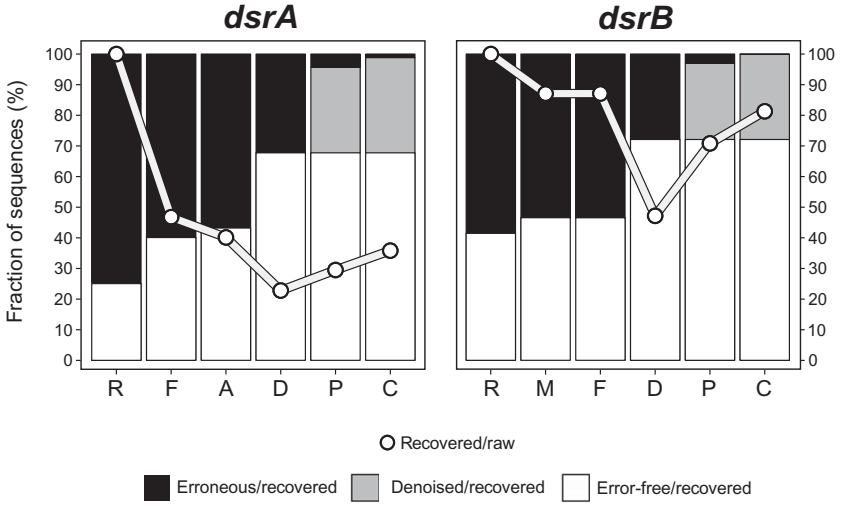

Fig. 2. The optimized sequence-processing pipeline for *dsrA* and *dsrB* reads produces high-quality data sets. Data are shown from the combined 90-sequence mock community sequence data sets. The white circles indicate the fractions of raw input sequences that are recovered after each step. The fraction of error-free sequences (white bars) was determined by dividing the number of recovered sequences that are 100% identical to any reference sequence from a mock community sequence to the total number of recovered sequences. The fractions of erroneous sequences are indicated as black bars. The fractions of slightly erroneous sequences that are assigned into mock community OTUs (denoised sequences) are indicated as grey bars. The sequential sequence-processing steps are shown on the x-axis: R, raw reads. F, quality and length filtering. A, assembly of non-overlapping paired-end reads into scaffolds (only for *dsrA*). M, merging of overlapping paired-end reads into contigs (only for *dsrB*). D, de-replication excluding singletons. P, pre-clustering at 99% sequence identity. C, clustering into species-level OTUs.

diagnostic markers thus allows a more realistic assessment of the abundance distribution of SRM community members.

Combining Ribosomal Database Project's (RDP's) Naïve Bayesian classifier and Evolutionary Placement Algorithm (EPA) for accurate taxonomic classification of dsrA *and* dsrB *sequences*

We tested the accuracy of the Naïve Bayesian classifier of RDP (Wang *et al*., 2007) and the EPA of RAxML (Berger *et al*., 2011) for assigning *dsrA* or *dsrB* sequences of varying sequence novelty to the different taxonomic categories of the reference *dsrAB* database (Müller *et al*., 2015). The classification accuracy at the approximate family level and at higher taxonomic levels was consistently higher for the EPA than for the Naïve Bayesian classifier. EPA accurately classified more than 90% of the mock community sequences at the family level, even when sequences in the reference tree shared < 80% identity to the query sequences (Fig. 4). The Naïve Bayesian classifier only outperformed the EPA when the query sequences were 100% identical to the sequences in the reference database/tree; 85% and 50% of the query sequences were correctly classified at the 'strain/clone' category by the Naïve Bayesian classifier and the EPA

Table 2. Recovery of mock community OTUs using the optimized sequence-processing pipeline.

	dsrA			*dsrB*		
	De-replicated	Pre-clustered	Clustered	De-replicated	Pre-clustered	Clustered
Expected OTUs	90	87	75	90	88	70
Total OTUs	1727	91	62	4330	91	68
MC-OTUs	61	56	51	76	74	58
Non MC-OTUs	1666	35	11	4254	17	10
Non MC-OTUs ≥ 90% identical to MC-OTUs	1494	27	3	4119	7	0
Non MC-OTUs ≥ 98% identical to MC-OTUs	1349	22	1	3837	4	0
Relative abundance of all non MC-OTU sequences	32.3%	4.3%	1.1%	27.9%	3.0%	0.1%

Absolute numbers of OTUs are shown after de-replication excluding singletons, pre-clustering at 99% nucleotide identity including *de novo* chimera detection, and after clustering at species-level. The combined 90-sequence mock community sequence data set of all nine different PCR cycle variations was used. The expected number of OTUs and the number of OTUs that are 100% identical to a reference sequence of a mock community sequence (MC-OTUs) are indicated. The number of expected OTUs was determined by clustering all mock community reference sequences at the given identity threshold.

© 2015 Society for Applied Microbiology and John Wiley & Sons Ltd,

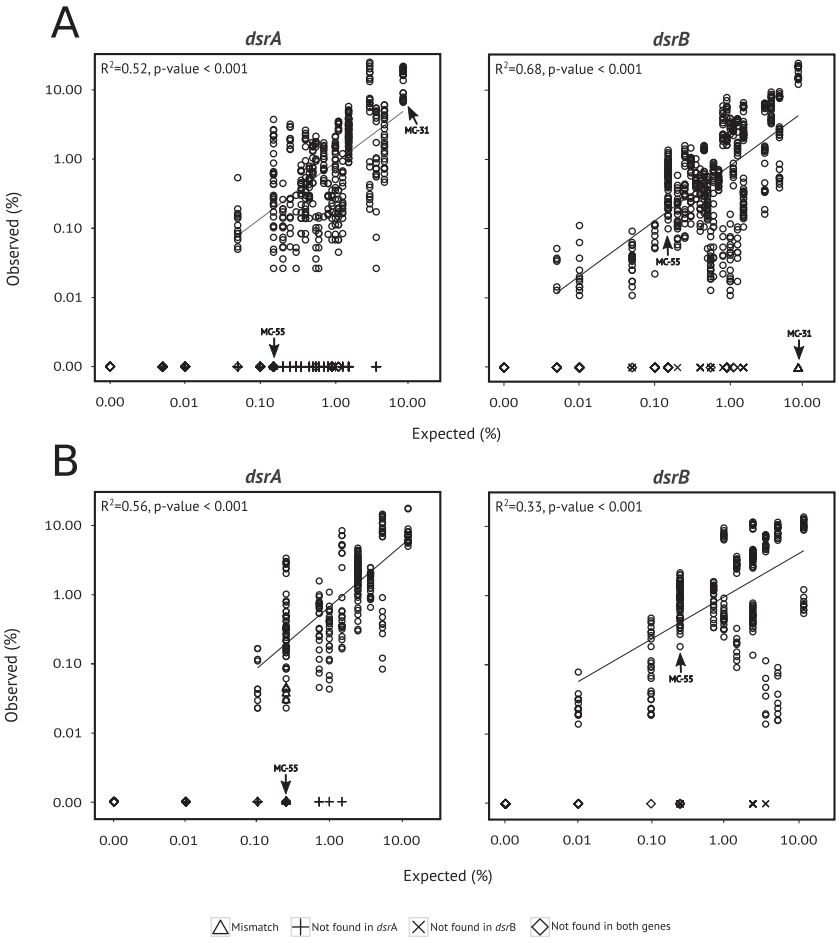

Fig. 3. Linear regression of expected versus observed relative abundance of mock community sequences. Data are shown from the 90-sequence (A) and 45-sequence (B) mock community sequence data sets after pre-clustering at 99% nucleotide identity. Only OTUs with 100% identity to any mock community reference sequence and that were observed in at least one data set were included in the linear model. Unambiguously identified mock community sequences and their respective relative abundances are shown as circles. Nine data points, which were derived from the nine different PCR cycle variations data sets, are shown for each mock community sequence. Triangles indicate mock community (MC) sequences MC-31 and MC-55 that were not amplified due to a primer mismatch. MC-31 had an expected relative abundance of ~8% and is only observed in the *dsrA* data set due to a mismatch in the *dsrB* primer-binding site of DSR1762Fmix. MC-55 had an expected relative abundance of ~0.15% and is only observed in the *dsrB* data set due to a mismatch in the *dsrA* primer-binding site of DSR190Fmix. Mock community sequences that were only found in the *dsrB* data set are indicated with straight crosses and mock community sequences that were only found in the *dsrA* data set are indicated with diagonal crosses. Diamonds indicate mock community sequences that were not found in any of the two data sets.

respectively (Fig. 4). Based on these observations, we suggest combining these two approaches for improved classification of environmental *dsrA* and *dsrB* sequences. The EPA has superior classification accuracy at the 'family' level and higher taxonomic levels, whereas the Naïve Bayesian classifier is best used for assignment into the 'strain/clone' category. However, classification at the 'strain/clone' level has only a high accuracy if 100% identical sequences are present in the reference database and should thus be interpreted with caution when applied to environmental *dsrA* and *dsrB* data (Fig. 4).

Diversity of dsrA *and* dsrB *in selected environmental samples*

To demonstrate its use for environmental *dsrAB* diversity surveys, the established *dsrA* and *dsrB* amplicon sequencing approach was applied to samples from three environments with well-studied SRM and *dsrAB*-containing communities, respectively, i.e. two Arctic surface sediments (from Greenland and Svalbard) (Canion *et al*., 2014) and a peat soil (from the Schlöppnerbrunnen II peatland in Germany) (Loy *et al*., 2004; Pester *et al*., 2012a,b). Analogous to the mock communities, DNA from all samples was amplified by using various combinations of cycle numbers in the first and second PCR steps (Table S2). As observed for the mock communities, the number of high-quality sequences that passed the stringent sequence processing was lower in the *dsrA* than in the *dsrB* data set (Table S2). Besides this difference in sensitivity, comparative diversity analyses and taxonomic classification showed generally similar results for both data sets. Although PCR cycle variations had some impact on the recovered sequence diversity, differences in diversity within a sample were always smaller than between samples, as shown for various alpha- and beta-diversity metrics (Fig. 5, Fig. S9, Table S2). Consistent with previous findings regarding *dsrAB* diversity in the Schlöppnerbrunnen II peatland, members of the *Syntrophobacteraceae* and the uncultured family-level lineage 8 represented abundant *dsrAB*-containing microorganisms in the peat soil (Fig. 5). Because members of uncultured family-level lineages are known to dominate in this peat (Pester *et al*., 2010; Steger *et al*., 2011), the unexpected overrepresentation of *Syntrophobacteraceae* in the *dsrA* but not in the *dsrB* data

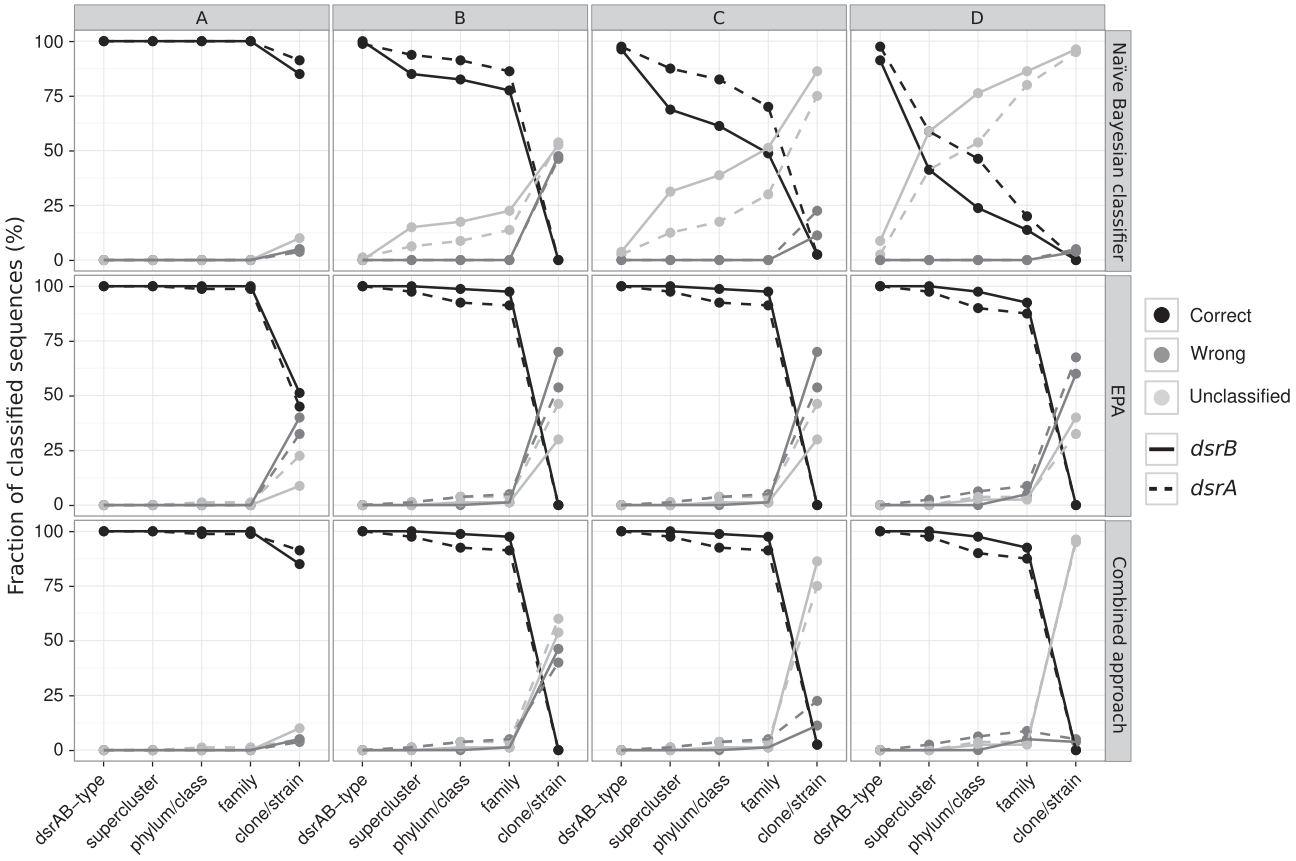

Fig. 4. The combining of results from the Evolutionary Placement Algorithm (EPA) with RDP's Naïve Bayesian classifier performs best for classifying *dsrA* and *dsrB* reads of varying dissimilarity to sequences in the reference database. Performance of RDP's Naïve Bayesian classifier, the EPA and a combination of both methods was tested by using the original mock community sequences. Sequences were classified into the five taxonomic levels of the original reference database (A), and modified versions of the reference database that did not contain any mock community sequence (B), or contained only sequences with less than 90% (C) or 80% (D) sequence identity to any mock community sequence. For the combined approach, classification results for the '*dsrAB* type' category to the 'family' category were inferred using EPA. The classification at the 'clone/strain' category was subsequently inferred by using the Naïve Bayesian classifier results, but only for sequences that showed matching results at the 'family' category by both methods.

set is possibly due to a primer bias during *dsrA* amplification. In contrast to the peat soil, most *dsrA*/*dsrB* sequences from Svalbard and Greenland sediments were affiliated with the *Desulfobacteraceae*, *Desulfobulbaceae* and *Syntrophobacteraceae*, which corroborate the known dominance of deltaproteobacterial SRM in Arctic and other coastal marine surface sediments (Ravenschlag *et al*., 2000; Park *et al*., 2011; Canion *et al*., 2014). The sediment samples additionally contained a sizable fraction of *dsrA/dsrB* sequences belonging to the environmental supercluster 1, which is solely composed of sequences from uncultured microorganisms and includes family-level lineage 9 that harbours many sequences from the marine environment (Müller *et al*., 2015). Taken together, although some level of biased amplification is unavoidable in an end-point PCR approach and by using degenerate primers, our results nevertheless demonstrate that the multiplex *dsrA* and *dsrB* amplicon sequencing approach is suitable for monitoring relative abundance changes/differences in *dsrAB* diversity and can now be applied to a large number of samples. The absolute abundances of selected groups of *dsrAB*-containing microorganisms, such as species-level OTUs, can subsequently be analysed by real-time PCR with specific primers that contain no or only very few degenerate nucleotides, as shown previously (Steger *et al*., 2011).

Conclusions

High-throughput DNA sequencing of small-subunit rRNA gene and cDNA amplicons enables extensive alpha- and beta-diversity analyses of microbial communities across many samples. Surprisingly, multiplex amplicon sequencing is still rarely applied to functional marker genes that are indicative of specific metabolic features and thus provide insights into the potential ecophysiology of microorganisms. By using *dsrAB*, encoding dissimilatory sulfite reductase, as targets genes and complex *dsrAB* mock

© 2015 Society for Applied Microbiology and John Wiley & Sons Ltd,

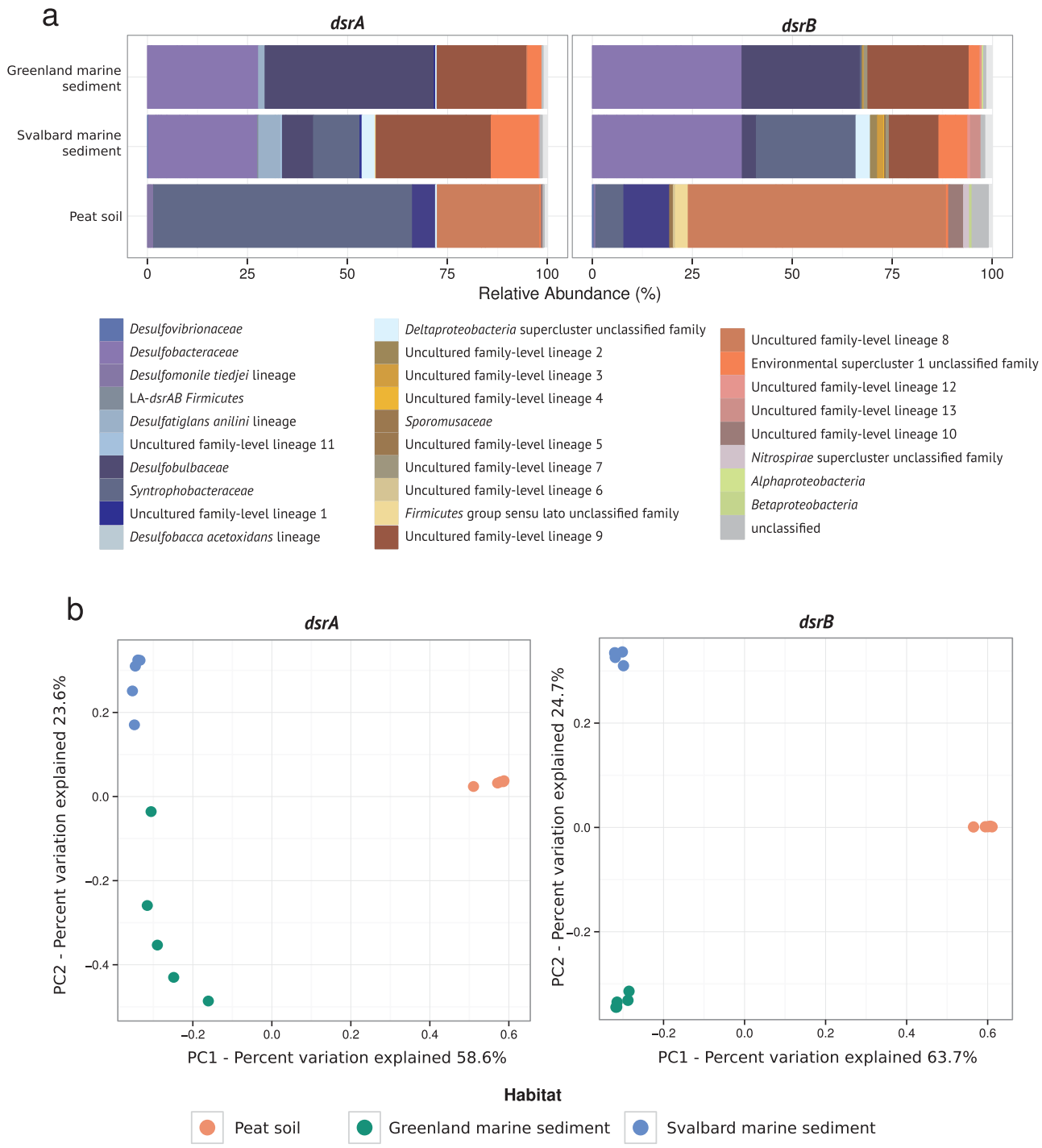

Fig. 5. Diversity of *dsrA* and *dsrB* sequences in selected environmental samples. The *dsrA* and *dsrB* amplicon sequencing approach was applied to Arctic marine sediments from Greenland and Svalbard and to a peat soil using different cycle number combinations (Table S2).
A. Relative abundances of families/uncultured family-level lineages in the combined data sets. Classification of representative OTU sequences was performed with the Evolutionary Placement Algorithm. Only families/uncultured family-level lineages with a total relative abundance of ≥ 1% in at least one sample are shown.
B. Principal coordinates analysis based on Bray–Curtis dissimilarity. Replicate dots for each habitat represent the individual cycle number combinations.

communities of defined diversity for testing, we combined available bioinformatics tools for processing and identification of short rRNA reads (Caporaso *et al*., 2010; Edgar, 2010; Berger *et al*., 2011) into a dedicated bioinformatics pipeline for analysis of functional gene reads. The development of new high-coverage primers sets for reductive bacterial-type *dsrAB* and use of a comprehensive, multilevel *dsrAB* reference taxonomy (Müller *et al*., 2015) for classification were essential for the performance of our functional gene amplicon sequencing approach, which now makes encompassing comparative surveys of sulfate/sulfite reducer diversity in the environment possible. Parallel sequencing of differently sized *dsrA* and *dsrB* amplicons from mock communities and environmental samples yielded comparable results. However, less high-quality sequences and species-level OTUs were obtained from data sets of non-overlapping paired-end *dsrA* sequences. For improved sensitivity (i.e. recovery of high-quality sequences and true-positive OTUs), it is thus recommended to select the size of the sequenced amplicon to generate overlapping paired-end sequences by a given NGS technology. The entire analytical workflow outlined in this study, from generation of barcoded amplicons for multiplex sequencing to processing and taxonomic classification of amplicon reads, is also applicable for oxidative-type *dsrAB* from sulfur oxidizers (Loy *et al*., 2009; Müller *et al*., 2015) and represents a reference for analysis of short sequence data derived from other functional genes.

Experimental procedures

DsrAB reference database and taxonomy

The core sequences ($n = 1292$, covering an ~1.9 kb *dsrAB* region) and the corresponding consensus tree of a recently published database of curated, aligned and phylogenetically classified *dsrAB*/DsrAB sequences (Müller *et al*., 2015) were used for primer design, evaluation of sequence processing and classification of unknown *dsrA* and *dsrB* sequences.

Evaluation and design of dsrAB-*targeted primers*

Forward primer sets DSR1Fmix and DSR1728Fmix and reverse primer sets DSR4Rmix and dsrB 4RSI1mix a-f (each set consisting of multiple individual primers with the same binding position) are commonly used for the amplification of ~1.9 kb *dsrAB* and ~0.35 kb *dsrB* fragments (Pester *et al*., 2010; Steger *et al*., 2011; Lever *et al*., 2013; Müller *et al*., 2015). We modified these primer sets to maximize coverage and minimize degeneracies and renamed them DSR187Fmix, DSR1762Fmix, DSR2113Rmix and DSR2107Rmix (Fig. 1, Table 1). Based on the amino acid conservation profile of reductive bacterial-type DsrAB (Müller *et al*., 2015), we designed two new primer sets DSR190Fmix and DSR916Rmix for PCR amplification of a ~0.75 kb *dsrA* fragment. Primers were (re)named according to their target position relative to the *Desulfovibrio vulgaris* Hildenborough DSM 644 *dsrAB* sequence (NC_002937, genome position 449888-452365). The coverages of primers DSR187Fmix, DSR190Fmix, DSR2107Rmix and DSR2113Rmix, and primer pairs that use at least one such primer, were determined with the ARB PROBE MATCH tool (Ludwig *et al*., 2004) based on 115 reductive bacterial-type *dsrAB* sequences from genomes and metagenomes (Müller *et al*., 2015). Coverages of primers DSR916Rmix and DSR1762Fmix were additionally determined based on 1110 reductive bacterial-type *dsrAB* sequences of the reference database.

Mock communities

Two diverse mock communities were constructed from 90 selected environmental clones, each carrying a ~1.9 kb-large *dsrAB* insert from an uncultured microorganism. The insert sequences have been determined previously by Sanger sequencing (Pester *et al*., 2010; Steger *et al*., 2011) (Fig. S1). Inserts from these clones were individually amplified using vector-targeted M13 primers. Amplicons of individual inserts were purified with Agencourt AMPure beads (Beckman Coulter Genomics), quantified with the PicoGreen dsDNA assay (Life Technologies) and mixed in defined ratios as shown in Fig. S1. The two mock communities consisted of 45 and 90 different *dsrAB* sequences with individual relative abundances of 0.001% to 12.5% and 0.001% to 8% respectively (Fig. S1). The 45-sequence and the 90-sequence mock communities had a total concentration of 3.5×10^9 and 4.7×10^9 *dsrAB* copies μl^{-1} respectively.

Environmental samples and DNA extraction

Environmental samples constituted a peat soil (Schlöppnerbrunnen II, Fichtelgebirge mountains, Germany, 50°07′55″N 11°52′52″E, September 2010) and Arctic marine surface sediments from Svalbard (Smeerenburgfjorden station J, water depth 214 m, 79°43′81″N, 11°05′19″E, July 2005) and Greenland (station 3 located outside of the Godthåbsfjord on the continental shelf in the Labrador Sea, water depth 498 m, 64°26′45″N, 52°47′39″E, August 2013) (Glombitza *et al*., 2015). Phenol-chloroform-based methods were used to extract DNA from peat soil and Greenland marine sediment according to protocols by Leininger and colleagues (Leininger *et al*., 2006) and Dumont and colleagues (Dumont *et al*., 2006) respectively. The PowerSoil DNA isolation kit (MO BIO Laboratories) was used to extract DNA from Svalbard Arctic sediment (Müller *et al*., 2014).

Barcoding and multiplex sequencing of PCR amplicons

Barcoded amplicons from mock communities and environmental DNA were prepared by using a two-step PCR approach (Herbold *et al*., 2015). In the first PCR, approximately 750 bp *dsrA* and 350 bp *dsrB* fragments were amplified using DSR190Fmix/DSR916Rmix and DSR1762Fmix/DSR2107Rmix primers, respectively, each primer with a 16 nt head sequence (5′-GCTATGCGCGAGCTGC-3′) at the 5′ end (Fig. 1, Table 1). In the second PCR, the first-step PCR product was used as a template for amplification with a

primer that consisted of the 16 nt head sequence and a unique, sample-specific 8 nt barcode at the 5′ end (5′-BARCODE-GCTATGCGCGAGCTGC-3′) (Fig. S3, Table S1). Each PCR reaction (20 μl in first step, 50 μl in second step) contained 1× DreamTaq buffer (Thermo Scientific), 0.2 mM dNTP mix (Thermo Scientific), 1 U DreamTaq (Thermo Scientific), 0.2 mg ml^{-1} bovine serum albumin (Thermo Scientific) and 1 μM of each forward and reverse primer mix and 1 μl of template. Thermal cycling during the first-step PCR was performed in 'touch down' mode: initial denaturation at 95°C for 3 min; 10–35 cycles of 30 s denaturation at 95°C, 30 s annealing at 60–50°C (temperature decreased by 1°C per cycle during the first 10 cycles) and elongation for 1 min at 72°C; final elongation at 72°C for 10 min. The first PCR reaction was performed in triplicate, screened by gel electrophoresis and pooled for use as a template in the second step. Thermal cycling during the second-step PCR was performed with a constant annealing temperature of 52°C and consisted of 5–20 cycles. In total, up to nine different cycle combinations of first- and second-step PCR (10:20, 15:15, 20:10, 25:5, 25:10, 30:10, 30:5, 35:10 and 35:10) were used for amplification of *dsrA* and *dsrB*. The barcoded amplicons were purified with Agencourt AMPure beads (Beckman Coulter Genomics) and quantified using a fluorescence dye assay (PicoGreen dsDNA Assay, Invitrogen). The individual barcoded amplicons were mixed in equimolar concentrations, with *dsrA* amplicons being added in double amounts. The barcoded amplicons from this study were part of a larger amplicon pool that was sequenced on an ILLUMINA MISEQ system by Microsynth AG (Balgach, Switzerland) as described previously (Herbold *et al.*, 2015). The MISEQ run was performed in the 2 × 300 cycle combination, which produces i.e. 2 × 300 nt paired-end reads. Sequence data sets are available in the NCBI Sequence Read Archive under study accession number SRP066402.

Sequence data processing and analysis

Sequence processing was based on recommendations of the UPARSE pipeline (Edgar, 2013) but was optimized for *dsrA* and *dsrB* paired-end MISEQ reads obtained in this study (Fig. S3) and additionally included tools from the programs QIIME 1.9.0 (Caporaso *et al.*, 2010), SINA V.1.2.9 (Pruesse *et al.*, 2012), BLAST (Altschul *et al.*, 1990) and USEARCH V.7.1090 (Edgar, 2010).

To be assigned to a sample, paired-end MISEQ reads were required to match the correct barcode and primer in at least one read and the corresponding primer in the second read (Herbold *et al.*, 2015). One mismatch was allowed in each barcode and primer sequence examined. Read pairs were then exported into individual files that were data set-specific (i.e. one data set per gene and sample). Primer and barcode fastq files were also generated at this step, using corrected barcodes and primers, to facilitate incorporation of the data sets into QIIME. Fastq reads within each data set were assigned to amplicon libraries using split_libraries_fastq.py in QIIME. Paired-end reads were then collapsed into a single continuous sequence by two different strategies because differences in *dsrA* and *dsrB* amplicon length resulted in non-overlapping and overlapping paired-end reads respectively.

For non-overlapping *dsrA* reads, the best combination of Q-score (i.e. 10 or 15) and trimmed read length (i.e. flexible length threshold based on Q-score or fixed at 75% of the minimum read length) to recover a maximal number of correct read pairs was determined by iterative testing with the 90-sequence mock community (see below). A Q-score of 15 was finally selected for de-multiplexing and trimming of *dsrA* reads. Subsequently, all *dsrA* reads were further trimmed to the same length with the -fastq_filter option in USEARCH at the first 3′ position with an average per base Q-score below 30 across the raw *dsrA* data set, i.e. the *dsrA* data sets of this study were trimmed at 53% of the minimum read length of 260 nt. Furthermore, sequences with a maximum expected error greater than 1 and shorter than 53% of the minimum read length was removed, which resulted in trimmed *dsrA* reads of 138 nt length [Note: Although all *dsrA* data in the paper are based on the aforementioned parameters, we found that using a Q-score of 10 or 15 in combination with trimming at 75% of the minimum read length and omitting the maximum expected error filtering step also yielded a comparable amount of high-quality sequences in the final *dsrA* data set (Fig. 2), but slightly less OTUs that perfectly matched the mock community sequences (Table 2) (i.e. Q-score 10: 29 000 quality-filtered sequences, with 99.9% in 45 perfect-match mock community OTUs; Q-score 15: 18 623 quality-filtered sequences, with 99.9% in 44 perfect-match mock community OTUs)]. Subsequently, non-*dsrA* sequences in the *dsrA* data were identified with tblastx against the reference database and removed if the bit-score was below 40. Before assembly of paired-end reads, forward and reverse *dsrA* reads were aligned with the SINA aligner against the *dsrAB* reference database using default settings. Forward and reverse *dsrA* read alignments were manually checked and truncated in the correct reading frame at the alignment position of the shortest read. Each read pair was assembled into a scaffold using an artificial separation of six 'N' characters between the forward read and the reverse-complement of the reverse read. This resulted in scaffolds of *dsrA* sequences of 220–260 nt length, which were unaligned before de-replication.

Overlapping *dsrB* paired-end reads were end-trimmed and assembled into contigs with join_paired_ends.py in QIIME with the default joining method (fastq-join). A range of Q-scores (0, 3, 10, 15, 20, 25, 30, 35, 36, 37, 38) was tested for end-trimming *dsrB* data sets. A Q-score of 15 resulted in the highest number of correct contigs, as evaluated with the 90-sequence mock community (see below). All *dsrB* contigs with a length < 75% of the approximate amplicon length or a maximum expected error greater than 1 were discarded by using the -fastq_filter option in USEARCH. Subsequently, non-*dsrB* sequences in the *dsrB* data were identified with tblastx against the reference database and removed if the bit-score was below 50. The length of the obtained *dsrB* contigs covered the entire *dsrB* amplicon and ranged from 310–350 nt.

Pre-processed *dsrA* scaffolds and *dsrB* contigs were de-replicated with simultaneous removal of singletons that occurred only in one sample of a data set with -derep_fulllength and the -sizeout option in USEARCH and then pre-clustered with -cluster_otus (-leftjust -rightjust -maxrejects 0 -maxaccepts 0) at 99% sequence identity with inherent *de novo* chimera detection. Pre-clustered

sequences were clustered into approximate species-level OTUs with gene-specific OTU thresholds (92% and 90% for *dsrA* and *dsrB* respectively) and without *de novo* chimera detection with -cluster_smallmem (-leftjust -rightjust -maxrejects 0 -maxaccepts 0 -id *dsrA*: 0.92 *dsrB*: 0.90) in USEARCH.

OTU abundances were determined by mapping all pre-processed *dsrA* scaffolds or *dsrB* contigs to the OTUs using -usearch_global (-leftjust -rightjust -maxrejects 0 -maxaccepts 0 -maxhits 1) with the gene-specific OTU thresholds mentioned above. The output file was converted into an OTU table with uc2otutab.py.

For alpha- and beta-diversity analyses, the OTU tables were imported into the R software environment (R Core Team, 2015) and processed within the package phyloseq (McMurdie and Holmes, 2013). The beta-diversity plot based on principal coordinate analysis of Bray–Curtis dissimilarities. The data sets were subsampled (1000 bootstraps) at the depth of the smallest library for each gene target. Rarefied OTU tables were then used to calculate alpha-diversity indices (observed OTUs, Chao1, Shannon diversity, Good's Coverage, rarefaction curves).

Mock community-based evaluation of the sequence-processing pipeline

The number of 100% correct sequences after each step of the sequence-processing pipeline (Fig. 2) was determined by using the -usearch_global option in USEARCH and the 90-sequence mock community input sequences as a reference database. For evaluation of raw data, paired-end reads were modified as follows: 90 nt fragments were truncated from the 5′ end of the read pairs and these were joined so that the resulting sequences had the structure 5′-90 nt forward read-NNNNNN-90 nt reverse read (reverse-complement)-3′. The reference sequences from the mock community were treated analogously for comparison. For evaluation of subsequent steps in the pipeline, *dsrA* scaffolds and *dsrB* contigs were directly compared with the mock community sequence database.

The conservation of the predicted mock community structure after sequence processing was evaluated by linear regression of the log-transformed expected to observe relative abundances of mock community sequences in the R software environment using the function lm(). Mock community sequences that were not observed in the respective data set were excluded from the analysis.

Taxonomic and phylogenetic classification of dsrA and dsrB sequences

The classification of the reference database was used for taxonomic assignment of novel sequences. The five phylogenetic levels of the reference taxonomy were named '*dsrAB* type' (for reductive bacterial-type or archaeal-type or oxidative bacterial-type *dsrAB* sequences), 'supercluster' (within the reductive bacterial-type *dsrAB* lineage), 'phylum/class' (based on the taxonomy of known isolates), 'family' (taxonomic families based on known isolates and uncultured family-level lineages) and 'strain/clone'. Taxonomic fields previously labelled as 'unclassified' were replaced by 'unclassified_supercluster', 'unclassified_phylum/class' or 'unclassified_family' to reflect their phylogenetic level (Müller *et al*., 2015).

Sequences were classified using three approaches. The first approach employed the k-mer-based Naïve Bayesian RDP classifier (Wang *et al*., 2007) in MOTHUR (Schloss *et al*., 2009) with a k-mer size of 8 nt and a cut-off of 90. The taxonomy file and the reference nucleotide sequence file for Naïve Bayesian classification are provided in the Supporting information (Files S1–S3).

The second approach was based on phylogenetic assignment of sequences into the reference DsrAB tree without modifying its topology by using the EPA in RAxML (Berger *et al*., 2011). Here, nucleotide sequences were initially translated into amino acid sequences and aligned to the DsrAB reference sequence alignment with MAFFT using the options -addfragments -reorder -thread 1 (Katoh *et al*., 2002). DsrA and DsrB sequences were aligned differently due to their different composition after processing of MISEQ paired-end reads. DsrB contig sequences were aligned to the original DsrB reference alignment. The DsrA reference alignment was adjusted by removing internal regions that are not represented in the DsrA scaffold sequences. Alignments were checked manually and regions with insertions and deletions (Müller *et al*., 2015) were removed prior to placement of sequences into the reference tree with EPA (-f v -m PROTCATDAYHOFF -p 1234). EPA-derived IDs for all nodes and leaves of the DsrAB reference tree were manually assigned to the respective taxonomic groups. The DsrAB reference tree file, the DsrAB reference alignment file and the corresponding taxonomy-ID mapping file are provided in the Supporting information (Files S1, S4, S5 and S6).

The third approach combined the results from both methods. Classification results for the '*dsrAB* type' level down to the 'family' level were inferred using EPA. The classification at the 'clone/strain' level was subsequently inferred by using the Naïve Bayesian classifier results, but only for sequences that showed matching results at the 'family' level by both methods.

The performances of the three classification approaches were tested *in silico* with the 80 mock community sequences that were represented in the reference database. For this purpose, the original mock community sequences were trimmed to the sizes of *dsrA* scaffolds or *dsrB* contigs as obtained after processing MISEQ paired-end reads. The trimmed mock community sequences were tested against four different versions of the reference database (original, $n = 1292$; without mock community sequences, $n = 1212$; without *dsrAB* sequences ≥ 90% identical to any mock community sequence, $n = 986$; without *dsrAB* sequences ≥ 80% identical to any mock community sequence, $n = 745$) to reveal how accurate sequences of varying similarity to the sequences in the reference database will be classified. The obtained classifications were compared with the known classifications of mock community sequences by using R.

Acknowledgements

We thank Captain Stig Henningsen, the crew of M/S Farm and all participants of the 2005 Svalbard cruise, which was

funded by the Max-Planck-Institute for Marine Microbiology, for help with sediment sampling. The Greenland sediment was collected during the R/V Sanna 2013 summer campaign, which was funded by the Arctic Research Centre, Aarhus University, and we thank Marit-Solveig Seidenkranz, Hans Røy and Kasper Kjeldsen for providing the samples. We further acknowledge Agathe Borejdo for library preparation, Daniela Greulich for sequencing, and other members of Microsynth AG for helpful discussions. Barbara Bayer and Kenneth Wasmund are acknowledged for critically revising the manuscript. Grants by the Austrian Science Fund (FWF, P25111-B22) and the Vienna Science and Technology Fund (WWTF, LS12-001) supported this study financially. The authors declare no conflict of interest.

Author contributions

CP, CWH and AL designed the experiments and the data analysis procedures with the help of all authors. CP performed experiments. CP, CWH and BH analysed data. CP and AL wrote the manuscript. CWH, BH, AM and MP revised the draft version and approved the final version of the manuscript.

References

Acinas, S.G., Sarma-Rupavtarm, R., Klepac-Ceraj, V., and Polz, M.F. (2005) PCR-induced sequence artifacts and bias: insights from comparison of two 16S rRNA clone libraries constructed from the same sample. *Appl Environ Microbiol* **71:** 8966–8969.

Altschul, S., Gish, W., Miller, W., Myers, E., and Lipman, D. (1990) Basic local alignment search tool. *J Mol Biol* **215:** 403–410.

Berger, S.A., Krompass, D., and Stamatakis, A. (2011) Performance, accuracy, and web server for evolutionary placement of short sequence reads under maximum likelihood. *Syst Biol* **60:** 291–302.

Brauman, A., Müller, J.A., Garcia, J.L., Brune, A., and Schink, B. (1998) Fermentative degradation of 3-hydroxybenzoate in pure culture by a novel strictly anaerobic bacterium, *Sporotomaculum hydroxybenzoicum* gen. nov., sp. nov. *Int J Syst Bacteriol* **48** (Part 1): 215–221.

Canion, A., Overholt, W.A., Kostka, J.E., Huettel, M., Lavik, G., and Kuypers, M.M.M. (2014) Temperature response of denitrification and anammox rates and microbial community structure in Arctic fjord sediments. *Environ Microbiol* **16:** 3331–3344.

Caporaso, J.G., Kuczynski, J., Stombaugh, J., Bittinger, K., Bushman, F.D., Costello, E.K., *et al.* (2010) QIIME allows analysis of high-throughput community sequencing data intensity normalization improves color calling in SOLiD sequencing. *Nat Methods* **7:** 335–336.

Carbonero, F., Benefiel, A.C., Alizadeh-Ghamsari, A.H., and Gaskins, H.R. (2012) Microbial pathways in colonic sulfur metabolism and links with health and disease. *Front Physiol* **3:** 448.

Collavino, M.M., Tripp, H.J., Frank, I.E., Vidoz, M.L., Calderoli, P.A., Donato, M., *et al.* (2014) *nifH* pyrosequencing reveals the potential for location-specific soil chemistry to influence N2-fixing community dynamics. *Environ Microbiol* **16:** 3211–3223.

Dumont, M.G., Radajewski, S.M., Miguez, C.B., McDonald, I.R., and Murrell, J.C. (2006) Identification of a complete methane monooxygenase operon from soil by combining stable isotope probing and metagenomic analysis. *Environ Microbiol* **8:** 1240–1250.

Edgar, R.C. (2010) Search and clustering orders of magnitude faster than BLAST. *Bioinformatics* **26:** 2460–2461.

Edgar, R.C. (2013) UPARSE: highly accurate OTU sequences from microbial amplicon reads. *Nat Methods* **10:** 996–998.

Esling, P., Lejzerowicz, F., and Pawlowski, J. (2015) Accurate multiplexing and filtering for high-throughput amplicon-sequencing. *Nucleic Acids Res* **43:** 2513–2524.

Finster, K. (2008) Microbiological disproportionation of inorganic sulfur compounds. *J Sulphur Chem* **29:** 281–292.

Franzosa, E.A., Hsu, T., Sirota-Madi, A., Shafquat, A., Abu-Ali, G., Morgan, X.C., and Huttenhower, C. (2015) Sequencing and beyond: integrating molecular 'omics' for microbial community profiling. *Nat Rev Microbiol* **13:** 360–372.

Glombitza, C., Jaussi, M., Seidenkrantz, M., Lomstein, B.A., and Barker, B. (2015) Formate, acetate and propionate as substrates for sulfate reduction in sub-arctic sediments of Southwest Greenland. *Front Microbiol* **6:** 846.

Herbold, C.W., Pelikan, C., Kuzyk, O., Hausmann, B., Angel, R., Berry, D., and Loy, A. (2015) A flexible and economical barcoding approach for highly multiplexed amplicon sequencing of diverse target genes. *Front Microbiol* **6:** 731.

Huse, S.M., Welch, D.M., Morrison, H.G., and Sogin, M.L. (2010) Ironing out the wrinkles in the rare biosphere through improved OTU clustering. *Environ Microbiol* **12:** 1889–1898.

Imachi, H., Sekiguchi, Y., Kamagata, Y., Loy, A., Qiu, Y.-L., Hugenholtz, P., *et al.* (2006) Non-sulfate-reducing, syntrophic bacteria affiliated with *Desulfotomaculum* cluster I are widely distributed in methanogenic environments. *Appl Environ Microbiol* **72:** 2080–2091.

Katoh, K., Misawa, K., Kuma, K., and Miyata, T. (2002) MAFFT: a novel method for rapid multiple sequence alignment based on fast Fourier transform. *Nucleic Acids Res* **30:** 3059–3066.

Kip, N., Dutilh, B.E., Pan, Y., Bodrossy, L., Neveling, K., Kwint, M.P., *et al.* (2011) Ultra-deep pyrosequencing of *pmoA* amplicons confirms the prevalence of *Methylomonas* and *Methylocystis* in *Sphagnum* mosses from a Dutch peat bog. *Environ Microbiol Rep* **3:** 667–673.

Laue, H., Friedrich, M., Ruff, J., and Cook, A.M. (2001) Dissimilatory sulfite reductase (Desulfoviridin) of the taurine-degrading, non-sulfate-reducing bacterium *Bilophila wadsworthia* RZATAU contains a fused DsrB-DsrD subunit. *J Bacteriol* **183:** 1727–1733.

Leininger, S., Urich, T., Schloter, M., Schwark, L., Qi, J., Nicol, G.W., *et al.* (2006) Archaea predominate among

ammonia-oxidizing prokaryotes in soils. *Nature* **442:** 806–809.

Lever, M.A., Rouxel, O., Alt, J.C., Shimizu, N., Ono, S., Coggon, R.M., *et al*. (2013) Evidence for microbial carbon and sulfur cycling in deeply buried ridge flank basalt. *Science* **339:** 1305–1308.

Loy, A., Küsel, K., Lehner, A., Drake, H.L., and Wagner, M. (2004) Microarray and functional gene analyses of sulfate-reducing prokaryotes in low-sulfate, acidic fens reveal cooccurrence of recognized genera and novel lineages. *Appl Environ Microbiol* **70:** 6998–7009.

Loy, A., Duller, S., Baranyi, C., Mussmann, M., Ott, J., Sharon, I., *et al*. (2009) Reverse dissimilatory sulfite reductase as phylogenetic marker for a subgroup of sulfur-oxidizing prokaryotes. *Environ Microbiol* **11:** 289–299.

Ludwig, W., Strunk, O., Westram, R., Richter, L., Meier, H., Yadhukumar, *et al*. (2004) ARB: a software environment for sequence data. *Nucleic Acids Res* **32:** 1363–1371.

McMurdie, P.J., and Holmes, S. (2013) phyloseq: an R package for reproducible interactive analysis and graphics of microbiome census data. *PLoS ONE* **8:** e61217.

Masella, A.P., Bartram, A.K., Truszkowski, J.M., Brown, D.G., and Neufeld, J.D. (2012) PANDAseq: paired-end assembler for Illumina sequences. *BMC Bioinformatics* **13:** 31.

Milucka, J., Ferdelman, T.G., Polerecky, L., Franzke, D., Wegener, G., Schmid, M., *et al*. (2012) Zero-valent sulphur is a key intermediate in marine methane oxidation. *Nature* **491:** 541–546.

Moreau, J.W., Zierenberg, R.A., and Banfield, J.F. (2010) Diversity of dissimilatory sulfite reductase genes (*dsrAB*) in a salt marsh impacted by long-term acid mine drainage. *Appl Environ Microbiol* **76:** 4819–4828.

Müller, A.L., de Rezende, J.R., Hubert, C.R.J., Kjeldsen, K.U., Lagkouvardos, I., Berry, D., *et al*. (2014) Endospores of thermophilic bacteria as tracers of microbial dispersal by ocean currents. *ISME J* **8:** 1153–1165.

Müller, A.L., Kjeldsen, K.U., Rattei, T., Pester, M., and Loy, A. (2015) Phylogenetic and environmental diversity of DsrAB-type dissimilatory (bi)sulfite reductases. *ISME J* **9:** 1152–1165.

Nelson, M.C., Morrison, H.G., Benjamino, J., Grim, S.L., and Graf, J. (2014) Analysis, optimization and verification of Illumina-generated 16S rRNA gene amplicon surveys. *PLoS ONE* **9:** e94249.

Parada, A., Needham, D.M., and Fuhrman, J.A. (2015) Every base matters: assessing small subunit rRNA primers for marine microbiomes with mock communities, time-series and global field samples. *Environ Microbiol*. doi:10.1111/1462-2920.13023.

Park, S.J., Park, B.J., Jung, M.Y., Kim, S.J., Chae, J.C., Roh, Y., *et al*. (2011) Influence of deglaciation on microbial communities in marine sediments off the coast of Svalbard, arctic circle. *Microb Ecol* **62:** 537–548.

Pester, M., Bittner, N., Deevong, P., Wagner, M., and Loy, A. (2010) A 'rare biosphere' microorganism contributes to sulfate reduction in a peatland. *ISME J* **4:** 1591–1602.

Pester, M., Knorr, K.H., Friedrich, M.W., Wagner, M., and Loy, A. (2012a) Sulfate-reducing microorganisms in wetlands – Fameless actors in carbon cycling and climate change. *Front Microbiol* **3:** 72.

Pester, M., Brambilla, E., Alazard, D., Rattei, T., Weinmaier, T., Han, J., *et al*. (2012b) Complete genome sequences of *Desulfosporosinus orientis* DSM765^T, *Desulfosporosinus youngiae* DSM17734^T, *Desulfosporosinus meridiei* DSM13257^T, and *Desulfosporosinus acidiphilus* DSM22704^T. *J Bacteriol* **194:** 6300–6301.

Pester, M., Rattei, T., Flechl, S., Gröngröft, A., Richter, A., Overmann, J., *et al*. (2012) *amoA*-based consensus phylogeny of ammonia-oxidizing archaea and deep sequencing of *amoA* genes from soils of four different geographic regions. *Environ Microbiol* **14:** 525–539.

Pester, M., Maixner, F., Berry, D., Rattei, T., Koch, H., Lücker, S., *et al*. (2013) *nxrB* encoding the beta subunit of nitrite oxidoreductase as functional and phylogenetic marker for nitrite-oxidizing *Nitrospira*. *Environ Microbiol* **16:** 3055–3071.

Polz, M.F., and Cavanaugh, C.M. (1998) Bias in template-to product ratios in multitemplate PCR. *Appl Environ Microbiol* **64:** 3724–3730.

Pruesse, E., Peplies, J., and Glöckner, F.O. (2012) SINA: accurate high-throughput multiple sequence alignment of ribosomal RNA genes. *Bioinformatics* **28:** 1823–1829.

R Core Team (2015) *R: A Language and Environment for Statistical Computing*. Vienna, Austria: R Foundation for Statistical Computing. URL: http://www.r-project.org/.

Rabus, R., Venceslau, S.S., Wöhlbrand, L., Voordouw, G., Wall, J.D., and Pereira, I.A. (2015) A post-genomic view of the ecophysiology, catabolism and biotechnological relevance of sulphate-reducing prokaryotes. *Adv Microb Physiol* **66:** 55–321.

Ravenschlag, K., Sahm, K., Knoblauch, C., Jørgensen, B.B., and Amann, R. (2000) Community structure, cellular rRNA content, and activity of sulfate-reducing bacteria in marine arctic sediments. *Appl Environ Microbiol* **66:** 3592–3602.

Reeder, J., and Knight, R. (2009) The 'rare biosphere': a reality check. *Nat Methods* **6:** 636–637.

Schloss, P.D., Westcott, S.L., Ryabin, T., Hall, J.R., Hartmann, M., Hollister, E.B., *et al*. (2009) Introducing mothur: open-source, platform-independent, community-supported software for describing and comparing microbial communities. *Appl Environ Microbiol* **75:** 7537–7541.

Seitz, V., Schaper, S., Dröge, A., Lenze, D., Hummel, M., and Hennig, S. (2015) A new method to prevent carry-over contaminations in two-step PCR NGS library preparations. *Nucleic Acids Res* **43:** e135.

Simon, J., Kroneck, P.M.H., Poole, I.R.K., and Press, A. (2013) Microbial sulfite respiration. *Adv Microb Physiol* **62:** 45–117.

Steger, D., Wentrup, C., Braunegger, C., Deevong, P., Hofer, M., Richter, A., *et al*. (2011) Microorganisms with novel dissimilatory (bi)sulfite reductase genes are widespread and part of the core microbiota in low-sulfate peatlands. *Appl Environ Microbiol* **77:** 1231–1242.

Suzuki, M.T., and Giovannoni, S.J. (1996) Bias caused by template annealing in the amplification of mixtures of 16S rRNA genes by PCR. *Appl Environ Microbiol* **62:** 625–630.

Tremblay, J., Singh, K., Fern, A., Kirton, E.S., He, S., Woyke, T., *et al*. (2015) Primer and platform effects on 16S rRNA tag sequencing. *Front Microbiol* **6:** 1–15.

© 2015 Society for Applied Microbiology and John Wiley & Sons Ltd,

Venceslau, S.S., Stockdreher, Y., Dahl, C., and Pereira, I.A. (2014) The 'bacterial heterodisulfide' DsrC is a key protein in dissimilatory sulfur metabolism. *Biochim Biophys Acta* **1837:** 1148–1164.

Wagner, M., Roger, A.J., Flax, J.L., Gregory, A., Stahl, D.A., and Brusseau, G.A. (1998) Phylogeny of dissimilatory sulfite reductases supports an early origin of sulfate respiration. *J Bacteriol* **180:** 2975–2982.

Wagner, M., Loy, A., Klein, M., Lee, N., Ramsing, N.B., Stahl, D.A., and Friedrich, M.W. (2005) Functional marker genes for identification of sulfate-reducing prokaryotes. *Methods Enzymol* **397:** 469–489.

Wang, Q., Garrity, G.M., Tiedje, J.M., and Cole, J.R. (2007) Naive Bayesian classifier for rapid assignment of rRNA sequences into the new bacterial taxonomy. *Appl Environ Microbiol* **73:** 5261–5267.

Wu, L., Wen, C., Qin, Y., Yin, H., Tu, Q., Van Nostrand, J.D., *et al*. (2015) Phasing amplicon sequencing on Illumina Miseq for robust environmental microbial community analysis. *BMC Microbiol* **15:** 125.

Zeleke, J., Sheng, Q., Wang, J.G., Huang, M.Y., Xia, F., Wu, J.H., and Quan, Z.X. (2013) Effects of *Spartina alterniflora* invasion on the communities of methanogens and sulfate-reducing bacteria in estuarine marsh sediments. *Front Microbiol* **4:** 243.

Zverlov, V., Klein, M., Friedrich, W., Kellermann, J., Stahl, D.A., and Wagner, M. (2005) Lateral gene transfer of dissimilatory (bi)sulfite reductase revisited. *J Bacteriol* **187:** 2203–2208.

Supporting information

Additional Supporting Information may be found in the online version of this article at the publisher's web-site:

Fig. S1. Compositions of the 90- and 45-sequence *dsrAB* mock communities. Rank abundance distribution and accession numbers of *dsrAB* reference sequences of (a) the 90-sequence mock community and (b) the 45-sequence mock community, which is a subset of the 90-sequence mock community. (c) Phylogeny of all mock community sequences. The *dsrAB* tree was calculated using RAxML with the GTR model.

Fig. S2. A gel picture of PCR products obtained with different combinations of *dsrA*- or *dsrB*-targeted primers from mock community or arctic marine sediment DNA. The primer sets were applied with and without the 16 nt head (5′-GCTATGCGCGAGCTGC- 3′) attached to the 5′ end. The upper gel picture shows the amplification with primers without head. The gel pictures below show results from the barcoding procedure, where a first PCR step is performed with headed primers for 30 cycles and a second barcoding PCR step for another 10 cycles. Gel electrophoresis was performed at 110V for 45 min and a 1% agarose gel. DNA bands were subsequently stained with the GelRedTM DNA stain (Biotium). L, GeneRuler 1 kb DNA ladder (Fermentas).

Fig. S3. A pipeline for generating, processing and classifying *dsrA* and *dsrB* amplicon sequence data. See the main text for further details. Barcoded amplicons of *dsrA* and *dsrB* are generated using a flexible two-step PCR procedure (Herbold *et al*., 2015), as shown here schematically for one sample. In the first PCR step, *dsrA* and *dsrB* are amplified with gene-specific primers that carry a generic 16 nt head sequence at the 5′ end. In the second PCR step, this head sequence is target for a barcoding primer consisting of the head sequence and a sample-specific 8 nt barcode sequence attached to its 5′ end. Barcoded amplicons from different samples are mixed in equimolar concentrations and the final amplicon pool is treated as a metagenome and sequenced (in this study: paired-end Illumina MiSeq sequencing). Pre-processing of raw reads is performed differently for longer amplicons that yield non-overlapping (*dsrA*) and for shorter amplicons that yield overlapping (*dsrB*) paired-end reads. Reads of *dsrA* are de-multiplexed at a Q-score of 15, length trimmed at the first position with an average Q-score of < 30 and filtered for reads with an expected average error of ≤ 1. Afterwards non-target genes are filtered from the data set. All paired-end *dsrA* reads are then aligned to the reference database, trimmed in the reading frame at the same position, unaligned and joined into scaffolds with forward and reverse reads separated by 6 ambiguous bases 'N'. All paired-end *dsrB* reads are de-multiplexed at a Q-score of 15, as revealed by iterative testing with the mock community data set, and assembled into contigs. Subsequently, *dsrB* contigs are quality filtered and non-target genes are removed. Pre-processed *dsrA* scaffolds and *dsrB* contigs are de-replicated with removal of singletons and then pre-clustered into OTUs of $\geq 99\%$ sequence identity, including *de novo* chimera detection and removal. Pre-clustered sequences are subsequently clustered into species-level OTUs at $\geq 92\%$ and $\geq 90\%$ sequence identity for *dsrA* scaffolds and *dsrB* contigs respectively. OTU count tables are generated for each sample. Representative OTU sequences are classified against the reference *dsrAB* database using a combination of phylogenetic assignment with the Evolutionary Placement Algorithm (EPA) (Berger *et al*., 2011) and RDP's Naïve Bayesian classifier (Wang *et al*., 2007).

Fig. S4. Inferred species-level thresholds for processed *dsrA* and *dsrB* amplicon sequence data. Pairwise nucleotide identities over the 1.9 kb long *dsrAB* region and the short *dsrA* scaffold/*dsrB* contig region were correlated for 1110 core sequences in the reference database. Red lines indicate the nucleotide identities of the short *dsrA* or *dsrB* sequences that correspond to the 90% sequence identity species-level threshold proposed for the long *dsrAB* region, as shown by the blue lines (Müller *et al*., 2015).

Fig. S5. Histogram of the average Q-scores of raw reads 1 and reads 2 in the *dsrA* and *dsrB* data sets. The average read length was 264 nt (259–285 nt).

Fig. S6. Relative abundance and sequence identity of non-mock community species-level OTUs. Data from the 90-sequence mock community data sets are shown separately for *dsrA* (A) and *dsrB* (B) and for all nine different PCR cycle combinations.

Fig. S7. Linear regressions of expected versus observed relative abundances of mock community sequences for all nine different PCR cycle combinations. Data from the 90-sequence mock community data sets are shown separately for *dsrA* and *dsrB* after pre-clustering at 99% nucleotide identity. Only OTUs with 100% identity to any mock community reference sequence and that were observed in at least one data set were included in the linear model.

Fig. S8. Impact of PCR cycle number on *dsrA* and *dsrB* community structure. The regression coefficients of observed versus expected relative abundances of mock community sequences (Fig. S7) were correlated with the number of cycles in the first PCR step (A, B), the second PCR step (C, D) and the first and second PCR step (E, F).

Fig. S9. Rarefaction curves of species-level OTUs in environmental samples. Data were sub-sampled ($n = 1000$) at the size of the smallest library (*dsrA*: $n = 143$, *dsrB*: $n = 1974$). The colour of each curve indicates the combination of cycles in the first and second PCR step.

Table S1. Number of *dsrA* and *dsrB* read pairs obtained from the 90- and the 45-sequence mock community using different PCR cycle number combinations.

Table S2. Number of sequences, diversity metrics and other parameters of *dsrA* and *dsrB* libraries from selected environmental samples.

Table S3. Number of mock community sequences that were not observed in the pre-clustered *dsrA* and *dsrB* sequencing data and potential explanations for their absence.

File S1. Description of Files S2–S6.

File S2. Reference *dsrAB* sequence file for classification of query sequences with MOTHUR's implementation of RDP's Naïve Bayesian classifier (classify.seqs). This multi-fasta file contains all 1292 core nucleotide sequences from the reference database (Müller *et al.*, 2015).

File S3. Reference *dsrAB* taxonomy file for classification of query sequences with MOTHUR's implementation of RDP's Naïve Bayesian classifier (classify.seqs). This file contains the taxonomic information of all 1292 core sequences. The first column is the identifier that matches the sequence header in File S2. The five hierarchical taxonomic levels are separated by semicolons and are '*dsrAB* type' (for reductive bacterial-type or archaeal-type or oxidative bacterial-type *dsrAB* sequences), 'supercluster' (within the reductive bacterial-type *dsrAB* lineage), 'phylum/class' (based on the taxonomy of known isolates), 'family' (taxonomic families based on known isolates or uncultured family-level lineages) and 'strain/clone'.

File S4. Reference DsrAB sequence alignment file for classification of query sequences with RAxML's Evolutionary Placement Algorithm (EPA). This multi-fasta file contains all aligned 1292 core amino acid sequences from the reference database (Müller *et al.*, 2015). Any query data set has to be aligned to this reference sequence alignment, i.e. by MAFFT (Katoh *et al.*, 2002). The format of the combined output file has to be changed from '.fasta' into '.phy' and can then be directly used as input for EPA.

File S5. Reference DsrAB tree file for placement with EPA. This file is an export of the consensus tree contained in the reference *dsrAB*/DsrAB ARB database (Müller *et al.*, 2015) in Newick format.

File S6. ID-mapping file for classification of sequences placed into the reference tree with EPA. The first column of the file shows the ID's that are generated for the 1292 core sequences by EPA with the reference DsrAB tree (File S5) as an input. The five hierarchical taxonomic levels are '*dsrAB* type' (for reductive bacterial-type or archaeal-type or oxidative bacterial-type *dsrAB* sequences), 'supercluster' (within the reductive bacterial-type *dsrAB* lineage), 'phylum/class' (based on the taxonomy of known isolates), 'family' (taxonomic families based on known isolates or uncultured family-level lineages) and 'strain/clone'. This file has to be compared with the EPA output file 'RAxML_classification' by using e.g. R or EXCEL.

© 2015 Society for Applied Microbiology and John Wiley & Sons Ltd,

Chapter 2

Glacial runoff promotes deep burial of sulfur cycling-associated microorganisms in marine sediments

Claus Pelikan, Marion Jaussi, Kenneth Wasmund, Marit-Solveig Seidenkrantz, Christof Pearce, Zou Zou Kuzyk, Craig W. Herbold, Hans Røy, Kasper Urup Kjeldsen, and Alexander Loy

Author contributions:

CP, HR, KUK, and AL designed the research. CP generated and analyzed the sequencing data. MSS, HR and ChP collected the cores, MJ, HR and KK obtained the samples and MJ performed most biogeochemical analyses. MSS, ChP and ZZK performed the age models. CP, KW and AL wrote the manuscript. All authors revised the manuscript.

Glacial runoff promotes deep burial of sulfur cycling-associated microorganisms in marine sediments

Claus Pelikan[1,2], Marion Jaussi[3], Kenneth Wasmund[1,2], Marit-Solveig Seidenkrantz[4], Christof Pearce[4], Zou Zou Kuzyk[5], Craig W. Herbold[1], Hans Røy[3], Kasper Urup Kjeldsen[3] and Alexander Loy[1,2]*

[1]*Division of Microbial Ecology, Centre for Microbiology and Environmental Systems Science, University of Vienna, Vienna, Austria*
[2]*Austrian Polar Research Institute, Vienna, Austria*
[3]*Center for Geomicrobiology, Department of Bioscience, Aarhus University, Aarhus, Denmark*
[4]*Department of Geoscience, Aarhus University, Denmark*
[5]*Department of Geological Sciences, University of Manitoba, Winnipeg, Canada*

*Correspondence: Alexander Loy (Tel: +43 1 4277 76605, loy@microbial-ecology.net)

Running Head: Microbial community composition of glaciated fjord sediments

Abstract

Marine fjords with active glacier outlets constitute a large proportion of high latitude shelf areas and are hot spots for organic matter burial in the sediments and subsequent microbial mineralization. Here, we investigated microbial community assembly in relation to sediment age and biogeochemistry over six meters of depth in subarctic glacier-influenced (GI) and non-glacier-influenced (NGI) marine sediments from south-western Greenland using an integrated correlation approach based on 16S rRNA gene and dissimilatory sulfite reductase-*dsrB* amplicon sequence data. Differences in sediment age-depth relationships and biogeochemical parameters, such as C/N ratios and sulfate reduction rates, were the strongest drivers of differential community assembly between GI and NGI sediments. Sediment age increased considerably with depth at NGI stations, suggesting lower rates of sedimentation. Only a few microorganisms of the surface community in NGI sediments persisted during burial and became abundant in the about 9,000 year-old subsurface. This scenario is largely consistent with previously documented, highly selective assembly patterns of the deep biosphere in energy-limited marine sediment layers. In contrast, a different community assembly was observed at GI stations where the deepest sediment zones were only a few hundred years old. Many key community members from the surface were abundantly present and strongly correlated to active sulfur-cycling throughout the GI

sediment cores. The persistence of important biogeochemical processes, e.g. sulfate reduction, and community members from surface sediments deep into the sediment subsurface was mediated by higher sedimentation rates at GI stations. In conclusion, our data suggests that glacier runoff, through increasing rates of sediment accumulation and associated changes in biogeochemistry, exerts a strong control on community assembly and metabolic activity of the deep biosphere in marine sediments.

Introduction

Arctic fjords with seaward glaciers constitute an important interface for sediment and freshwater influx from land into the sea, thereby creating physical and chemical variation in adjacent water and sediment ecosystems (Etherington *et al.*, 2007; Svendsen *et al.*, 2002). The largest impact on life in glacier-associated fjords is the high influx of sedimentary materials, e.g., minerals and organic matter, which strongly influences animal (Hop *et al.*, 2002) and microbial (Bourgeois *et al.*, 2016; Park *et al.*, 2011) community distributions in marine sediments. Increased water turbidity in close proximity to the glacier (Zajączkowski, 2008) can negatively influence surface water primary production (Etherington *et al.*, 2007). However, glacial meltwater is also an important source for nutrients (Meire *et al.*, 2015; Statham *et al.*, 2008) and can thereby stimulate phytoplankton growth (Sørensen *et al.*, 2015). Consequences of increased primary production are a net CO_2 uptake in arctic fjords (Meire *et al.*, 2015) as well as rapid burial of fresh detrital phytoplankton biomass in the underlying sediments (Bourgeois *et al.*, 2016; Smith *et al.*, 2015). Fjord sediments also receive significant amounts of terrigenous organic matter, which results in high C/N ratios of the sediment organic matter pool (Goñi *et al.*, 2013; Wehrmann *et al.*, 2014). The labile fraction of organic matter in sediments is initially degraded by hydrolytic and fermenting microorganisms (Müller *et al.*, 2018). These largely unidentified microbial species typically have a wide range of enzymatic capabilities for organic matter breakdown (Orsi *et al.*, 2018; Teske *et al.*, 2011). Degradation metabolites are either further degraded by secondary fermenters or are mineralized to CO_2 via microbial respiration (Arndt *et al.*, 2013).

Of prime importance is the respiratory reduction of sulfate to sulfide, which has been shown to be responsible for up to 69% of the total organic matter mineralization in arctic fjord sediments (Sørensen *et al.*, 2015). Other key electron acceptors are metals that can be introduced via glacial runoff to marine sediments and are subjected to redox cycling (Bhatia *et al.*, 2013; Laufer *et al.*, 2016; Wehrmann *et al.*, 2014). Fe(III) and Mn(IV) facilitate the oxidation of reduced sulfur compounds (Wehrmann *et al.*, 2014; Zopfi *et al.*, 2004) and thereby fuel a cryptic sulfur cycle in glacier-influenced sediments (Wehrmann *et al.*, 2017).

Because glacial influences on the assembly of the marine sediment microbiota are not well understood, we investigated microbial diversity and community composition of glacier-influenced (GI) and non-glacier-influenced (NGI) coastal sediments in the Godthåbsfjord region of Greenland. Compositions of the entire microbiota and the community of putative sulfite/sulfate-reducing microorganisms (SRM), as analyzed by 16S rRNA and dissimilatory sulfite reductase (*dsrB*) gene amplicon sequencing, respectively, were compared across sediment samples of different depths and ages. Co-occurrence analyses of operational taxonomic units (OTUs) and correlation with biogeochemical data revealed key environmental factors that were driving the major community differences between GI and NGI sediments and identified microorganisms that were associated with sulfur cycling. Our results contribute to a better understanding of the assembly and depth zonation of microbial communities in coastal arctic sediments.

Materials and Methods

Sediment sampling

Sampling of the cores for this study was described previously (Glombitza *et al.*, 2015). In brief, up to 6 m long gravity cores were recovered from four sites on the open shelf and within the Godthåbsfjord (Nuup Kangerlua) in South West Greenland (Table 1 and Supplementary Figure S1) in August 2013. The four stations can be broadly subdivided into two groups: glacier-influenced (GI) and non-glacier influenced (NGI). Station 3 and station 6 were NGI stations and were located outside the fjord on the continental shelf of the Labrador Sea and in the Kapisigdit Kanderdluat (a side-fjord without glaciers), respectively. Station 5, which was located in the main channel of the Godthåbsfjord, although not directly in front of a glacier (material released from the glacier is transported towards the Labrador Sea across this site), and station 8 located in close proximity to a glacier front at the northernmost outlet of the Greenland ice sheet in the Kangersuneq fjord belonged to the GI stations. For molecular analyses, sediment cores were sampled by cutting small holes across the core liner and scraping off the surface with sterile spatulas before collecting sediment samples in duplicates with sterile 5 mL cut-off syringes. The sediment was immediately packed in Whirl-Pak bags and frozen at -80°C. Porewater was extracted from the sediment cores as described previously (Glombitza *et al.*, 2015).

Analytical methods

Sulfate, hydrogen sulfide and DIC concentration measurements, as well as sulfate reduction rate (SRR) measurements were previously described in Glombitza *et al.*, (2015). In addition, ferrous iron, total organic carbon (TOC), total nitrogen (TN) and sediment age were analyzed. For analyses of ferrous iron (Fe^{2+}) concentrations, porewater was amended with 0.5 M HCl (1:1, v/v) and stored at 4°C. One mL of ferrozine

solution (1 g L^{-1} in 50 mM HEPES-buffer at pH 7) was subsequently added to 20 µL of acid-preserved porewater, producing a magenta color reaction (Sørensen, 1982, Phillips & Lovley, 1987). The absorbance was measured at 562 nm (Stookey, 1970) with a spectrophotometer (FLUOstar Omega, BMG Labtech GMBH). To determine total organic carbon (TOC) and total nitrogen (TN), sediment samples were treated with sulfurous acid (5-6% w/w) to remove inorganic carbon. Once dried, 50 mg of acidified sediment were packed into cleaned tin cups and burned in the elemental analyzer (FLASH EA 1112 series, Thermo Scientific). TOC and TN concentrations were calculated from a standard curve with wheat flour, which contains 43.37% of carbon and 2.31% of nitrogen. The C/N ratio was calculated as the molar ratio of total organic carbon to total nitrogen. For determination of methane concentrations, 2 cm^3 sediment was transferred to 20 mL GC vials containing 2.5 mL saturated NaCl with excess crystalline salt. The bottles were vigorously shaken to release methane into the head space of the GC vials and stored upside down at -20°C until further analysis. Methane concentrations in the vial headspace were subsequently measured by gas chromatography (SRI 310C GC, SRI Instruments Europe GmbH) with a flame ionization detector. Ammonium concentrations were determined from 2 mL of porewater. Concentrations were analyzed spectrophotometrically as previously described (Dansk-Standard, 1975; Bower & Holm-Hansen, 1980).

Sediment age of cores from stations 3, 5 and 6 were based on radiocarbon dating and age modeling. For ^{14}C age determination, calcareous mollusk shells, benthic foraminifera and sea weed samples were collected from cores and the ^{14}C concentrations were determined by Accelerator Mass Spectrometry. The ^{14}C ages were calibrated using the Marine13 radiocarbon calibration curve (Reimer *et al.*, 2013) with a reservoir correction of $\Delta R = 140 \pm 35$ years. Age-depth models for cores from station 3 and 6 were calculated using the software Oxcal v4.2 (Ramsey, 2008). The presence of rapidly deposited turbidite sequences in the core from station 5 made a detailed age model difficult.

In the core retrieved from station 8 no material usable for ^{14}C dating was found, and thus radiocarbon dating was not possible. Instead, the sediment age was estimated from ^{210}Pb, ^{137}Cs, and ^{226}Ra measurements of freeze-dried, homogenized sediment samples. The water content of each sample was determined before and after freeze-drying and results were reported on a dry-weight basis, salt-corrected for bottom-water salinity at the time of sampling. Core sections were analyzed by gamma spectroscopy using a CANBERRA® Broad Energy Germanium with a P-type detector (model BE3830). Detector efficiency and self-absorption were corrected by counting reference material from the International Atomic Energy Agency (IAEA) within the same geometry. The reproducibility errors, determined by counting the same sample four times, were 5.7, 8.8, and 3.8%, for ^{210}Pb, ^{137}Cs, and ^{226}Ra, respectively. ^{210}Pb was also determined from its ^{210}Po daughter isotope using alpha spectroscopy (n=23 sediment sections). The samples

were prepared according to (Flynn, 1968). A ^{209}Po tracer, calibrated against a ^{210}Po NIST standard (Isotope Product Laboratories) was employed for quantitation. The reproducibility error was less than 1%. Sedimentation rate, that was used for the age model presented in this study, was estimated from the least-squares fit to the natural log of the excess ^{210}Pb (^{210}Pb*ex*) in the core and the output of a one-dimensional two-layer advection diffusion model that accounts for both biomixing and compaction with depth (Lavelle *et al.*, 1985, Kuzyk *et al.*, 2015).

To estimate the loss of surface sediment by gravity coring and to correct the age-depth model, we compared the porewater profiles of ammonium, dissolved inorganic carbon and the carbon isotope ratio ^{13}C/^{12}C of DIC (data not shown) between Rumohr cores collected during the same cruise and the gravity cores presented in this study. The upper 18 cm of the gravity core retrieved at station 3 and the upper 10 cm of the the core retrieved at station 6 were missing. The depths of potential surface sediment loss at the two GI stations were corrected as the mean values of the two first cores (14 cm) since the Rumohr core casts at the GI station were not successful. Finally, sediment age was recalculated as “actual age”, i.e., the surface of the seafloor was considered as 0 year old at the time of sampling, based on the age models and the above mentioned depth correction.

DNA extraction and preparation of 16S rRNA gene and dsrB amplicon libraries

Approximately 0.5 to 1 g of sediment was used for DNA extraction according to a previously established protocol (Kjeldsen *et al.*, 2007). Per station, 8 to 10 samples from different depths were selected for further analyses (Supplementary Table 1). Barcoded 16S rRNA gene amplicons were produced using a two-step PCR barcoding approach (Herbold *et al.*, 2016) with the general primers U519F (5’-CAGCMGCCGCGGTAATWC-3’) and 802R (5’-TACNVGGGTATCTAATCC-3’) for initial amplification (Klindworth *et al.*, 2013). These primers were modified with a 16 bp head sequence as described previously (Herbold *et al.*, 2016). First amplification was performed in triplicates with 12.5 µL per reaction volume. The reaction mix contained 1xTaq buffer (Thermo Scientific), 0.2 mM dNTP mix (Thermo Scientific), 2 mM MgCl2, 0.25 U Taq polymerase (Thermo Scientific), 0.2 µM of each primer and approximately 1-10 ng DNA. The first PCR started with a denaturation at 95°C for 3 min, followed by 30 cycles of 95°C for 30 s, 48°C for 30 s and 72°C for 30 s and a final elongation at 72°C for 2 min. The subsequent barcoding PCR (50 µL total volume) was performed with 1x Taq buffer (Thermo Scientific), 0.2 mM dNTP mix (Thermo Scientific), 2 mM MgCl2, 1 U Taq polymerase (Thermo Scientific), 0.2 µM of each primer and 2 µL of the pooled triplicate PCR products from the first PCR reaction. The thermal cycling program consisted of an initial denaturation at 95°C for 3 min, 12 cycles of 95°C for 30 s, 52°C for 30 s and 72°C for 30 s followed by a final elongation at 72°C for 2 min. *dsrB* amplicons were produced according to an established protocol (Pelikan *et al.*, 2016). Barcoded amplicons were

mixed and further prepared for multiplexed, paired-end MiSeq sequencing (Herbold *et al.*, 2016).

Sequence data processing

16S rRNA gene and *dsrB* amplicon raw reads were demultiplexed, filtered and clustered as described previously (Herbold *et al.*, 2016; Pelikan *et al.*, 2016) using fastq-join (Aronesty, 2013) to merge reads and UPARSE version 8.1.1861 (Edgar, 2013) to generate OTUs. Phylum/class-level classification of 16S rRNA-OTUs was performed with the Ribosomal Database Project naïve Bayesian classifier in MOTHUR (Schloss *et al.*, 2009; Wang *et al.*, 2007) using the SILVA database v.128 (Quast *et al.*, 2013) as a reference. *dsrB*-OTUs were classified by phylogenetic placement of representative sequences into a DsrAB reference tree (Müller *et al.*, 2015), which was updated with novel sequences from diverse candidate phyla (Anantharaman *et al.*, 2017a; Hausmann *et al.*, 2018; Parks *et al.*, 2017). The DsrAB reference tree was constructed by de-replicating novel DsrA and DsrB sequences with less than 100 % similarity to any DsrAB sequence in the original reference database and subsequently aligning them to the reference alignments of DsrA and DsrB (Müller *et al.*, 2015) using MAFFT (Katoh *et al.*, 2002). The combined DsrA and DsrB alignments were then concatenated and sequences with a total length of less than 500 amino acids were removed. The concatenated DsrAB alignment was clustered at 70 % sequence identity with usearch (Edgar, 2010), and alignment positions were kept if they were conserved in at least 10 % of all sequences in the 70 %-clustered alignment (56 sequences). The unclustered DsrAB alignment (2985 sequences) was then filtered for conserved alignment positions and was used to generate a maximum likelihood tree with FastTree (Price *et al.*, 2010). 16S rRNA gene and *dsrB* OTU tables were processed in R using native functions (R Core Team, 2015) and the R software package phyloseq (McMurdie and Holmes, 2013). OTU counts were rarefied, i.e., sub-sampled at the smallest library size (*dsrB*: 1521; 16S rRNA gene: 4517) and transformed into relative abundances for all further analyses, except for network analyses, which were performed with the unrarefied OTU count matrices (Friedman and Alm, 2012).

Statistical analyses

Shannon alpha diversity was calculated using R (R Core Team, 2015). Beta diversity analyses were performed with the R software package vegan (Oksanen *et al.*, 2017), including calculations of Bray-Curtis distances with the function vegdist() and nonmetric multidimensional scaling ordination analysis with the function nMDS(). Environmental variables were tested for effects on the overall community composition by mantel tests using the native R function mantel(). Obtained p-values were corrected for multiple testing with the native R function p-adjust() using the Benjamini-Hochberg correction method. Correlations of individual OTUs with environmental variables were calculated

with the native R function cor() using the Spearman correlation coefficient. P-values were generated by permuting the values of each environmental variable followed by correlation of individual OTU abundances with the permuted environmental variable. This process was repeated 1000 times and the obtained p-values were corrected as described above.

OTU co-occurrence networks were calculated using SparCC (Friedman and Alm, 2012). Count matrices were filtered prior to network calculation for increased sensitivity of the network analyses (Berry and Widder, 2014). Only OTUs with more than 10 reads per sample in at least 20% of all samples (n=7) were kept. P-values were generated as described above. Only positive OTU correlations >0.5 were considered. Attributes of individual OTUs, i.e,. sampling station and sediment age at which the OTU was found at the highest relative abundance, were assigned to OTUs in R and networks were visualized in Cytoscape (Shannon *et al.*, 2003). Significant OTU clusters, i.e., significantly more interactions between OTUs within the community cluster than with OTUs outside the community cluster, were defined by Mann-Whitney U tests, using the Cytoscape plugin "clusterONE" (Nepusz *et al.*, 2012).

Phylogenetic analysis

Representative sequences of 16S rRNA-OTUs were aligned with the SINA aligner (Pruesse *et al.*, 2012) using the SILVA database v.128 (Quast *et al.*, 2013) as a reference. Sequences that were closely related to 16S rRNA-OTUs were extracted from the SILVA database and used to construct a reference tree with FastTree (Price *et al.*, 2010). Subsequently, 16S rRNA-OTU sequences were placed into the reference tree using the EPA algorithm (Berger *et al.*, 2011) in RAxML (Stamatakis, 2014). The placement trees of 16S rRNA-OTUs and *dsrB*-OTUs (utilized for *dsrB*-OTU classification) were visualized with iTOL (Letunic and Bork, 2007).

Results

Depth profiles of sediment age and porewater chemistry differ substantially between non-glacier-influenced and glacier-influenced sediments

A goal of the present study was to identify environmental factors (biogeochemical data is partially described in Glombitza *et al.*, 2015) that shape the microbial community composition and interactions in marine sediments, with a focus on the differences between NGI and GI sediments. NGI stations 3 and 6 were characterized by a strong gradient of sediment age due to comparably low sedimentation rates that seemed more or less constant over the respective time periods covered by the two cores (Supplementary Figure S2). Sediment from 5 - 6 meters depth corresponded to 9000 - 12000 years of age. Furthermore, NGI stations had high concentrations of organic carbon (TOC) and nitrogen (TN) as well as low C/N ratios. SRR decreased with depth at

both stations and sulfate became depleted in the bottom of the core from station 3 but not in the core from station 6. At station 3, hydrogen sulfide concentrations gradually increased with depth and decreased again below a depth of 400 cmbsf coinciding with appearance of methane in the porewater. At station 6, hydrogen sulfide was present in lower amounts and methane did not accumulate at any depth.

In comparison, GI stations 5 and 8 were characterized by high sedimentation rates as indicated by the low sediment ages, i.e., around 200 years at the bottom of the core at station 8 and around 500 years at the bottom of the core at station 5 (Supplementary Figure S2). GI stations had high C/N ratios of up to 48. The porewater contained free Fe^{2+} in the upper 250 cmbsf at both GI stations. High rates of sulfate reduction were measured in deeper sediment layers at the GI stations. Notably, SRR in the deep sediments of station 8 were higher than those measured in surface sediments from station 3. Despite substantial SRR, no hydrogen sulfide was detected at any depth.

Glacier run-off and sediment age are strong determinants of microbial community composition

In total, 6755 16S rRNA-OTUs and 1094 *dsrB*-OTUs were obtained by amplicon sequencing. NGI and GI sediments differed clearly in 16S rRNA gene and *dsrB* OTU composition and these differences increased with depth at NGI stations (Supplementary Figure S3 A and B). Mantel correlations with environmental factors revealed that the 16S rRNA- and *dsrB*-OTU compositions were mostly impacted by sediment age and C/N ratio of organic matter (Table 2). This indicated that the microbial communities at GI stations were affected by the prevalent physicochemical properties, i.e., high sedimentation and high C/N ratios (Supplementary Figure S2). In addition, some of the differences in 16S rRNA gene and *dsrB* OTU composition between GI sediments might be explained by sediment structure (i.e. density and porosity), TOC, TN, SRR and Fe^{2+} concentrations (the latter two parameters were only significant for the 16S rRNA gene OTU data) (Table 2). Gradually increasing sediment age with depth at NGI stations (Supplementary Figure S2) was associated with increased 16S rRNA gene and *dsrB* beta-diversity (Supplementary Figure S3 A and B).

16S rRNA gene and *dsrB* alpha-diversity at the NGI stations gradually decreased with depth (Supplementary Figure S3 C and D). In contrast, alpha-diversity in GI stations remained rather high with increasing depth to approximately 600 cmbsf (Supplementary Figure S3 C and D). Accordingly, relative abundance patterns of most phyla/classes and DsrAB families at stations 5 and 8 did not follow a gradual change in compositions with increasing sediment depth like at stations 3 and 6, but remained rather constant, with some fluctuations between taxa (Figure 1). *Alpha-*, *Delta-*, and *Gammaproteobacteria, Campylobacterota and Cyanobacteria* were overall more abundant at GI sediments as compared to NGI sediments (Figure 1 A). Furthermore, the *dsrAB*-containing community in GI sediments had higher relative abundances of *Desulfobacteraceae*,

Desulfobulbaceae, uncultured DsrAB family-level lineages 4, 7, and 9 and unclassified DsrAB sequences from the *Firmicutes* group and the *Nitrospira* supercluster (Figure 1 B). At NGI stations, several phyla/classes (*Acidobacteria*, *Bacteroidetes*, *Deltaproteobacteria*, *Dependentiae* (TM6), *Gammaproteobacteria, Omnitrophica* (OP3), *Planctomycetes* and *Woesarchaeota* (DHVEG-6); including taxa that were more abundant at GI stations) decreased in relative abundance with depth, particularly at station 3 (Figure 1 A). The phyla *Atribacter* (JS1), *Aerophobetes* (BHI80−139), *Aminicenantes* (OP8), *Alphaproteobacteria, Betaproteobacteria*, *Chloroflexi* increased in relative 16S rRNA gene abundance with depth at both NGI stations. Subsurface *Bathyarchaeota* were found in deeper sediments at station 3 but there overall relative abundance was below one percent. The relative abundance of the following *dsrAB*-containing groups decreased with depth at NGI stations; *Desulfobacteraceae*, *Syntrophobacteraceae*, the uncultured family-level lineages 7 and 9, and uncultured bacteria within the Environmental supercluster 1 (Figure 1 B). In contrast, representatives of the uncultured family-level lineage 3, as well as uncultured bacteria within the *Deltaproteobacteria* supercluster and the *Firmicutes* group increased in relative abundance with depth at the NGI stations.

SRR-correlated OTUs have high inter-species connectivity in young sediments

Correlation network analyses of 16S rRNA- and *dsrB*-OTUs were performed to highlight potential synergistic interactions between microbial community members. Network analyses revealed two nearly separated 16S rRNA-OTU clusters and two completely separated *dsrB*-OTU clusters, which were structured along a sediment age gradient (Figure 2 A and B). One cluster included OTUs that were most abundant in old NGI sediments and the other one included OTUs that were most abundant in young GI and NGI sediments. These separate network clusters in ‘young’ and ‘old’ sediments largely overlapped with regions of particularly high inter-species OTU correlations. The separation of these ‘young’ and ‘old’ sediment OTU clusters corresponds to a sediment age of around 300-400 years (Figure 2 C and D).

The OTUs in the 16S rRNA gene and *dsrB* networks were additionally subjected to correlation analyses with environmental parameters (Supplementary Figures S4 and S5). The ‘young’ and ‘old’ sediment clusters consisted mainly of OTUs that were positively correlated with SRR and sediment age, respectively (Figure 2 A and B). Notably, most OTUs that correlated positively with SRR also correlated negatively with sediment age and vice versa (Supplementary Figures S4 and S5). SRR-correlated OTUs showed distinct distributions in relative abundances i.e., highest abundances in the surface sediments of NGI stations and mostly ubiquitous distributions throughout the whole core at GI stations (Figure 3). Many of these 16S rRNA-OTUs (n=10) and most of the *dsrB*-OTUs belonged to the family *Desulfobacteraceae* (Supplementary Figures S6 and S7). Other SRR-correlated 16S rRNA-OTUs belonged to the families *Desulfobulbaceae*, *Desulfarculaceae,* and *Syntrophobacteraceae* and to the phyla/classes *Acidobacteria*, *Actinobacteria*,

Alphaproteobacteria, *Bacteroidetes*, *Ignavibacteria*, *Gammaproteobacteria*, *Planctomycetes,* and *Woesarchaeota* (Supplementary Figure S6). Besides the prevalence of *Desulfobacteraceae,* SRR-correlated *dsrB*-OTUs were affiliated with the uncultured family-level lineages 7 and 9 (Supplementary Figure S7). The *dsrB*-OTUs 40 and 41 were also affiliated with the Environmental Supercluster 1. Interestingly, OTU 40 belonged to a sequence cluster of uncultured bacteria, and was related to a *Chloroflexi* metagenome bin (Supplementary Figure S7).

Sediment age-correlated OTUs were affiliated with diverse taxa (Figure 4). The phyla/classes that were represented by at least two age-correlated 16S rRNA-OTUs were *Aerophobetes* (BHI80−13), *Alphaproteobacteria*, *Aminicenantes* (OP8), *Atribacter* (JS1), *Chloroflexi*, *Deltaproteobacteria*, *Euryarchaeota* (Marine Benthic Group D)*, Omnitrophica* (OP3), and *Planctomycetes* (Supplementary Figure S6). Three age-correlated *dsrB*-OTUs were affiliated to the family *Desulfobacteraceae* (Supplementary Figure S7). OTU 16 belonged to a group of uncultured bacteria in the *Deltaproteobacteria* supercluster, OTU 58 could only be assigned to the *Firmicutes* group, and OTU 1 was affiliated with the family *Syntrophobacteraceae*.

Discussion

Glacier-runoff affects age-depth relationships and microbial community assembly in marine sediments

Rates and amounts of glacial inputs into sedimentary environments of fjords have a major impact on their biogeochemistry (Glombitza *et al.*, 2015). Here, we compared microbial community structure between NGI and GI sediments, and highlight the environmental factors that underlie the observed differences in community assembly with sediment depth. 16S rRNA gene and *dsrB* diversity were mainly structured along the sediment age gradients and C/N ratios in GI sediments (Table 2), which resulted in separate clustering of microbial communities from NGI and GI sediments (Supplementary Figure S3 A and B). Sulfate is the key terminal electron acceptor in marine sediments of the Godthåbsfjord (Sørensen *et al.*, 2015), but the connection between depth, SRR, and community structure differed between NGI and GI sediments.

In NGI sediments, steep gradients of SRR indicated that most of the labile organic matter deposited from marine primary production is mineralized at the seafloor surface (Flury *et al.*, 2016; Røy *et al.*, 2012). Microbial communities in NGI sediments became less diverse with depth (Supplementary Figure S3 C and D) and increasingly distinct from the surface communities (Supplementary Figure S3 A and B). These shifts in community composition with depth were attributed to increasing sediment age (Table 2), and are likely the result of highly selective survival of surface community members during long-term burial into subsurface sediments (Petro *et al.*, 2017).

In contrast, the two GI sediments were characterized by higher sedimentation rates as indicated by low porosity (station 8), young ages, and high C/N ratios (Supplementary Figure S2); the latter being caused by influx of terrestrial organic matter (Meyers, 1994; Goñi *et al.*, 2013; Wehrmann *et al.*, 2014). However, terrestrial organic matter transported by the glacier is diagenetically altered and likely unavailable for microbial degradation (Wehrmann *et al.*, 2014). On average higher SRR throughout the GI sediment cores were thus possibly sustained by reactive organic matter that was deposited from algal blooms in nutrient-rich waters of glaciated fjords (Bourgeois *et al.*, 2016; Smith *et al.*, 2015). Glacier runoff also contains considerable amounts of iron and manganese (Bhatia *et al.*, 2013; Wehrmann *et al.*, 2014). Accumulation of dissolved Fe^{2+} suggested that Fe(III) reduction contributed to organic matter mineralization in upper GI station sediments (Supplementary Figure S2). Lack of sulfide accumulation with depth indicated immediate re-oxidation or scavenging of sulfide produced from high sulfate reduction activity (Supplementary Figure S2). In agreement with previous research (Bourgeois *et al.*, 2016; Park *et al.*, 2011), higher rates of sedimentation had a major influence on the composition of the seafloor microbial community in glaciated fjords.

Identities and potential functional interactions of sulfur cycling-associated taxa

16S rRNA gene and *dsrB* correlation network analyses (Weiss *et al.*, 2016) revealed two main OTU interaction clusters in both amplicon sequence datasets (Figure 2). Each cluster was predominantly and exclusively composed of either SRR- or sediment age-correlated OTUs. The relative abundances of SRR-correlated OTUs were highest in 'young' sediments (up to about 400 years of age), i.e. they were present at high abundances throughout the sediment cores at GI stations and only in surface sediments at NGI stations (Figure 3).

Most SRR-correlated 16S rRNA gene- and *dsrB*-OTUs were affiliated with the family *Desulfobacteraceae* as well as other *bona fide* deltaproteobacterial SRM taxa from marine sediments (Wasmund *et al.*, 2017) (Figure 3). In addition, several SRR-correlated *dsrB*-OTUs were affiliated with uncultured DsrAB lineages. Some of these lineages contain metagenome-derived sequences of uncultivated bacteria from the phyla *Acidobacteria* (DsrAB family-level lineage 9), *Planctomycetes* or *Chloroflexi* (Supplementary Figure S7) (Anantharaman *et al.*, 2017; Wasmund *et al.*, 2016). Interestingly, also several SRR-correlated 16S rRNA-OTUs were affiliated with these phyla, supporting their putative involvement in sulfite/sulfate reduction in the Godthåbsfjord sediments.

Rapid oxidation of sulfide apparently contributed to active sulfur-cycling in deep GI station sediments. Since oxygen and nitrate are typically depleted within millimeters to few centimeters of the sediment surface (Froelich *et al.*, 1979; Thamdrup *et al.*, 1994), abiotic or biotic sulfide oxidation is likely linked to reduction of metals (Wehrmann *et al.*, 2014). Several SRR-correlated 16S rRNA-OTUs were affiliated with taxa containing sulfur-

oxidizing microorganisms (SOM) such as the candidate genus PHOS-HE36 (phylum *Ignavibacteriae*) (Koenig *et al.*, 2005), the *Woeseiaceae*/JTB255 sediment group (*Gammaproteobacteria*) (Dyksma *et al.*, 2016; Mußmann *et al.*, 2017), and the *Rhodobacteriaceae* (*Alphaproteobacteria*) (Lenk *et al.*, 2012; Thrash *et al.*, 2017) (Supplementary Figure S6). In addition, OTU 30 affiliated with the SOM genus *Sulfurovum* (Supplementary Figure S6) was solely responsible for the high relative abundance of *Campylobacterota* at GI station 5 (Figure 2 A).

We also identified numerous SRR-correlated OTUs that were affiliated with taxa not known to have a sulfur-based energy metabolism. While these OTUs could represent new sulfur-cycling microorganisms, they may also be degraders of organic matter that fuel sulfate reduction with fermentation products. For instance, some SRR-correlated 16S rRNA-OTUs were affiliated with BD2-2 (phylum *Bacteroidetes*), *Phycisphaera* (phylum *Planctomycetes*) or OM1 (phylum *Actinobacteria*) (Supplementary Figure S6). Representatives of these phyla hydrolyze and ferment organic polymers in marine sediments and are able to form syntrophic associations with SRM (Baker *et al.*, 2015; Schauer *et al.*, 2011; Trembath-Reichert *et al.*, 2016; Webster *et al.*, 2011).

Microbiota transitions from young to old sediments and assembly of a deep subsurface biosphere in NGI sediments

OTU correlation analysis showed that OTU clusters, and thus the microbial communities of young and old sediment zones in NGI sediments became ‘disconnected’ at a sediment age of about 300-400 years (Figure 2 C and D). This age corresponds to a sediment depth of approximately 30-40 and 20-30 cmbsf at stations 3 and 6, respectively. This is in line with observations that a considerably shift in microbial community structure occurs in marine sediments at the transition from surface sediments into deeper sediment zones (Starnawski *et al.*, 2017; Jochum *et al.*, 2017). It was hypothesized that bioturbation in the sediment surface introduces fresh organic matter that supports SRM activity and that the transition to the unmixed sediment below is a main site of assembly of the subsurface SRM community (Jochum *et al.*, 2017). Most sediment age-correlated OTUs in NGI sediments were affiliated with taxa known to harbour members that selectively persist from the surface into deep subsurface sediments, e.g., *Chloroflexi*, *Aerophobetes*, *Atribacter* (JS1), *Aminicenantes* (OP8), *Alphaproteobacteria,* and *Deltaproteobacteria* (Figure 4) (Orcutt *et al.*, 2011; Wang *et al.*, 2016). Members of these taxa, such as the genus *Desulfatiglans* (Starnawski *et al.*, 2017; Jochum *et al.*, 2017), the deltaproteobacterial candidate lineage SEEP-SRB1 (Schreiber *et al.*, 2010) or the euryarchaeal Marine Benthic Group D (Kaster *et al.*, 2014; Lloyd *et al.*, 2013; Nobu *et al.*, 2016; Robbins *et al.*, 2016; Wasmund *et al.*, 2014; Wang *et al.*, 2016) are postulated to have the necessary traits, such as fermentation, sulfate reduction or acetogenesis, to cope with the energy-limitations in most subsurface sediment environments. Although the *in situ* physiology of these OTUs is unknown, some might be involved in

organoclastic sulfate reduction that is sustained throughout the NGI sediment cores (Glombitza *et al.*, 2015).

Conclusions

Coastal marine ecosystems in arctic and sub-arctic oceans are poised for being increasingly impacted by climate change-induced melting of glaciers. In this comparative study, we found that glacier runoff was a main determinant of the depth-dependent microbial community assembly in GI and NGI sediments of a sub-arctic fjord. Increasing differences in community composition between GI and NGI sediments with depth were largely explained by sediment age. High sedimentation rates enabled a complex community of SRR-correlated microorganisms to continuously thrive at high relative abundances from the surface deep into GI sediments. Similar communities of SRR-correlated microorganisms were also present in the surface of NGI sediments. However, these very active sulfur-cycling-associated surface communities were largely replaced by sediment age-correlated microorganisms that selectively survived burial into the more energy-limited subsurface of NGI sediments. In summary, our results suggest that increased glacier runoff promotes higher sedimentation rates that allow abundant surface processes and associated community members to be rapidly buried and maintained at high abundances in deep subsurface sediments.

Acknowledgments

The authors would like to thank the crew of the R/V Sanna and the scientific party during the 2013 campaign. The cruise was funded by the Arctic Research Centre, Aarhus University and led by Marit-Solveig Seidenkranz. This work was financially supported by the Austrian Science Fund (P29426-B29 to KW; P25111-B22 to AL) with additional funding by the Independent Research Fund Denmark / Natural Science (G-Ice project grant no 7014-00113B/FNU). The authors declare no conflict of interest.

Tables

Table 1. Description of the sampling stations and cores, including sampling position, water depth and core length. Table was modified from Glombitza *et al.*, 2015. The exact location of the sampling stations is indicated in Supplementary Figure S1.

Station	Core name	Latitude (N)	Longitude (W)	Water depth [m]	Core length [cm]
3	SA13-ST3-20G	6426.7425'	5247.6486'	498.2	587
5	A13-ST5-30G	6425.3479'	5130.6209'	622.4	607
6	SA13-ST6-40G	6429.0604'	5042.3240'	389	562
8	SA13-ST8-47G	6440.7078'	5017.4672'	475.8	569

Table 2. Mantel correlations between 16S rRNA gene and *dsrB* community compositions and physicochemical parameters. Only significant values ($p < 0.05$) are shown in the table. Parameters with the strongest effect on the 16S rRNA gene or *dsrB* community compositions are indicated in bold.

	16S rRNA gene		***dsrB***	
	Mantel statistic	p-value	Mantel statistic	p-value
Sediment age [actual years]	**0.380**	0.003	**0.538**	0.002
Sulfate [mmol L^{-1}]	0.179	0.016	0.390	0.002
DIC [mmol L^{-1}]	0.108	0.047	0.207	0.010
H_2S [µmol L^{-1}]	0.227	0.003	0.418	0.002
Fe^{2+} [µmol L^{-1}]	0.262	0.003	-	-
Density [g cc^{-1}]	0.234	0.003	0.349	0.002
Porosity	0.213	0.003	0.364	0.002
TOC [µmol g dw^{-1}]	0.228	0.005	0.329	0.002
C/N ratio	**0.471**	0.003	**0.478**	0.002
SRR [nmol Sulfate cm^{-3} d^{-1}]	0.260	0.003	-	-
Methane [µmol L^{-1}]	-	-	0.310	0.002

DIC, dissolved inorganic carbon; TOC, total organic carbon; SRR, sulfate reduction rate

References

Anantharaman, K., Jungbluth, S. P., Kantor, R. S., Lavy, A., Warren, L. A., Rappé, M. S., *et al.* (2017) Dramatic expansion of microbial groups that shape the global sulfur cycle. *ISME J.* **12**: 1715-1728.

Arndt, S., Jørgensen, B. B., LaRowe, D. E., Middelburg, J. J., Pancost, R. D., and Regnier, P. (2013) Quantifying the degradation of organic matter in marine sediments: A review and synthesis. *Earth-Sci. Rev.* **123**: 53–86.

Aronesty, E. (2013) Comparison of Sequencing Utility Programs. *Open Bioinforma. J.* **7**: 1–8.

Baker, B. J., Lazar, C. S., Teske, A. P., and Dick, G. J. (2015) Genomic resolution of linkages in carbon, nitrogen, and sulfur cycling among widespread estuary sediment bacteria. *Microbiome* **3**: 14.

Berger, S. A., Krompass, D., and Stamatakis, A. (2011) Performance, accuracy, and Web server for evolutionary placement of short sequence reads under maximum likelihood. *Syst. Biol.* **60**: 291–302.

Berry, D., and Widder, S. (2014) Deciphering microbial interactions and detecting keystone species with co-occurrence networks. *Front. Microbiol.* **5**: 219.

Bhatia, M. P., Kujawinski, E. B., Das, S. B., Breier, C. F., Henderson, P. B., and Charette, M. A. (2013) Greenland meltwater as a significant and potentially bioavailable source of iron to the ocean. *Nat. Geosci.* **6**: 503–503.

Bourgeois, S., Kerhervé, P., Calleja, M. L., Many, G., and Morata, N. (2016) Glacier inputs influence organic matter composition and prokaryotic distribution in a high Arctic fjord (Kongsfjorden, Svalbard) *J. Mar. Syst.* **164**: 112–127.

Bower, C.E. and Holm-Hansen, T. (1980) A Salicylate–Hypochlorite Method for Determining Ammonia in Seawater. Can. J. Fish. Aquat. Sci. **37**: 794–798.

Dansk-Standard. (1975) DS 224: Vandundersøgelse. Bestemmelse af ammonium-nitrogen. 6 pp.

Dyksma, S., Bischof, K., Fuchs, B. M., Hoffmann, K., Meier, D., Meyerdierks, A., *et al.* (2016) Ubiquitous Gammaproteobacteria dominate dark carbon fixation in coastal sediments. *ISME J.* **10**:1939–1953.

Edgar, R. C. (2010) Search and clustering orders of magnitude faster than BLAST. *Bioinformatics* **26**: 2460–2461.

Edgar, R. C. (2013) UPARSE: highly accurate OTU sequences from microbial amplicon reads. *Nat. Methods* **10**: 996–998.

Etherington, L. L., Hooge, P. N., Hooge, E. R., and Hill, D. F. (2007) Oceanography of Glacier Bay, Alaska: Implications for biological patterns in a glacial fjord estuary. *Estuaries Coasts* **30**: 927–944.

Flury, S., Røy, H., Dale, A. W., Fossing, H., Tóth, Z., Spiess, V., *et al.* (2016) Controls on subsurface methane fluxes and shallow gas formation in Baltic Sea sediment (Aarhus Bay, Denmark). *Geochim. Cosmochim. Acta* **188**: 297–309.

Flynn, W. (1968) The determination of low levels of polonium-210 in environmental materials. *Anal. Chim. Acta* **43**: 221-226.

Friedman, J., and Alm, E. J. (2012) Inferring Correlation Networks from Genomic Survey Data. *PLoS Comput. Biol.* **8**: e1002687.

Froelich, P. N., Klinkhammer, G. P., Bender, M. L., Luedtke, N. A., Heath, G. R., Cullen, D., *et al.* (1979) Early oxidation of organic matter in pelagic sediments of the eastern equatorial Atlantic: suboxic diagenesis. *Geochim. Cosmochim. Acta* **43**: 1075–1090.

Glombitza, C., Jaussi, M., Røy, H., Seidenkrantz, M.-S., Lomstein, B. A., and Jørgensen, B. B. (2015) Formate, acetate, and propionate as substrates for sulfate reduction in sub-arctic sediments of Southwest Greenland. *Front. Microbiol.* **6**: 846.

Goñi, M. A., O'Connor, A. E., Kuzyk, Z. Z., Yunker, M. B., Gobeil, C., and Macdonald, R. W. (2013) Distribution and sources of organic matter in surface marine sediments across the North American Arctic margin. *J. Geophys. Res. C: Oceans* **118**: 4017–4035.

Hausmann, B., Pelikan, C., Herbold, C. W., Köstlbacher, S., Albertsen, M., Eichorst, S. A., *et al.* (2018) Peatland Acidobacteria with a dissimilatory sulfur metabolism. *ISME J.* **12**: 1729-1742.

Herbold, C. W., Pelikan, C., Kuzyk, O., Hausmann, B., Angel, R., Berry, D., *et al.* (2016) Corrigendum: A flexible and economical barcoding approach for highly multiplexed amplicon sequencing of diverse target genes. *Front. Microbiol.* **7**: 870.

Hop, H., Pearson, T., Hegseth, E. N., Kovacs, K. M., Wiencke, C., Kwasniewski, S., *et al.* (2002) The marine ecosystem of Kongsfjorden, Svalbard. *Polar Res.* **21**: 167–208.

Jochum, L. M., Chen, X., Lever, M. A., Loy, A., Jørgensen, B. B., Schramm, A., *et al.* (2017) Depth Distribution and Assembly of Sulfate-Reducing Microbial Communities in Marine Sediments of Aarhus Bay. *Appl. Environ. Microbiol.* **83**: e01547-17.

Kaster, A.-K., Mayer-Blackwell, K., Pasarelli, B., and Spormann, A. M. (2014) Single cell genomic study of Dehalococcoidetes species from deep-sea sediments of the Peruvian Margin. *ISME J.* **8**: 1831–1842.

Katoh, K., Misawa, K., Kuma, K.-I., and Miyata, T. (2002) MAFFT: a novel method for rapid multiple sequence alignment based on fast Fourier transform. *Nucleic Acids Res.* **30**: 3059–3066.

Kjeldsen, K. U., Loy, A., Jakobsen, T. F., Thomsen, T. R., Wagner, M., and Ingvorsen, K. (2007) Diversity of sulfate-reducing bacteria from an extreme hypersaline sediment, Great Salt Lake (Utah). *FEMS Microbiol. Ecol.* **60**: 287–298.

Klindworth, A., Pruesse, E., Schweer, T., Peplies, J., Quast, C., Horn, M., *et al.* (2013) Evaluation of general 16S ribosomal RNA gene PCR primers for classical and next-generation sequencing-based diversity studies. *Nucleic Acids Res.* **41**: e1.

Koenig, A., Zhang, T., Liu, L.-H., and Fang, H. H. P. (2005) Microbial community and biochemistry process in autosulfurotrophic denitrifying biofilm. *Chemosphere* **58**: 1041–1047.

Kuzyk Z. A., Macdonald, R. W. and Johannessen, S. C. (2015) Calculating Rates and Dates and Interpreting Contaminant Profiles in Biomixed Sediments. In: *Developments in Paleoenvironmental Research*., pp. 61–87.

Laufer, K., Byrne, J. M., Glombitza, C., Schmidt, C., Jørgensen, B. B., and Kappler, A. (2016) Anaerobic microbial Fe(II) oxidation and Fe(III) reduction in coastal marine sediments controlled by organic carbon content. *Environ. Microbiol.* **18**: 3159–3174.

Lavelle J. W., Massoth, G. J. and Crecelius, E. A. (1985) Sedimentation rates in Puget Sound from ^{210}Pb measurements. NOAA Technical Memorandum ERL PMEL-61. Pacific Marine Environmental Laboratory, Seattle, WA. 43 pp.

Lenk, S., Moraru, C., Hahnke, S., Arnds, J., Richter, M., Kube, M., *et al.* (2012) Roseobacter clade bacteria are abundant in coastal sediments and encode a novel combination of sulfur oxidation genes. *ISME J.* **6**: 2178–2187.

Letunic, I., and Bork, P. (2007) Interactive Tree Of Life (iTOL): an online tool for phylogenetic tree display and annotation. *Bioinformatics* **23**: 127–128.

Lloyd, K. G., Schreiber, L., Petersen, D. G., Kjeldsen, K. U., Lever, M. A., Steen, A. D., *et al.* (2013) Predominant archaea in marine sediments degrade detrital proteins. *Nature* **496**: 215–218.

McMurdie, P. J., and Holmes, S. (2013) phyloseq: An R Package for Reproducible Interactive Analysis and Graphics of Microbiome Census Data. *PLoS One* **8**: e61217.

Meire, L., Søgaard, D. H., Mortensen, J., Meysman, F. J. R., Soetaert, K., Arendt, K. E., *et al.* (2015) Glacial meltwater and primary production are drivers of strong CO_2 uptake in fjord and coastal waters adjacent to the Greenland Ice Sheet. *Biogeosciences* **12**: 2347–2363.

Meyers, P. A. (1994) Preservation of elemental and isotopic source identification of sedimentary organic matter. *Chem. Geol.* **114**: 289–302.

Müller, A. L., Kjeldsen, K. U., Rattei, T., Pester, M., and Loy, A. (2015) Phylogenetic and environmental diversity of DsrAB-type dissimilatory (bi)sulfite reductases. *ISME J.* **9**: 1152–1165.

Müller, A. L., Pelikan, C., de Rezende, J. R., Wasmund, K., Putz, M., Glombitza, C., *et al.* (2018) Bacterial interactions during sequential degradation of cyanobacterial necromass in a sulfidic arctic marine sediment. *Environ. Microbiol.* **20**: 2927–2940.

Mußmann, M., Pjevac, P., Krüger, K., and Dyksma, S. (2017) Genomic repertoire of the Woeseiaceae/JTB255, cosmopolitan and abundant core members of microbial communities in marine sediments. *ISME J.* **11**: 1276–1281.

Nepusz, T., Yu, H., and Paccanaro, A. (2012) Detecting overlapping protein complexes in protein-protein interaction networks. *Nat. Methods* **9**: 471–472.

Nobu, M. K., Dodsworth, J. A., Murugapiran, S. K., Rinke, C., Gies, E. A., Webster, G., *et al.* (2016) Phylogeny and physiology of candidate phylum "Atribacteria" (OP9/JS1) inferred from cultivation-independent genomics. *ISME J.* **10**: 273–286.

Oksanen, J., Blanchet, F. G., Friendly, M., Kindt, R., Legendre, P., McGlinn, D., *et al.* (2017) vegan: Community Ecology Package. *Available online at: http:// CRAN.R-project.org/package=vegan.*

Orcutt, B. N., Sylvan, J. B., Knab, N. J., and Edwards, K. J. (2011) Microbial ecology of the dark ocean above, at, and below the seafloor. *Microbiol. Mol. Biol. Rev.* **75**: 361–422.

Orsi, W. D., Richards, T. A., and Francis, W. R. (2018) Predicted microbial secretomes and their target substrates in marine sediment. *Nat. Microbiol.* **3**: 32–37.

Parks, D. H., Rinke, C., Chuvochina, M., Chaumeil, P.-A., Woodcroft, B. J., Evans, P. N., *et al.* (2017) Recovery of nearly 8,000 metagenome-assembled genomes substantially expands the tree of life. *Nat. Microbiol.* **2**: 1533–1542.

Park, S.-J., Park, B.-J., Jung, M.-Y., Kim, S.-J., Chae, J.-C., Roh, Y., *et al.* (2011) Influence of deglaciation on microbial communities in marine sediments off the coast of Svalbard, Arctic Circle. *Microb. Ecol.* **62**: 537–548.

Pelikan, C., Herbold, C. W., Hausmann, B., Müller, A. L., Pester, M., and Loy, A. (2016) Diversity analysis of sulfite- and sulfate-reducing microorganisms by multiplex dsrA and dsrB amplicon sequencing using new primers and mock community-optimized bioinformatics. *Environ. Microbiol.* **18**: 2994–3009.

Petro, C., Starnawski, P., Schramm, A., and Kjeldsen, K. U. (2017) Microbial community assembly in marine sediments. *Aquat. Microb. Ecol.* **79**: 177–195.

Phillips E. J. P. and Lovley, D. R. (1987) Determination of Fe(III) and Fe(II) in oxalate extracts of sediments. *Soil Sci. Soc. of Am. J.* **51**: 938-941.

Price, M. N., Dehal, P. S., and Arkin, A. P. (2010) FastTree 2 – Approximately Maximum-Likelihood Trees for Large Alignments. *PLoS One* **5**: e9490.

Pruesse, E., Peplies, J., and Glöckner, F. O. (2012) SINA: accurate high-throughput multiple sequence alignment of ribosomal RNA genes. *Bioinformatics* **28**: 1823–1829.

Quast, C., Pruesse, E., Yilmaz, P., Gerken, J., Schweer, T., Yarza, P., *et al.* (2013) The SILVA ribosomal RNA gene database project: improved data processing and web-based tools. *Nucleic Acids Res.* **41**: D590–6.

R Core Team (2015) R: The R Project for Statistical Computing. *Available online at: http://www.r-project.org/.*

Ramsey C. B. (2008) Deposition models for chronological records. *Quat. Sci. Rev.* **27**: 42-60.

Reimer P. J., Bard, E., Bayliss, A., Beck, J. W., Blackwell, P. G., Ramsey, C. B., *et al.* (2013) IntCal13 and Marine13 radiocarbon age calibration curves 0–50,000 years cal BP. Radiocarbon **55**: 1869-1887.

Robbins, S. J., Evans, P. N., Parks, D. H., Golding, S. D., and Tyson, G. W. (2016) Genome-Centric Analysis of Microbial Populations Enriched by Hydraulic Fracture Fluid Additives in a Coal Bed Methane Production Well. *Front. Microbiol.* **7**: 731.

Røy, H., Kallmeyer, J., Adhikari, R. R., Pockalny, R., Jørgensen, B. B., and D'Hondt, S. (2012) Aerobic microbial respiration in 86-million-year-old deep-sea red clay. *Science* **336**: 922–925.

Schauer, R., Røy, H., Augustin, N., Gennerich, H.-H., Peters, M., Wenzhoefer, F., *et al.* (2011) Bacterial sulfur cycling shapes microbial communities in surface sediments of an ultramafic hydrothermal vent field. *Environ. Microbiol.* **13**: 2633–2648.

Schloss, P. D., Westcott, S. L., Ryabin, T., Hall, J. R., Hartmann, M., Hollister, E. B., *et al.* (2009) Introducing mothur: open-source, platform-independent, community-supported software for describing and comparing microbial communities. *Appl. Environ. Microbiol.* **75**: 7537–7541.

Schreiber, L., Holler, T., Knittel, K., Meyerdierks, A., and Amann, R. (2010) Identification of the dominant sulfate-reducing bacterial partner of anaerobic methanotrophs of the ANME-2 clade. *Environ. Microbiol.* **12**: 2327–2340.

Shannon, P., Markiel, A., Ozier, O., Baliga, N. S., Wang, J. T., Ramage, D., *et al.* (2003) Cytoscape: a software environment for integrated models of biomolecular interaction networks. *Genome Res.* **13**: 2498–2504.

Smith, R. W., Bianchi, T. S., Allison, M., Savage, C., and Galy, V. (2015) High rates of organic carbon burial in fjord sediments globally. *Nat. Geosci.* **8**: 450–453.

Sørensen, H. L., Meire, L., Juul-Pedersen, T., de Stigter, H. C., Meysman, F., Rysgaard, S., *et al.* (2015) Seasonal carbon cycling in a Greenlandic fjord: an integrated pelagic and benthic study. *Mar. Ecol. Prog. Ser.* **539**: 1–17.

Sørensen J. (1982) Reduction of ferric iron in anaerobic, marine sediment and interaction with reduction of nitrate and sulfate. *Applied and Environmental Microbiology* **43**: 319-324.

Stamatakis, A. (2014) RAxML version 8: a tool for phylogenetic analysis and post-analysis of large phylogenies. *Bioinformatics* **30**: 1312–1313.

Starnawski, P., Bataillon, T., Ettema, T. J. G., Jochum, L. M., Schreiber, L., Chen, X., *et al.* (2017) Microbial community assembly and evolution in subseafloor sediment. *Proc. Natl. Acad. Sci. U. S. A.* **114**: 2940–2945.

Statham, P. J., Skidmore, M., and Tranter, M. (2008) Inputs of glacially derived dissolved and colloidal iron to the coastal ocean and implications for primary productivity. *Global Biogeochem. Cycles* **22**: GB3013.

Stookey L. L. (1970) Ferrozine - a new spectrophotometric reagent for iron. *Analytical Chemistry* **42**: 779-781.

Svendsen, H., Beszczynska-Møller, A., Hagen, J. O., Lefauconnier, B., Tverberg, V., Gerland, S., *et al.* (2002) The physical environment of Kongsfjorden–Krossfjorden, an Arctic fjord system in Svalbard. *Polar Res.* **21**: 133–166.

Teske, A., Durbin, A., Ziervogel, K., Cox, C., and Arnosti, C. (2011) Microbial community composition and function in permanently cold seawater and sediments from an arctic fjord of svalbard. *Appl. Environ. Microbiol.* **77**: 2008–2018.

Thamdrup, B., Fossing, H., and Jørgensen, B. B. (1994) Manganese, iron and sulfur cycling in a coastal marine sediment, Aarhus bay, Denmark. *Geochim. Cosmochim. Acta* **58**: 5115–5129.

Thrash, J. C., Seitz, K. W., Baker, B. J., Temperton, B., Gillies, L. E., Rabalais, N. N., *et al.* (2017) Metabolic Roles of Uncultivated Bacterioplankton Lineages in the Northern Gulf of Mexico “Dead Zone.” *MBio* **8**: e01017–17.

Trembath-Reichert, E., Case, D. H., and Orphan, V. J. (2016) Characterization of microbial associations with methanotrophic archaea and sulfate-reducing bacteria through statistical comparison of nested Magneto-FISH enrichments. *PeerJ* **4**: e1913.

Wang, Q., Garrity, G. M., Tiedje, J. M., and Cole, J. R. (2007) Naive Bayesian classifier for rapid assignment of rRNA sequences into the new bacterial taxonomy. *Appl. Environ. Microbiol.* **73**: 5261–5267.

Wang, Y., Gao, Z.-M., Li, J.-T., Bougouffa, S., Tian, R. M., Bajic, V. B., *et al.* (2016) Draft genome of an Aerophobetes bacterium reveals a facultative lifestyle in deep-sea anaerobic sediments. *Sci Bull. Fac. Agric. Kyushu Univ.* **61**: 1176–1186.

Wasmund, K., Cooper, M., Schreiber, L., Lloyd, K. G., Baker, B. J., Petersen, D. G., *et al.* (2016) Single-Cell Genome and Group-Specific dsrAB Sequencing Implicate Mari ne Members of the Class Dehalococcoidia (Phylum Chloroflexi) in Sulfur Cycling. *MBio* **7**: e00266-16.

Wasmund, K., Mußmann, M., and Loy, A. (2017) The life sulfuric: microbial ecology of sulfur cycling in marine sediments. *Environ. Microbiol. Rep.* **9**: 323–344.

Wasmund, K., Schreiber, L., Lloyd, K. G., Petersen, D. G., Schramm, A., Stepanauskas, R., *et al.* (2014) Genome sequencing of a single cell of the widely distributed marine subsurface Dehalococcoidia, phylum Chloroflexi. *ISME J.* **8**: 383–397.

Webster, G., Sass, H., Cragg, B. A., Gorra, R., Knab, N. J., Green, C. J., *et al.* (2011) Enrichment and cultivation of prokaryotes associated with the sulphate-methane transition zone of diffusion-controlled sediments of Aarhus Bay, Denmark, under heterotrophic conditions. *FEMS Microbiol. Ecol.* **77**: 248–263.

Wehrmann, L. M., Formolo, M. J., Owens, J. D., Raiswell, R., Ferdelman, T. G., Riedinger, N., *et al.* (2014) Iron and manganese speciation and cycling in glacially influenced high-latitude fjord sediments (West Spitsbergen, Svalbard): Evidence for a benthic recycling-transport mechanism. *Geochim. Cosmochim. Acta* **141**: 628–655.

Wehrmann, L. M., Riedinger, N., Brunner, B., Kamyshny, A., Hubert, C. R. J., Herbert, L. C., *et al.* (2017) Iron-controlled oxidative sulfur cycling recorded in the distribution and isotopic composition of sulfur species in glacially influenced fjord sediments of west Svalbard. *Chem. Geol.* **466**: 678–695.

Weiss, S., Van Treuren, W., Lozupone, C., Faust, K., Friedman, J., Deng, Y., *et al.* (2016) Correlation detection strategies in microbial data sets vary widely in sensitivity and precision. *ISME J.* **10**: 1669–1681.

Zopfi, J., Ferdelman, T. G., and Fossing, H. (2004) Distribution and fate of sulfur intermediates—sulfite, tetrathionate, thiosulfate, and elemental sulfur—in marine sediments. In *Sulfur Biogeochemistry - Past and Present.* Amend, J.P., Edwards, K.J., and Lyons, T.W. (eds). Boulder Colorado, USA: Geological Society of America, pp. 97–116.

Figure 1

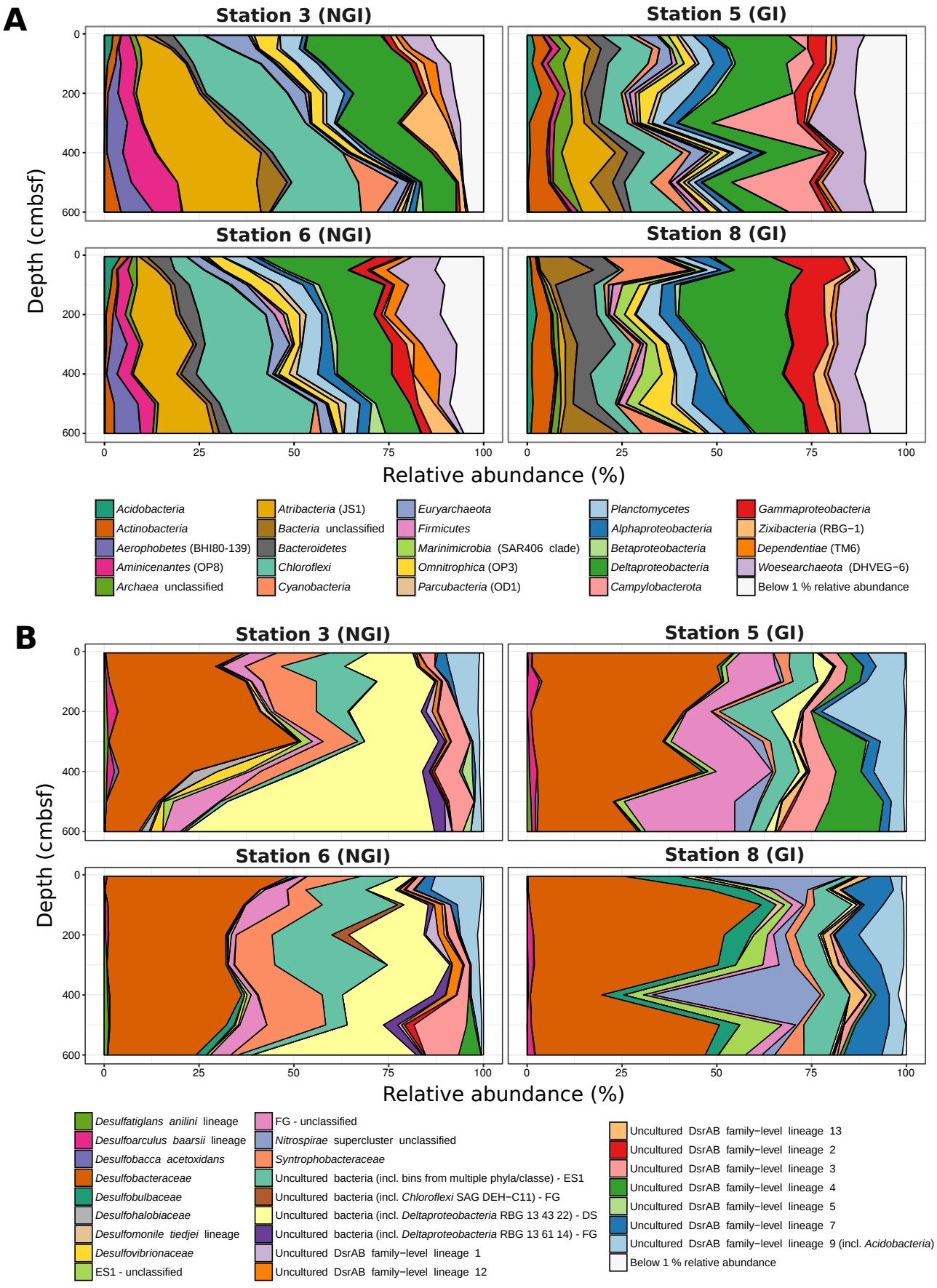

Figure 1. Microbial community composition in non-glacier-influenced (NGI) and glacier-influenced (GI) sediment cores. Indicated are gradual changes in 16S rRNA phylum/class (A) and DsrAB-family (B) abundances with sediment depth. Only phyla/classes and DsrAB-families with a relative abundance above 1 % are shown. DS, *Deltaproteobacteria* supercluster. ES1, Environmental supercluster 1. FG, *Firmicutes* group. NS, *Nitrospira* supercluster.

Figure 2

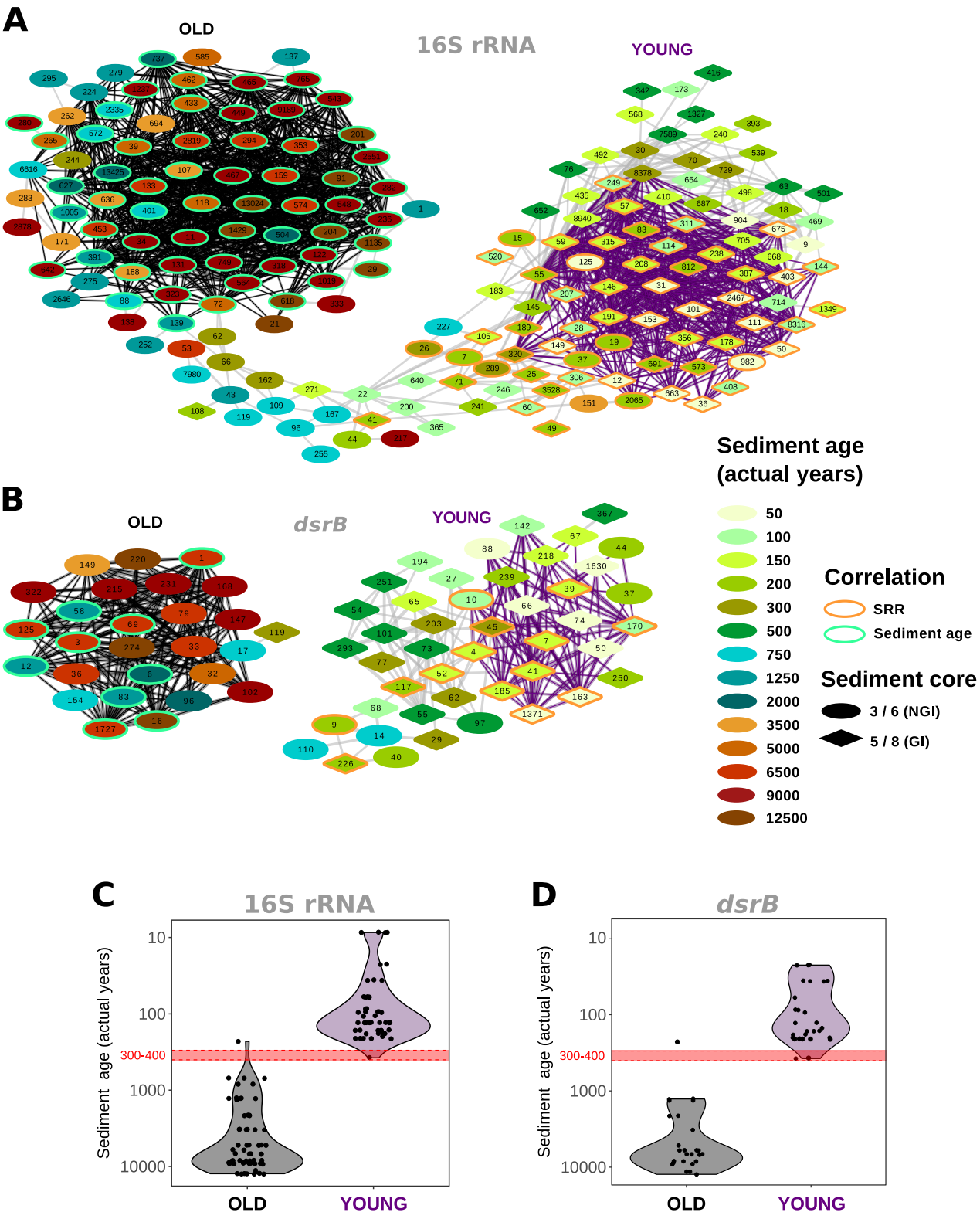

Figure 2. Co-occurrence of abundant OTUs across non-glacier-influenced (NGI) and glacier-influenced (GI) sediment cores. Inter-species correlations are indicated for 16S rRNA gene (A) and *dsrB* (B) OTUs. Only edges with p ≤ 0.01 and an estimate value of ≥ 0.5 are shown. OTUs are colored and shaped according to the rounded sediment age and sampling station at which they were found at the highest relative abundance, respectively. The orange and green border color of OTUs indicates significant correlations to sulfate reduction rates and sediment age, respectively. OTUs that are connected by black and purple edges formed significant community clusters in old and young sediments, respectively. C and D, Sediment age at which OTUs of the significant community clusters were found at the highest relative abundance. Black and purple background colors indicate OTUs of the old and young community cluster, respectively.

Figure 3

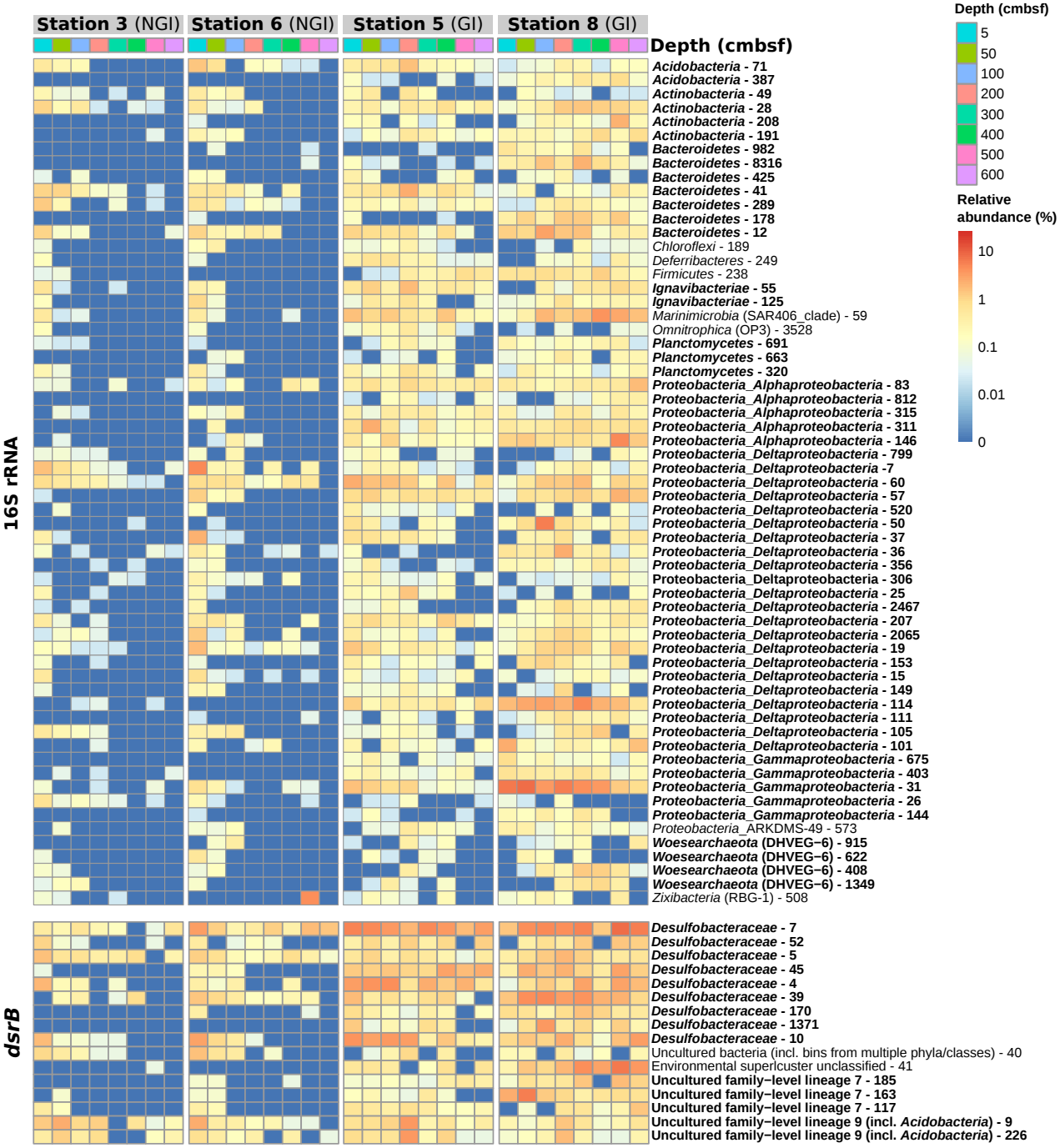

Figure 3. Relative abundance of 16S rRNA- and *dsrB*-OTUs with significant correlations to sulfate reduction in non-glacier-influenced (NGI) and glacier-influenced (GI) sediment cores. The column annotation indicates the sampling depth in centimeter below seafloor (cmbsf). The color range from blue to red indicates the relative abundance of OTUs. Phyla/classes and DsrAB-families that were represented by more than one OTU are indicated in bold.

Figure 4

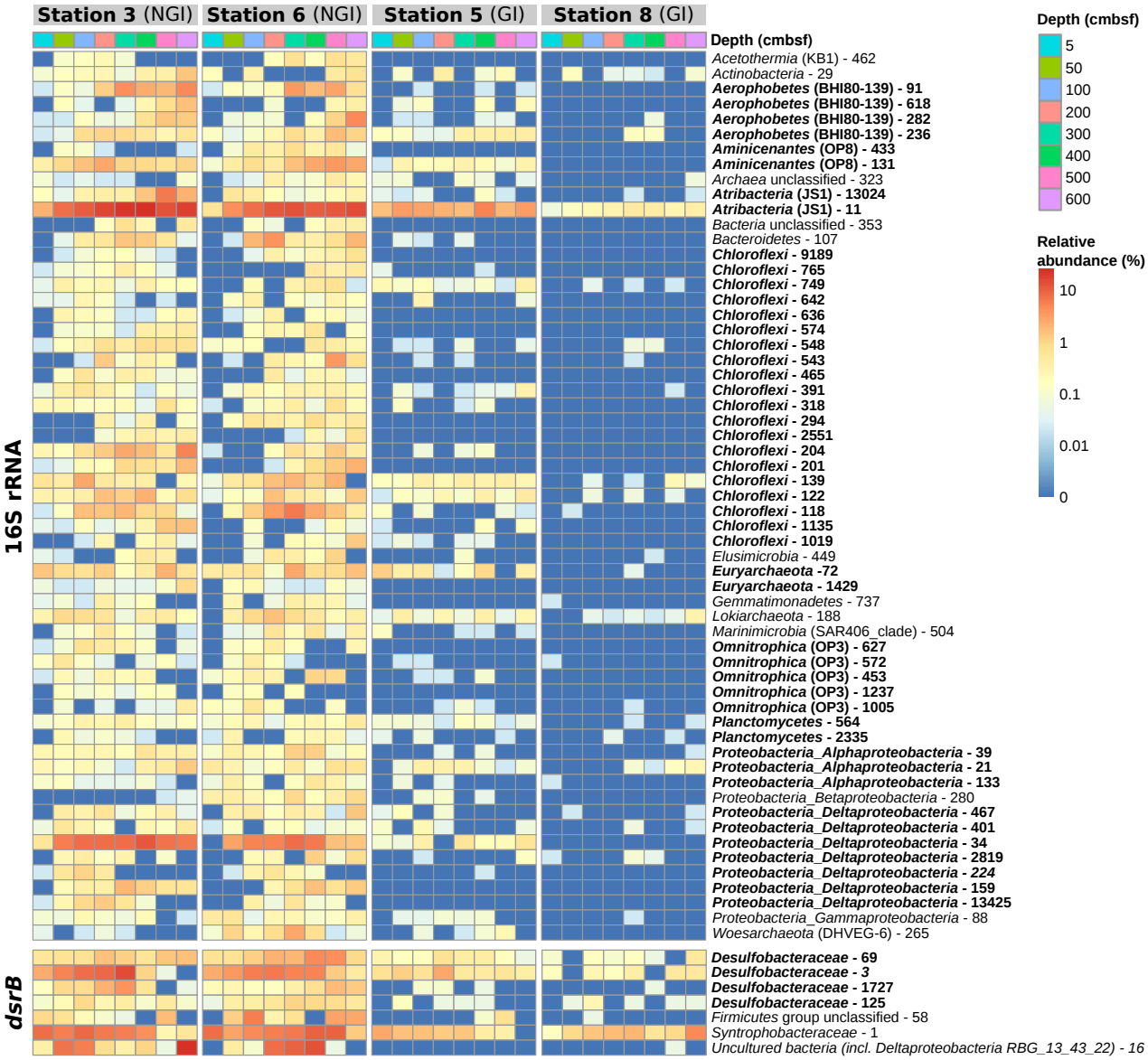

Figure 4. Relative abundance of 16S rRNA- and *dsrB*-OTUs with significant correlations to sediment age in non-glacier-influenced (NGI) and glacier-influenced (GI) sediment cores. The column annotation indicates the sampling depth in centimeter below seafloor (cmbsf). The color range from blue to red indicates the relative abundance of OTUs. Phyla/classes and DsrAB-families that were represented by more than one OTU are indicated in bold.

Supplementary Information

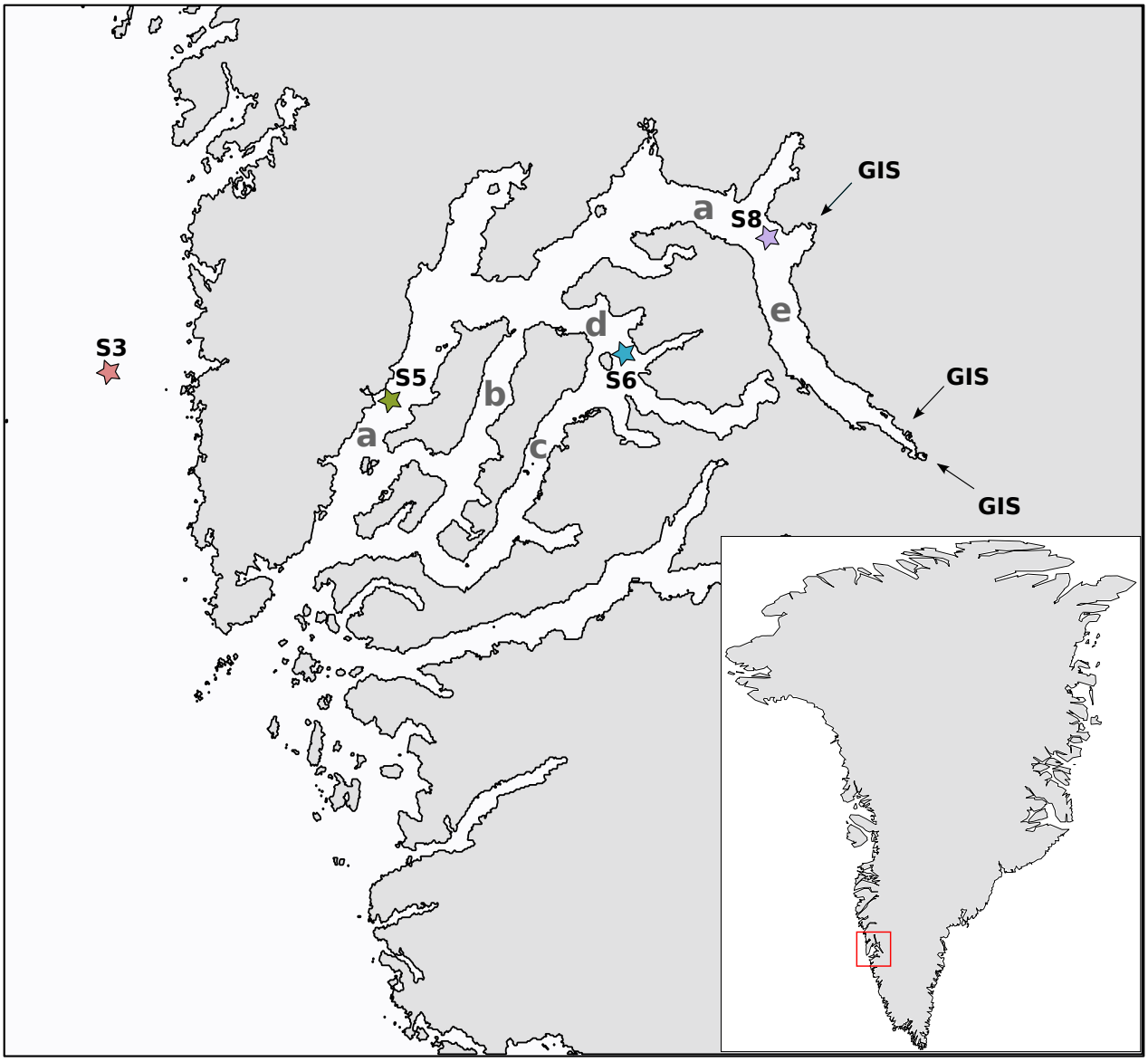

Supplementary Figure S1. Locations of the four sampling stations in the Godthåbsfjord region. The exact coordinates of the stations are indicated in Table 1. S3 and S6, Non-glacier-influenced stations 3 and 6. S5 and S8, Glacier-influenced stations 5 and 8. GIS, Greenland Ice Sheet glacier outlet into the Kangersuneq fjord. a, main fjord (Nûp Kangerdlua). b, Qôrnup Suvdlua. c, Ûmánap Suvdlua. d, Kapisigdlit Kanderdluat. e, Kangersuneq. The map was modified from Glombitza *et al.*, 2015.

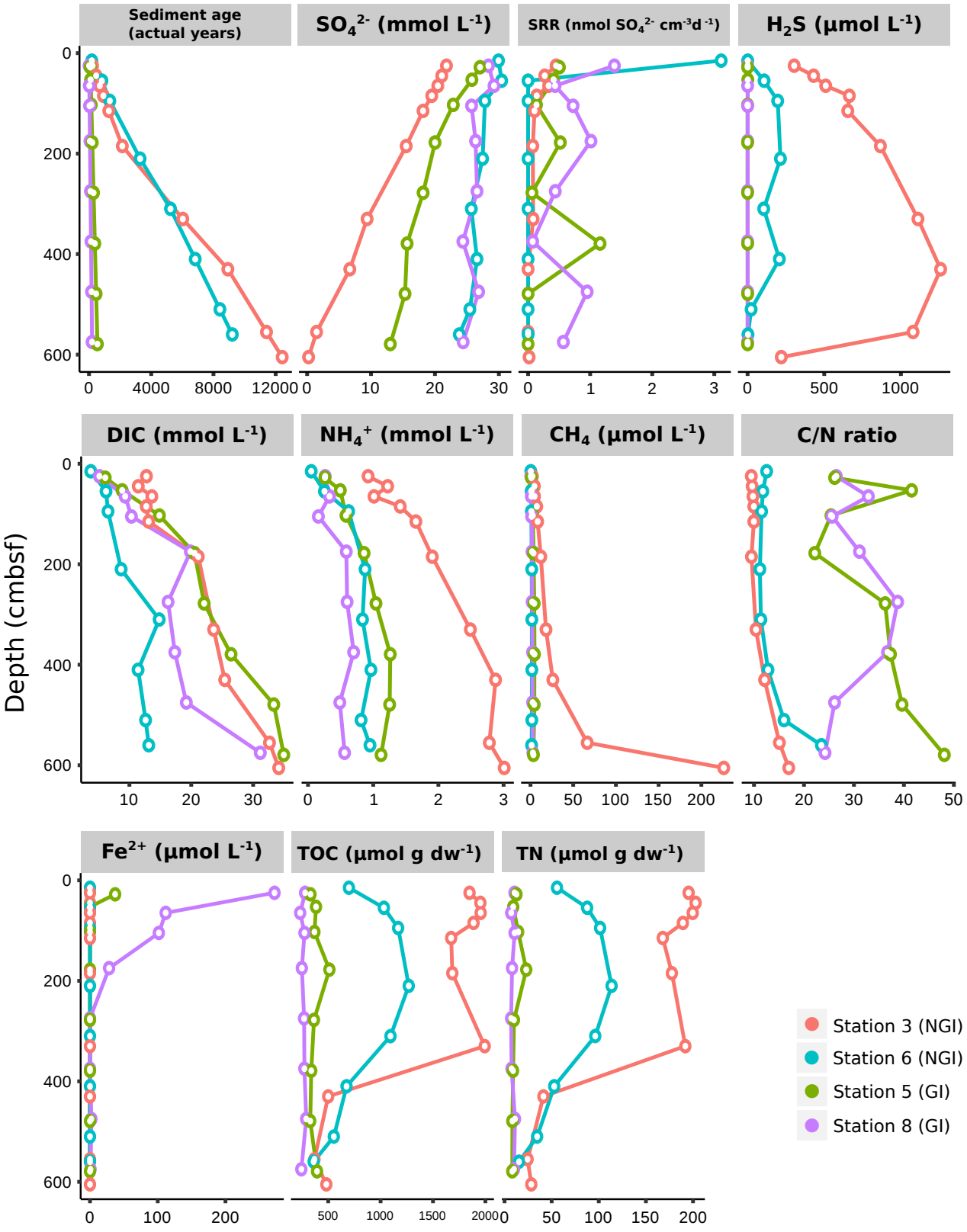

Supplementary Figure S2. Physicochemical sediment properties in non-glacier-influenced (NGI) and glacier-influenced (GI) sediment cores. Colours indicate the sampling station. Note that the scales are different for each physicochemical parameter. Data on SRR and DIC, as well as, sulfate and sulfide contentrations were taken from Glombitza *et al.*, 2015.

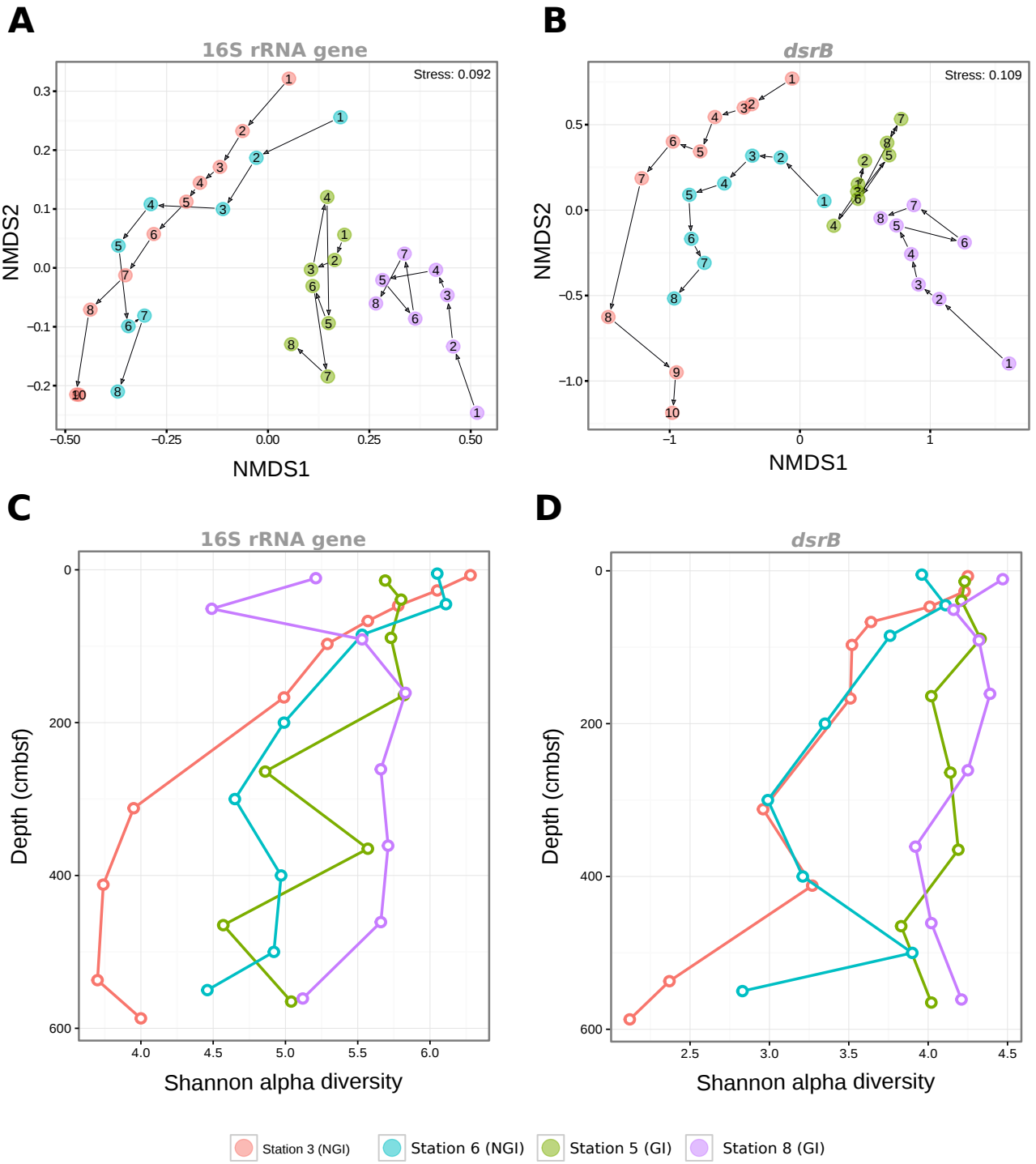

Supplementary Figure S3. Microbial diversity across non-glacier-influenced (NGI) and glacier-influenced (GI) sediment cores and sediment depth. A and B, Nonmetric multidimensional scaling ordinations (NMDS) of Bray-Curtis distances between 16S rRNA gene and *dsrB* communities. C and D, Shannon alpha diversity indices of 16S rRNA gene and *dsrB* communities. Colours indicate the sampling station. Numbers indicate the sediment depth according to Supplementary Table 1.

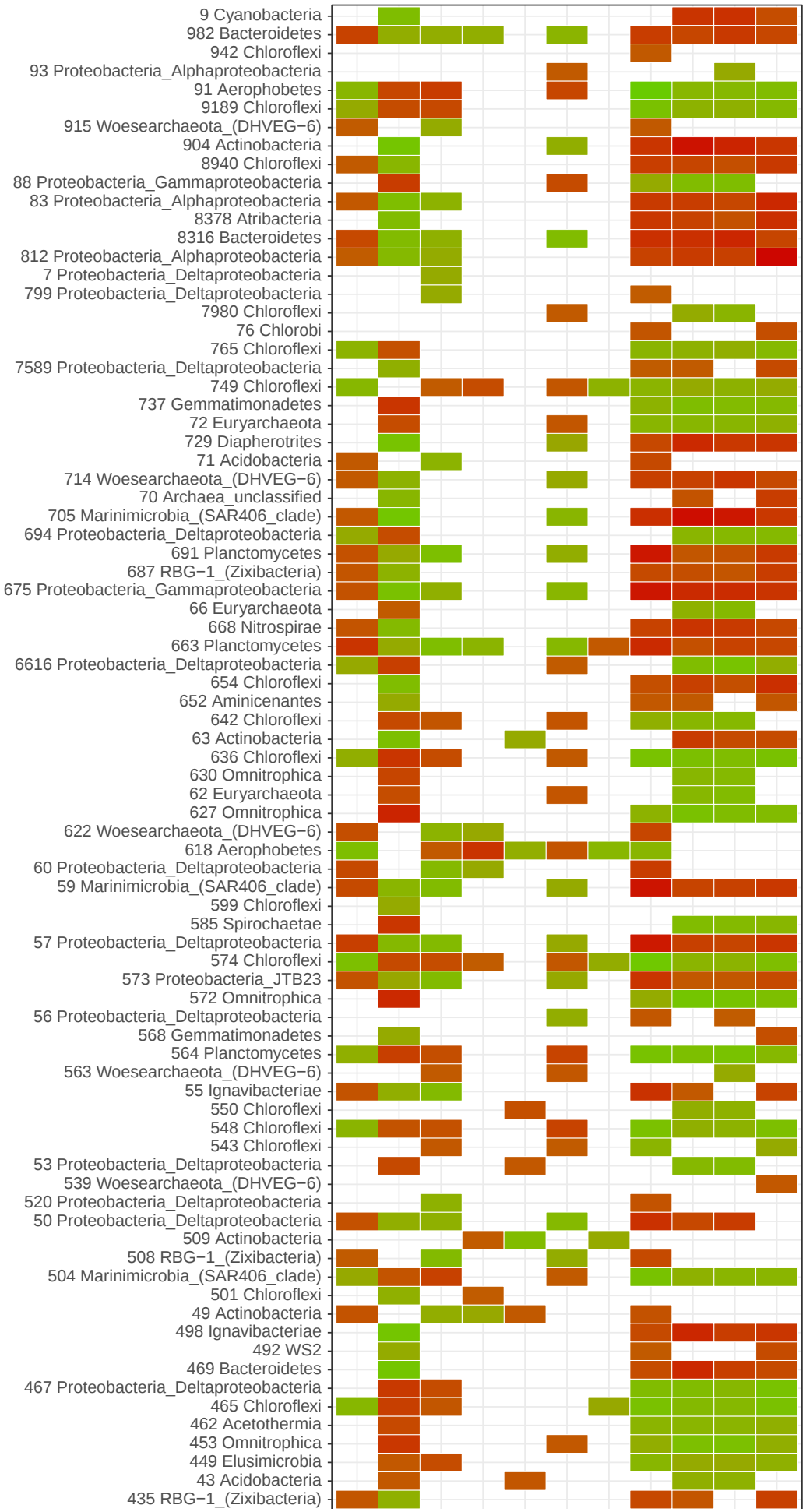
9 Cyanobacteria
982 Bacteroidetes
942 Chloroflexi
93 Proteobacteria_Alphaproteobacteria
91 Aerophobetes
9189 Chloroflexi
915 Woesearchaeota_(DHVEG−6)
904 Actinobacteria
8940 Chloroflexi
88 Proteobacteria_Gammaproteobacteria
83 Proteobacteria_Alphaproteobacteria
8378 Atribacteria
8316 Bacteroidetes
812 Proteobacteria_Alphaproteobacteria
7 Proteobacteria_Deltaproteobacteria
799 Proteobacteria_Deltaproteobacteria
7980 Chloroflexi
76 Chlorobi
765 Chloroflexi
7589 Proteobacteria_Deltaproteobacteria
749 Chloroflexi
737 Gemmatimonadetes
72 Euryarchaeota
729 Diapherotrites
71 Acidobacteria
714 Woesearchaeota_(DHVEG−6)
70 Archaea_unclassified
705 Marinimicrobia_(SAR406_clade)
694 Proteobacteria_Deltaproteobacteria
691 Planctomycetes
687 RBG−1_(Zixibacteria)
675 Proteobacteria_Gammaproteobacteria
66 Euryarchaeota
668 Nitrospirae
663 Planctomycetes
6616 Proteobacteria_Deltaproteobacteria
654 Chloroflexi
652 Aminicenantes
642 Chloroflexi
63 Actinobacteria
636 Chloroflexi
630 Omnitrophica
62 Euryarchaeota
627 Omnitrophica
622 Woesearchaeota_(DHVEG−6)
618 Aerophobetes
60 Proteobacteria_Deltaproteobacteria
59 Marinimicrobia_(SAR406_clade)
599 Chloroflexi
585 Spirochaetae
57 Proteobacteria_Deltaproteobacteria
574 Chloroflexi
573 Proteobacteria_JTB23
572 Omnitrophica
56 Proteobacteria_Deltaproteobacteria
568 Gemmatimonadetes
564 Planctomycetes
563 Woesearchaeota_(DHVEG−6)
55 Ignavibacteriae
550 Chloroflexi
548 Chloroflexi
543 Chloroflexi
53 Proteobacteria_Deltaproteobacteria
539 Woesearchaeota_(DHVEG−6)
520 Proteobacteria_Deltaproteobacteria
50 Proteobacteria_Deltaproteobacteria
509 Actinobacteria
508 RBG−1_(Zixibacteria)
504 Marinimicrobia_(SAR406_clade)
501 Chloroflexi
49 Actinobacteria
498 Ignavibacteriae
492 WS2
469 Bacteroidetes
467 Proteobacteria_Deltaproteobacteria
465 Chloroflexi
462 Acetothermia
453 Omnitrophica
449 Elusimicrobia
43 Acidobacteria
435 RBG−1_(Zixibacteria)


433 Aminicenantes
425 Bacteroidetes
41 Bacteroidetes
416 Actinobacteria
410 Actinobacteria
408 Woesearchaeota_(DHVEG−6)
403 Proteobacteria_Gammaproteobacteria
401 Proteobacteria_Deltaproteobacteria
39 Proteobacteria_Alphaproteobacteria
393 Woesearchaeota_(DHVEG−6)
391 Chloroflexi
387 Acidobacteria
37 Proteobacteria_Deltaproteobacteria
36 Proteobacteria_Deltaproteobacteria
365 Chloroflexi
356 Proteobacteria_Deltaproteobacteria
353 Bacteria_unclassified
3528 Omnitrophica
34 Proteobacteria_Deltaproteobacteria
323 Archaea_unclassified
320 Planctomycetes
31 Proteobacteria_Gammaproteobacteria
318 Chloroflexi
315 Proteobacteria_Alphaproteobacteria
311 Proteobacteria_Alphaproteobacteria
30 Proteobacteria_Epsilonproteobacteria
306 Proteobacteria_Deltaproteobacteria
29 Actinobacteria
295 Chloroflexi
294 Chloroflexi
28 Actinobacteria
289 Bacteroidetes
2878 Chloroflexi
2859 Planctomycetes
283 Spirochaetae
282 Aerophobetes
2819 Proteobacteria_Deltaproteobacteria
280 Proteobacteria_Betaproteobacteria
279 Nitrospirae
275 Chloroflexi
26 Proteobacteria_Gammaproteobacteria
268 Thaumarchaeota
265 Woesearchaeota_(DHVEG−6)
2646 Marinimicrobia_(SAR406_clade)
262 Euryarchaeota
261 Chloroflexi
25 Proteobacteria_Deltaproteobacteria
2568 Euryarchaeota
2551 Chloroflexi
252 Aminicenantes
249 Deferribacteres
2467 Proteobacteria_Deltaproteobacteria
244 Euryarchaeota
241 Planctomycetes
240 Woesearchaeota_(DHVEG−6)
238 Firmicutes
236 Aerophobetes
235 Bathyarchaeota
2335 Planctomycetes
227 Proteobacteria_Deltaproteobacteria
224 Proteobacteria_Deltaproteobacteria
220 Firmicutes
21 Proteobacteria_Alphaproteobacteria
209 RBG−1_(Zixibacteria)
208 Actinobacteria
207 Proteobacteria_Deltaproteobacteria
2065 Proteobacteria_Deltaproteobacteria
204 Chloroflexi
201 Chloroflexi
19 Proteobacteria_Deltaproteobacteria
191 Actinobacteria
18 Bacteria_unclassified
189 Chloroflexi
188 Lokiarchaeota
187 Proteobacteria_Gammaproteobacteria
183 Proteobacteria_Deltaproteobacteria
178 Bacteroidetes
171 Spirochaetae
162 Aminicenantes
15 Proteobacteria_Deltaproteobacteria
Estimate_value
0.5
0.0
−0.5

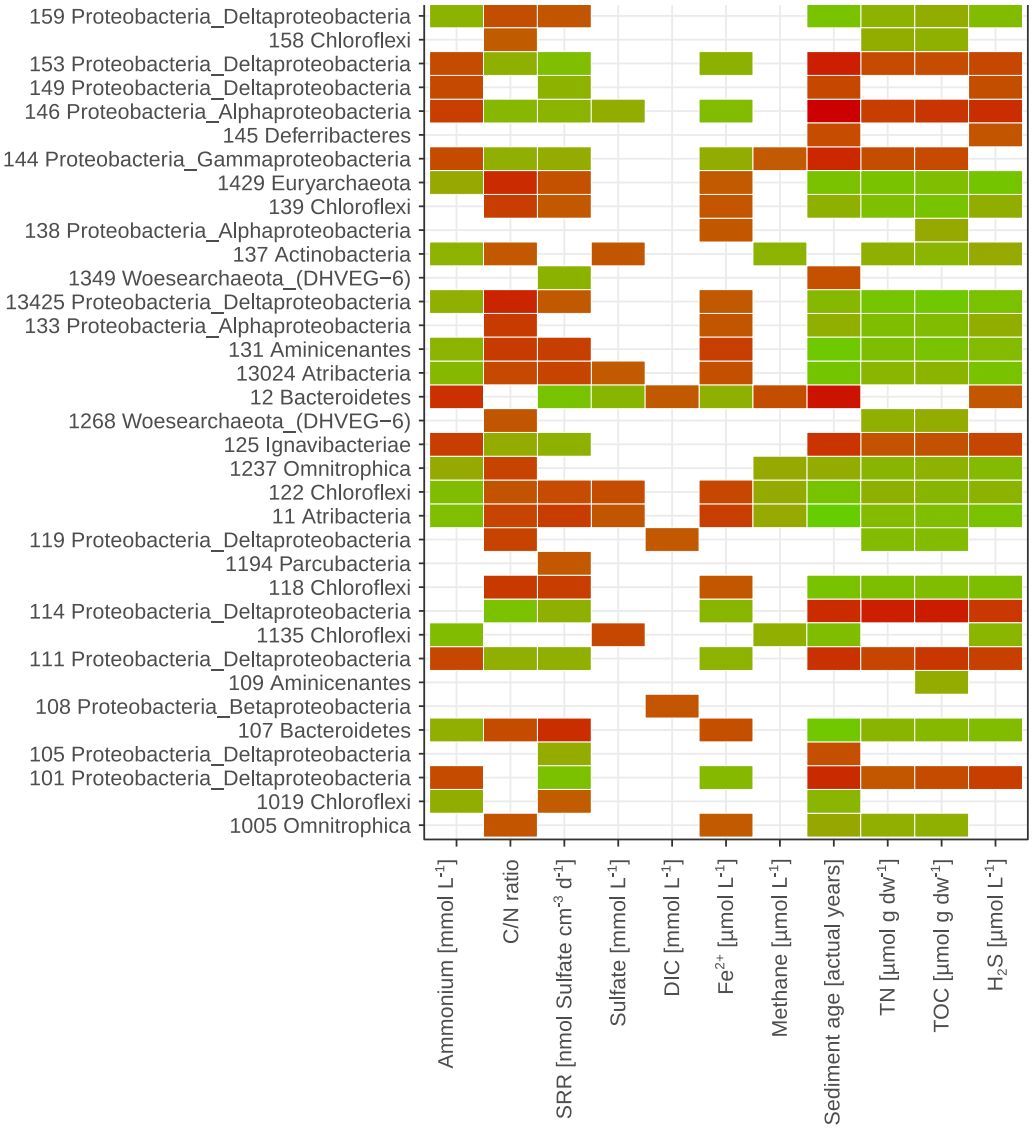

Supplementary Figure S4. Spearman correlations between relative abundances of rRNA-OTUs and physicochemical parameters. Indicated are OTUs with significant ($p \leq$ Spearman correlations to any of the tested parameters.

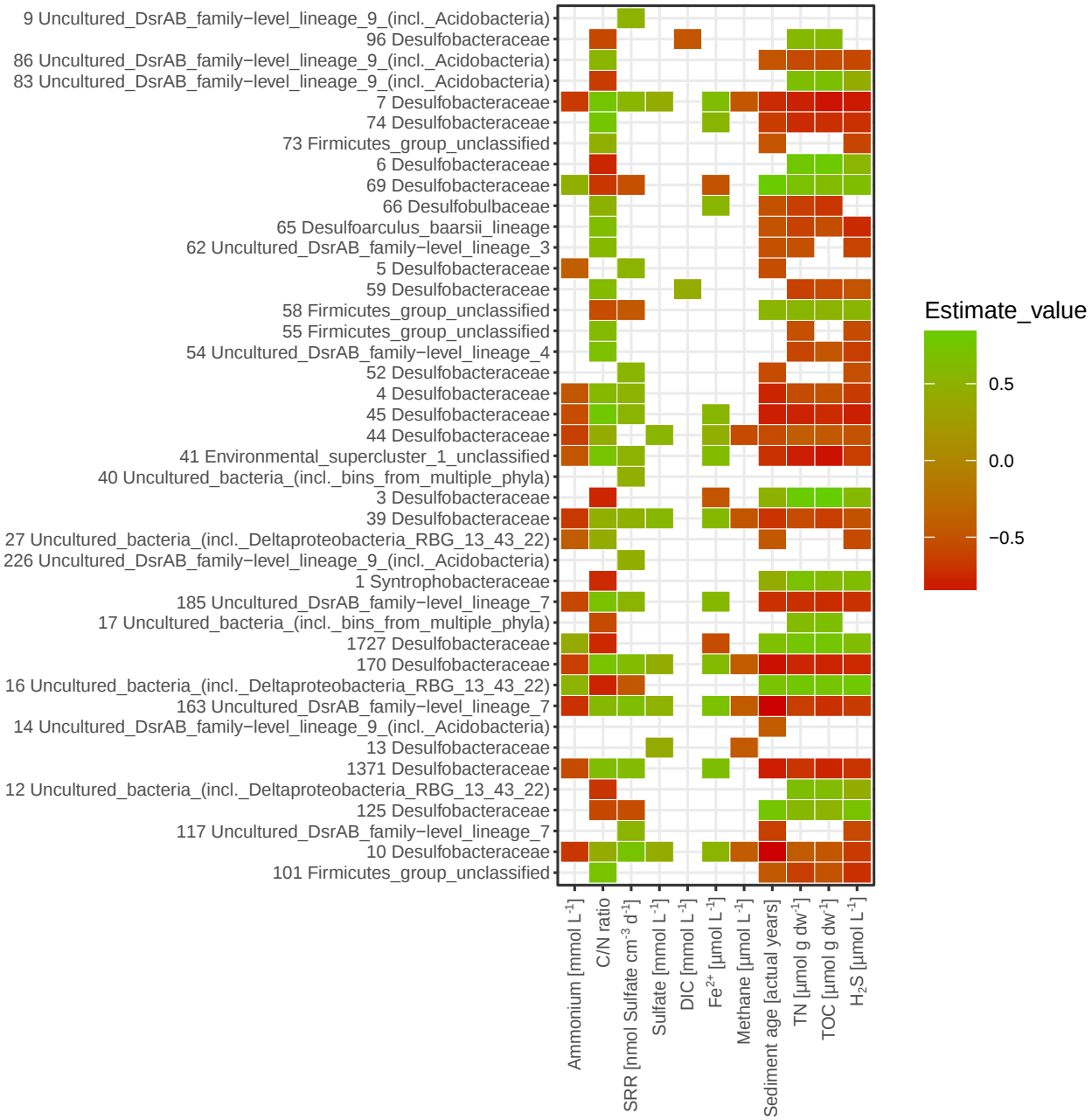

Supplementary Figure S5. Spearman correlations between relative abundances of *dsrB*-OTUs and physicochemical parameters. Indicated are OTUs with significant ($p \leq 0.5$) Spearman correlations to any of the tested parameters.

Supplementary Figure S6. Phylogenetic placement of 16S rRNA-OTUs. Only OTUs with significant correlations to sulfate reduction rates or sediment age are shown. The reference tree was built from sequences that were closely related to 16S rRNA-OTUs. These were extracted from the SILVA database v.128 (Quast *et al.*, 2013), and used for tree construction with FastTree (Price *et al.*, 2010). 16S rRNA-OTUs were aligned to the SILVA database using the SINA aligner (Pruesse *et al.*, 2012), and placed into the reference tree using the EPA algorithm (Berger *et al.*, 2011) in RAxML (Stamatakis, 2014). The placement tree was visualized with iTOL (Letunic and Bork, 2007). OTUs that are colored in orange and green were significantly correlated to sulfate reduction rates (Figure 3) and sediment age (Figure 4), respectively. Clades that contained only OTUs with significant correlations to either sulfate reduction rates or sediment age are colored accordingly. Gray clades contain OTUs with correlations to sulfate reduction rates and OTUs with correlations to sediment age.

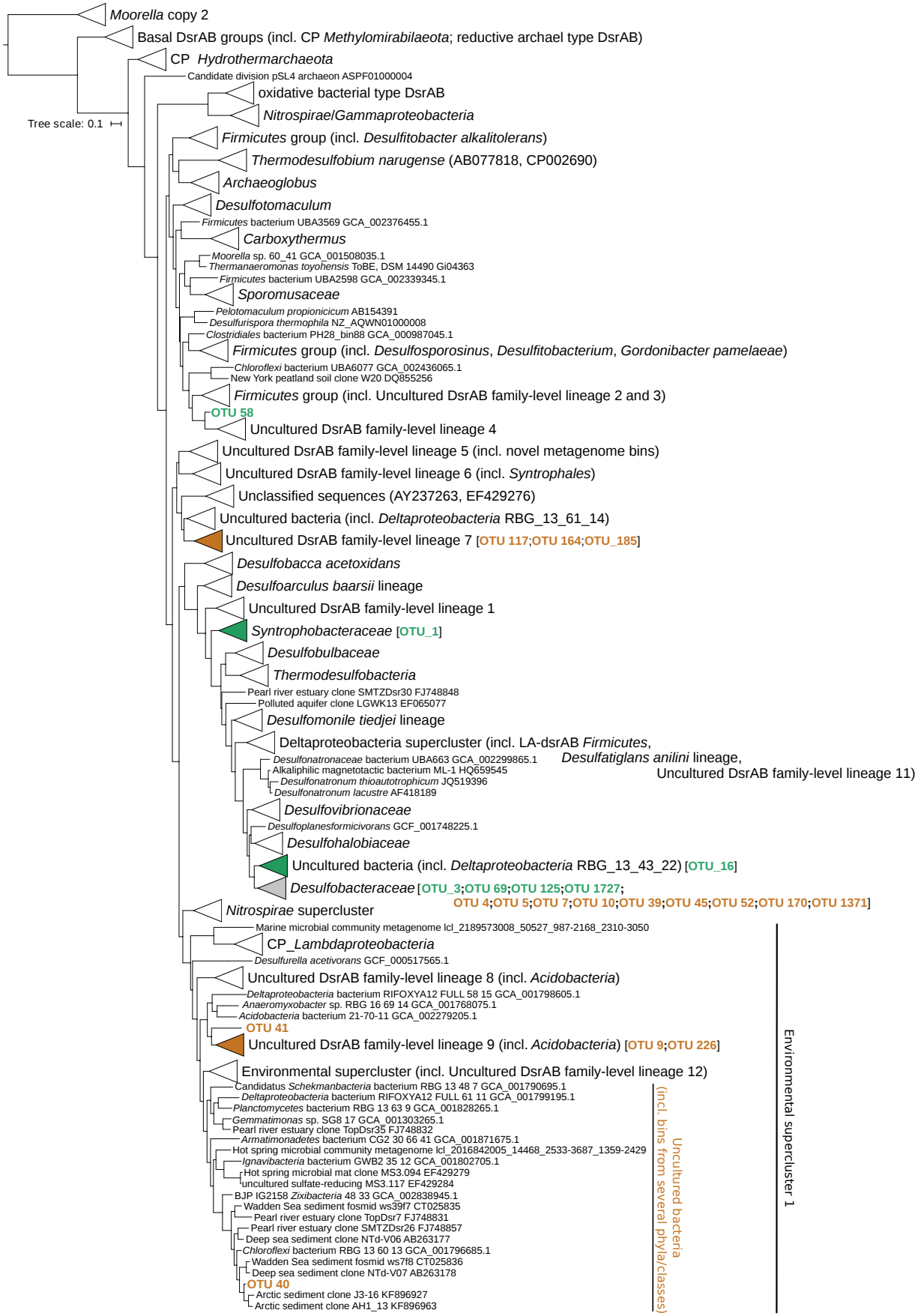

Supplementary Figure S7. Phylogenetic placement of *dsrB*-OTUs. Only OTUs with significant correlations to sulfate reduction rates or sediment age are shown. The reference tree was built from an extended reference alignment that contained DsrAB sequences from Müller *et al.*, 2015 and novel DsrAB sequences from recent metagenomic surveys (Anantharaman *et al.*, 2017; Parks *et al.*, 2017). The reference tree was constructed with FastTree (Price *et al.*, 2010). *dsrB*-OTUs were aligned to the extended reference alignment using MAFFT (Katoh *et al.*, 2002), and added to the reference tree using the EPA algorithm (Berger *et al.*, 2011) in RAxML (Stamatakis, 2014). The placement tree was visualized with iTOL (Letunic and Bork, 2007). OTUs that are colored in orange and green were significantly correlated to sulfate reduction rates (Figure 3) and sediment age (Figure 4), respectively. Clades that contained only OTUs with significant correlations to either sulfate reduction rates or sediment age are colored accordingly. Gray clades contain OTUs with correlations to sulfate reduction rates and OTUs with correlations to sediment age.

Supplementary Table S1. Sample numbering and sediment depth of the four sediment cores.

Coring station	Sample numbering	Sediment depth (cmbsf)
Station 3	1	25
Station 3	2	45
Station 3	3	65
Station 3	4	85
Station 3	5	115
Station 3	6	185
Station 3	7	330
Station 3	8	430
Station 3	9	555
Station 3	10	605
Station 5	1	28
Station 5	2	53
Station 5	3	103
Station 5	4	178
Station 5	5	278
Station 5	6	379
Station 5	7	479
Station 5	8	579
Station 6	1	15
Station 6	2	55
Station 6	3	95
Station 6	4	210
Station 6	5	310
Station 6	6	410
Station 6	7	510
Station 6	8	560
Station 8	1	25
Station 8	2	65
Station 8	3	105
Station 8	4	175
Station 8	5	275
Station 8	6	375
Station 8	7	475
Station 8	8	575

References

Anantharaman, K., Jungbluth, S. P., Kantor, R. S., Lavy, A., Warren, L. A., Rappé, M. S., *et al.* (2017) Dramatic expansion of microbial groups that shape the global sulfur cycle. *ISME J.* **12**: 1715-1728.

Berger, S. A., Krompass, D., and Stamatakis, A. (2011) Performance, accuracy, and Web server for evolutionary placement of short sequence reads under maximum likelihood. *Syst. Biol.* **60**: 291–302.

Glombitza, C., Jaussi, M., Røy, H., Seidenkrantz, M.-S., Lomstein, B. A., and Jørgensen, B. B. (2015) Formate, acetate, and propionate as substrates for sulfate reduction in sub-arctic sediments of Southwest Greenland. *Front. Microbiol.* **6**: 846.

Katoh, K., Misawa, K., Kuma, K.-I., and Miyata, T. (2002) MAFFT: a novel method for rapid multiple sequence alignment based on fast Fourier transform. *Nucleic Acids Res.* **30**: 3059–3066.

Letunic, I., and Bork, P. (2007) Interactive Tree Of Life (iTOL): an online tool for phylogenetic tree display and annotation. *Bioinformatics* **23**: 127–128.

Müller, A. L., Kjeldsen, K. U., Rattei, T., Pester, M., and Loy, A. (2015) Phylogenetic and environmental diversity of DsrAB-type dissimilatory (bi)sulfite reductases. *ISME J.* **9**: 1152–1165.

Parks, D. H., Rinke, C., Chuvochina, M., Chaumeil, P.-A., Woodcroft, B. J., Evans, P. N., *et al.* (2017) Recovery of nearly 8,000 metagenome-assembled genomes substantially expands the tree of life. *Nat. Microbiol.* **2**: 1533–1542.

Price, M. N., Dehal, P. S., and Arkin, A. P. (2010) FastTree 2 – Approximately Maximum-Likelihood Trees for Large Alignments. *PLoS One* **5**: e9490.

Pruesse, E., Peplies, J., and Glöckner, F. O. (2012) SINA: accurate high-throughput multiple sequence alignment of ribosomal RNA genes. *Bioinformatics* **28**: 1823–1829.

Quast, C., Pruesse, E., Yilmaz, P., Gerken, J., Schweer, T., Yarza, P., *et al.* (2013) The SILVA ribosomal RNA gene database project: improved data processing and web-based tools. *Nucleic Acids Res.* **41**: D590–6.

Stamatakis, A. (2014) RAxML version 8: a tool for phylogenetic analysis and post-analysis of large phylogenies. *Bioinformatics* **30**: 1312–1313.

Chapter 3

Bacterial interactions during sequential degradation of cyanobacterial necromass in a sulfidic arctic marine sediment

Albert L. Müller*, **Claus Pelikan***, Julia R. de Rezende, Kenneth Wasmund, Martina Putz, Clemens Glombitza, Kasper U. Kjeldsen, Bo Barker Jørgensen, and Alexander Loy
*Contributed equally to this study

Reference:

Environmental Microbiology 20, 2927-2940 (2018), doi:10.1111/1462-2920.14297

Supplementary information available at:
https://onlinelibrary.wiley.com/doi/full/10.1111/1462-2920.14297

Author contributions:

AM, CP and AL designed the research. AM performed the incubation experiments, extracted DNA and generated amplicons for sequencing, performed initial sequence analysis and wrote a first manuscript draft. MP helped with the experiments. CP and KW designed FISH probes and performed RAMAN analyses. JR and KK analyzed VFAs and determined sulfate reduction rates. CG calculated Gibbs Energy for acetoclastic sulfate reduction in the sediments. CP and AL wrote the manuscript. AM, JR, KW, MP, CG, KK and BJ revised the the draft versions of the manuscript and approved the final version of the paper.

environmental microbiology

Environmental Microbiology (2018) **20**(8), 2927–2940 doi:10.1111/1462-2920.14297

Bacterial interactions during sequential degradation of cyanobacterial necromass in a sulfidic arctic marine sediment

Albert L. Müller,[1†] Claus Pelikan,[1,2] Julia R. de Rezende,[3‡] Kenneth Wasmund,[1,2] Martina Putz,[1§] Clemens Glombitza,[4] Kasper U. Kjeldsen,[3] Bo Barker Jørgensen[3] and Alexander Loy[1,2*]

[1]*Division of Microbial Ecology, Department of Microbiology and Ecosystem Science, Research Network Chemistry meets Microbiology, University of Vienna, Vienna, Austria.*

[2]*Austrian Polar Research Institute, Vienna, Austria.*

[3]*Center for Geomicrobiology, Department of Bioscience, Aarhus University, Aarhus, Denmark.*

[4]*NASA Ames Research Center, Moffett Field, CA, USA.*

Summary

Seafloor microorganisms impact global carbon cycling by mineralizing vast quantities of organic matter (OM) from pelagic primary production, which is predicted to increase in the Arctic because of diminishing sea ice cover. We studied microbial interspecies-carbon-flow during anaerobic OM degradation in arctic marine sediment using stable isotope probing. We supplemented sediment incubations with ^{13}C-labeled cyanobacterial necromass (spirulina), mimicking fresh OM input, or acetate, an important OM degradation intermediate and monitored sulfate reduction rates and concentrations of volatile fatty acids (VFAs) during substrate degradation. Sequential 16S rRNA gene and transcript amplicon sequencing and fluorescence *in situ* hybridization combined with Raman microspectroscopy revealed that only few bacterial species were the main degraders of ^{13}C-spirulina necromass. *Psychrilyobacter, Psychromonas, Marinifilum, Colwellia, Marinilabiaceae* and *Clostridiales* species were likely involved in the primary hydrolysis and fermentation of spirulina. VFAs, mainly acetate, produced from spirulina degradation were mineralized by sulfate-reducing bacteria and an *Arcobacter* species. Cellular activity of *Desulfobacteraceae* and *Desulfobulbaceae* species during acetoclastic sulfate reduction was largely decoupled from relative 16S rRNA gene abundance shifts. Our findings provide new insights into the identities and physiological constraints that determine the population dynamics of key microorganisms during complex OM degradation in arctic marine sediments.© 2018 Society for Applied Microbiology and John Wiley & Sons Ltd

Received 21 February, 2018; revised 2 May, 2018; accepted 24 May, 2018. *For correspondence. E-mail loy@microbial-ecology.net; Tel. + 431427776605; Fax + 4314277876605. Present addresses: †Albert Müller, Department of Civil and Environmental Engineering, Stanford,CA, USA; ‡Julia R. de Rezende, The Lyell Centre for Earth and Marine Science and Technology, Edinburgh, Scotland, UK; §Martina Putz, Department of Forest Mycology and Plant Pathology, Swedish University of Agricultural Sciences, Uppsala, Sweden. Albert L. Müller and Claus Pelikan contributed equally to this study

Introduction

The Earth's seafloor is habitat for more than half of the microbial cells in the marine environment (Kallmeyer *et al*., 2012). Microorganisms in marine sediments are highly dependent on energy and carbon that is derived from the degradation of detrital organic matter (OM) (Jørgensen and Boetius, 2007), which is produced by marine phytoplankton (Arndt *et al*., 2013). Although only 1% of the OM exported from surface waters reaches the seafloor on a global scale (Hedges and Keil, 1995), regional differences are high and sediments in coastal regions receive approximately 6–12% of pelagic primary production (Dunne *et al*., 2007). The labile fraction of OM that reaches the seafloor is gradually degraded and mineralized by the concerted activity of diverse anaerobic microorganisms (Arndt *et al*., 2013; Orsi *et al*., 2018). Cellular macromolecules such as proteins, nucleic acids, lipids and polysaccharides that make-up the majority of phytoplankton debris (Burdige, 2007) are degraded by mostly unknown microorganisms into oligomers and monomers, which are subsequently fermented to a range of products, including volatile fatty acids (VFAs), H_2 and CO_2 (Burdige, 2007; Muyzer and Stams, 2008). In continental shelf sediments, the most favorable electron acceptors (O_2, Fe(III), Mn(IV), NO_3^-) are depleted first (Froelich *et al*., 1979) and sulfate reduction is the predominant process that accounts for the oxidation of half

© 2018 The Authors. Environmental Microbiology published by Society for Applied Microbiology and John Wiley & Sons Ltd. This is an open access article under the terms of the Creative Commons Attribution License, which permits use, distribution and reproduction in any medium, provided the original work is properly cited.

of the VFAs that are produced during anaerobic OM breakdown (Jørgensen, 1982). Thus, on a global scale sulfate-reducing microorganisms (SRM) facilitate the remineralization of approximately 29% of the total OM flux to the entire seafloor (Bowles *et al*., 2014).

The Arctic is severely impacted by climate change, resulting in a constant decline of the arctic sea ice cover (Vaughan *et al*. 2013). This allows marine primary production to prevail (Arrigo *et al*., 2008) and predictions suggest this will initially cause an increased export of OM to the seafloor (Lalande *et al*., 2009; Sørensen *et al*., 2015). OM degradation rates and pathways in arctic marine sediments have been intensively studied in Svalbard fjords with a focus on enzymatic hydrolysis, sulfate reduction, iron reduction and denitrification (Arnosti and Jørgensen, 2006; Finke *et al*., 2007; Canion *et al*., 2014). Intriguingly, OM-degrading microorganisms in permanently cold sediments are relatively active at temperatures close to the freezing point (Kostka *et al*., 1999; Arnosti and Jørgensen, 2003; Robador *et al*., 2016), because of psychrophilic adaptations (Knoblauch and Jørgensen, 1999; Cavicchioli, 2016). The microbial communities in Svalbard fjord sediments are highly diverse (Teske *et al*., 2011), and dominated by representatives of the classes *Deltaproteobacteria, Gammaproteobacteria* and the phylum *Bacteroidetes* (Ravenschlag *et al*., 1999–2001). Even though a variety of specific members of this arctic sediment microbial community could be isolated (Knoblauch *et al*., 1999; Sahm *et al*., 1999; Wang *et al*., 2015), the identity and population dynamics of most microorganisms that are responsible for the degradation of complex OM under cold, anoxic conditions in marine sediments is unknown.

In this study, we conducted microcosm experiments with ^{13}C-labelled substrates in order to directly link OM degradation processes in arctic marine sediments with specific microorganisms (Supporting Information Fig. S1). We used sediment samples from a fjord in Svalbard (Smeerenburgfjorden, station J) where sulfate reduction is the predominant terminal remineralization process (Finke *et al*., 2007). Anoxic sediment incubations were either supplemented with a low dose (LD) or a high dose (HD) of ^{13}C-labelled cyanobacterial necromass (spirulina) in order to mimic a pulse of bulk OM input to the seabed or ^{13}C-labelled acetate, an important organic carbon degradation intermediate and electron donor for anaerobic respiration in marine sediments. We investigated bacterial community responses to substrate supplementation by amplicon-sequencing of 16S rRNA genes and transcripts in light of changes in VFA concentrations and sulfate reduction rates, and by single-cell Raman microspectroscopy. This allowed us to (i) identify species-level phylotypes involved in the degradation cascade of cyanobacterial necromass and in the terminal oxidation of acetate, (ii) reveal main products of cyanobacterial necromass degradation and provide evidence for their consumption by SRM and microorganisms that use alternative electron acceptors for energy conservation and (iii) confirm the specific incorporation of substrate-derived ^{13}C into individual target cells via a combination of catalyzed reporter deposition fluorescence *in situ* hybridization (CARD-FISH) and Raman microspectroscopy.

Results

Enhanced sulfate reduction rates in spirulina necromass- and acetate-amended microcosms

Sulfate reduction rates in the unamended controls ranged from 9 to 18 nmol cm^{-3} d^{-1} (Fig. 1 A and B). The addition of cyanobacterial necromass significantly enhanced sulfate reduction rates to 18–40 nmol cm^{-3} d^{-1} ($P < 0.001$) and to 45–64 nmol cm^{-3} d^{-1} ($P < 0.001$) in LD and HD ^{13}C-spirulina incubations respectively (Fig. 1A). Amendment of ^{13}C-acetate also significantly increased sulfate reduction rates to 14–34 nmol cm^{-3} d^{-1} ($P < 0.001$) and to 22–40 nmol cm^{-3} d^{-1} ($P < 0.001$) in LD and HD incubations respectively (Fig. 1B). Sulfate reduction rates were below the detection limit in incubations with molybdate as inhibitor (Fig. 1A and B).

Acetate is the main volatile fatty acid produced from spirulina degradation

Average background concentrations of VFAs in the unamended control microcosms were low (12 μM acetate, 9 μM formate, 4 μM lactate and < 1 μM propionate, pyruvate, butyrate and valerate) (Fig. 1 and Supporting Information Fig. S2). The concentrations of VFAs differed substantially between the incubations with ^{13}C-spirulina and ^{12}C-spirulina (Fig. 1C and D), which suggests considerable differences in the composition of the purchased spirulina products (Supporting Information Results and Discussion). Only results from the ^{13}C-spirulina incubations are discussed in the main text. A pulse of ^{13}C-spirulina was added at the beginning of the experiment and its degradation led to the production of mainly ^{13}C-acetate and several other VFAs (Fig. 1C and D). Compared to uninhibited incubations, concentrations of VFAs increased more over time in incubations with the sulfate-reduction inhibitor molybdate. Exceptions were HD ^{13}C-spirulina incubations where ^{13}C-acetate increased to similarly high concentrations (> 1.1 mM) with and without molybdate (Fig. 1D). In LD ^{13}C-spirulina incubations, ^{13}C-acetate only accumulated in the presence of molybdate and reached concentrations of 35 μM (Fig. 1C). Other VFAs that consistently accumulated in molybdate-

© 2018 The Authors. Environmental Microbiology published by Society for Applied Microbiology and John Wiley & Sons Ltd.,

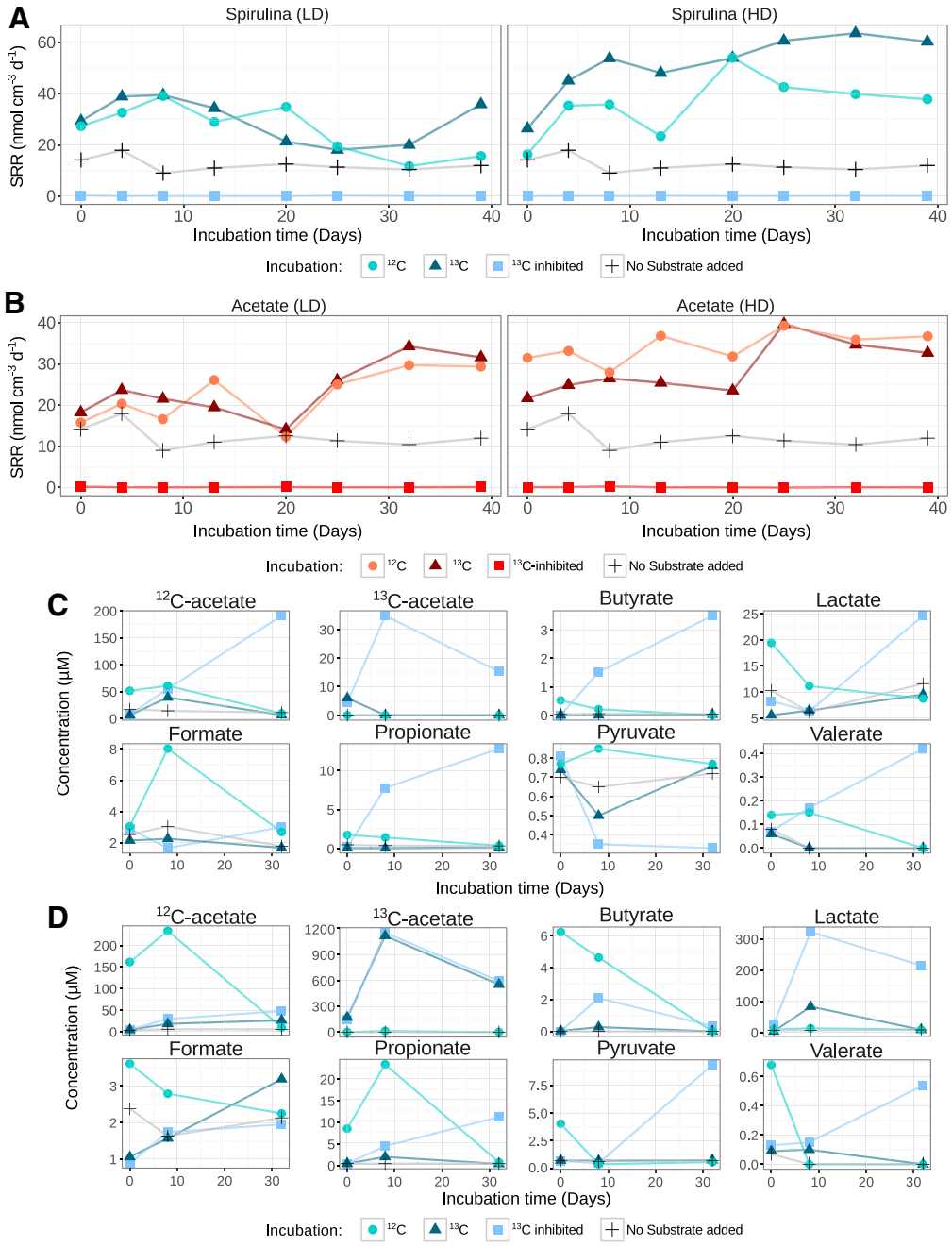

Fig. 1. Sulfate reduction rates and volatile fatty acid concentrations in substrate-supplemented sediment incubations. Sulfate reduction rates (nmol cm^{-1} d^{-1}) are shown for incubations supplemented with spirulina (A) and acetate (B). Concentrations of volatile fatty acids are indicated for LD (C) and HD (D) incubations with spirulina. ^{13}C-inhibited, sediment incubations with ^{13}C-substrate and molybdate. LD, low substrate dose (50 µg ml^{-1} spirulina or 50 µM acetate). HD, high substrate dose (1 mg ml^{-1} spirulina or 1 mM acetate). Note that the scales are different for each treatment and VFA.

inhibited ^{13}C-spirulina microcosms were formate, propionate, butyrate and valerate, which reached concentrations of 25 µM, 11 µM, 4 µM and 0.42 µM in LD incubations and 324 µM, 13 µM, 2 µM and 0.52 µM in HD incubations. Pyruvate increased up to 9 µM but only in HD ^{13}C-spirulina incubations (Fig. 1D) and not in LD ^{13}C-spirulina incubations (Fig. 1C). Lactate concentrations were always comparable to the unamended controls (Fig. 1C and D). Intriguingly, low amounts of ^{12}C-acetate accumulated in molybdate-inhibited ^{13}C-spirulina incubations (up to 191 and 48 µM in LD and HD incubations respectively), indicating that addition of fresh cyanobacterial necromass additionally stimulated the breakdown of endogenous OM (van Nugteren *et al*., 2009).

© 2018 The Authors. Environmental Microbiology published by Society for Applied Microbiology and John Wiley & Sons Ltd.,

Concentrations of acetate, formate, propionate, butyrate and valerate remained mostly unchanged in incubations with repeated amendments of acetate (Supporting Information Fig. S2). Similar to spirulina incubations, inhibition with molybdate led to an accumulation of acetate, butyrate, propionate and valerate (Supporting Information Fig. S2). However, the concentrations of these VFAs were consistently lower in molybdate-inhibited incubations with ^{13}C-acetate than with ^{13}C-spirulina. This further suggests that a substantial part of the VFAs that accumulated in the inhibited ^{13}C-spirulina incubations came from breakdown of the supplemented substrate.

An assemblage of eleven phylotypes from diverse taxa is associated with degradation of spirulina necromass under sulfidic conditions

We monitored changes in the relative abundance and ribosomal activity of bacterial community members during the microcosm experiments by pyrosequencing of 16S rRNA gene and transcript amplicons. The sediment community at the start of the experiment (day 0) was dominated by *Deltaproteobacteria, Bacteroidetes, Gammaproteobacteria* and *Planctomycetes* (Fig. 2); these taxa also harboured 21 of the 25 abundant phylotypes (≥ 1% 16S rRNA gene and/or transcript abundance) (Supporting Information Table S1). The other four abundant phylotypes were affiliated with *Fusobacteria, Betaproteobacteria*, candidate group Milano-WF1B-44 and *Cyanobacteria-Chloroplast* (Supporting Information Table S1). Amendments with acetate did not trigger considerable changes in 16S rRNA gene or transcript alpha- (Supporting Information Table S2) and beta-diversity (Supporting Information Fig. S3). In contrast, incubations with ^{13}C-spirulina led to LD- and HD-dependent shifts in 16S rRNA gene and transcript composition (Supporting Information Figs S3 and S4).

We identified individual phylotypes that responded to the added substrates by comparing their relative 16S rRNA gene and transcript abundances in incubations with substrate versus unamended controls. Overall, eleven responsive phylotypes of the phyla/classes *Gammaproteobacteria, Deltaproteobacteria, Epsilonbacteraeota, Bacteroidetes, Firmicutes* and *Fusobacteria* were identified by two-proportion *T*-tests ($P \leq 0.01$); of which seven were only associated with spirulina amendments, one with acetate amendment alone and three with both substrate amendments (Fig. 3). Ten of these phylotypes had a relative 16S rRNA gene abundance of ≥ 0.1% at the start of the incubations (including four phylotypes with ≥ 1%) (Supporting Information Fig. S5), demonstrating that the majority of the responsive consortium are abundant microbiota members in the sulfidic zone of the arctic

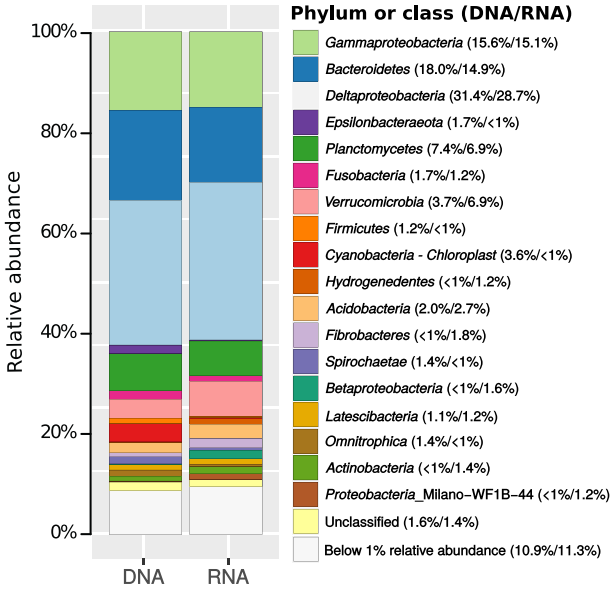

Fig. 2. Bacterial community composition in sulfidic Smeerenburgfjorden surface sediment at the start of the incubation experiments (day 0). Average (n = 4) relative 16S rRNA gene (DNA) and transcript (RNA) abundance of bacterial phyla or proteobacterial classes. Only phyla/classes with a relative abundance ≥ 1% on DNA or RNA level are indicated.

marine sediment *in situ.* Five phylotypes (1452, 4400, 4749, 7435, 10615) responded by significant increases in relative abundances of both 16S rRNA genes and transcripts, while six (2011, 4982, 7234, 7300, 9869, 10263) responded only by increases in relative 16S rRNA transcript abundance, including three deltaproteobacterial phylotypes that were stimulated by the amendment of acetate. The fourth, putative acetate-utilizing *Arcobacter* phylotype 10615 was low in abundance and ribosomal activity (< 0.1%) at day 0, but became dominant in spirulina- and acetate-amended incubations (Fig. 3). Four deltaproteobacterial phylotypes, including *Desulfobacteraceae* phylotype 2011 and [*Desulfobacterium*] phylotype 4982 that responded to acetate, were considered as putative SRM because they were inhibited by molybdate. The other two SRM phylotypes (*Desulfobacteraceae* phylotype 11380 and *Desulfobulbaceae* phylotype 3944) did not respond significantly to spirulina or acetate amendments (Fig. 3).

Single cell stable isotope probing revealed ^{13}C-incorporation in phylotypes that responded to substrate supplementation

Raman microspectroscopy of randomly selected cells from day 32 of the HD ^{13}C-spirulina incubations showed that only 4% of cells displayed a low level of ^{13}C labelling, which supports the finding that only a small part of

© 2018 The Authors. Environmental Microbiology published by Society for Applied Microbiology and John Wiley & Sons Ltd.,

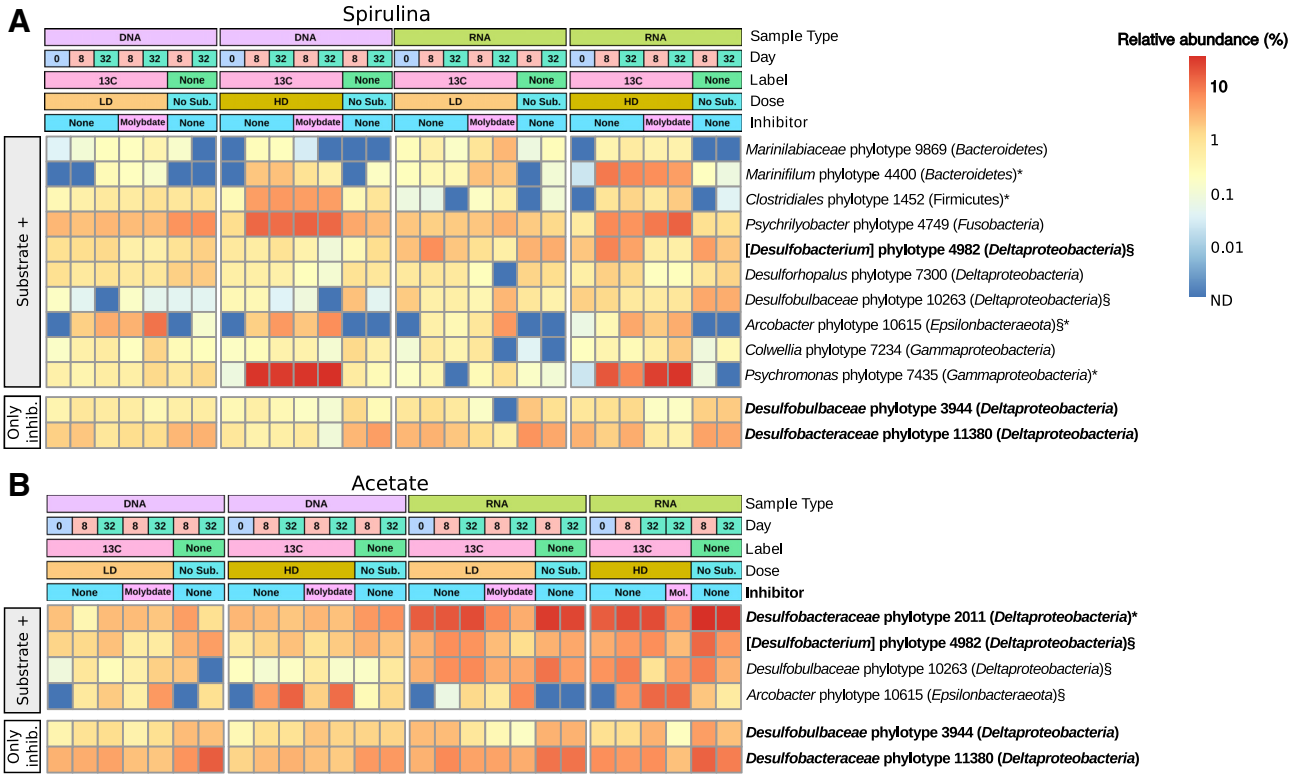

Fig. 3. Relative abundance heat-maps of substrate-responsive and molybdate-inhibited 16S rRNA phylotypes. Depicted are phylotypes that responded to substrate amendment and/or molybdate inhibition in spirulina (A) and acetate (B) incubations with significant relative abundance changes in at least two 16S rRNA gene or transcript libraries as compared to unamended or uninhibited incubations. SRM (i.e., molybdate-inhibited) phylotypes are highlighted in bold. Phylotypes that responded to both spirulina and acetate amendments are indicated with a section sign (§). Phylotypes that were analyzed by CARD-FISH-Raman microspectroscopy are indicated with an asterisk (*). Substrate + , phylotypes that responded to substrate additions. Only inhib., phylotypes that did not respond to substrate addition but were inhibited by molybdate. No Sub., no-substrate control incubation. Mol., Molybdate.

the native sediment community is involved in the degradation of spirulina necromass (Fig. 4). We further combined CARD-FISH and Raman microspectroscopy to confirm ^{13}C-substrate utilization and assimilation by individual cells of selected taxa that responded to the substrate additions. The used or newly developed CARD-FISH probes covered four putative hydrolytic/fermenting phylotypes, i.e., *Clostridiales* phylotype 1452, *Marinifilum* phylotype 4400, *Psychrilyobacter* phylotype 4749 and *Psychromonas* phylotype 7435 and two putative acetate-utilizing phylotypes, i.e., *Desulfobacteraceae* phylotype 2011 and *Arcobacter* phylotype 10615 (Supporting Information Fig. S6). All phylotypes that responded to ^{13}C-spirulina, including *Arcobacter* phylotype 10615 that responded to ^{13}C-spirulina and ^{13}C-acetate, showed significant cellular ^{13}C-incorporation at day 32 of the HD ^{13}C-spirulina incubations (Fig. 4). *Desulfobacteraceae* phylotype 2011 was also significantly enriched in comparison to the ^{12}C-spirulina control but only a small fraction (11%) of the cells were labelled at low level (Fig. 4). The fraction of ^{13}C-labeled *Desulfobacteraceae* phylotype 2011 cells was larger (37%) in HD ^{13}C-acetate incubations but individual cells had low ^{13}C/^{12}C phenylalanine peak height ratios, indicating only minor ^{13}C-incorporation.

Discussion

Different cellular responses of members of a bacterial consortium involved in mineralization of organic matter in an arctic marine sediment

OM in anoxic, sulfidic marine sediments is mainly degraded by the joint activity of hydrolysers, fermenters and SRM (Arndt *et al*., 2013). In order to investigate the microorganisms involved in sequential OM degradation, we performed anoxic incubation experiments at 0°C with arctic marine sediments from Smeerenburgfjorden (Svalbard). In these sediments sulfate reduction is the dominant carbon mineralization process, with important contributions by iron reduction (Finke *et al*., 2007). Sulfate reduction rates in sediment incubations without

© 2018 The Authors. Environmental Microbiology published by Society for Applied Microbiology and John Wiley & Sons Ltd.,

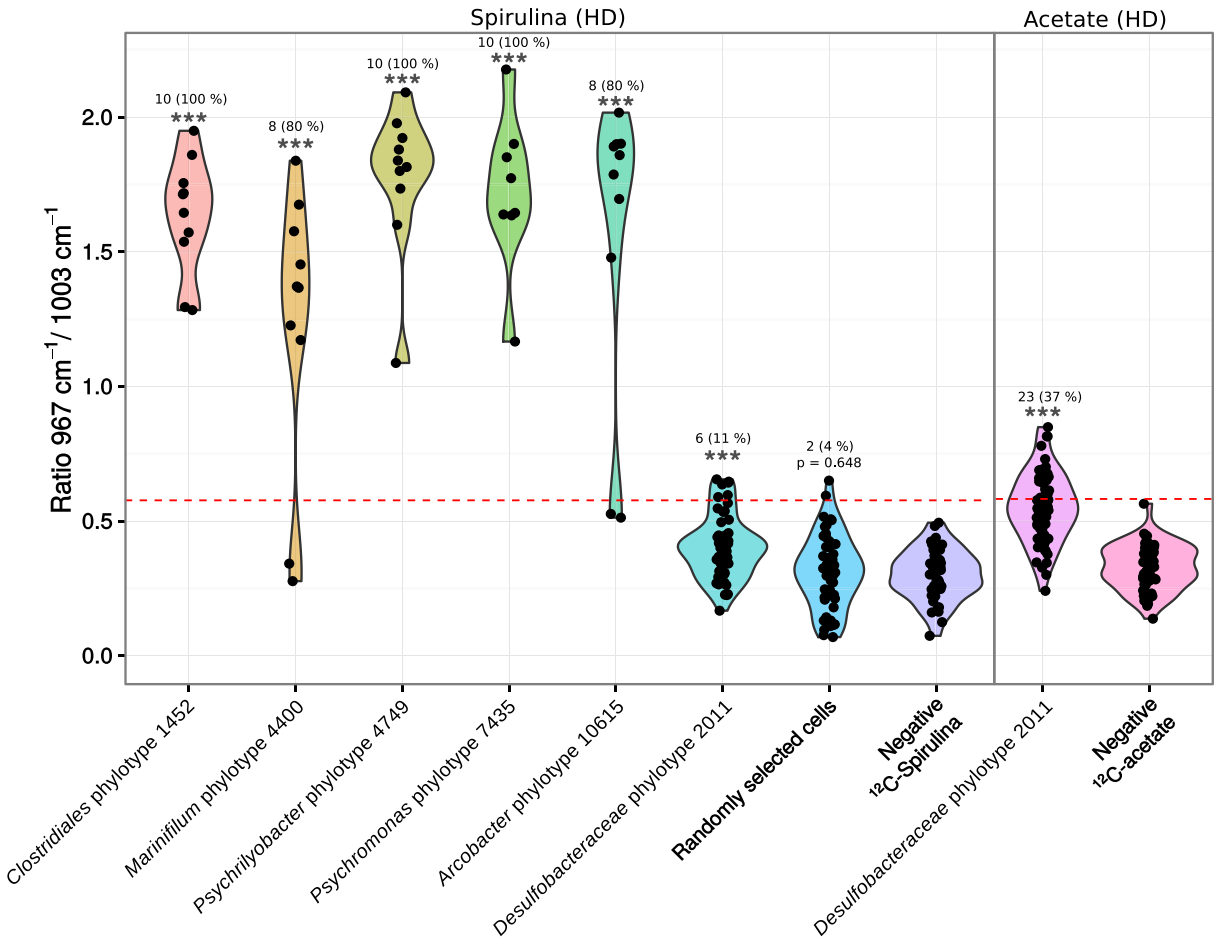

Fig. 4. ^{13}C-labelling of individual cells of substrate responsive phylotypes. CARD-FISH-Raman microspectroscopy analysis of ^{13}C-labelled probe-targeted cell populations (including selected substrate-responsive phylotypes) at day 32 in high dose (HD) ^{13}C-spirulina (1 mg ml^{-1}) and ^{13}C-acetate (1 mM) incubations. Stars (***) indicate significant ($P < 0.001$) ^{13}C-labelling, as revealed by comparing ^{13}C-labelled target populations to the respective negative control using Wilcoxon Rank Sum tests. Negative ^{12}C-spirulina, randomly selected cells from incubations with ^{12}C-spirulina at day 0. Negative ^{12}C-acetate, cells of *Desulfobacteraceae* phylotype 2011 (*Deltaproteobacteria*) from incubations with ^{12}C-acetate at day 0. The red dashed line shows the threshold for detection of ^{13}C-labelling in an individual cell.

external substrates (9–18 nmol cm^{-3} d^{-1}) (Fig. 1A and B) were in the range of previously determined mean *in situ* rates of 15–20 nmol cm^{-3} d^{-1} in the sulfate reduction zone of Smeerenburgfjorden sediments (Jørgensen *et al*., 2010; Sawicka *et al*., 2012; Robador *et al*., 2016). Supplementation of spirulina and acetate, each at two different doses, to individual sediment microcosms immediately triggered significant increases in sulfate reduction rates, which were more pronounced in spirulina incubations (Fig. 1A). Interestingly, a 20-fold increase in substrate concentration resulted in only 55% and 38% increased sulfate reduction rates in spirulina and acetate incubations respectively. This indicated that the SRM community had almost reached maximal physiological activity at the lower substrate dose. Hydrolysis and fermentation of spirulina biomass predominantly generated acetate and smaller amounts of butyrate, propionate, valerate, formate and pyruvate (Fig. 1C and D). Accumulation of these VFAs in sulfate reduction-inhibited incubations confirmed that mineralization of OM and utilization of VFAs in this sediment is largely dependent on the activity of SRM.

Smeerenburgfjorden sediments harbor a cold-adapted microbial community that is primarily composed of *Deltaproteobacteria, Gammaproteobacteria* and representatives of the phylum *Bacteroidetes* (Ravenschlag *et al*., 1999–2001). These classes/phyla were also dominant in the sediments analyzed in the present study (Fig. 2). Here, we show that only eleven species-level phylotypes of this complex sediment microbiota responded significantly to spirulina or acetate supplementation during a 38 days incubation period at 0°C. Responsive phylotypes either only increased in relative 16S rRNA transcript abundance, which suggests response by increased ribosomal activity, or additionally in relative 16S rRNA gene abundance, which suggests response by growth

© 2018 The Authors. Environmental Microbiology published by Society for Applied Microbiology and John Wiley & Sons Ltd.,

(Hausmann *et al*., 2016). Acetate mainly triggered increases in ribosomal activity in SRM phylotypes 2011 and 4982, whereas four (phylotypes 4400, 1452, 4749, 7435) of the six phylotypes involved in the fermentation of spirulina necromass and the acetate-utilizing, non-sulfate-reducing *Arcobacter* phylotype 10615, also responded by increased relative 16S rRNA gene abundance (Fig. 3). Differences in spirulina- and acetate-based ^{13}C-labeling of individual cells confirmed different cellular response patterns of the diverse functional guilds in anaerobic carbon decomposition (Fig. 4). This difference in cellular response could relate to frequently observed higher process rates of hydrolysis as compared to the mineralization of VFAs (Arnosti, 2011). Hydrolytic microorganisms in marine sediments can respond to increased substrate availability by synthesis of extracellular enzymes (Brüchert and Arnosti, 2003), which might even persist in sediments and enable a fast response to new OM input (Fabiano and Danovaro, 1998). It has also been speculated that glucose-utilizing fermenters in arctic marine sediments have substantially higher growth yields than acetate-utilizing SRM (Kirchman *et al*., 2014). SRM in marine sediments require several days to upregulate their VFA turnover (Arnosti *et al*., 2005). The calculated energy yield from acetoclastic sulfate reduction at *in situ* conditions in Smeerenburgfjorden sediment (Supporting Information Material and Methods; Table S3) was –93.3 kJ mol^{-1}, which is much higher than the energetic limit of this process of –30 kJ mol^{-1} (Jin and Bethke, 2009; Glombitza *et al*., 2015). Thus, SRM in our sediment microcosms seemed not to be energy-limited even at low *in situ* acetate concentrations. However, most of the substrate might be funnelled through catabolic pathways for energy conservation as opposed to also supplying elements and energy for anabolism and thus growth and cell division (Rabus *et al*., 2013). Additionally, doubling times of previously isolated, psychrophilic SRM at 0°C are considerably lower than at their optimal growth temperatures, i.e., 30–170 h at 7–18°C (Knoblauch and Jørgensen, 1999). Cell physiological constraints of SRM might further limit the uptake of substrate from the sediment and intracellular activation (Schauder *et al*., 1986; Glombitza *et al*., 2015), and also adsorption of VFAs by the sediment matrix can significantly reduce substrate uptake and mineralization (Shaw *et al*., 1984; Finke *et al*., 2007). Increase in relative 16S rRNA gene abundance, i.e., putative growth of the non-sulfate-reducing *Arcobacter* phylotype in acetate incubations (Fig. 3) is conflicting. However, this may be explained by the use of the energetically more favourable electron acceptors manganese, nitrate or iron, which result in higher energy yields during OM oxidation than the use of sulfate (Froelich *et al*., 1979; LaRowe and Amend, 2014).

Psychrophilic fermenters of cyanobacterial necromass

Six phylotypes were considered hydrolysers/fermenters, because they showed a significant response to spirulina amendments, did not respond to the amendment of acetate, were not negatively impacted by amendment of the sulfate reduction inhibitor molybdate, and were related to described species with hydrolytic and/or fermentative metabolic capabilities (Fig. 5). Four of the phylotypes (*Psychromonas* phylotype 7435, *Gammaproteobacteria*; *Psychrilyobacter* phylotype 4749, *Fusobacteria*; *Marinifilum* phylotype 4400, *Bacteroidetes*; *Clostridiales* phylotype 1452, *Firmicutes*) grew (Fig. 3A) and incorporated spirulina-derived ^{13}C into their cells (Fig. 4). These phylotypes thus seemed to be primarily r-selected (Lynch and Neufeld, 2015) and thus able to quickly take advantage and grow upon availability of larger amounts of OM that, for example, are available during spring bloom-like events of primary producers that deposit to the seafloor upon cell death (Hebbeln and Wefer, 1991). In contrast, *Colwellia* phylotype 7234 (*Gammaproteobacteria*) and *Marinilabiliaceae* phylotype 9869 (*Bacteroidetes*) only responded by relative increase in ribosomal activity (Fig. 5). *Colwellia* phylotype 7234 was of high relative abundance in the native sediment (day 0) (Supporting Information Table S1), which suggests that it retains a more stable population size in periods of low nutrient supply.

Bacterial cellular biomass is composed of thousands of individual molecules and metabolites (Engelking, 2015), but amendment of spirulina necromass activated only very few members of the complex sediment microbiota, as observed in another study (Graue *et al*., 2012). Dry spirulina cell extract is mostly composed of crude protein (64-74%), carbohydrates (12-20%) and lipids (9-14%) (Ciferri, 1983), which thus represent the dominant food sources for the responsive bacteria and is in agreement with the various fermentative capabilities of their phylogenetically most closely related species (Supporting Information Results and Discussion).

SRM utilizing acetate and other electron donors

All four phylotypes that were inhibited by molybdate, and thus identified as SRM (Fig. 5), are members of the class *Deltaproteobacteria* (Fig. 3B), which contains the majority of ecologically relevant SRM in marine sediments (Wasmund *et al*., 2017). The abundant *Desulfobacteraceae* phylotype 2011 belongs to the globally distributed Sva0081 group of yet uncultured sediment bacteria (Supporting Information Fig. S5). Phylotype 4982 (*Desulfobulbaceae*) is very closely related to [*Desulfobacterium*] *catecholicum* (99% 16S rRNA identity) (Supporting Information Fig. S5), a complete oxidizer of acetate and other VFAs (Szewzyk and Pfennig, 1987). Both phylotypes responded to acetate amendment but mainly by increased ribosomal activity

© 2018 The Authors. Environmental Microbiology published by Society for Applied Microbiology and John Wiley & Sons Ltd.,

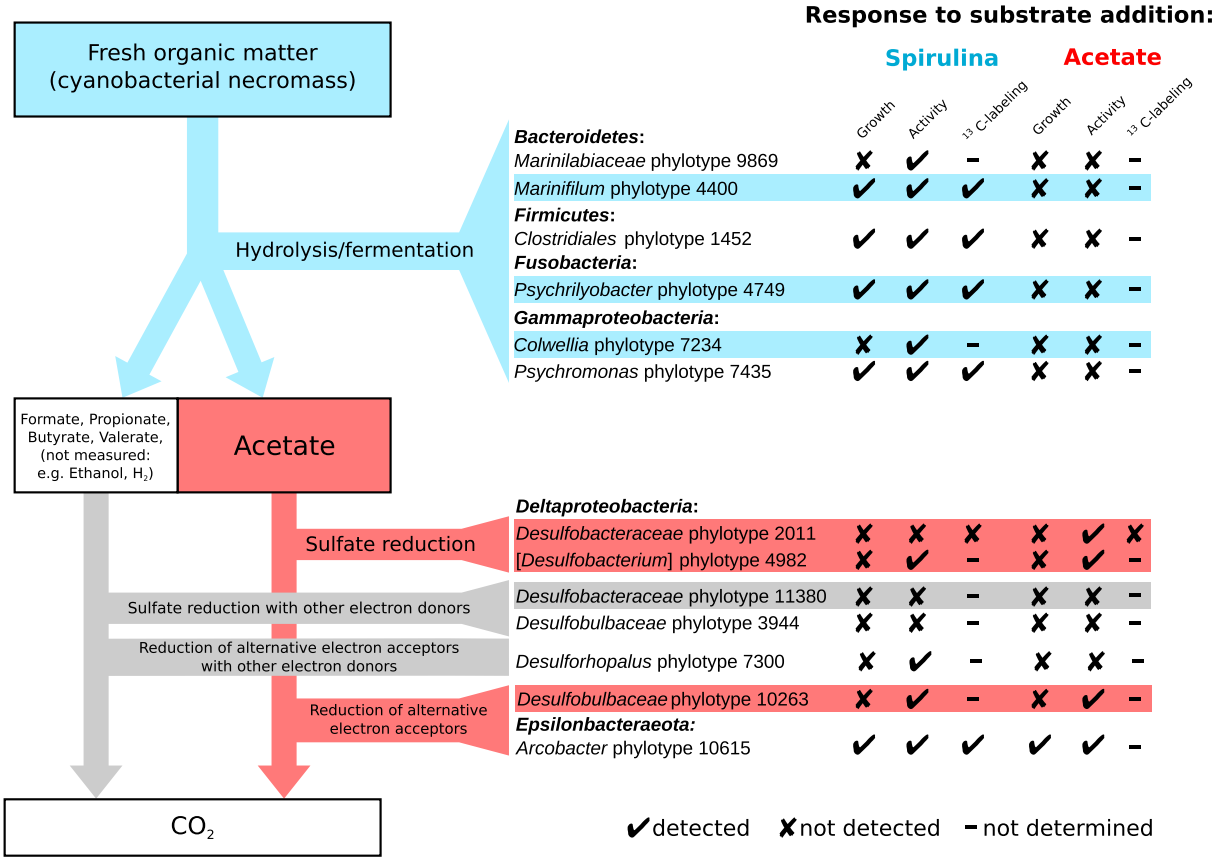

Fig. 5. A bacterial interaction model for organic matter degradation in sulfidic arctic marine sediments of Smeerenburgfjorden, Svalbard. Fresh biomass that is introduced into the system by sedimentation is utilized by hydrolytic and fermentative bacteria and degraded to VFAs, mainly acetate, which are further utilized by SRM or microorganisms that use alternative electron acceptors. Putative roles in organic carbon degradation are shown for identified phylotypes (Fig. 3). Growth, significant response in relative 16S rRNA gene abundance. Activity, significant response in relative 16S rRNA transcript abundance. ^{13}C-labelling, significant ^{13}C-incorporation by > 50% of phylotype cells from ^{13}C-spirulina or ^{13}C-acetate as revealed by single-cell CARD-FISH-Raman (Fig. 4). Responsive phylotypes that are highly abundant and/or ribosomally active in native sediment, i.e., ≥ 1% abundance in 16S rRNA gene or transcript libraries at day 0 (Supporting Information Table S1), are shaded.

(Fig. 3B). Additionally, *Desulfobacteraceae* phylotype 2011 incorporated only small amounts of ^{13}C from acetate into its biomass (Fig. 4). Our results suggest that cellular activity of acetate-utilizing SRM in arctic marine sediments is largely decoupled from an increase in their population size. We postulate that populations of SRM in marine surface sediments with constantly cold temperatures are rather stable (Robador *et al*., 2009), and only change slowly in response to long-term changes in substrate availability.

Besides the two acetate-utilizing SRM-phylotypes, we also identified *Desulfobulbaceae* phylotype 3944 and *Desulfobacteraceae* phylotype 11380 to be suppressed in incubations with molybdate (Fig. 3). Both phylotypes did not respond significantly to either spirulina or acetate amendments, which suggests that they utilize other, endogenous electron donors for sulfate reduction (Fig. 5). Alternatively, they might have other energy metabolisms that are inhibited by molybdate, e.g., utilization of taurine (Lie *et al*., 1999) or disproportionation of thiosulfate or elemental sulfur (Finster *et al*., 1998).

Bacteria that utilize VFAs but are not strictly dependent on sulfate reduction

Three VFA-utilizing phylotypes were not suppressed by molybdate (Fig. 5); *Arcobacter* phylotype 10615, *Desulfobulbaceae* phylotype 10263 and *Desulforhopalus* phylotype 7300. The first two responded to spirulina and acetate amendments (Figs 3 and 4), which indicated that both phylotypes primarily utilized the spirulina fermentation product acetate. In contrast *Desulforhopalus* phylotype 7300 only responded to spirulina incubations (Fig. 3A), potentially by consuming spirulina degradation intermediates other than acetate. Given that *Arcobacter* phylotype 10615 responded to acetate with particularly massive relative abundance increases (Fig. 3B), we hypothesize that it used electron acceptors more energetically favorable than sulfate for the oxidation of VFAs (Fig. 5). *Arcobacter*-related microorganisms use manganese, iron or nitrate as electron acceptors (Thamdrup *et al*., 2000; Vandieken *et al*., 2012; Canion *et al*., 2013;

© 2018 The Authors. Environmental Microbiology published by Society for Applied Microbiology and John Wiley & Sons Ltd.,

Vandieken and Thamdrup, 2013). Also, the SRM *Desulfobulbus propionicus*, which is related to *Desulfobulbaceae* phylotype 10263 (94.4% 16S rRNA identity) (Supporting Information Fig. S5), has similar metabolic capabilities in the absence of sulfate (Dannenberg *et al*., 1992; Lovley and Phillips, 1994; Holmes *et al*., 2004). *Desulforhopalus* phylotype 7300 was closely related to *Desulforhopalus singaporensis* (Supporting Information Fig. S5), which besides sulfate can also use nitrate, sulfite and thiosulfate as electron acceptor (Lie *et al*., 1999). Iron and nitrate reduction contribute to organic carbon oxidation in Svalbard fjord sediments (Kostka *et al*., 1999; Finke *et al*., 2007; Canion *et al*., 2014) and many SRM use intermediate sulfur species for respiration (Wasmund *et al*., 2017). Thus, iron, nitrate or intermediate sulfur species might have been utilized by the phylotypes that were not inhibited by molybdate.

Conclusions

We investigated degradation of complex OM in sulfidic Smeerenburgfjorden sediment from the arctic archipelago of Svalbard. We propose a metabolic and species interaction model for dead biomass mineralization in the conditions studied that may be found in permanently cold and sulfate-reduction-dominated sediments (Fig. 5). Deposited organic biomass was primarily degraded by a limited number of species from diverse phyla. Initial hydrolysis and fermentation of mainly proteins, carbohydrates and lipids to diverse VFAs were catalyzed by *Psychrilyobacter* (*Fusobacteria*), *Marinifilum* and *Marinilabiaceae* (*Bacteroidetes*), *Colwellia* and *Psychromonas* (*Gammaproteobacteria*) and *Clostridiales* species (*Firmicutes*). Acetate, the main fermentation product, was mineralized by sulfate-reducing species of the families *Desulfobacteraceae* and *Desulfobulbaceae* (*Deltaproteobacteria*) and by *Arcobacter* (*Epsilonbacteraeota*) and *Desulfobulbaceae (Deltaproteobacteria)* species that presumably used other electron acceptors than sulfate. Interestingly, cellular activation (i.e., increases in relative 16S rRNA transcript abundance and in single-cell ^{13}C-labelling) upon availability of new substrate was coupled to relative population growth (i.e., increases in relative 16S rRNA gene abundance) in microorganisms able to directly hydrolyze/ferment cyanobacterial necromass and in the acetate-utilizing *Arcobacter* species, but not in acetate-utilizing SRM. These different cellular responses of each species have important implications for the population dynamics of the different functional guild members in marine sediments. It is tempting to speculate that the taxa identified here will play increasing roles in the future mineralization of the predicted increased phyto-detrital organic material in arctic benthic systems (Lalande *et al*., 2009; Sørensen *et al*., 2015), and in determining the extent of burial of organic material into the subsurface.

Experimental procedures

Marine sediment sampling

Arctic marine sediment samples were collected from Smeerenburgfjorden, Svalbard (station J; 79°43′N, 11°05′E; water depth 216 m) in August 2011. Sediment from 5 to 10 cm depth was collected from several HAPS cores (KC Denmark A/S, Silkeborg, Denmark) (Kanneworff and Nicolaisen, 1972), transferred into gastight plastic bags (Hansen *et al*., 2000) and stored on ice at 0°C for up to 2.5 months prior to incubations.

Sediment incubations

Approximately 2 l of anoxic sediment slurry was prepared per set of substrate and concentrations (Supporting Information Fig. S1A) by homogenizing sediment with anoxic bottom water from station J at a 1:1 (w/w) ratio under constant flow of N_2 gas. 200 ml of slurry was distributed into 250 ml serum bottles, amended with different substrates, sealed with butyl rubber stoppers (Geo-Microbial Technologies) and incubated at 0°C (Supporting Information Fig. S1A). Incubations were performed with either acetate or spirulina (Sigma-Aldrich, Steinheim, Germany). Spirulina consists of freeze-dried cells of the cyanobacterium *Arthrospira platensis.* Incubations were performed with two different substrate concentrations; i.e., a low dose (LD) and a high dose (HD) with 50 μg ml^{-1} and 1 mg ml^{-1} of spirulina and with 50 μM and 1 mM of acetate respectively (Supporting Information Fig. S1A). Spirulina was added as a one-time pulse at the beginning of the experiment, whereas acetate was continuously added every four to seven days (Supporting Information Fig. S1B) in order to compensate for the supposedly high acetate turnover (Finke *et al*., 2007). LD acetate supplementation was in the range of concentrations measured *in situ* in Svalbard sediments (Finke *et al*., 2007). Parallel incubations were performed with ^{13}C-labeled acetate or ^{13}C-labelled spirulina (both Sigma Aldrich, 99 atom% ^{13}C), ^{12}C-substrates (unlabeled control), ^{13}C-labelled substrate in combination with 5 mM molybdate as a sulfate-reduction inhibitor (inhibited control) and an unamended control incubation (no-substrate control) (Supporting Information Fig. S1A). Molybdate was added at day 0 and after 3 weeks of incubation. At days 0, 4, 8, 13, 20, 25, 32 and 39 after the start of the incubations, subsamples were taken through the rubber stopper with a sterile 16-gauge needle (Braun) attached to a 10 ml Omnifix syringe (Braun). At each sampling time point, a subsample of 6.5 ml was taken and stored

© 2018 The Authors. Environmental Microbiology published by Society for Applied Microbiology and John Wiley & Sons Ltd.,

either at −80°C for VFA and nucleic acid analyses or fixed for CARD-FISH analyses as described below.

Biogeochemical analyses

Concentrations of the VFAs acetate, formate, propionate, butyrate, valerate, lactate and pyruvate were measured in the supernatant by 2-dimensional ion chromatography-mass spectrometry (IC-IC-MS; Dionex ICS-3000 coupled to an MSQ Plus™, both Thermo Scientific), equipped with an Ion Pack™ AS 24 as the first column to separate the VFAs from chloride, and an Ion Pack™ AS 11 HC as the second column) (Glombitza *et al*., 2014). Prior to the analyses, samples were thawed and filtered through disposable syringe filters (Acrodisc™ 13 mm, IC grade, polyethersulfone (PES) membrane with 0.2 μM pore size), that were previously cleaned by rinsing with 10 ml Milli-Q water (Utrapure, Type 1) (Glombitza *et al*., 2014). Both isotopic variants of acetate were analyzed in parallel in separate selected ion monitoring (SIM) channels, i.e., ^{12}C-acetate (m/z 59) and ^{13}C-acetate (m/z 61). The Gibbs Energy of acetoclastic sulfate reduction was calculated as described in Supporting Information Materials and Methods. Parallel incubations were set up with ^{35}S-labelled carrier-free sulfate tracer and sulfate reduction rates were determined using a single-step cold chromium distillation method (Kallmeyer *et al*., 2004). Significance of SRR differences between no substrate controls and substrate amended incubations were determined by Wilcoxon tests using the function wilcox.test() from the R statistical package (R Core Team, 2015).

16S rRNA gene and transcript sequence analyses

Nucleic acid extraction and preparation of 16S rRNA gene and transcript libraries is described in Supporting Information Material and Methods. Sequencing was performed on a GS FLX + instrument using Titanium chemistry (Roche, Mannheim, Germany) by Eurofins MWG Operon (Ebersberg, Germany). Sequencing reads were filtered using mothur's implementation of PyroNoise (Schloss *et al*., 2009; Quince *et al*., 2011) and clustered into phylotypes of approximate species-level at 97% sequence identity using UCLUST (Edgar, 2010) as evaluated previously (Berry *et al*., 2012). Representative sequences (mean length of 220 bp) were aligned with mothur using default settings. Chimeras that were detected with Chimera Slayer (Haas *et al*., 2011) were excluded from further analysis. Altogether we obtained 344,867 high quality reads (on average 4732 reads per sample) that clustered into 11,548 species-level phylotypes. Phylum/class-level classification was performed using mothur's implementation of the Ribosomal Database Project naïve Bayesian classifier (Wang *et al*., 2007; Schloss *et al*., 2009) with default settings. Note that reclassification of the class *Epsilonproteobacteria* into the new phylum *Epsilonbacteraeota* was recently proposed (Waite *et al*., 2017). Alpha diversity metrics were calculated (Caporaso *et al*., 2010) with re-sampling (100 re-samples) at 3250 reads to avoid sample based artifacts (Lozupone *et al*., 2011). Principal coordinates analysis (PCoA) was performed in the R software environment (R Core Team, 2015) on the re-sampled phylotype table based on Bray-Curtis dissimilarities using the software package phyloseq (McMurdie and Holmes, 2013). Phylotypes with a relative abundance of ≥ 1% of the community in at least one sample were aligned against the SILVA database SSU_Ref_NR99_128 (Quast *et al*., 2013) using SINA (Pruesse *et al*., 2012). A phylogenetic tree was calculated with FastTree (Price *et al*., 2009) using an alignment of closely related sequences that were selected from the non-redundant SILVA database SSU_Ref_NR99_128 (Quast *et al*., 2013). Phylotype sequences were subsequently added to the resulting tree using the EPA algorithm (Berger *et al*., 2011) in RAxML (Stamatakis, 2014). Trees were visualized using iTOL (Letunic and Bork, 2016). The sequence similarity between phylotypes and representative strains in the non-redundant SILVA database SSU_Ref_NR99_128 (Quast *et al*., 2013) was calculated using t_coffe (Notredame *et al*., 2000). Phylotypes associated with the utilization of the added substrate at a given dose or with sulfate reduction had to be significantly enriched in at least two 16S rRNA gene and/or transcript libraries (n = 4 for substrate utilization, n = 8 for sulfate reduction) compared to the respective control (no substrate control or inhibited control). Significant enrichment of phylotypes was determined using a two-proportion T-test (Müller *et al*., 2014; Robador *et al*., 2016). P-values were corrected for multiple comparisons using the Benjamini-Hochberg false discovery rate method with p.adjust() from the R statistical package (R Core Team, 2015). Corrected P-values of ≤ 0.01 were considered significant.

Sequence data

16S rRNA gene and transcript sequence data is available in the NCBI Short Read Archive under accession number SRP133170.

Catalyzed reporter deposition-fluorescence in situ hybridization coupled with raman microspectroscopy (CARD-FISH-raman)

Microbial cells were extracted from arctic marine sediment as described in Supporting Information Materials and Methods. The extracted cells were collected by filtration on polycarbonate filters (GTTP type, pore size

© 2018 The Authors. Environmental Microbiology published by Society for Applied Microbiology and John Wiley & Sons Ltd.,

0.2 μm, Millipore) and identified by CARD-FISH or two-step CARD-FISH (Supporting Information Materials and Methods). Hybridized cells were extracted from the filters (Supporting Information Materials and Methods) and spotted onto an aluminum-coated slide (A1136; EMF Corporation) for analysis on a LabRAM HR800 confocal Raman microscope (Horiba Jobin-Yvon) as outlined previously (Huang *et al*., 2007). The obtained single cell spectra were baseline-corrected using a polynomial function. Spectra were then aligned according to the phenylalanine peak region and normalized by dividing the spectral intensity at each wavelength by the total spectral intensity. Ratios between the height of the ^{13}C-phenylalanine peak (wavelength of 960–970 cm^{-1}) and the height of the ^{12}C-phenylalanine peak (wavelength of 1000–1005 cm^{-1}) were calculated. Significance of the peak height ratio differences between ^{13}C-labeled probe-targeted cell populations and negative controls were determined in the R software environment (R Core Team, 2015) with wilcoxon.test(). Testing for spirulina uptake was performed between probe-targeted cells in ^{13}C-spirulina incubations and populations of cells randomly selected from ^{12}C-spirulina incubations. Testing for acetate uptake by *Desulfobacteraceae* phylotype 2011 was performed between populations from ^{13}C-acetate and ^{12}C-acetate incubations respectively. The threshold for detection of ^{13}C-labeled cells was calculated by adding three times the standard deviation of the negative (^{12}C) control to the mean of the negative control.

Acknowledgements

We thank Laura Wehrmann for the excellent organization of the 2011 Svalbard cruise, Kristian Lund (captain) and Klaus Ryberg (first mate) of the MS Farm and cruise participants Carol Arnosti, Andy Canion, Patrick Chanton and Kolja Kindler for their assistance with sample collection. Furthermore, we thank Marc Mußmann for provide us with the CARD-FISH probe DSS1431. This work was financially supported by the Austrian Science Fund (FWF, P29426-B29 to KW; P25111-B22 to AL). The authors declare no conflict of interest.

References

Arndt, S., Jørgensen, B.B., LaRowe, D.E., Middelburg, J.J., Pancost, R.D., and Regnier, P. (2013) Quantifying the degradation of organic matter in marine sediments: A review and synthesis. *Earth-Sci Rev* **123**: 53–86.

Arnosti, C. (2011) Microbial extracellular enzymes and the marine carbon cycle. *Ann Rev Mar Sci* **3**: 401–425.

Arnosti, C., Finke, N., Larsen, O., and Ghobrial, S. (2005) Anoxic carbon degradation in Arctic sediments: Microbial transformations of complex substrates. *Geochim Cosmochim Acta* **69**: 2309–2320.

Arnosti, C., and Jørgensen, B.B. (2003) High activity and low temperature optima of extracellular enzymes in Arctic sediments: Implications for carbon cycling by heterotrophic microbial communities. *Mar Ecol Prog Ser* **249**: 15–24.

Arnosti, C., and Jørgensen, B.B. (2006) Organic carbon degradation in Arctic marine sediments, Svalbard: A comparison of initial and terminal steps. *Geomicrobiol J* **23**: 551–563.

Arrigo, K.R., van Dijken, G., and Pabi, S. (2008) Impact of a shrinking Arctic ice cover on marine primary production. *Geophys Res Lett* **35**: L19603.

Berger, S.A., Krompass, D., and Stamatakis, A. (2011) Performance, accuracy, and Web server for evolutionary placement of short sequence reads under maximum likelihood. *Syst Biol* **60**: 291–302.

Berry, D., Schwab, C., Milinovich, G., Reichert, J., Ben Mahfoudh, K., and Decker, T. (2012) Phylotype-level 16S rRNA analysis reveals new bacterial indicators of health state in acute murine colitis. *ISME J* **6**: 2091–2106.

Bowles, M.W., Mogollón, J.M., Kasten, S., Zabel, M., and Hinrichs, K.-U. (2014) Global rates of marine sulfate reduction and implications for sub-sea-floor metabolic activities. *Science* **344**: 889–891.

Brüchert, V., and Arnosti, C. (2003) Anaerobic carbon transformation: experimental studies with flow-through cells. *Mar Chem* **80**: 171–183.

Burdige, D.J. (2007) Preservation of organic matter in marine sediments: Controls, mechanisms, and an imbalance in sediment organic carbon budgets? *Chem Rev* **107**: 467–485.

Canion, A., Overholt, W.A., Kostka, J.E., Huettel, M., Lavik, G., and Kuypers, M.M.M. (2014) Temperature response of denitrification and anaerobic ammonium oxidation rates and microbial community structure in Arctic fjord sediments. *Environ Microbiol* **16**: 3331–3344.

Canion, A., Prakash, O., Green, S.J., Jahnke, L., Kuypers, M.M.M., and Kostka, J.E. (2013) Isolation and physiological characterization of psychrophilic denitrifying bacteria from permanently cold Arctic fjord sediments (Svalbard, Norway). *Environ Microbiol* **15**: 1606–1618.

Caporaso, J.G., Kuczynski, J., Stombaugh, J., Bittinger, K., Bushman, F.D., and Costello, E.K. (2010) QIIME allows analysis of high-throughput community sequencing data. *Nat Methods* **7**: 335–336.

Cavicchioli, R. (2016) On the concept of a psychrophile. *ISME J* **10**: 793–795.

Ciferri, O. (1983) Spirulina, the edible microorganism. *Microbiol Rev* **47**: 551–578.

Dannenberg, S., Kroder, M., Dilling, W., and Cypionka, H. (1992) Oxidation of H2, organic compounds and inorganic sulfur compounds coupled to reduction of O2 or nitrate by sulfate-reducing bacteria. *Arch Microbiol* **158**: 93–99.

Dunne, J.P., Sarmiento, J.L., and Gnanadesikan, A. (2007) A synthesis of global particle export from the surface ocean and cycling through the ocean interior and on the seafloor. *Global Biogeochem Cycles* **21**.

Edgar, R.C. (2010) Search and clustering orders of magnitude faster than BLAST. *Bioinformatics* **26**: 2460–2461.

Engelking, L.R. (2015) Chemical composition of living cells. In *Textbook of Veterinary Physiological Chemistry*. New York, USA: Elsevier, pp. 2–6.

© 2018 The Authors. Environmental Microbiology published by Society for Applied Microbiology and John Wiley & Sons Ltd.,

Fabiano, M., and Danovaro, R. (1998) Enzymatic activity, bacterial distribution, and organic matter composition in sediments of the Ross Sea (Antarctica). *Appl Environ Microbiol* **64**: 3838–3845.

Finke, N., Vandieken, V., and Jã¸Rgensen, B.B. (2007) Acetate, lactate, propionate, and isobutyrate as electron donors for iron and sulfate reduction in Arctic marine sediments, Svalbard. *FEMS Microbiol Ecol* **59**: 10–22.

Finster, K., Liesack, W., and Thamdrup, B. (1998) Elemental sulfur and thiosulfate disproportionation by *Desulfocapsa sulfoexigens* sp. nov., a new anaerobic bacterium isolated from marine surface sediment. *Appl Environ Microbiol* **64**: 119–125.

Froelich, P.N., Klinkhammer, G.P., Bender, M.L., Luedtke, N. A., Heath, G.R., Cullen, D., *et al*. (1979) Early oxidation of organic matter in pelagic sediments of the eastern equatorial Atlantic: Suboxic diagenesis. *Geochim Cosmochim Acta* **43**: 1075–1090.

Glombitza, C., Jaussi, M., Røy, H., Seidenkrantz, M.-S., Lomstein, B.A., and Jørgensen, B.B. (2015) Formate, acetate, and propionate as substrates for sulfate reduction in sub-arctic sediments of Southwest Greenland. *Front Microbiol* **6**: 846.

Glombitza, C., Pedersen, J., Røy, H., and Jørgensen, B.B. (2014) Direct analysis of volatile fatty acids in marine sediment porewater by two-dimensional ion chromatography-mass spectrometry. *Limnol Oceanogr Methods* **12**: 455–468.

Graue, J., Engelen, B., and Cypionka, H. (2012) Degradation of cyanobacterial biomass in anoxic tidal-flat sediments: A microcosm study of metabolic processes and community changes. *ISME J* **6**: 660–669.

Haas, B.J., Gevers, D., Earl, A.M., Feldgarden, M., Ward, D. V., Giannoukos, G., *et al*. (2011) Chimeric 16S rRNA sequence formation and detection in Sanger and 454-pyrosequenced PCR amplicons. *Genome Res* **21**: 494–504.

Hansen, J.W., Thamdrup, B., and Jørgensen, B.B. (2000) Anoxic incubation of sediment in gas-tight plastic bags: A method for biogeochemical process studies. *Mar Ecol Prog Ser* **208**: 273–282.

Hausmann, B., Knorr, K.-H., Schreck, K., Tringe, S.G., Glavina Del Rio, T., Loy, A., and Pester, M. (2016) Consortia of low-abundance bacteria drive sulfate reduction-dependent degradation of fermentation products in peat soil microcosms. *ISME J* **10**: 2365–2375.

Hebbeln, D., and Wefer, G. (1991) Effects of ice coverage and ice-rafted material on sedimentation in the Fram Strait. *Nature* **350**: 409–411.

Hedges, J.I., and Keil, R.G. (1995) Sedimentary organic matter preservation: An assessment and speculative synthesis. *Mar Chem* **49**: 81–115.

Holmes, D.E., Bond, D.R., and Lovley, D.R. (2004) Electron transfer by *Desulfobulbus propionicus* to Fe(III) and graphite electrodes. *Appl Environ Microbiol* **70**: 1234–1237.

Huang, W.E., Stoecker, K., Griffiths, R., Newbold, L., Daims, H., Whiteley, A.S., and Wagner, M. (2007) Raman--FISH: Combining stable-isotope Raman spectroscopy and fluorescence in situ hybridization for the single cell analysis of identity and function. *Environ Microbiol* **9**: 1878–1889.

Jin, Q., and Bethke, C.M. (2009) Cellular energy conservation and the rate of microbial sulfate reduction. *Geology* **37**: 1027–1030.

Jørgensen, B.B. (1982) Mineralization of organic matter in the sea bed—the role of sulphate reduction. *Nature* **296**: 643–645.

Jørgensen, B.B., and Boetius, A. (2007) Feast and famine–microbial life in the deep-sea bed. *Nat Rev Microbiol* **5**: 770–781.

Jørgensen, B.B., Dunker, R., Grünke, S., and Røy, H. (2010) Filamentous sulfur bacteria, Beggiatoa spp., in arctic marine sediments (Svalbard, 79 degrees N). *FEMS Microbiol Ecol* **73**: 500–513.

Kallmeyer, J., Ferdelman, T.G., Weber, A., Fossing, H., and Jørgensen, B.B. (2004) A cold chromium distillation procedure for radiolabeled sulfide applied to sulfate reduction measurements. *Limnol Oceanogr Methods* **2**: 171–180.

Kallmeyer, J., Pockalny, R., Adhikari, R.R., Smith, D.C., and D'Hondt, S. (2012) Global distribution of microbial abundance and biomass in subseafloor sediment. *Proc Natl Acad Sci U S A* **109**: 16213–16216.

Kanneworff, E., and Nicolaisen, W. (1972) The "Haps" a frame-supported bottom corer. *Ophelia* **10**: 119–128.

Kirchman, D.L., Hanson, T.E., Cottrell, M.T., and Hamdan, L. J. (2014) Metagenomic analysis of organic matter degradation in methane-rich Arctic Ocean sediments. *Limnol Oceanogr* **59**: 548–559.

Knoblauch, C., and Jørgensen, B.B. (1999) Effect of temperature on sulphate reduction, growth rate and growth yield in five psychrophilic sulphate-reducing bacteria from Arctic sediments. *Environ Microbiol* **1**: 457–467.

Knoblauch, C., Sahm, K., and Jørgensen, B.B. (1999) Psychrophilic sulfate-reducing bacteria isolated from permanently cold arctic marine sediments: Description of *Desulfofrigus oceanense* gen. nov., sp. nov., *Desulfofrigus fragile* sp. nov., *Desulfofaba gelida* gen. nov., sp. nov., *Desulfotalea psychrophila* gen. nov., sp. nov. and *Desulfotalea arctica* sp. nov. *Int J Syst Bacteriol* **49**: 1631–1643.

Kostka, J.E., Thamdrup, B., Glud, R.N., and Canfield, D.E. (1999) Rates and pathways of carbon oxidation in permanently cold Arctic sediments. *Mar Ecol Prog Ser* **180**: 7–21.

Lalande, C., Bélanger, S., and Fortier, L. (2009) Impact of a decreasing sea ice cover on the vertical export of particulate organic carbon in the northern Laptev Sea, Siberian Arctic Ocean. *Geophys Res Lett* **36**: 1–5.

LaRowe, D., and Amend, J. (2014) Energetic constraints on life in marine deep sediments. In *Life in Extreme Environments: Microbial Life of the Deep Biosphere*. Kallmeyer, J., and Wagner, D. (eds). Berlin: De Gruyter, pp. 279–302.

Letunic, I., and Bork, P. (2016) Interactive tree of life (iTOL) v3: An online tool for the display and annotation of phylogenetic and other trees. *Nucleic Acids Res* **44**: W242–W245.

Lie, T.J., Clawson, M.L., Godchaux, W., and Leadbetter, E. R. (1999) Sulfidogenesis from 2-aminoethanesulfonate (taurine) fermentation by a morphologically unusual sulfate-reducing bacterium, *Desulforhopalus singaporensis* sp. nov. *Appl Environ Microbiol* **65**: 3328–3334.

© 2018 The Authors. Environmental Microbiology published by Society for Applied Microbiology and John Wiley & Sons Ltd.,

Lovley, D.R., and Phillips, E.J. (1994) Novel processes for anaerobic sulfate production from elemental sulfur by sulfate-reducing bacteria. *Appl Environ Microbiol* **60**: 2394–2399.

Lozupone, C., Lladser, M.E., Knights, D., Stombaugh, J., and Knight, R. (2011) UniFrac: An effective distance metric for microbial community comparison. *ISME J* **5**: 169–172.

Lynch, M.D.J., and Neufeld, J.D. (2015) Ecology and exploration of the rare biosphere. *Nat Rev Microbiol* **13**: 217–229.

McMurdie, P.J., and Holmes, S. (2013) phyloseq: An R package for reproducible interactive analysis and graphics of microbiome census data. *PLoS One* **8**: e61217.

Müller, A.L., de Rezende, J.R., Hubert, C.R.J., Kjeldsen, K. U., Lagkouvardos, I., Berry, D., *et al*. (2014) Endospores of thermophilic bacteria as tracers of microbial dispersal by ocean currents. *ISME J* **8**: 1153–1165.

Muyzer, G., and Stams, A.J.M. (2008) The ecology and biotechnology of sulphate-reducing bacteria. *Nat Rev Microbiol* **6**: 441–454.

Notredame, C., Higgins, D.G., and Heringa, J. (2000) T-Coffee: A novel method for fast and accurate multiple sequence alignment. *J Mol Biol* **302**: 205–217.

van Nugteren, P., Moodley, L., Brummer, G.-J., Heip, C.H. R., Herman, P.M.J., and Middelburg, J.J. (2009) Seafloor ecosystem functioning: The importance of organic matter priming. *Mar Biol* **156**: 2277–2287.

Orsi, W.D., Richards, T.A., and Francis, W.R. (2018) Predicted microbial secretomes and their target substrates in marine sediment. *Nat Microbiol* **3**: 32–37.

Price, M.N., Dehal, P.S., and Arkin, A.P. (2009) FastTree: Computing large minimum evolution trees with profiles instead of a distance matrix. *Mol Biol Evol* **26**: 1641–1650.

Pruesse, E., Peplies, J., and Glöckner, F.O. (2012) SINA: Accurate high-throughput multiple sequence alignment of ribosomal RNA genes. *Bioinformatics* **28**: 1823–1829.

Quast, C., Pruesse, E., Yilmaz, P., Gerken, J., Schweer, T., Yarza, P., Peplies, J., and Glöckner, F.O. (2013) The SILVA ribosomal RNA gene database project: Improved data processing and web-based tools. *Nucleic Acids Res* **41**: D590–D596.

Quince, C., Lanzen, A., Davenport, R.J., and Turnbaugh, P. J. (2011) Removing noise from pyrosequenced amplicons. *BMC Bioinformatics* **12**: 38.

Rabus, R., Hansen, T.A., and Widdel, F. (2013) Dissimilatory sulfate- and sulfur-reducing prokaryotes. In *The Prokaryotes*. Dworkin, M., Falkow, S., Rosenberg, E., Schleifer, K.-H., Stackebrandt, E. (eds). New York: Springer, pp. 309–404.

Ravenschlag, K., Sahm, K., Pernthaler, J., and Amann, R. (1999) High bacterial diversity in permanently cold marine sediments. *Appl Environ Microbiol* **65**: 3982–3989.

Ravenschlag, K., Sahm, K., Knoblauch, C., Jørgensen, B.B., and Amann, R. (2000) Community structure, cellular rRNA content, and activity of sulfate-reducing bacteria in marine arctic sediments. *Appl Environ Microbiol* **66**: 3592–3602.

Ravenschlag, K., Sahm, K., and Amann, R. (2001) Quantitative molecular analysis of the microbial community in marine arctic sediments (Svalbard). *Appl Environ Microbiol* **67**: 387–395.

R Core Team (2015) *R: A language and environment for statistical computing*. Vienna, Austria: R Foundation for Statistical Computing. URL: http://www.r-project.org/

Robador, A., Brüchert, V., and Jørgensen, B.B. (2009) The impact of temperature change on the activity and community composition of sulfate-reducing bacteria in arctic versus temperate marine sediments. *Environ Microbiol* **11**: 1692–1703.

Robador, A., Müller, A.L., Sawicka, J.E., Berry, D., Hubert, C. R.J., Loy, A., *et al*. (2016) Activity and community structures of sulfate-reducing microorganisms in polar, temperate and tropical marine sediments. *ISME J* **10**: 796–809.

Sahm, K., Knoblauch, C., and Amann, R. (1999) Phylogenetic affiliation and quantification of psychrophilic sulfate-reducing isolates in marine Arctic sediments. *Appl Environ Microbiol* **65**: 3976–3981.

Sawicka, J.E., Jørgensen, B.B., and Brüchert, V. (2012) Temperature characteristics of bacterial sulfate reduction in continental shelf and slope sediments. *Biogeosci Discuss* **9**: 3425–3700.

Schauder, R., Eikmanns, B., Thauer, R.K., Widdel, F., and Fuchs, G. (1986) Acetate oxidation to CO_2 in anaerobic bacteria via a novel pathway not involving reactions of the citric acid cycle. *Arch Microbiol* **145**: 162–172.

Schloss, P.D., Westcott, S.L., Ryabin, T., Hall, J.R., Hartmann, M., Hollister, E.B., *et al*. (2009) Introducing mothur: Open-source, platform-independent, community-supported software for describing and comparing microbial communities. *Appl Environ Microbiol* **75**: 7537–7541.

Shaw, D.G., Alperin, M.J., Reeburgh, W.S., and McIntosh, D.J. (1984) Biogeochemistry of acetate in anoxic sediments of Skan Bay, Alaska. *Geochim Cosmochim Acta* **48**: 1819–1825.

Sørensen, H.L., Meire, L., Juul-Pedersen, T., de Stigter, H. C., Meysman, F., Rysgaard, S., *et al*. (2015) Seasonal carbon cycling in a Greenlandic fjord: An integrated pelagic and benthic study. *Mar Ecol Prog Ser* **539**: 1–17.

Stamatakis, A. (2014) RAxML version 8: A tool for phylogenetic analysis and post-analysis of large phylogenies. *Bioinformatics* **30**: 1312–1313.

Szewzyk, R., and Pfennig, N. (1987) Complete oxidation of catechol by the strictly anaerobic sulfate-reducing *Desulfobacterium catecholicum* sp. nov. *Arch Microbiol* **147**: 163–168.

Teske, A., Durbin, A., Ziervogel, K., Cox, C., and Arnosti, C. (2011) Microbial community composition and function in permanently cold seawater and sediments from an arctic fjord of svalbard. *Appl Environ Microbiol* **77**: 2008–2018.

Thamdrup, B., Rosselló-Mora, R., and Amann, R. (2000) Microbial manganese and sulfate reduction in Black Sea shelf sediments. *Appl Environ Microbiol* **66**: 2888–2897.

Vandieken, V., Pester, M., Finke, N., Hyun, J.-H., Friedrich, M.W., Loy, A., and Thamdrup, B. (2012) Three manganese oxide-rich marine sediments harbor similar communities of acetate-oxidizing manganese-reducing bacteria. *ISME J* **6**: 2078–2090.

Vandieken, V., and Thamdrup, B. (2013) Identification of acetate-oxidizing bacteria in a coastal marine surface sediment by RNA-stable isotope probing in anoxic slurries and intact cores. *FEMS Microbiol Ecol* **84**: 373–386.

© 2018 The Authors. Environmental Microbiology published by Society for Applied Microbiology and John Wiley & Sons Ltd.,

Vaughan, D.G., Comiso, J.C., Allison, I., Carrasco, J., Kaser, G., Kwok, R., *et al*. (2013) Observations: Cryosphere. In *Climate Change 2013: The Physical Science Basis. Contribution of Working Group I to the Fifth Assessment Report of the Intergovernmental Panel on Climate Change*. Cambridge University Press, Cambridge.

Waite, D.W., Vanwonterghem, I., Rinke, C., Parks, D.H., Zhang, Y., Takai, K., *et al*. (2017) Comparative genomic analysis of the class *Epsilonproteobacteria* and proposed reclassification to *Epsilonbacteraeota* (phyl. nov.). *Front Microbiol* **8**: 682.

Wang, F.-Q., Lin, X.-Z., Chen, G.-J., and Du, Z.-J. (2015) *Colwellia arctica* sp. nov., isolated from Arctic marine sediment. *Antonie Van Leeuwenhoek* **107**: 723–729.

Wang, Q., Garrity, G.M., Tiedje, J.M., and Cole, J.R. (2007) Naive Bayesian classifier for rapid assignment of rRNA sequences into the new bacterial taxonomy. *Appl Environ Microbiol* **73**: 5261–5267.

Wasmund, K., Mußmann, M., and Loy, A. (2017) The life sulfuric: Microbial ecology of sulfur cycling in marine sediments. *Environ Microbiol Rep* **9**: 323–344.

Supporting Information

Additional Supporting Information may be found in the online version of this article at the publisher's web-site:

Fig. S1. Experimental overview.

A. Setup of anoxic sediment incubations.

B. Timeline for substrate additions and sampling. LD, low substrate dose (50 μg ml^{-1} spirulina and 50 μM acetate). HD, high substrate dose (1 mg ml^{-1} spirulina and 1 mM acetate). SR-inhibitor, the sulfate reduction inhibitor molybdate.

Fig. S2. Volatile fatty acids concentrations in acetate incubations. Concentrations of volatile fatty acids in (A) LD and (B) HD incubations with acetate. ^{13}C-inhibited, sediment incubations with ^{13}C-substrate and molybdate. Note that acetate was periodically added (black arrows) right before the measurement. LD, low dose (50 μM) of acetate. HD, high dose (1 mM) of acetate. Note that the scales are different for each treatment and each VFA.

Fig. S3. Principal coordinates analysis of bacterial beta-diversity in anoxic sediment incubations. The analyses were based on Bray-Curtis dissimilarities of relative 16S rRNA gene (DNA) and transcript (RNA) abundances of bacterial phylotypes. Sample colour indicates type and concentration of added substrate. Sample shape indicates the day of sampling.

Fig. S4. Bacterial community dynamics in spirulina and acetate amended anoxic sediment incubations. Only phyla/classes with a relative 16S rRNA gene (DNA) and/or transcript (RNA) abundance of ≥ 1% at day 0 are indicated. ^{13}C., sediment incubations with ^{13}C-substrate. ^{13}Ci., sediment incubations with ^{13}C-substrate and molybdate. ^{12}C., sediment incubations with ^{12}C-substrate. None., no-substrate control. LD, low substrate dose (50 μg ml^{-1} spirulina or 50 μM acetate). HD, high substrate dose (1 mg ml^{-1} spirulina or 1 mM acetate).

Fig. S5. Phylogeny of abundant phylotypes. Only phylotypes with ≥ 1% relative 16S rRNA gene or transcript abundance in at least one incubation sample are shown. The tree was calculated using FastTree (Price *et al*., 2009) and an alignment of close relatives of phylotypes selected from the SILVA database SSU_Ref_NR99_128 (Quast *et al*., 2013). Short amplicon sequences were subsequently aligned with SINA (Pruesse *et al*., 2012) and added to the reference tree without changing its topology using the EPA algorithm (Berger et al., 2011) in RAxML (Stamatakis, 2014). Numbers in parentheses indicate average relative 16S rRNA gene/transcript abundances at day 0. Blue and red squares indicate significant enrichment ($P \leq 0.01$) in spirulina and acetate incubations respectively, compared to the no substrate control. Numbers within the squares give the number of samples (of 24 spirulina and 22 acetate incubation samples in total) in which the phylotype was significantly enriched. Yellow squares indicate sulfate-reduction-associated phylotypes, numbers in the square indicate numbers of samples (of 15 in total) in which the phylotype was significantly enriched in uninhibited incubations with substrate compared to molybdate-inhibited controls.

Fig. S6. Raman spectra of responsive phylotypes and their relative sequence abundance.

A. Overlays of single cell Raman spectra are displayed for the CARD-FISH- probe-labelled phylotypes in ^{13}C-spirulina (1 mg ml^{-1}) or ^{13}C-acetate (1 mM) incubations. *Clostridiales* phylotype 1452 (*Firmicutes), Marinifilum* phylotype 4400 (*Bacteroidetes), Psychrilyobacter* phylotype 4749 (*Fusobacteria), Psychromonas* phylotype 7435 (*Gammaproteobacteria), Arcobacter* phylotype 10615 (*Epsilonbacteraeota*) and *Desulfobacteraceae* phylotype 2011 (*Deltaproteobacteria*). Random, Raman spectra from randomly selected cells in the ^{13}C-spirulina (1 mg ml^{-1}) incubations. Negative ^{13}C-spirulina, Raman spectra from randomly selected cells from the ^{12}C-spirulina incubations. Negative ^{13}C- acetate, Raman spectra from cells of *Desulfobacteraceae* phylotype 2011 (*Deltaproteobacteria*) from incubations with ^{12}C-acetate at day 0. Insets show enlarged Raman spectrum regions containing ^{13}C-phenylalanine (wavelength of 960–970 cm^{-1}) and ^{12}C-phenylalanine (wavelength of 1000–1005 cm^{-1}) peaks.

B. Relative 16S rRNA gene and transcript abundance of CARD-FISH targeted cell populations in the respective substrate supplemented sediment incubation.

Table S1. Relative abundances of phylotypes with ≥ 1% of all bacterial 16S rRNA genes or transcripts at day 0.

Table S2. Read number, coverage and alpha-diversity of bacterial 16S rRNA gene and transcript libraries.

Table S3. Data for calculation of *in situ* Gibbs energy of acetoclastic sulfate reduction.

Table S4. Thermodynamic properties used for the calculation of standard state Gibbs energy change of reaction [DG_0 (T, p)]. Using the SUPCRT92 software (Johnson *et al*., 1992). References: (a) Schock, (1995) and (b) Schock and Helgeson (1988).

Table S5. 16S rRNA-targeted FISH probes.

© 2018 The Authors. Environmental Microbiology published by Society for Applied Microbiology and John Wiley & Sons Ltd.,

Chapter 4

Microorganisms that degrade protein and lipid macromolecules in Arctic marine sediment

Claus Pelikan, Kenneth Wasmund, Clemens Glombitza, Bela Hausmann, Craig W. Herbold, Hans Røy, Kasper Urup Kjeldsen, and Alexander Loy

Author contributions:

HR and KK provided sediment samples. CP and KW performed microcosm incubations, extracted DNA and prepared DNA-SIP gradients. CP measured sulfate concentrations and performed amplicon sequencing and metagenome analyses. CG measured volatile fatty acid concentrations. CP wrote the draft manuscript, with contributions from KW. AL revised a first version of the manuscript.
NOTE: Manuscript was not yet send to CG, BH, CWG, HR, and KUK for revisions.

Microorganisms that degrade protein and lipid macromolecules in Arctic marine sediment

Claus Pelikan[1,2], Kenneth Wasmund[1,2], Clemens Glombitza[3,4], Bela Hausmann[1], Craig W. Herbold[1], Hans Røy[3], Kasper Urup Kjeldsen[3] and Alexander Loy[1,2]*

[1]*Division of Microbial Ecology, Centre for Microbiology and Environmental Systems Science, University of Vienna, Vienna, Austria*
[2]*Austrian Polar Research Institute, Vienna, Austria*
[3]*Center for Geomicrobiology, Department of Bioscience, Aarhus University, Aarhus, Denmark*
[4]*NASA Ames Research Center, Mountain View, CA, United States*

*Correspondence: Alexander Loy (Tel: +43 1 4277 76605, loy@microbial-ecology.net)

Running Head: Protein and lipid degradation in arctic marine sediments

Abstract

Microorganisms mineralize substantial quantities of organic matter released from decaying cells. Proteins and lipids are abundant components of organic matter, however, the identity and function of microorganisms that degrade these cellular macromolecules remain understudied. Here, we incubated arctic marine sediment microcosms with ^{13}C-labelled proteins and lipids under sulfate-reducing conditions and tracked the microbial uptake of ^{13}C-carbon via DNA-based stable isotope probing (DNA-SIP). Microbial community dynamics and enrichment in ^{13}C-DNA among SIP fractions was examined by high-throughput sequencing of 16S rRNA genes and dissimilatory sulfite reductase-*dsrB* for sulfate-reducing microorganisms (SRM). We show that proteins were initially hydrolyzed and catabolized by *Psychrilyobacter*, *Psychromonas*, *Photobacterium*, *Fusibacter,* and *Clostridia* species, whereas primary degradation of lipids was mainly conducted by *Vibrio* and *Psychromonas* species. ^{13}C-labelling of a *Psychromonas* species-level OTU from both proteins and lipids was explained by sub-OTU diversity, whereby four distinct sub-OTUs degraded the different substrates. All metagenome-derived genomes of the identified primary hydrolyzers encoded secretion systems to release enzymes for extracellular hydrolysis of macromolecules, with the exception of *Psychrilyobacter*. The *Psychrilyobacter* might instead take-up digested peptides or use an unknown secretion mechanism. Sulfate-reducing *Deltaproteobacteria* species primarily utilized degradation intermediates, i.e., formate, lactate, butyrate and iso-butyrate. Genomic predictions suggested that a new *Desulfoluna*-related sulfate-reducing species could additionally scavenge long-chain fatty acids. Our findings elucidated the identities and functions of several key microorganisms and provided

important insights into niche partitioning during protein and lipid degradation in arctic marine sediments.

Introduction

The majority of marine sediments that underlie the Earth's oceans are dominated by heterotrophic processes and are primarily sustained by “pelagic-benthic” coupling (Hop *et al.*, 2002), i.e., a constant supply of organic matter from photosynthetic planktonic organisms that thrive in the overlying water column and settle with particulate aggregates to the seafloor after their death (Arndt *et al.*, 2013). The amount and composition of organic matter that reaches the seafloor is strongly dependent on water depth, whereby continental shelfs and shallow sediments generally receive greater inputs compared to deep sea sediments (Dunne *et al.*, 2007). In cold polar regions with lower microbial activities in the water column (Christian and Karl, 1995), a large fraction of phytodetritus from spring bloom-like events reaches the underlying sediments (Fabiano and Pusceddu, 1998). Additionally, organic matter inputs from land-derived sources can be substantial in areas close to land and rivers, as well as polar regions subjected to melting (Arndt *et al.*, 2013; Wehrmann *et al.*, 2014).

Organic matter in marine sediments is largely composed of an immense diversity of macromolecules (Thurman, 1985), of which a substantial component can be deconstructed by microorganisms and utilized as nutrient and energy sources (Arndt *et al.*, 2013). Proteins and lipids typically constitute 10% and 5-10% of the organic matter found in marine sediments, respectively (Hedges and Oades, 1997; Burdige, 2007). Proteins, peptides and amino acids are sources of nitrogen (McCarthy *et al.*, 1997), which become particularly important in sediment habitats when inorganic nitrogen sources are depleted (Vetter and Deming, 1994). Lipids generally consist of an alkyl chain that is ester- or ether-bound to a polar head group such as phospho-glycerol or a glycerol that is glycosidically bound to a sugar moiety. They are major components of phytoplankton biomass (Parsons *et al.*, 1961; Hudson and Karis, 1974), of which the less labile fraction survives degradation in the water column (Wakeham *et al.*, 1984), and is microbially degraded in the underlying sediments (Harvey *et al.*, 1986).

Most macromolecules are too large to be directly imported into cells (Meyer-Reil, 1991). Hydrolysis of macromolecules via the activity of extracellular enzymes is the rate limiting step during organic matter mineralization in heterotrophic marine sediments (Meyer-Reil, 1991), which teem with microorganisms that encode a large diversity of extracellular hydrolases (Orsi et al., 2017). Interestingly, peptidase activity is negatively correlated to amount of phytodetritus input, whereas lipase activity is positively correlated (Vetter and Deming, 1994). This indicates that peptidases are excreted in times of nutrient limitation, whereas lipases are excreted when organic matter availability is high (Vetter and Deming, 1994). Thus, niche partitioning of protein and lipid degraders

might not only reflect substrate preferences but might additionally indicate differences in ecological response strategies to organic matter supply.

The degradation of organic matter such as proteins and lipids in anoxic marine sediments is a complex microbial process (Müller *et al.*, 2018). The hydrolysis of macromolecules results in the generation of oligomers and monomers, which are then fermented to alcohols, lactate and volatile fatty acids (VFAs), such as butyrate, propionate, acetate and formate. These fermentation products are subsequently mineralized to CH_4, CO_2 and H_2 (Muyzer and Stams, 2008). Sulfate is the second most abundant anion in seawater and penetrates into sediments where it can be used as electron acceptor during anaerobic respiration. Thus, sulfate-reducing microorganisms (SRM) contribute significantly to the degradation and turnover of organic matter on a global scale (Jørgensen, 1982; Bowles *et al.*, 2014). SRM in marine sediments are primarily known to oxidize and mineralize fermentation products such as acetate (Knoblauch *et al.*, 1999; Sahm *et al.*, 1999; Webster *et al.*, 2006; Na *et al.*, 2015; Müller *et al.*, 2018). However, many incompletely and completely oxidizing SRM are also known to oxidize higher fatty acids (Rabus *et al.*, 2013). In marine sediments, SRM are thus possibly important for both, the terminal mineralization of protein and lipid degradation products, as well as direct oxidation of long-chain fatty acids. Even though, the biogeochemistry of organic matter degradation in anoxic sediments is relatively well understood (e.g. Zinke *et al.*, 2018), the microbial key players that are responsible for hydrolysis, fermentation and terminal mineralization of organic matter and the trophic links between these processes remain understudied.

In the present study, we supplemented ^{13}C-labelled proteins and ^{13}C-labelled lipids to anoxic 4°C-cold microcosms of arctic marine sediment incubated under sulfate-reduction-inhibited and uninhibited conditions. Catabolism and assimiliation of ^{13}C-labelled substrates by the sediment microorganisms was investigated by DNA-based stable isotope probing (DNA-SIP) and amplicon sequencing of 16S rRNA and dissimilatory sulfite reductase-*dsrB*. The degradation of organic matter was monitored by measuring concentrations of VFAs and sulfate. Metagenome sequencing and genome-resolved analyses were used to predict excreted enzymes and reconstruct organic matter degradation pathways in key organisms identified by DNA-SIP. This study revealed (i) the identities and foraging strategies of several key protein- and lipid-consuming bacteria in arctic marine sediments, (ii) that niche partitioning among *Psychromonas* subspecies was based on differential protein and lipid utilization, (iii) and that SRM of the family *Desulfobacteraceae* mainly utilized macromolecule degradation intermediates, i.e., butyrate, lactate and formate, but that a newly-identified SRM species could also utilize higher fatty acids as substrates.

Materials and methods

Sediment incubations

Sediment slurries were produced with surface sediment (0-30 cm) from Greenland (Nuuk fjord 'station 3', water depth 498m, August 2013, 64°26′45″N, 52°47'39''E) mixed 1:1 (v/v) with anoxic artificial seawater (Graue *et al.*, 2012) containing approximately 28 mM sulfate. For each microcosm, 40 ml of this slurry was distributed into 250 ml serum vials under anoxic conditions. Triplicate microcosms were either supplemented with a single dose of 300 µg C g^{-1} ^{13}C-labelled substrate (Algal lipid mixture-^{13}C, 99 atom% ^{13}C or Algal crude protein extract-^{13}C, 98 atom% ^{13}C, Sigma aldrich), with 300 µg C g^{-1} ^{13}C labelled substrates and the dissimilatory sulfate reduction inhibitor molybdate (28mM; (Newport and Nedwell, 1988)), or were left without supplementation. Microcosms were maintained at 4°C during all incubations. The microcosms were sampled after 2, 5, 10, 17, 25 and 48 days of incubation in an anoxic glove-box (nitrogen atmosphere containing approximately 2% hydrogen, 10% CO_2). Sediment samples were taken for analysis of volatile fatty acids and sulfate (1 ml), as well as for DNA-based analyses (0.5 ml). Samples were stored on pre-cooled ice packs in the anoxic glove box and were transferred immediately to the -80 °C freezer after sampling.

Determination of sulfate and volatile fatty acid concentrations

Sulfate concentrations in interstitial water samples were determined by capillary electrophoresis (P/ACETM MDQ molecular characterization system, Beckman Coulter) with the CEofixTM anions 5 kit (Analis). Standards were produced by dissolving known concentrations of Na_2SO_4 in artificial seawater. The concentrations of VFAs were determined as follows: samples were defrosted, vortexed and centrifuged at 10,000 rpm for 10 minutes. 100 µL of the supernatant were diluted 1:10 (v/v) in Milli-Q water. Syringe filters (Acrodisc IC grade filter, d=13 mm, Suprapor® membrane with 0.2 µm pore size) were first rinsed with 10 ml Milli-Q water followed by 0.5 ml of diluted sample to minimize further dilution with the rinsing water. Another 0.5 ml of sample were then filtered and measured by 2-dimensional ion chromatography-mass spectrometry (IC-IC-MS; Dionex ICS-3000 coupled to an MSQ Plus™, both Thermo Scientific), equipped with an Ion Pack™ AS 24 as the first column to separate the VFAs from chloride, and an Ion Pack™ AS 11 HC as the second column (Glombitza *et al.*, 2014).

DNA extraction

For DNA-SIP gradients and PCR-based amplicon sequencing, DNA was extracted using a combination of bead beating, cetyltrimethylammonium bromide-containing buffer and phenol-chloroform extractions. 0.5 g of sediment slurry was added to in Lysing Matrix E tubes (MP Biomedicals) and were suspended in 0.675 ml cetyltrimethylammonium bromide containing extraction buffer, as described previously (Dumont *et al.*, 2006). The

tubes were placed on a rotary shaker (200 rpm) and incubated at 37°C for 30 minutes. The samples were supplemented with 75 µL of sodium dodecyl sulfate (20% w/v) and were then incubated for 1 hour at 65°C (tubes were inverted every 20 minutes). Samples were subjected to 2 rounds of bead beating with a speed of '6' for 30 s using a FastPrep®-24 bead beater (MP Biomedicals). In between the beat beating steps, samples were cooled on ice. Debris was collected by centrifugation at 6,000 g for 10 minutes at 25°C and supernatant was collected into a clean tube. An equal volume of phenol:chloroform:isoamyl alcohol (ROTH) was added to the supernatant and tubes were repeatedly inverted to mix, followed by centrifugation at 16,000 g for 10 min at 25°C. The aqueous phase (upper layer) was transferred into a clean 1.5 ml tube, supplemented with 0.6 volume of 2-propanol and incubated for 1 hour at 4°C to to precipitate DNA. The precipitate was then pelleted by centrifugation at 16,000 g for 30 min at 4°C. DNA pellets were washed with 250 µL of 70% (v/v) ethanol, air dried and resuspended in 50 µL Tris buffer [10mM Tris-HCl (pH 8.0)]. For metagenome sequencing, DNA was extracted from the sediment at day 0 and from protein and lipid supplemented sediment microcosms at days 5, 17 and 25 using the Ultra Pure Power Soil Kit (MoBio).

DNA-SIP gradients

$CsCl_2$ gradients with 5 µg DNA were prepared in temperature controlled room at 23°C according to a previously published protocol (Neufeld *et al.*, 2007). The gradient mixtures were added to ultracentrifuge tubes (Beckman Coulter) and were centrifuged in an Optima L-100XP ultracentrifuge (Beckman Coulter) using the VTi 90 rotor for >48 hours at 49,500 rpm at 20 °C. After centrifugation, gradients were fractionated into 250 µL fractions by puncturing the bottom of the tube with a sterile needle and adding water to the gradient tube at the top using a sterile needle and a syringe pump (World Precision Instruments). The density of collected fractions was determined by using a digital refractometer (AR 200; Reichert Analytical Instrument) at 23 °C. Afterwards, DNA was precipitated with 500 µL sterile PEG 6000 (30% polyethylene glycol 6000 and 1.6 M NaCl) and 1 µL of glycogen (5 µg/ml) and subsequently purified as described previously (Neufeld *et al.*, 2007). Bacterial DNA in SIP fractions was quantified by real-time PCR (qPCR) using the primers 341F 5'-CCT ACG GGA GGC AGC AG-3' and 534R 5'-ATT ACG GCG GCT GCT GGC A-3'. The 20 µL qPCR mix contained 1x IQ™ SYBR Green Supermix (BIO-RAD), 0.25 µM of each primer and 1 µL of 1:10 diluted DNA from individual gradient fractions. The thermal cycling program consisted of 3 min at 95°C, 39 cycles of 95°C for 15 seconds, 60°C for 30 seconds and 72°C for 39 seconds followed by a melting curve from 60°C to 95°C by increments of 0.5°C every 5 seconds.

Amplicon sequencing and analysis

Barcoded 16S rRNA gene and *dsrB* amplicons for Illumina MiSeq sequencing were produced using a previously established two-step PCR approach (Herbold *et al.*, 2016;

Pelikan *et al.*, 2016). 16S rRNA gene and *dsrB* amplicon raw reads were processed as described previously (Herbold *et al.*, 2016; Pelikan *et al.*, 2016). The identity thresholds used for species-level OTU clustering were 97% and 90% for 16S rRNA genes and *dsrB*, respectively. Sub-OTU diversity at single-nucleotide resolution in the amplicon data was investigated using cluster-free filtering (Tikhonov *et al.*, 2015). An OTU was considered to be ^{13}C-enriched when it was significantly more abundant in 'heavy' SIP fractions, i.e., density higher than 1.726 g ml^{-1}, compared to 'light' fractions, i.e., density lower than 1.720 g ml^{-1}, obtained from the same incubation, as determined using Deseq2 (version 1.10.1) (Love et al. 2014) in the R software environment (R core team, 2014). The sequence abundance of each OTU in the heavy part of the DNA-SIP gradient (numerator), was compared to its sequence abundance in the light part of the DNA-SIP gradient (denominator). Only OTUs with more than 5 read counts per sample in at least 5 samples, i.e., 16% of the whole dataset, were considered during Deseq2 analyses. Results were extracted with the command results(cooksCutoff = FALSE, altHypothesis = c("greater")) and were only considered significant if (i) the adjusted p-value was below 0.1 and (ii) the respective OTU was not significantly enriched in the heavy fractions of the DNA-SIP gradient from the no substrate incubations. OTU counts were normalized with Deseq2 and heatmaps of enriched OTUs were created with R software package pheatmap (version 1.0.8; https://CRAN.R-project.org/package=pheatmap).

Metagenome sequencing and differential coverage binning

Metagenome libraries were produced with the Nextera XT DNA Library Preparation Kit (Illumina) and paired-end sequencing was performed on an Illumina Hiseq 2500 at the Vienna Biocenter Core Facilities Next Generation Sequencing facility (Vienna, Austria). Bam files were first translated into fastq files using SAMtools (Li *et al.*, 2009). Reads with a q-score below 10 were removed and sequence coverage was normalized across samples using bbnorm with an average read depth of 100 and a minimum read depth of 3 (BBmap package v. 33.57 http://sourceforge.net/projects/bbmap/). Normalized read files were assembled with IDBA-UD (Peng *et al.*, 2012) and SPAdes (Bankevich *et al.*, 2012) using default parameters. Reads of each sample were mapped to the each assembly using BWA (Li and Durbin, 2009), and coverage information was obtained using SAMtools (Li *et al.*, 2009). Differential coverage binning was performed with MetaBAT (Kang *et al.*, 2015), MaxBin (Wu *et al.*, 2016), and CONCOCT (Alneberg *et al.*, 2014). Following the programs default mode, only contigs with a minimum length of 2,500 and 1,000 bp were used for binning with MetaBAT and MaxBin/CONCOCT, respectively. The resulting metagenome-assembled genomes (MAGs) generated from different assemblies and binning programs were aggregated with DAS Tool (Sieber *et al.*, 2018) and de-replicated with dRep using the programs default parameters (Olm *et al.*, 2017). MAGs that could be linked to ^{13}C-incorporating OTUs during protein and lipid hydrolysis, i.e., because the MAG contained a matching 16S rRNA gene and/or *dsrB* sequence, were further analyzed.

Selected MAGs were evaluated for completion and contamination using checkM (Parks *et al.*, 2015), and classified using the Genome Taxonomy Database (GTDB) (Parks *et al.*, 2018). A genome tree of MAGs, the genome of the type strain of *Psychrilyobacter atlanticus* and closely related reference genomes was constructed from the concatenated marker gene alignment provided by GTDB (Parks *et al.*, 2018). A tree was built from this concatenated marker gene alignment with FastTree (Price *et al.*, 2010) and visualized with iTOL (Letunic and Bork, 2007). Average nucleotide identities (ANI) and average amino acid identities (AAI) of selected MAGs and closely related reference genomes were determined using all-vs-all FastANI 1.1 with default parameters (Jain *et al.*, 2018) and CompareM 0.0.23 (aai_wf) with default parameters (https://github.com/dparks1134/CompareM), respectively.

Genome annotation

MAGs were annotated with the MicroScope annotation platform (Vallenet *et al.*, 2017). The annotations of proteins were confirmed by DIAMOND blastp searches (Buchfink *et al.*, 2015) against the NCBI-nr database (e-value 10^{-5}), hidden Markov model-based searches using Interproscan (Jones *et al.*, 2014) with the databases Pfam-A (Finn *et al.*, 2013) and TIGRFAM (Haft *et al.*, 2003), and online blastp searches against the UniProt database (UniProt Consortium, 2018). Possible hydrolytic enzymes were examined for secretion signal peptide sequences and transmembrane helices using the Phobius online server (Kall *et al.*, 2007). Furthermore, peptidases and lipases/esterases were additionally compared to the databases MEROPS (Rawlings, 2000) and ESTHER (Lenfant *et al.*, 2013), respectively, using DIAMOND blastP searches (e-value > 10^{-5}, identity ≥ 30). The selection of potentially catabolic peptidases encoded by genomes/MAGs was based on two recent studies about extracellular peptidases in marine sediments (Steen *et al.*, 2016; Zinke *et al.*, 2018). Non-peptidase homologues and peptidases with regulatory functions, as indicated by MEROPS database descriptions, were not considered. The selection of catabolic lipases/esterases was based on the ESTHER database descriptions. The selected hydrolytic enzymes are listed in Supplementary Table S1.

Phylogenetic analyses of 16S rRNA *OTU and dsrB OTU sequences*

16S rRNA OTUs and 16S rRNA gene sequences from MAGs were aligned and classified with the SINA aligner (Pruesse *et al.*, 2012), using the SILVA database v.128 (Quast *et al.*, 2013). Full-length sequences of close relatives of 16S rRNA OTUs were extracted from the SILVA database and combined with the aligned 16S rRNA genes sequences that were obtained from MAGs. A reference tree was constructed from this combined alignment using FastTree (Price *et al.*, 2010). Subsequently, 16S rRNA OTUS and partial 16S rRNA genes from MAGs were added to the reference tree using the EPA algorithm (Berger *et al.*, 2011) in RAxML (Stamatakis, 2014). *dsrB* OTUs were translated, aligned to a reference DsrAB alignment (Pelikan *et al.*, in prep) using MAFFT (Katoh *et al.*, 2002), and then placed into a

reference tree using the EPA algorithm (Berger *et al.*, 2011) in RAxML (Stamatakis, 2014). Both trees were visualized in iTOL (Letunic and Bork, 2007).

Results

Sulfate removal and development of VFAs during organic matter degradation

Sulfate was almost completely consumed after 48 days in all incubation treatments except those in which sulfate reduction was inhibited by molybdate (Figure 1 A). Sulfate removal was most pronounced between days 5 and 25. Supplementation of proteins and lipids to the incubations resulted in moderately higher concentrations of acetate, propionate, butyrate and iso-butyrate as compared to the no-substrate controls (Figure 1 B). VFA dynamics were largely similar between protein- and lipid-amended microcosms, only that more iso-butyrate was produced at earlier time points in the protein incubations. Molybdate-inhibited incubations supplemented with proteins and lipids showed increased accumulation of formate, butyrate, and iso-butyrate, but decreased production of acetate and propionate. Lactate only accumulated in molybdate-inhibited incubations with lipid supplementations (Figure 1 B).

^{13}C-labelling of OTUs and sub-OTUs during protein and lipid catabolism and assimilation

To evaluate incorporation of ^{13}C from the added ^{13}C-labelled proteins or lipids into the DNA of replicating community members, bacterial 16S rRNA genes were quantified by qPCR of DNA that was extracted from individual SIP fractions (Supplementary Figure S1). Higher copy numbers in the “heavy” fractions of the gradient (i.e. density >1,726 g ml^{-1}) at days 5 and 10 in both ^{13}C-substrate incubations, indicated ^{13}C-uptake and incorporation already at these early time points. At days 17 and 25, only very small or no differences between ^{13}C-substrate incubations and the no substrate controls were observed.

Microbial community analysis of SIP fractions by 16S rRNA gene amplicon sequencing identified five OTUs (*Psychrilyobacter* OTU 5, *Psychromonas* OTU 4, *Fusibacter* OTU 38, JTB215 OTU 1 and *Photobacterium* OTU 54) that were enriched in ‘heavy’ fractions of the ^{13}C-protein incubations at day 5 (Figure 2 A; Supplementary Table S2). At day 10 we identified 19 additional OTUs with significant enrichment in ^{13}C-SIP fractions of incubations with protein amendments (Figure 2 A). These were affiliated with the classes *Deltaproteobacteria* (OTUs 2, 19, 36, 44, 67, 183, 232, 892, 4719), *Gammaproteobacteria* (OTUs 80, 128, 205, 285) and the phyla *Bacteroidetes* (OTUs 124 and 184), *Firmicutes* (OTUs 202 and 4050) and *Marinimicrobia* (OTU 123) or were unclassified (OTU 312) (Supplementary Figure S3).

In SIP gradients from ^{13}C-lipid amended incubations at day 5, significant ^{13}C-enrichment was revealed for only two gammaproteobacterial OTUs, *Psychromonas* OTU 4 and *Vibrio* OTU 80, which were also ^{13}C-enriched in protein amended incubations. An analysis of the microdiversity within OTU 4 indicated that four *Psychromonas* sub-OTUs

(4, 192, 9, 43) with more than 99% sequence identity to each other responded differently in incubations with protein or lipid amendments. The sub-OTUs 4 and 192, which were significantly enriched in ^{13}C-SIP fractions of ^{13}C-lipid incubations (Figure 3 A), were more closely related to each other than to sub-OTUs 9 and 43 (Figure3 B). Furthermore, the relative abundance of sub-OTUs 4 and 192 increased in ^{13}C-lipid incubations over time (Figure 3 C). Notably, sub-OTU 4 was also slightly enriched in ^{13}C-SIP fractions of ^{13}C-protein incubations (Figure 3 A). Sub-OTUs 9 and 43 were significantly enriched in ^{13}C-SIP fractions of ^{13}C-protein incubations, but only sub-OTU 9 increased in relative abundance in ^{13}C-protein incubations over time (Figure 3 C). No sub-OTU diversity was detected in any other ^{13}C-labelled OTU. At day 10, we identified three additional OTUs enriched in the ^{13}C-SIP fractions of ^{13}C-lipid incubations that were affiliated with the phylum *Firmicutes* (OTUs 1 and 4141) and the *class Deltaproteobacteria* (OTU 13310) (Figure 2 A).

We also monitored the temporal relative abundance changes of the identified, ^{13}C-enriched 16S rRNA OTUs (n= 26) in the protein- and lipid-treated microcosms. Between day 5 and 10, ten OTUs (1, 2, 4, 5, 19, 54, 80, 285, 4141 and 13310) increased in relative abundances in substrate amended incubations as compared to the no-substrate controls (Supplementary Figure S2 A). Furthermore, comparisons between microcosms incubated under sulfate-reducing conditions and incubations in which sulfate reduction was inhibited by molybdate identified OTUs 1, 2, 67, 4050 and 4141 as putative SRM or microorganisms that potentially interacted with SRM.

Amplicon sequencing of *dsrB* corroborated the involvement of SRM in protein and lipid degradation. Two *Desulfobacteraceae dsrB* OTUs (2 and 18) were significantly enriched in ^{13}C-SIP fractions of ^{13}C-lipid incubations at day 10 (Figure 2 B; Supplementary Table S3). In incubations with ^{13}C-protein, five *dsrB* OTUs were enriched in ^{13}C-SIP fractions at day 10, i.e., two *Desulfobacteraceae* OTUs (39 and 5), a *Desulfobulbaceae* OTU (75) and two OTUs that were affiliated with the uncultured DsrAB family-level lineages 9 (OTU 14) and 13 (OTU 20) (Figure 2 B; Supplementary Figure S4). The *dsrB* OTUs 2 and 18 were inhibited by molybdate, whereas the other five *dsrB* OTUs were not (Supplementary Figure S2 B).

Genomic evidence for extracellular hydrolysis of proteins and lipids

Metagenome sequencing and genome binning recovered nine metagenome-assembled genomes (MAGs) with good quality, i.e., completeness >80% and contamination <10%. Three of these MAGs were related to OTUs that incorporated ^{13}C-carbon from protein or lipid hydrolysis, and were thus selected for further analyses (Supplementary Table S4). These three MAGs were named *Psychromonas* GLG-1, *Desulfoluna* GLD-1 and *Clostridia* GPF-1. *Psychromonas* GLG-1 was most closely related to *Psychromonas aquimarina* ATCC BAA-1526 and encoded a 16S rRNA sequence that was identical to sub-OTU 4 (Supplementary Figure S3). The MAG *Desulfoluna* GLD-1 was most closely related to

Desulfoluna spongiiphila and encoded a *dsrB* sequence that was identical to *dsrB* OTU 2 (Supplementary Figure S4). *Clostridia* GPF-1 was distantly related to any publicly available genome (Supplementary Figure S5), with an AAI to the closest genome, i.e., *Caloranaerobacter azorensis* DSM 13643, of only 53.39% (alignment fraction: 37%). A 16S rRNA fragment (92 bp) was retrieved from *Clostridia* GPF-1, which was identical to 16S rRNA OTU 1 (Supplementary Figure S3). All bins that were affiliated with the genus *Psychrilyobacter* were very incomplete (<20%) (data not shown). Therefore, we analyzed the publicly available genome of *Psychrilyobacter atlanticus* DSM 19335, which encoded a 16S rRNA sequence that was identical to 16S rRNA OTU 5 (Supplementary Figure S3). Based on the DNA-SIP results and since we could link genomes/MAGs to specific OTU sequences, the aforementioned four genomes/MAGs were analyzed for their ability to degrade proteins (*P. atlanticus* corresponding to 16S rRNA OTU 5), lipids (*Psychromonas* GLG-1 corresponding to sub-OTU 4; *Desulfoluna* GLD-1 corresponding to *dsrB* OTU 2) or both macromolecules (*Clostridia* GPF-1 corresponding to 16S rRNA OTU 1).

The genome of *P. atlanticus* encoded a variety of peptidases (n=24), which were likely involved in breakdown of peptides for further catabolism of amino acids (Supplementary Table S5). Two of these peptidases (i.e. M3 and M24) encoded signal peptides for translocation across the cytoplasmic membrane (Figure 4). The secretion machinery of *P. atlanticus* was incomplete, i.e., the SEC pathway to transfer proteins to the periplasm was present, but Type II or Type III 'general' secretion systems could not be identified (Supplementary Table S5). Instead, the genome of *P. atlanticus* encoded a Type IV secretion system and Type V autotransporters. Overall, the genome of *P. atlanticus* encoded a copious array of predicted peptide (n=19) and amino acid transporters (n=38), especially when compared to the MAGs of the putative lipid degraders *Psychromonas* GLG-1 (peptide transporter, n=6; amino acid transporter, n=14) and *Desulfoluna* GLD-1 (peptide transporter, n=8; amino acid transporter, n=11) (Supplementary Table S5). In addition, the genome of *P. atlanticus* was the only analyzed genome that encoded for proton-dependent peptide transportation (Supplementary Table S5). The genome of *P. atlanticus* also encoded a glycerol-3-phosphate transporter, a glycerol facilitator and a short-chain fatty acid transporter (Supplementary Table S5).

Clostridia GPF-1 encoded the largest number of peptidases (n= 29) of all analyzed genomes (Supplementary Table S5). Three of these peptidases (M20, M24 and S8) have predicted secretion signals and might be excreted into the extracellular space via the SEC pathway (Figure 4). Similar to *P. atlanticus*, *Clostridia* GPF-1 encoded a broad array of peptide (n=14) and amino acid (n=24) transporters. In accordance with the DNA-SIP study, *Clostridia* GPF-1 also has the potential for catabolic breakdown of lipids. The MAG encoded one potentially secreted catabolic esterase/lipase that correspond to the ESTHER family Bacterial_EstLip_FamX, and two membrane bound esterases/lipases that correspond to the ESTHER families Bacterial_EstLip_Fam and Carboxylesterase, type B (Supplementary Table S5). Despite the potential of *Clostridia* GPF-1 to hydrolyze ester bonds between

glycerol and fatty acids, genes for known fatty acid transporters were not found. Nonetheless, we found a glycerol-3-phosphate transporter and a putative glycerol facilitator in close vicinity to a glycerol kinase (Supplementary Table S5).

The lipid-metabolizing capability of *Psychromonas* GLG-1 was supported by a gene for a carboxylesterase with a signal peptide, which corresponds to the ESTHER family Carboxylesterase, type B (Supplementary Table S5). In addition, *Psychromonas* GLG-1 encoded a great variety (n=14) of extracellular glycoside hydrolases (Supplementary Table S5), of which some might be able to hydrolyze glycosidic bonds between carbohydrate moieties or between carbohydrates and glycerol in glycolipids like the spirulina lipid digalactosyl diglyceride. *Psychromonas* GLG-1 encoded a complete SEC pathway, a TAT pathway and a Type II secretion system for enzyme secretion (Figure 4). The long chain fatty acids resulting from extracellular degradation of acyl chain esters, were likely incorporated by two long-chain fatty acid transporters (Supplementary Table S5). Glycerol transporters were not detected in the genome of *Psychromonas* GLG-1.

The *dsrB* OTU 2 related MAG *Desulfoluna* GLD-1 encoded no catabolic peptidases and lipases with secretion signals (Supplementary Table S5). However, we found a long-chain fatty acid transport protein that could be used to take up long-chain fatty acids and butyrate from the environment (Figure 5).

Intracellular catabolism of protein and lipid degradation intermediates

The genome of *P. atlanticus* encoded 22 intracellular peptidases with possible catabolic roles (Supplementary Table S5). In comparison, the genomes of the two putative lipid degraders, i.e., *Psychromonas* GLG-1 and *Desulfoluna* GLD-1, both encoded only 7 and 9 intracellular peptidases, respectively. A multitude of different routes of amino acid degradation exist in microorganisms. In this study, we focused on amino acid degradation processes, which form glutamate and/or keto-acids that are part of the central carbon metabolism and could explain incorporation of ^{13}C-carbon from the ^{13}C-labelled proteins into their own DNA, as well as the development of specific VFAs in our incubations (Figure 4). The genome of *P. atlanticus* encoded several aminotransferases and other amino acid degrading enzymes (i.e. alanine dehydrogenases, cystathionine gamma-lyase, serine/threonine ammonia-lyase, tryptophanase, methionine gamma-lyase) (Supplementary Table S5). These can convert amino acids to the keto-acids pyruvate and oxobutanoate, which could be further fermented to formate and either acetate or propionate, respectively (Figure 4). Some amino acid degrading enzymes were also present in the genomes of putative lipid degraders (Supplementary Table S5), but the genome of *P. atlanticus* encoded three specific amino acid degradation pathways that were largely not found in the other three genomes. These included pathways for the fermentation of lysine to butyrate and acetate (7 of 8 genes), the catabolism of glutamate to acetate and pyruvate via the methylaspartate pathway (2 of 4 genes), and the

catabolism of glutamate to butyrate via the hydroxyglutarate pathway (9 of 10 genes) (Supplementary Table S5).

The genome of the putative protein and lipid degrader *Clostridia* GPF-1 encoded for the broadest array of intracellular peptidases of all investigated genomes (n=26) (Supplementary Table S5). The catabolism of amino acids in *Clostridia* GPF-1 to propionate, acetate and formate, i.e., via aminotransferases and other amino acid degrading enzymes (i.e. L-threoninie 3-dehydrogenase, cystathionine β-synthase, cystathionine gamma-lyase, serine/threonine ammonia-lyase, methionine gamma-lyase) was mostly similar to the predicted routes used by *P. atlanticus*, although no genes for lysine fermentation were found and the glutamate degradation pathways were rather incomplete (Supplementary Table S5). Instead, *Clostridia* GPF-1 encoded for enzymes that initiate valine degradation, i.e., two branched-chain amino acid transferases and the gene 2-keto-isovalerate dehydrogenase, which is part of the branched-chain α-keto acid dehydrogenase complex only found in the genome of *Clostridia* GPF-1 (Supplementary Table S5). The enzyme 2-keto-isovalerate dehydrogenase converts 2-oxoisovalerate to isobutyryl-CoA, which might then be converted to isobutyrate by an unknown mechanism or isomerized by isobutyryl-CoA mutase to butyryl-CoA (Figure 4). Isobutyryl-CoA and the accompanying enzymes that are required for isomerization were only present in the genome of *Clostridia* GPF-1 (Supplementary Table S5). Butyryl-CoA could be further converted to butyrate in a fermentative manner (Figure 4). The genome of *Clostridia* GPF-1 encoded all genes necessary for the conversion of glycerol and glycerol-3-phosphate to pyruvate (Supplementary Table S5), which is in line with the ^{13}C-enrichment of 16S rRNA OTU 1 in ^{13}C-lipid incubations (Figure 2).

The putative lipid degrader *Psychromonas* GLG-1 encoded enzymes required for fatty acid beta-oxidation, including a probable multienzyme complex that contains the two enzymes enoyl-CoA hydratase/isomerase and 3-hydroxyacyl-CoA dehydrogenase (Supplementary Table S5). Through beta-oxidation, *Psychromonas* GLG-1 could convert even- and odd-chain fatty acids to propionyl- and acetyl-CoA, which might be further fermented to acetate and propionate, respectively (Figure 4). In comparison to *P.atlanticus* and *Clostridia* GPF-1, which seemed to be strict fermenters, MAG *Psychromonas* GLG-1 also encoded a complete TCA cycle, which might have enabled a respiratory conversion of acetyl-CoA to CO_2 (Figure 4). When oxygen is available, *Psychromonas* GLG-1 might use one of the two encoded high affinity oxidases for respiration, i.e., cbb3-type cytochrome c oxidase and cytochrome bd–type oxidase (Supplementary Table S5). In oxygen depleted sediments, e.g., in our microcosm incubations, *Psychromonas* GLG-1 might still be able to respire using nitrate or fumarate as terminal electron acceptors (Supplementary Table S5). In contrast to *Clostridia* GPF-1, enzymes for the intracellular degradation of glycerol were not found in *Psychromonas* GLG-1 (Supplementary Table S5). Despite the presence of several extracellular glycosyl hydrolases in the genome of *Psychromonas* GLG-1 and a complete glycolysis pathway,

enzymes for feeding galactose, i.e., from spirulina galactosyl diglycerides, into glycolysis were not identified (Supplementary Table S5).

Desulfoluna GLD-1 also encoded a full beta-oxidation pathway, several acyl-CoA synthetases and a butanoate CoA-transferase (Supplementary Table S5). The latter enzyme converts butyrate to butyryl-CoA, which can be funneled into beta-oxidation (Figure 5). Long-chain fatty acids and butyrate could thereby be converted to acetate and propionate, respectively. The metabolic intermediate acetyl-CoA could also be converted to CO_2 via the TCA cycle (Figure 5). For lactate degradation, *Desulfoluna* GLD-1 encoded several lactate dehydrogenases and a lactate utilization operon (Supplementary Table S5). Resulting pyruvate is likely converted to acetyl-CoA, which might be further processed to acetate or CO_2 as mentioned above. *Desulfoluna* GLD-1 also encoded a formate dehydrogenase enzyme complex (Supplementary Table S5), which converts formate to CO_2 and H_2 (Figure 5). In agreement with the inhibition of *dsrB* OTU 2 in molybdate amended incubations, *Desulfoluna* GLD-1 encoded all enzymes that are required for sulfate reduction.

Discussion

This study unravels the identities and functions of various poorly understood microbial populations, and remarkably, distinct sub-populations of the same species, which are key players in the degradation and turnover of two of the major macromolecules present in marine sediments, i.e, proteins and lipids. SIP indicated that ^{13}C-carbon from protein and lipid hydrolysis was incorporated into microbial DNA already within 5-10 days. Since sulfate depletion and accumulation of most VFAs was only observed after day 5, OTUs with ^{13}C-enrichment already at day 5 likely represented the primary hydrolyzers of proteins and lipids. Labelling of various microorganisms affiliated with the phyla/classes *Deltaproteobacteria*, *Gammaproteobacteria* and *Firmicutes* at day 10 also indicated fast transfer of ^{13}C-carbon among trophic levels of the microbial food web, since many of these taxa are known consumers of fermentation products.

Sequencing of 16S rRNA genes across DNA-SIP gradients revealed that the primary hydrolysis of proteins was mostly performed by *Psychrilyobacter* (OTU 5), various populations of *Psychromonas* (sub-OTUs 4, 9 and 43) *Photobacterium* (OTU 54), *Fusibacter* (OTU 38) and JTB215 (OTU 1). In comparison, only one population of *Psychromonas* (sub-OTU 4) and *Vibrio* (OTU 80) were enriched in ^{13}C-lipid incubations at day 5, indicating that only a few specialized microorganisms were involved in the primary catabolism of spirulina lipids. Importantly, most of those microorganisms were also enriched in relative abundances in microcosms with substrate additions versus no-substrate controls, thereby indicating that these populations indeed oxidized molecules from proteins or lipids and used the acquired energy for growth. Intriguingly, many more OTUs incorporated ^{13}C-carbon from proteins as compared to lipids possibly

due to higher proportions of proteins in sediment organic matter (Hedges and Oades, 1997; Burdige, 2007) and a greater susceptibility of proteins to degradation as compared to lipids (Wakeham and Canuel, 2006). However, sediment microorganisms are known to scavenge organic nitrogen sources in times of low nutrient supply (Vetter and Deming, 1994), which might additionally explain high numbers of secondary responders in incubations with protein amendments.

Our SIP analyses showed that *Psychrilyobacter* OTU 5 was a prominent protein and/or amino acid degrader. Furthermore, strong increases in relative abundances upon protein supplementation indicated population growth from these organisms. Genomic analyses also showed that the analyzed reference genome of *Psychrilyobacter atlanticus* (Zhao *et al.*, 2009), indeed encoded various routes for the degradation of peptides and fermentation of amino acids that may have driven this growth (Figure 4). Members of this genus were previously shown to be important for 'bulk' organic matter degradation of total cyanobacterial biomass in marine sediments (Graue *et al.*, 2012; Müller *et al.*, 2018). Here, we provide important first evidence that detrital protein is a primary nutrient and energy source for *Psychrilyobacter* spp., and that these organisms are therefore key players in the mineralization of proteinaceous material in the seabed.

To facilitate protein degradation, *P. atlanticus* encoded 24 peptidases that were predicted to be important for the catabolism of proteins or peptides. Two of them encoded secretion signal peptides for export from the cytoplasm to the periplasm and possibly also to the extracellular environment. Although we did not find Type-II or -III secretion systems that are typically used for protein secretion to extracellular space, *P. atlanticus* encoded for a Type IV secretion system and Type V autotransporters that might instead perform this function (Desvaux *et al.*, 2005). Furthermore, we cannot not rule-out that alternative secretion pathways exist. On the other hand, known *Fusobacteria* generally do not secrete proteins to the extracellular space (Kapatral *et al.*, 2003). A plausible alternative explanation could be that they rely on other microorganisms to secrete extracellular peptidases. Indeed, recent studies have shown that diverse bacterial and archaeal lineages encode extracellular peptidases in marine sediments (Orsi *et al.*, 2018; Zinke *et al.*, 2018), strongly indicating that this abundant and valuable macromolecule is a highly valued nutrient source for diverse taxa. Furthermore, extracellular enzymes are known to persist in marine sediments for prolonged times and thereby act on newly available substrates as soon as they become available (Fabiano and Danovaro, 1998). Thus, we hypothesize that it might be an advantageous strategy for *Psychrilyobacter*-related microbes to avoid costly investment in extracellular peptidase production. Such a strategy might also explain why they encode a particularly broad array of peptide (n=19) and amino acid transporters (n=38), as well as the presence of proton dependent peptide transporters. Genomic evidence also indicated that once *P. atlanticus* organisms imported peptides and/or amino acids into the cytoplasm, they have the potential to catabolize and ferment various amino acids such as alanine, tryptophane, lysine and glutamate, into the

volatile fatty acids acetate, butyrate and propionate (Figure 4). In accordance with our results, amino acids are considered a primary substrate for *P. atlanticus* (Zhao *et al.*, 2009), as well as for other *Fusobacteria* (Potrykus *et al.*, 2008).

The MAG *Clostridia* GPF-1 that harboured an identical 16S rRNA gene sequence to JTB215 OTU 1, had less than 54% AAI to any available genome, and therefore our data represents the first insights into the potential metabolism of this enigmatic group of sediment bacteria. The JTB215 OTU 1 population was ^{13}C-labelled in SIP analyses from both ^{13}C-protein and ^{13}C-lipid incubations. Our genomic analyses indicated that these *Clostridia*-related microorganisms might be versatile, with the potential to utilize peptides, amino acids and glycerol, as substrates (Figure 4). Most strikingly, *Clostridia* GPF-1 encoded a copious number of peptidases (n= 29), of which, three were predicted to be excreted via the SEC pathway. Further, numerous peptide (n=14) and amino acid (n=24) transporters were identified. Upon import of peptides and/or amino acids, *Clostridia* GPF-1 has the potential to degrade amino acids into VFAs, as indicated by a wide range of aminotransferase and other amino acid degrading enzymes. Iso-butyrate was predicted to be produced by *Clostridia* GPF-1, and indeed accumulation of iso-butyrate was pronounced from amendments of proteins and is a typical end-product of valine degradation in related *Clostridium* spp. (Lovitt *et al.*, 1987). Additionally, iso-butyrate could be converted to butyrate, which was identified as a major substrate for SRM. *Clostridia* GPF-1 also had the potential to hydrolyze lipids, i.e., genes for predicted secreted Bacterial_EstLip_FamX esterase/lipase and two membrane bound Bacterial_EstLip_FamX and Carboxylesterase and type B esterases/lipases were identified in the genome. Since no fatty acid transporters were found, it was possible that only glycerol moieties were utilized as substrates after lipid hydrolysis. Accordingly, *Clostridia* GPF-1 encoded several enzymes involved in glycerol utilization, and no genes for enzymes for beta-oxidation.

An outstanding finding from this study was that several sub-OTUs of a *Psychromonas* species (OTU 4) showed highly distinct labelling patterns in DNA-SIP analyses from either protein or lipid additions. Although we did not recover multiple MAGs representative of each of these sub-species, the 16S rRNA sequence of *Psychromonas* GLG-1 matched sub-OTU 4. This sub-OTU was strongly enriched in heavy SIP fractions from ^{13}C-lipid amended microcosms and also increased in relative abundance over time in incubations with this macromolecule (Figure 3). The gene content of *Psychromonas* GLG-1 indicated lipolytic activity, since it encoded an extracellular esterase, as well as two long-chain fatty acid transporters and a beta oxidation pathway (Figure 4). In contrast, *Psychromonas* GLG-1 encoded no extracellular peptidases, considerably fewer peptide and amino acid transporters compared to the other MAGs analysed here, and only very few complete amino acid degradation pathways. Therefore, the weak ^{13}C-labelling of sub-OTU 4 also observed from incubations with ^{13}C-protein, might results from utilization of protein degradation intermediates. Representatives of the genus *Psychromonas* were

previously shown to be involved in bulk organic matter degradation in arctic sediments (Müller *et al.*, 2018), and were also shown to be highly correlated with fluxes of phytodetritus into marine sediments (Bienhold *et al.*, 2011). Our data indicated that *Psychromonas*-related microorganisms have a high phylogenetic and metabolic diversity, and that different sub-OTUs play key roles in either protein or lipid turnover in arctic marine sediments.

In addition to ^{13}C-enriched OTUs from day 5 that could be linked to genomes or MAGs, we also found ^{13}C-enrichment of *Fusibacter* OTU 38 and *Photobacterium* OTU 54 in ^{13}C-protein incubations, and of *Vibrio* OTU 80 in ^{13}C-lipid incubations. Representatives of the genera *Photobacterium* and *Vibrio* are facultative anaerobes that are considered seawater bacteria, which can also thrive in marine sediments (Vezzulli *et al.*, 2009; Chase *et al.*, 2015; Zhang *et al.*, 2015). Close relatives to OTU 54 were lipolytic (Seo, 2005; Yoon and -H. Yoon, 2005), and proteolytic (Zhang *et al.*, 2015; Li *et al.*, 2017), indicating a broad substrate spectrum of this very diverse genus. The majority of OTU-80 related *Vibrio spp*. on the other hand are able to degrade sugars and glycerol and some are lipolytic (Shieh *et al.*, 2000; Shieh, 2003; Rameshkumar *et al.*, 2010; Sheu *et al.*, 2011; Wang *et al.*, 2011; Lucena *et al.*, 2012), indicating that *Vibrio* OTU 80 might have been involved in the catabolism of several subcomponents of spirulina lipids. *Fusibacter* OTU 38 was closely related to isolates that respire simple carbohydrates and amino acids (Ravot *et al.*, 1999; Ben Hania *et al.*, 2012; Smii *et al.*, 2015; Serrano *et al.*, 2017). Interestingly, representatives of the genus *Fusibacter* were shown to be involved in the degradation of DNA subcomponents (i.e., nucleobases) in marine sediments (Wasmund *et al.*, 2019). Our study further indicates an involvement of *Fusibacter spp*. in protein degradation in arctic marine sediments, and together with previous studies, suggests they are a highly versatile group of bacteria.

In addition to the primary hydrolyzers described above that were already ^{13}C-labelled at day 5, various microorganisms also became labelled at day 10 (Figure 2). These taxa had potential roles in direct catabolism of monomers released by primary hydrolyzers (e.g., amino or fatty acids), or became labelled due to cross-feeding on fermentation products (e.g., VFAs). Some of the taxa that became labelled at day 10 were proposed to be directly or indirectly dependent on sulfate-reduction, as indicated by their inhibition in molybdate amended incubations (Newport and Nedwell, 1988). These sulfate-reduction dependent microorganisms included the two deltaproteobacterial *dsrB* OTUs (2 and 18), which were ^{13}C-enriched in ^{13}C-lipid incubations. *Desulfoluna* GLD-1 encoded a *dsrB* sequence that was identical to *dsrB* OTU 2 and metabolic capabilities of this MAG included the potential for butyrate, lactate and formate degradation coupled to sulfate reduction. Interestingly, butyrate, lactate and formate were major fermentation products from primary hydrolysis, and therefore utilization of these VFAs likely explains ^{13}C-enrichment of *dsrB* OTU 2 in ^{13}C-lipid incubations. The butyrate degradation pathway encoded by *Desulfoluna* GLD-1, i.e., a predicted long-chain fatty acid transport protein

and a beta-oxidation pathway, may however also be utilized for catabolizing long-chain fatty acids (Figure 5). Since the oxidation of higher fatty acids is common among SRM isolates (Rabus *et al.*, 2013), it is conceivable that *Desulfoluna*-affiliated microorganisms are capable of this function *in situ*.

Conclusions

Proteins and lipids are major components of organic matter in marine sediments, and their concentrations and compositions in marine sediments have major implications for the diversity and abundance of microorganisms in sediments. Our analyses revealed that *Psychrilyobacter*, *Psychromonas*, *Photobacterium*, *Fusibacter* and *Clostridia* were involved in protein hydrolysis, whereas lipids were hydrolyzed by *Vibrio* and *Psychromonas*. Excitingly, this phylogenetic partitioning during protein and lipid degradation was also observed on the sub-OTU level between different *Psychromonas* sub-OTUs. Analyses of genomes of key protein and lipid degraders revealed their potential metabolisms in arctic marine sediments. *Clostridia* are capable of hydrolyzing extracellular proteins and subsequently utilize (branched-chain) amino acids and/or hydrolyze lipids to scavenge glycerol moieties. *Psychrilyobacter* have the potential to feed on peptides and amino acids for which it may depend on other sediment bacteria, such as *Clostridia*, for the production and release of extracellular peptidases. Lipid-degrading *Psychromonas* sub-OTUs hydrolyze lipids extracellularly and utilize fatty acids moieties, whereas the released glycerol might serve as substrate for other microorganisms. Primary substrates of SRM were protein and lipid degradation intermediates such as formate, lactate and butyrate. Further, we propose long-chain fatty acids, probably released by lipolytic sediment microorganisms, could serve some SRM such as *Desulfoluna* spp. as alternative substrates. In summary, our study provided new insights into the identities, functions and possible metabolisms of various protein and lipid degrading microorganisms in marine sediments. This information will ultimately lead to a better understanding of the anaerobic carbon cycle in arctic marine sediments.

Acknowledgements

The authors would like to thank the crew of the R/V Sanna 2013 summer sampling campaign, which was funded by the Arctic Research Centre, Aarhus University, and Marit-Solveig Seidenkranz for providing the samples. Furthermore the authors want to thank Carmen Czepe from the Vienna Biocenter Core Facilities Next Generation Sequencing facility for sequencing of metagenomic libraries on the Illumina Hiseq2500 instrument. This work was financially supported by the Austrian Science Fund (P29426-B29 to KW; P25111-B22 to AL). The authors declare no conflict of interest.

References

Alneberg, J., Bjarnason, B.S., de Bruijn, I., Schirmer, M., Quick, J., Ijaz, U.Z., et al. (2014) Binning metagenomic contigs by coverage and composition. *Nat. Methods* **11**: 1144–1146.

Arndt, S., Jørgensen, B.B., LaRowe, D.E., Middelburg, J.J., Pancost, R.D., and Regnier, P. (2013) Quantifying the degradation of organic matter in marine sediments: A review and synthesis. *Earth-Sci. Rev.* **123**: 53–86.

Bankevich, A., Nurk, S., Antipov, D., Gurevich, A.A., Dvorkin, M., Kulikov, A.S., et al. (2012) SPAdes: a new genome assembly algorithm and its applications to single-cell sequencing. *J. Comput. Biol.* **19**: 455–477.

Ben Hania, W., Fraj, B., Postec, A., Fadhlaoui, K., Hamdi, M., Ollivier, B., and Fardeau, M.-L. (2012) Fusibacter tunisiensis sp. nov., isolated from an anaerobic reactor used to treat olive-mill wastewater. *Int. J. Syst. Evol. Microbiol.* **62**: 1365–1368.

Berger, S.A., Krompass, D., and Stamatakis, A. (2011) Performance, accuracy, and Web server for evolutionary placement of short sequence reads under maximum likelihood. *Syst. Biol.* **60**: 291–302.

Bienhold, C., Boetius, A., and Ramette, A. (2011) The energy–diversity relationship of complex bacterial communities in Arctic deep-sea sediments. *ISME J.* **6**: 724–732.

Bowles, M.W., Mogollón, J.M., Kasten, S., Zabel, M., and Hinrichs, K.-U. (2014) Global rates of marine sulfate reduction and implications for sub-sea-floor metabolic activities. *Science* **344**: 889–891.

Buchfink, B., Xie, C., and Huson, D.H. (2015) Fast and sensitive protein alignment using DIAMOND. *Nat. Methods* **12**: 59–60.

Burdige, D.J. (2007) Preservation of organic matter in marine sediments: controls, mechanisms, and an imbalance in sediment organic carbon budgets? *Chem. Rev.* **107**: 467–485.

Chase, E., Young, S., and Harwood, V.J. (2015) Sediment and vegetation as reservoirs of Vibrio vulnificus in the Tampa Bay Estuary and Gulf of Mexico. *Appl. Environ. Microbiol.* **81**: 2489–2494.

Christian, J.R. and Karl, D.M. (1995) Bacterial ectoenzymes in marine waters: Activity ratios and temperature responses in three oceanographic provinces. *Limnol. Oceanogr.* **40**: 1042–1049.

Desvaux, M., Khan, A., Beatson, S.A., Scott-Tucker, A., and Henderson, I.R. (2005) Protein secretion systems in Fusobacterium nucleatum: genomic identification of Type 4 piliation and complete Type V pathways brings new insight into mechanisms of pathogenesis. *Biochim. Biophys. Acta* **1713**: 92–112.

Dumont, M.G., Radajewski, S.M., Miguez, C.B., McDonald, I.R., and Murrell, J.C. (2006) Identification of a complete methane monooxygenase operon from soil by combining stable isotope probing and metagenomic analysis. *Environ. Microbiol.* **8**: 1240–1250.

Dunne, J.P., Sarmiento, J.L., and Gnanadesikan, A. (2007) A synthesis of global particle export from the surface ocean and cycling through the ocean interior and on the seafloor. *Global Biogeochem. Cycles* **21**: 1–16.

Fabiano, M. and Danovaro, R. (1998) Enzymatic activity, bacterial distribution, and organic matter composition in sediments of the ross sea (Antarctica). *Appl. Environ. Microbiol.* **64**: 3838–3845.

Fabiano, M. and Pusceddu, A. (1998) Total and hydrolizable particulate organic matter (carbohydrates, proteins and lipids) at a coastal station in Terra Nova Bay (Ross Sea, Antarctica). *Polar Biol.* **19**: 125–132.

Finn, R.D., Bateman, A., Clements, J., Coggill, P., Eberhardt, R.Y., Eddy, S.R., et al. (2013) Pfam: the protein families database. *Nucleic Acids Res.* **42**: D222–D230.

Glombitza, C., Pedersen, J., Røy, H., and Jørgensen, B.B. (2014) Direct analysis of volatile fatty acids in marine sediment porewater by two-dimensional ion chromatography-mass spectrometry. *Limnol. Oceanogr. Methods* **12**: 455–468.

Graue, J., Engelen, B., and Cypionka, H. (2012) Degradation of cyanobacterial biomass in anoxic tidal-flat sediments: a microcosm study of metabolic processes and community changes. *ISME J.* **6**: 660–669.

Haft, D.H., Selengut, J.D., and White, O. (2003) The TIGRFAMs database of protein families. *Nucleic Acids Res.* **31**: 371–373.

Harvey, H.R., Rodger Harvey, H., Fallon, R.D., and Patton, J.S. (1986) The effect of organic matter and oxygen on the degradation of bacterial membrane lipids in marine sediments. *Geochim. Cosmochim. Acta* **50**: 795–804.

Hedges, J.I. and Oades, J.M. (1997) Comparative organic geochemistries of soils and marine sediments. *Org. Geochem.* **27**: 319–361.

Herbold, C.W., Pelikan, C., Kuzyk, O., Hausmann, B., Angel, R., Berry, D., and Loy, A. (2016) Corrigendum: A flexible and economical barcoding approach for highly multiplexed amplicon sequencing of diverse target genes. *Front. Microbiol.* **7**: 870.

Hop, H., Pearson, T., Hegseth, E.N., Kovacs, K.M., Wiencke, C., Kwasniewski, S., et al. (2002) The marine ecosystem of Kongsfjorden, Svalbard. *Polar Res.* **21**: 167–208.

Hudson, B.J. and Karis, I.G. (1974) The lipids of the alga Spirulina. *J. Sci. Food Agric.* **25**: 759–763.

Jain, C., Rodriguez-R, L.M., Phillippy, A.M., Konstantinidis, K.T., and Aluru, S. (2018) High throughput ANI analysis of 90K prokaryotic genomes reveals clear species boundaries. *Nat. Commun.* **9**: 5114.

Jones, P., Binns, D., Chang, H.-Y., Fraser, M., Li, W., McAnulla, C., et al. (2014) InterProScan 5: genome-scale protein function classification. *Bioinformatics* **30**: 1236–1240.

Jørgensen, B.B. (1982) Mineralization of organic matter in the sea bed—the role of sulphate reduction. *Nature* **296**: 643–645.

Kall, L., Krogh, A., and Sonnhammer, E.L.L. (2007) Advantages of combined transmembrane topology and signal peptide prediction--the Phobius web server. *Nucleic Acids Res.* **35**: W429–W432.

Kang, D.D., Froula, J., Egan, R., and Wang, Z. (2015) MetaBAT, an efficient tool for accurately reconstructing single genomes from complex microbial communities. *PeerJ* **3**: e1165.

Kapatral, V., Ivanova, N., Anderson, I., Reznik, G., Bhattacharyya, A., Gardner, W.L., et al. (2003) Genome analysis of F. nucleatum sub spp vincentii and its comparison with the genome of F. nucleatum ATCC 25586. *Genome Res.* **13**: 1180–1189.

Katoh, K., Misawa, K., Kuma, K.-I., and Miyata, T. (2002) MAFFT: a novel method for rapid multiple sequence alignment based on fast Fourier transform. *Nucleic Acids Res.* **30**: 3059–3066.

Knoblauch, C., Sahm, K., and Jørgensen, B.B. (1999) Psychrophilic sulfate-reducing bacteria isolated from permanently cold arctic marine sediments: description of Desulfofrigus oceanense gen. nov., sp. nov., Desulfofrigus fragile sp. nov., Desulfofaba gelida gen. nov., sp. nov., Desulfotalea psychrophila gen. nov., sp. nov. and Desulfotalea arctica sp. nov. *Int. J. Syst. Bacteriol.* **49**: 1631–1643.

Lenfant, N., Hotelier, T., Velluet, E., Bourne, Y., Marchot, P., and Chatonnet, A. (2013) ESTHER, the database of the α/β-hydrolase fold superfamily of proteins: tools to explore diversity of functions. *Nucleic Acids Res.* **41**: D423–9.

Letunic, I. and Bork, P. (2007) Interactive Tree Of Life (iTOL): an online tool for phylogenetic tree display and annotation. *Bioinformatics* **23**: 127–128.

Li, H. and Durbin, R. (2009) Fast and accurate short read alignment with Burrows-Wheeler transform. *Bioinformatics* **25**: 1754–1760.

Li, H., Handsaker, B., Wysoker, A., Fennell, T., Ruan, J., Homer, N., et al. (2009) The Sequence Alignment/Map format and SAMtools. *Bioinformatics* **25**: 2078–2079.

Li, Y., Zhou, M., Wang, F., Wang, E.T., Du, Z., Wu, C., et al. (2017) Photobacterium proteolyticum sp. nov., a protease-producing bacterium isolated from ocean sediments of Laizhou Bay. *Int. J. Syst. Evol. Microbiol.* **67**: 1835–1840.

Lovitt, R.W., Kell, D.B., and Morris, J.G. (1987) The physiology of Clostridium sporogenes NCIB 8053 growing in defined media. *J. Appl. Bacteriol.* **62**: 81–92.

Lucena, T., Ruvira, M.A., Arahal, D.R., Macián, M.C., and Pujalte, M.J. (2012) Vibrio aestivus sp. nov. and Vibrio quintilis sp. nov., related to Marisflavi and Gazogenes clades, respectively. *Syst. Appl. Microbiol.* **35**: 427–431.

McCarthy, M., Pratum, T., Hedges, J., and Benner, R. (1997) Chemical composition of dissolved organic nitrogen in the ocean. *Nature* **390**: 150–154.

Meyer-Reil, L.-A. (1991) Ecological Aspects of Enzymatic Activity in Marine Sediments. In, *Brock/Springer Series in Contemporary Bioscience*., pp. 84–95.

Müller, A.L., Pelikan, C., de Rezende, J.R., Wasmund, K., Putz, M., Glombitza, C., et al. (2018) Bacterial interactions during sequential degradation of cyanobacterial necromass in a sulfidic arctic marine

sediment. *Environ. Microbiol.* **20**: 2927–2940.

Muyzer, G. and Stams, A.J.M. (2008) The ecology and biotechnology of sulphate-reducing bacteria. *Nat. Rev. Microbiol.* **6**: 441–454.

Na, H., Lever, M.A., Kjeldsen, K.U., Schulz, F., and Jørgensen, B.B. (2015) Uncultured Desulfobacteraceae and Crenarchaeotal group C3 incorporate 13C-acetate in coastal marine sediment. *Environ. Microbiol. Rep.* **7**: 614–622.

Neufeld, J.D., Vohra, J., Dumont, M.G., Lueders, T., Manefield, M., Friedrich, M.W., and Murrell, J.C. (2007) DNA stable-isotope probing. *Nat. Protoc.* **2**: 860–866.

Newport, P.J. and Nedwell, D.B. (1988) The mechanisms of inhibition of Desulfovibrio and Desulfotomaculum species by selenate and molybdate. *J. Appl. Bacteriol.* **65**: 419–423.

Olm, M.R., Brown, C.T., Brooks, B., and Banfield, J.F. (2017) dRep: a tool for fast and accurate genomic comparisons that enables improved genome recovery from metagenomes through de-replication. *ISME J.* **11**: 2864–2868.

Orsi, W.D., Richards, T.A., and Francis, W.R. (2018) Predicted microbial secretomes and their target substrates in marine sediment. *Nat Microbiol* **3**: 32–37.

Parks, D.H., Chuvochina, M., Waite, D.W., Rinke, C., Skarshewski, A., Chaumeil, P.-A., and Hugenholtz, P. (2018) A standardized bacterial taxonomy based on genome phylogeny substantially revises the tree of life. *Nat. Biotechnol.* **36**: 996–1004.

Parks, D.H., Imelfort, M., Skennerton, C.T., Hugenholtz, P., and Tyson, G.W. (2015) CheckM: assessing the quality of microbial genomes recovered from isolates, single cells, and metagenomes. *Genome Res.* **25**: 1043–1055.

Parsons, T.R., Stephens, K., and Strickland, J.D.H. (1961) On the Chemical Composition of Eleven Species of Marine Phytoplankters. *J. Fish. Res. Board Can.* **18**: 1001–1016.

Pelikan, C., Herbold, C.W., Hausmann, B., Müller, A.L., Pester, M., and Loy, A. (2016) Diversity analysis of sulfite- and sulfate-reducing microorganisms by multiplex dsrA and dsrB amplicon sequencing using new primers and mock community-optimized bioinformatics. *Environ. Microbiol.* **18**: 2994–3009.

Peng, Y., Leung, H.C.M., Yiu, S.M., and Chin, F.Y.L. (2012) IDBA-UD: a de novo assembler for single-cell and metagenomic sequencing data with highly uneven depth. *Bioinformatics* **28**: 1420–1428.

Potrykus, J., White, R.L., and Bearne, S.L. (2008) Proteomic investigation of amino acid catabolism in the indigenous gut anaerobe Fusobacterium varium. *Proteomics* **8**: 2691–2703.

Price, M.N., Dehal, P.S., and Arkin, A.P. (2010) FastTree 2 – Approximately Maximum-Likelihood Trees for Large Alignments. *PLoS One* **5**: e9490.

Pruesse, E., Peplies, J., and Glöckner, F.O. (2012) SINA: accurate high-throughput multiple sequence alignment of ribosomal RNA genes. *Bioinformatics* **28**: 1823–1829.

Quast, C., Pruesse, E., Yilmaz, P., Gerken, J., Schweer, T., Yarza, P., et al. (2013) The SILVA ribosomal RNA gene database project: improved data processing and web-based tools. *Nucleic Acids Res.* **41**: D590–6.

Rabus, R., Hansen, T.A., and Widdel, F. (2013) Dissimilatory Sulfate- and Sulfur-Reducing Prokaryotes. In, *The Prokaryotes*., pp. 309–404.

Rameshkumar, N., Sproer, C., Lang, E., and Nair, S. (2010) Vibrio mangrovi sp. nov., a diazotrophic bacterium isolated from mangrove-associated wild rice (Poteresia coarctata Tateoka). *FEMS Microbiol. Lett.* **307**: 35–40.

Ravot, G., Magot, M., Fardeau, M.L., Patel, B.K., Thomas, P., Garcia, J.L., and Ollivier, B. (1999) Fusibacter paucivorans gen. nov., sp. nov., an anaerobic, thiosulfate-reducing bacterium from an oil-producing well. *Int. J. Syst. Bacteriol.* **49**: 1141–1147.

Rawlings, N.D. (2000) MEROPS: the peptidase database. *Nucleic Acids Res.* **28**: 323–325.

Sahm, K., Knoblauch, C., and Amann, R. (1999) Phylogenetic affiliation and quantification of psychrophilic sulfate-reducing isolates in marine Arctic sediments. *Appl. Environ. Microbiol.* **65**: 3976–3981.

Seo, H.J. (2005) Photobacterium aplysiae sp. nov., a lipolytic marine bacterium isolated from eggs of the sea hare Aplysia kurodai. *Int. J. Syst. Evol. Microbiol.* **55**: 2293–2296.

Serrano, A.E., Escudero, L.V., Tebes-Cayo, C., Acosta, M., Encalada, O., Fernández-Moroso, S., and Demergasso,

C. (2017) First draft genome sequence of a strain from the genus Fusibacter isolated from Salar de Ascotán in Northern Chile. *Stand. Genomic Sci.* **12**: 43.

Sheu, S.-Y., Jiang, S.-R., Chen, C.A., Wang, J.-T., and Chen, W.-M. (2011) Vibrio stylophorae sp. nov., isolated from the reef-building coral Stylophora pistillata. *Int. J. Syst. Evol. Microbiol.* **61**: 2180–2185.

Shieh, W.Y. (2003) Vibrio ruber sp. nov., a red, facultatively anaerobic, marine bacterium isolated from sea water. *Int. J. Syst. Evol. Microbiol.* **53**: 479–484.

Shieh, W.Y., Chen, A.L., and Chiu, H.H. (2000) Vibrio aerogenes sp. nov., a facultatively anaerobic marine bacterium that ferments glucose with gas production. *Int. J. Syst. Evol. Microbiol.* **50**: 321–329.

Sieber, C.M.K., Probst, A.J., Sharrar, A., Thomas, B.C., Hess, M., Tringe, S.G., and Banfield, J.F. (2018) Recovery of genomes from metagenomes via a dereplication, aggregation, and scoring strategy. Nat Microbiol **3**: 836–843.

Smii, L., Ben Hania, W., Cayol, J.-L., Joseph, M., Hamdi, M., Ollivier, B., and Fardeau, M.-L. (2015) Fusibacter bizertensis sp. nov., isolated from a corroded kerosene storage tank. *Int. J. Syst. Evol. Microbiol.* **65**: 117–121.

Stamatakis, A. (2014) RAxML version 8: a tool for phylogenetic analysis and post-analysis of large phylogenies. *Bioinformatics* **30**: 1312–1313.

Steen, A.D., Kevorkian, R.T., Bird, J.T., Dombrowski, N., Baker, B.J., Hagen, S.M., et al. (2016) Extracellular peptidases in subsurface sediments of the White Oak River estuary, NC, suggest microbial community adaptation to oxidize degraded organic matter. doi: https://doi.org/10.1101/080671

Thurman, E.M. (1985) Organic Geochemistry of Natural Waters.

Tikhonov, M., Leach, R.W., and Wingreen, N.S. (2015) Interpreting 16S metagenomic data without clustering to achieve sub-OTU resolution. *ISME J.* **9**: 68–80.

UniProt Consortium, T. (2018) UniProt: the universal protein knowledgebase. *Nucleic Acids Res.* **46**: 2699.

Vallenet, D., Calteau, A., Cruveiller, S., Gachet, M., Lajus, A., Josso, A., et al. (2017) MicroScope in 2017: an expanding and evolving integrated resource for community expertise of microbial genomes. *Nucleic Acids Res.* **45**: D517–D528.

Vetter, Y.A. and Deming, J.W. (1994) Extracellular enzyme activity in the Arctic Northeast Water polynya. *Mar. Ecol. Prog. Ser.* **114**: 23–34.

Vezzulli, L., The VibrioSea Consortium, Pezzati, E., Moreno, M., Fabiano, M., Pane, L., and Pruzzo, C. (2009) Benthic ecology of Vibrio spp. and pathogenic Vibrio species in a coastal Mediterranean environment (La Spezia Gulf, Italy). *Microb. Ecol.* **58**: 808–818.

Wakeham, S.G. and Canuel, E.A. (2006) Degradation and Preservation of Organic Matter in Marine Sediments. In, *The Handbook of Environmental Chemistry*., pp. 295–321.

Wakeham, S.G., Lee, C., Farrington, J.W., and Gagosian, R.B. (1984) Biogeochemistry of particulate organic matter in the oceans: results from sediment trap experiments. *Deep Sea Res. A* **31**: 509–528.

Wang, H., Liu, J., Wang, Y., and Zhang, X.-H. (2011) Vibrio marisflavi sp. nov., isolated from seawater. *Int. J. Syst. Evol. Microbiol.* **61**: 568–573.

Wasmund, K., Pelikan, C., Watzka, M., Richter, A., Noel, A.C., Hubert, C.R.J., et al. (2019) DNA-foraging bacteria in the seafloor. doi: https://doi.org/10.1101/528695

Webster, G., Watt, L.C., Rinna, J., Fry, J.C., Evershed, R.P., Parkes, R.J., and Weightman, A.J. (2006) A comparison of stable-isotope probing of DNA and phospholipid fatty acids to study prokaryotic functional diversity in sulfate-reducing marine sediment enrichment slurries. *Environ. Microbiol.* **8**: 1575–1589.

Wehrmann, L.M., Formolo, M.J., Owens, J.D., Raiswell, R., Ferdelman, T.G., Riedinger, N., and Lyons, T.W. (2014) Iron and manganese speciation and cycling in glacially influenced high-latitude fjord sediments (West Spitsbergen, Svalbard): Evidence for a benthic recycling-transport mechanism. *Geochim. Cosmochim. Acta* **141**: 628–655.

Wu, Y.-W., Simmons, B.A., and Singer, S.W. (2016) MaxBin 2.0: an automated binning algorithm to recover genomes from multiple metagenomic datasets. *Bioinformatics* **32**: 605–607.

Yoon, J.-H. and -H. Yoon, J. (2005) Photobacterium lipolyticum sp. nov., a bacterium with lipolytic activity isolated from the Yellow Sea in Korea. *Int. J. Syst. Evol. Microbiol.* **55**: 335–339.

Zhang, X.-Y., Han, X.-X., Chen, X.-L., Dang, H.-Y., Xie, B.-B., Qin, Q.-L., et al. (2015) Diversity of cultivable protease-producing bacteria in sediments of Jiaozhou Bay, China. *Front. Microbiol.* **6**: 1021.

Zhao, J.-S., -S. Zhao, J., Manno, D., and Hawari, J. (2009) Psychrilyobacter atlanticus gen. nov., sp. nov., a marine member of the phylum Fusobacteria that produces H2 and degrades nitramine explosives under low temperature conditions. *Int. J. Syst. Evol. Microbiol.* **59**: 491–497.

Zinke, L.A., Glombitza, C., Bird, J.T., Røy, H., Jørgensen, B.B., Lloyd, K.G., et al. (2018) Microbial organic matter degradation potential in Baltic Sea sediments influenced by depositional conditions and in situ geochemistry. *Appl. Environ. Microbiol.* ***85****: e02164-18*

Figure 1

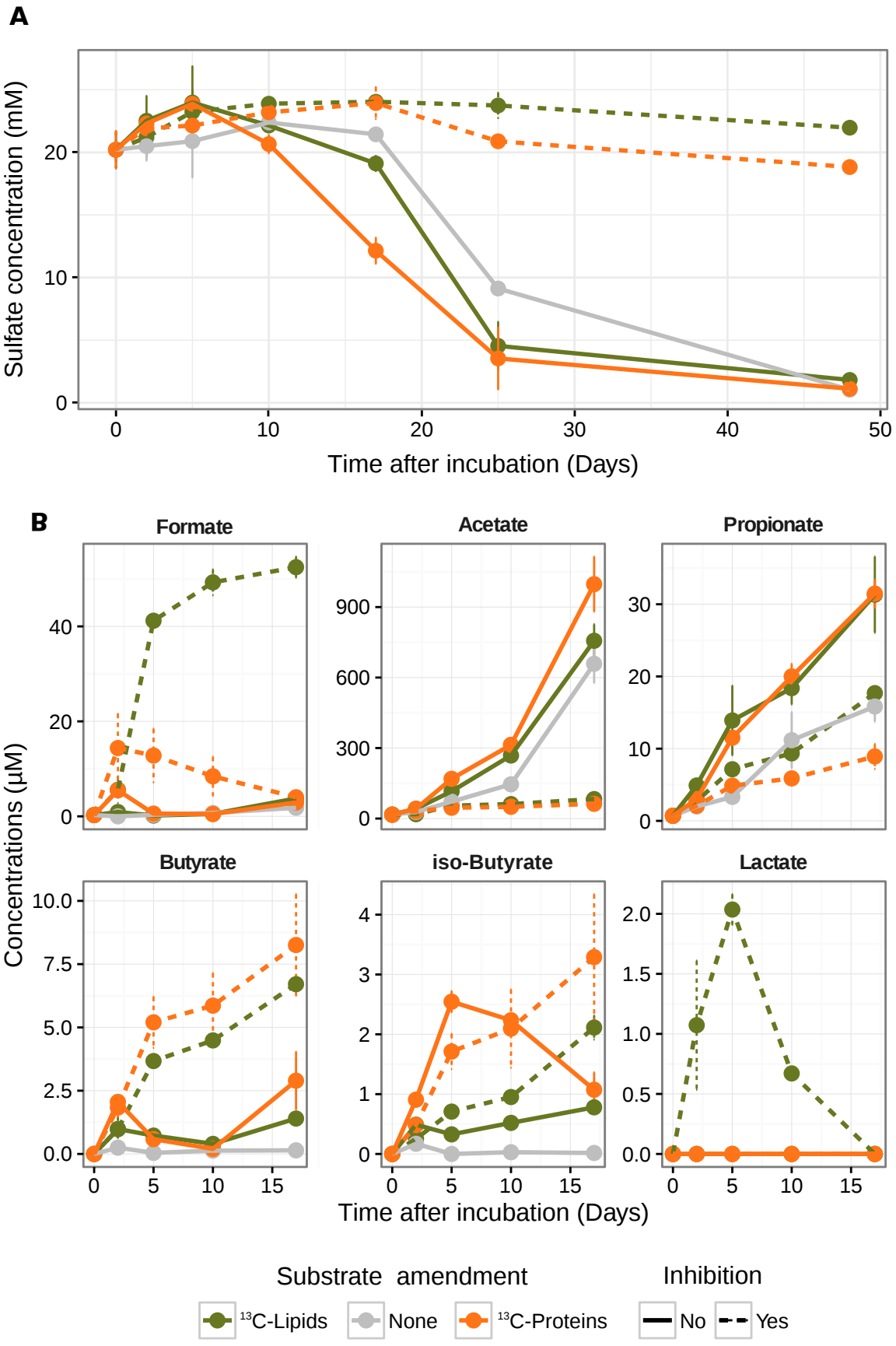

Figure 1. Dynamics of sulfate and volatile fatty acid concentrations in arctic marine sediment microcosms. Concentrations of sulfate (A) and volatile fatty acids (B) were determined in incubations with protein and lipids under sulfate-reduction-inhibited, i.e., molybdate amended, and uninhibited conditions. Negative control microcosms without substrate amendements were incubated under uninhibited conditions. Error bars represent standard deviations of measurements from replicate samples.

Figure 2

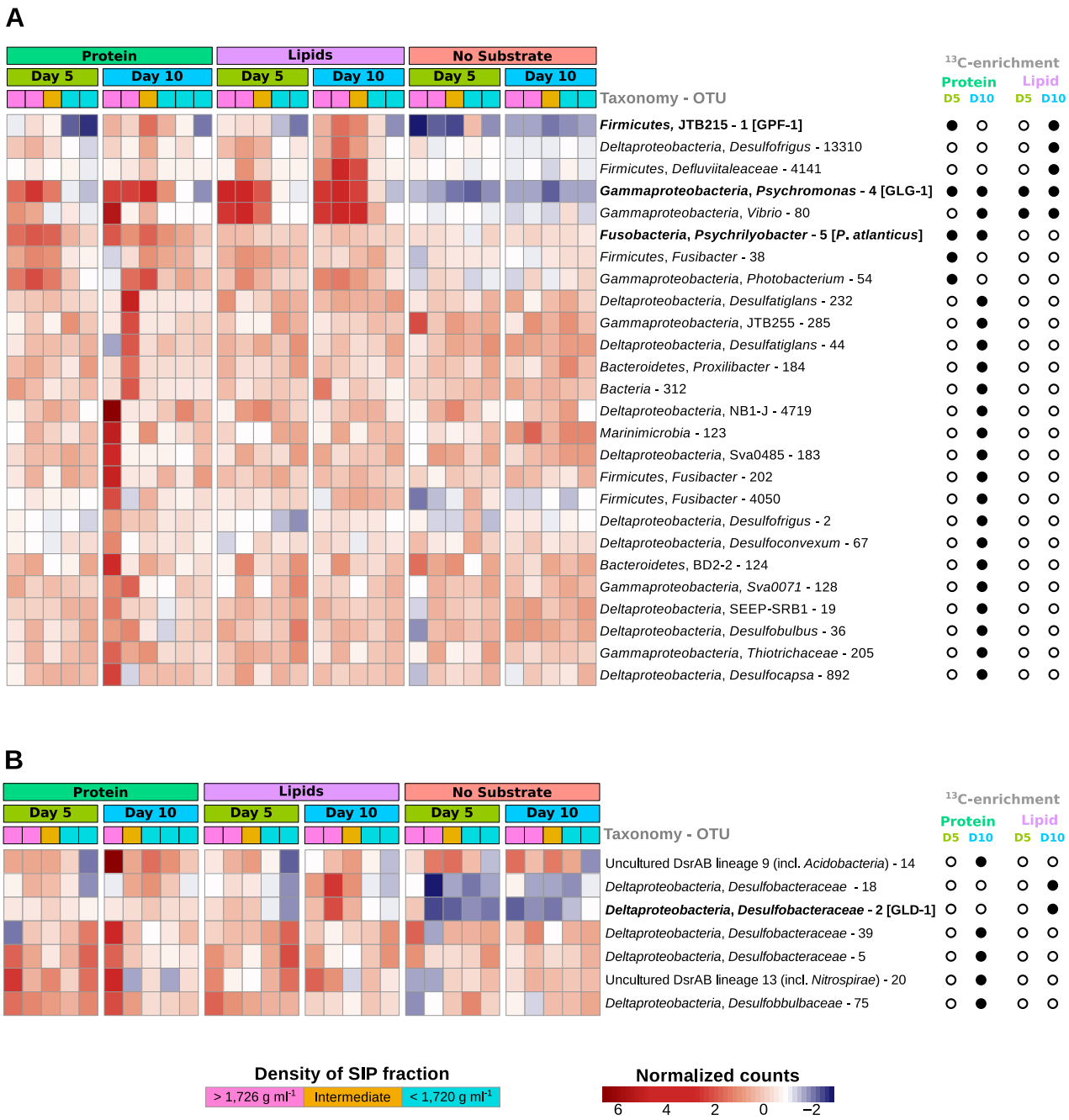

Figure 2. Relative abundance of 16S rRNA (A) and *dsrB* (B) OTUs in DNA-SIP gradients. Significant ^{13}C-enrichment of OTUs was determined by differential abundance analysis between high density (>1,726 g ml^{-1}) and low density (<1,720 g ml^{-1}) DNA-SIP fractions. The heatmap was clustered based on euclidean distances between relative abundance patterns of OTUs in DNA-SIP gradients. 16S rRNA and *dsrB* OTUs that correspond to 16S rRNA gene and *dsrB* sequences of genomes/MAGs are indicated in bold.

Figure 3

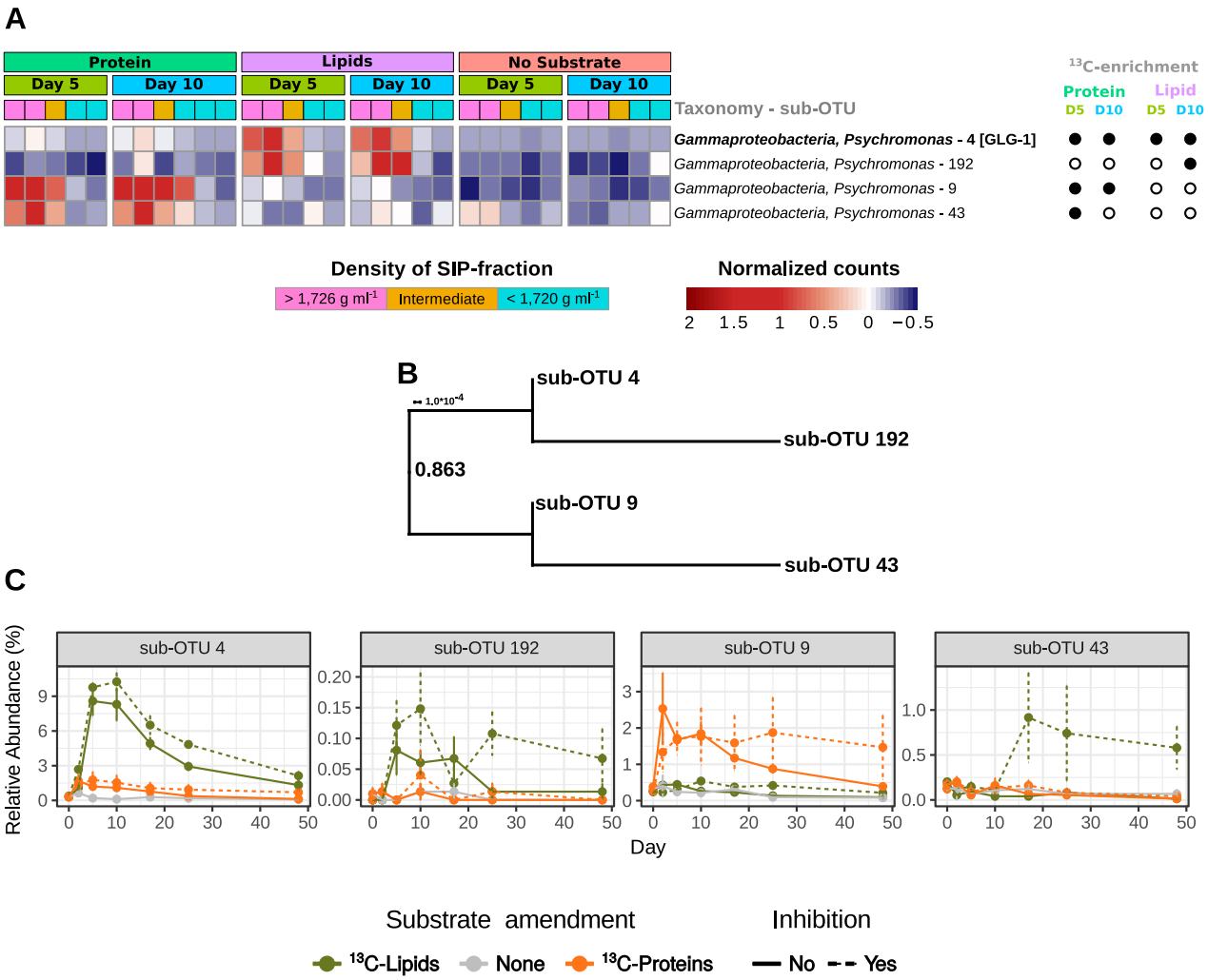

Figure 3. Sub-OTU diversity within 16S rRNA OTU 4. A., Relative abundances of 16S rRNA OTU 4 related sub-OTUs in DNA-SIP gradients. Significant ^{13}C-enrichment was determined by differential abundance analysis between high density (>1,726 g ml^{-1}) and low density (<1,720 g ml^{-1}) DNA-SIP fractions. The heatmap was clustered based on euclidean distances between relative abundance patterns of sub-OTUs in DNA-SIP gradients. Sub-OTU 4, which correspond to the 16S rRNA gene sequence of MAG *Psychromonas* GLG-1, is indicated in bold. B., Phylogenetic relationships of OTU 4 related sub-OTU sequences. The sequences were aligned with MAFFT (Katoh *et al.*, 2002) and the tree was calculated with FastTree (Price *et al.*, 2010). C., Relative abundance of OTU 4 related sub-OTUs over time in protein, lipid and no substrate incubations with or without the sulfate-reduction inhibitor molybdate.

Figure 4

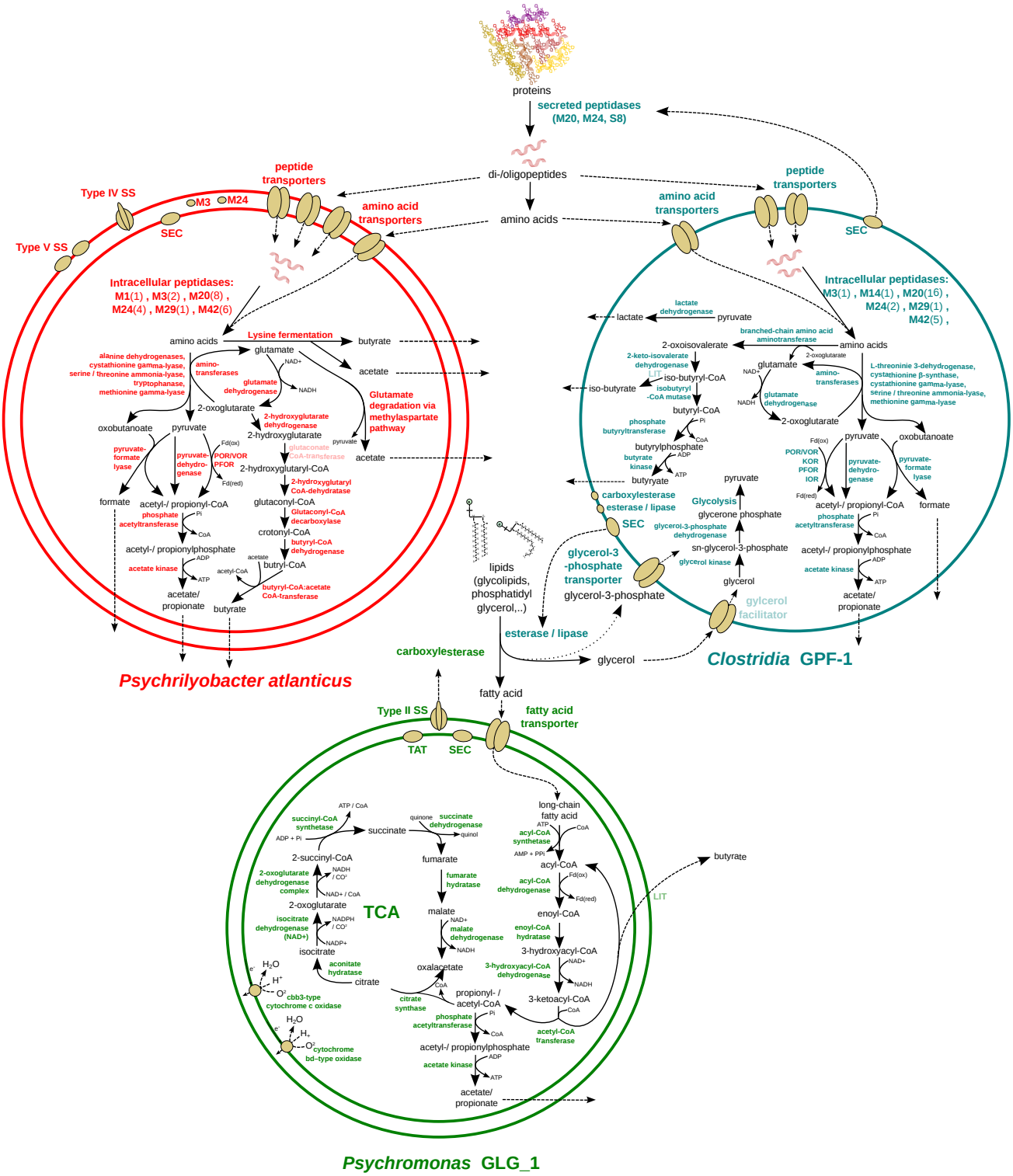

Figure 4. Model for protein and lipid hydrolysis in arctic marine sediment microcosms. The three hydrolyzer genomes/MAGs *Psychrilyobacter atlanticus*, *Clostridia* GPF-1 and *Psychromonas* GLG-1 are depicted. They correspond to the 16S rRNA OTUs 5, 1 and sub-OTU 4, respectively. The model indicates processes and enzymes that explain observed VFA dynamics and ^{13}C-enrichment of corresponding 16S rRNA OTUs. Enzymes that are indicated in pale colour were not found in the respective genome/MAG. SS,. Secretion system, TCA., tricarboxylic acid cycle, TAT., Twin-arginine translocation pathway, SEC., Sec secretion system, LIT., process has physiological evidence but the involved enzymes are not identified yet.

Figure 1

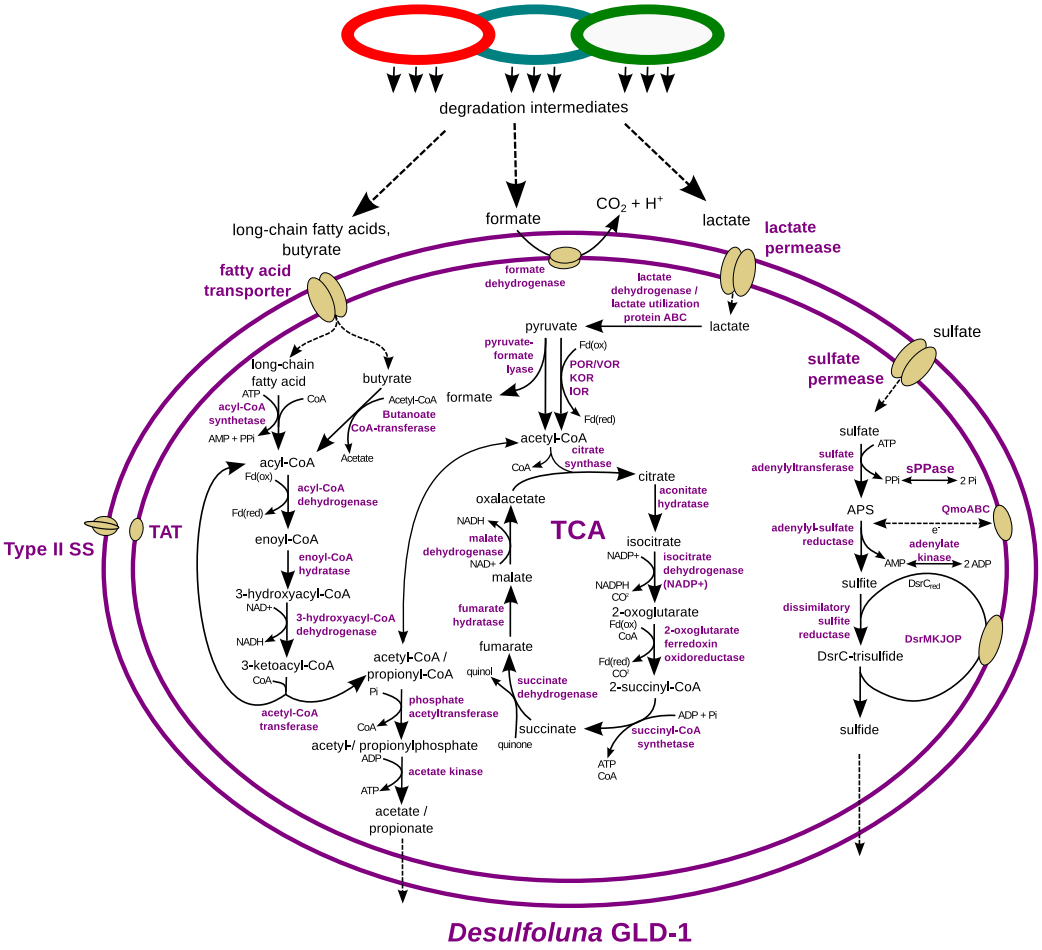

Figure 5. Model for utilization of degradation intermediates by SRM. The MAG *Desulfoluna* GLD-1 is depicted, which corresponds to *dsrB* OTU 2. The model indicates processes and enzymes that explain observed VFA dynamics and ^{13}C-enrichment of the corresponding *dsrB* OTU 2. SS,. Secretion system, TCA., tricarboxylic acid cycle.

Supplementary Information

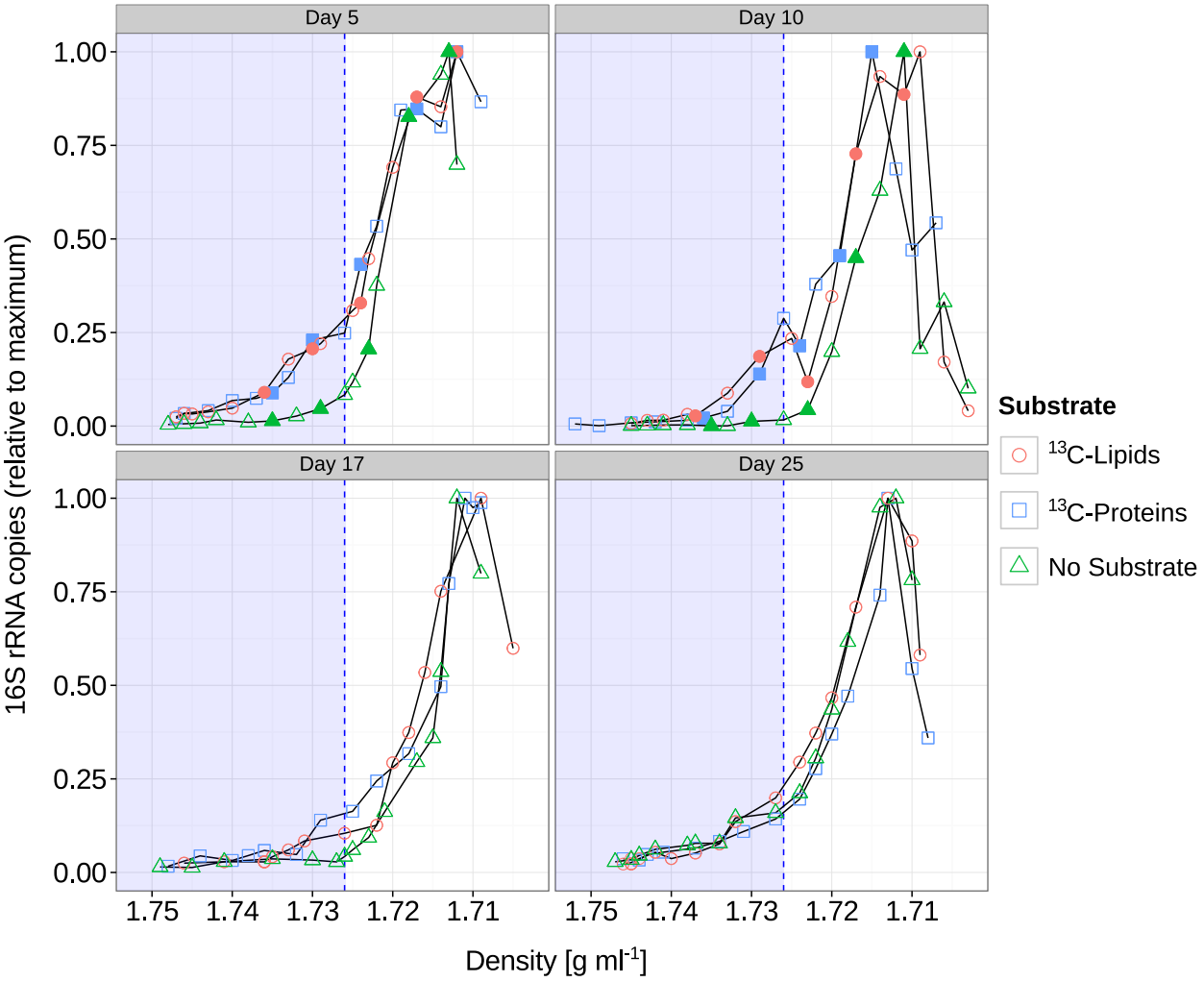

Supplemntary Figure S1. Proportions of 16S rRNA gene copies recovered from fractions of DNA-SIP gradients. Color and shape of data points indicate the amended substrate. Filled symbols indicate that DNA from the respective fraction of the DNA-SIP gradient was used as template for amplicon sequencing. The blue shaded area indicates the density (1.726 g ml^{-1}) of the gradient above which ^{13}C-labelled DNA is expected to accumulate.

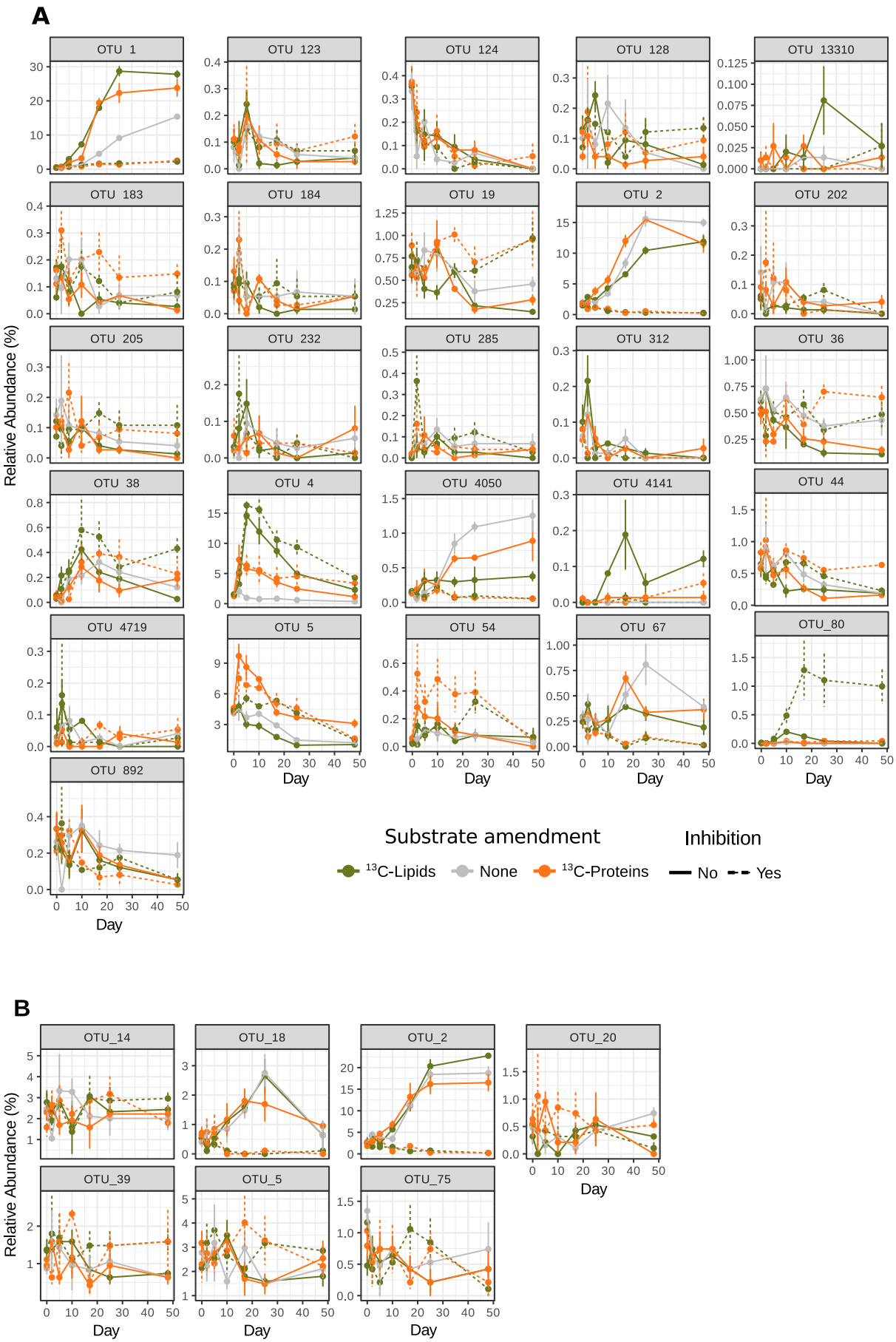

Supplementary Figure S2. Relative abundance of selected OTUs over time in protein, lipid and no substrate incubations with or without the sulfate-reduction inhibitor molybdate. Panels A and B indicate relative abundances of 16S rRNA and *dsrB* OTUs that incorporated ^{13}C-carbon during protein or lipid hydrolysis, respectively.

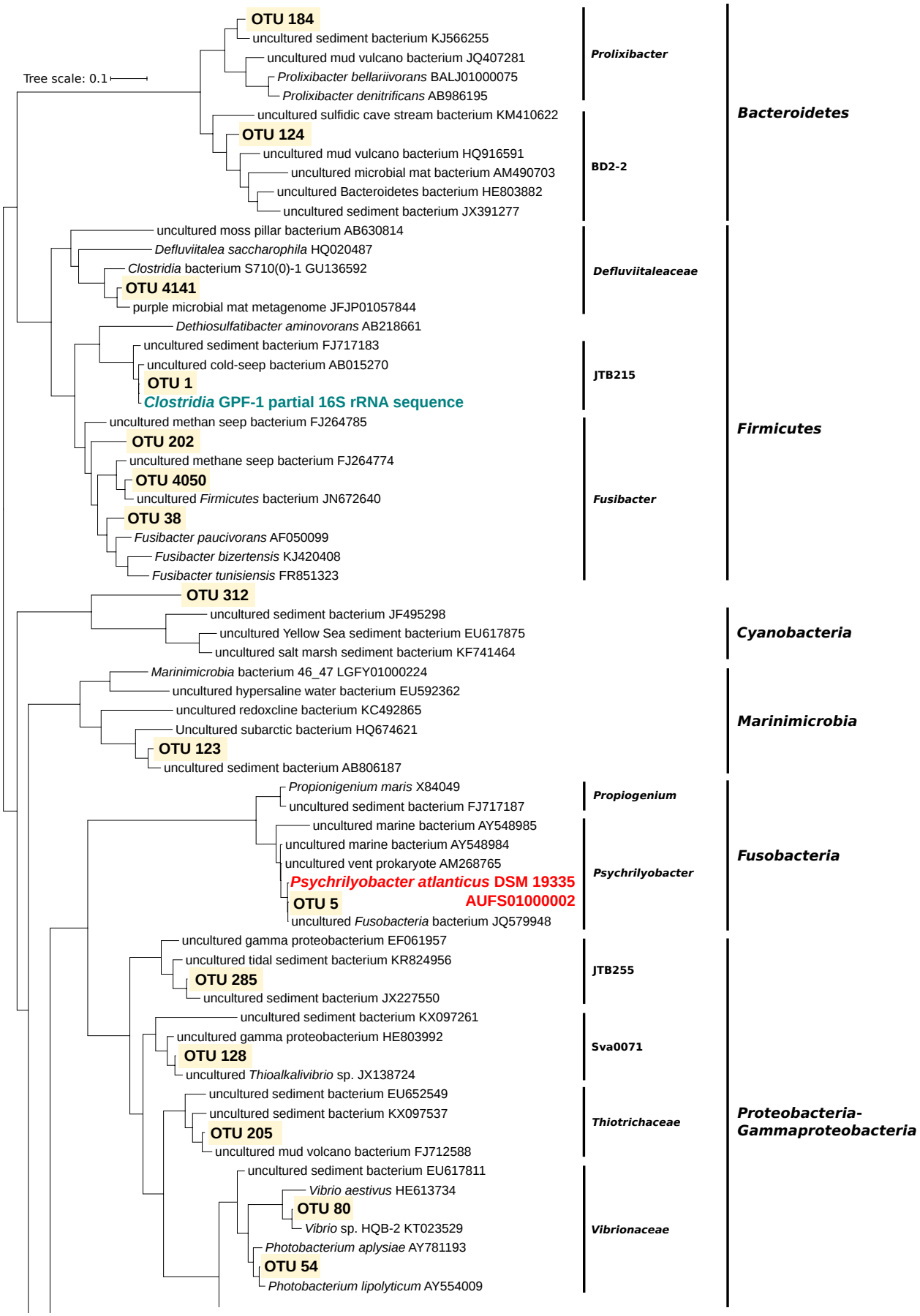
Tree scale: 0.1
OTU 184
uncultured sediment bacterium KJ566255
uncultured mud vulcano bacterium JQ407281
Prolixibacter bellariivorans BALJ01000075
Prolixibacter denitrificans AB986195
Prolixibacter
uncultured sulfidic cave stream bacterium KM410622
OTU 124
uncultured mud vulcano bacterium HQ916591
uncultured microbial mat bacterium AM490703
uncultured Bacteroidetes bacterium HE803882
uncultured sediment bacterium JX391277
BD2-2
Bacteroidetes
uncultured moss pillar bacterium AB630814
Defluviitalea saccharophila HQ020487
Clostridia bacterium S710(0)-1 GU136592
OTU 4141
purple microbial mat metagenome JFJP01057844
Defluviitaleaceae
Dethiosulfatibacter aminovorans AB218661
uncultured sediment bacterium FJ717183
uncultured cold-seep bacterium AB015270
OTU 1
Clostridia GPF-1 partial 16S rRNA sequence
JTB215
uncultured methan seep bacterium FJ264785
OTU 202
uncultured methane seep bacterium FJ264774
OTU 4050
uncultured Firmicutes bacterium JN672640
OTU 38
Fusibacter paucivorans AF050099
Fusibacter bizertensis KJ420408
Fusibacter tunisiensis FR851323
Fusibacter
Firmicutes
OTU 312
uncultured sediment bacterium JF495298
uncultured Yellow Sea sediment bacterium EU617875
uncultured salt marsh sediment bacterium KF741464
Cyanobacteria
Marinimicrobia bacterium 46_47 LGFY01000224
uncultured hypersaline water bacterium EU592362
uncultured redoxcline bacterium KC492865
Uncultured subarctic bacterium HQ674621
OTU 123
uncultured sediment bacterium AB806187
Marinimicrobia
Propionigenium maris X84049
uncultured sediment bacterium FJ717187
Propiogenium
uncultured marine bacterium AY548985
uncultured marine bacterium AY548984
uncultured vent prokaryote AM268765
Psychrilyobacter atlanticus DSM 19335
AUFS01000002
OTU 5
uncultured Fusobacteria bacterium JQ579948
Psychrilyobacter
Fusobacteria
uncultured gamma proteobacterium EF061957
uncultured tidal sediment bacterium KR824956
OTU 285
uncultured sediment bacterium JX227550
JTB255
uncultured sediment bacterium KX097261
uncultured gamma proteobacterium HE803992
OTU 128
uncultured Thioalkalivibrio sp. JX138724
Sva0071
uncultured sediment bacterium EU652549
uncultured sediment bacterium KX097537
OTU 205
uncultured mud volcano bacterium FJ712588
Thiotrichaceae
uncultured sediment bacterium EU617811
Vibrio aestivus HE613734
OTU 80
Vibrio sp. HQB-2 KT023529
Photobacterium aplysiae AY781193
OTU 54
Photobacterium lipolyticum AY554009
Vibrionaceae
Proteobacteria-
Gammaproteobacteria

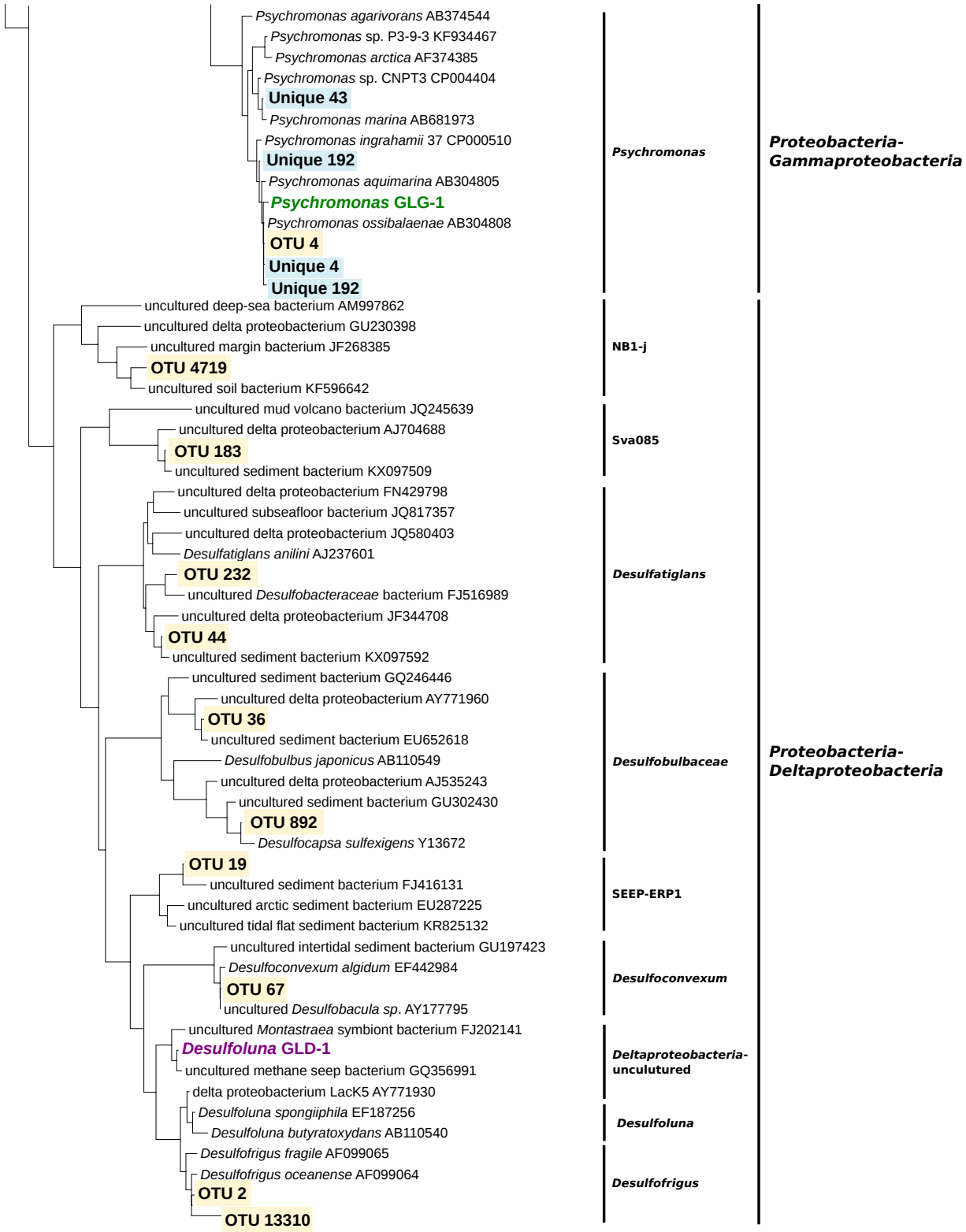

Supplementary Figure S3. Phylogenetic affiliation of 16S rRNA OTU and sub-OTU sequences. Tree was constructed from close relative sequences of SIP-enriched OTUs and sub-OTUs in the SILVA database v.128 (Quast *et al.*, 2013) and full-length 16S rRNA genes from MAGs with Fasttree (Price *et al.*, 2010). Full-length MAG derived 16S rRNA genes were aligned to the SILVA database v.128 (Quast *et al.*, 2013) with the SINA aligner (Pruesse *et al.*, 2012) prior to tree construction. 16S rRNA OTUs, sub-OTUs and partial 16S rRNA genes from MAGs were aligned to the SILVA database and then placed into the reference tree using the EPA algorithm (Berger *et al.*, 2011) in RAxML (Stamatakis, 2014). The tree was visualized in iTOL (Letunic and Bork, 2007).

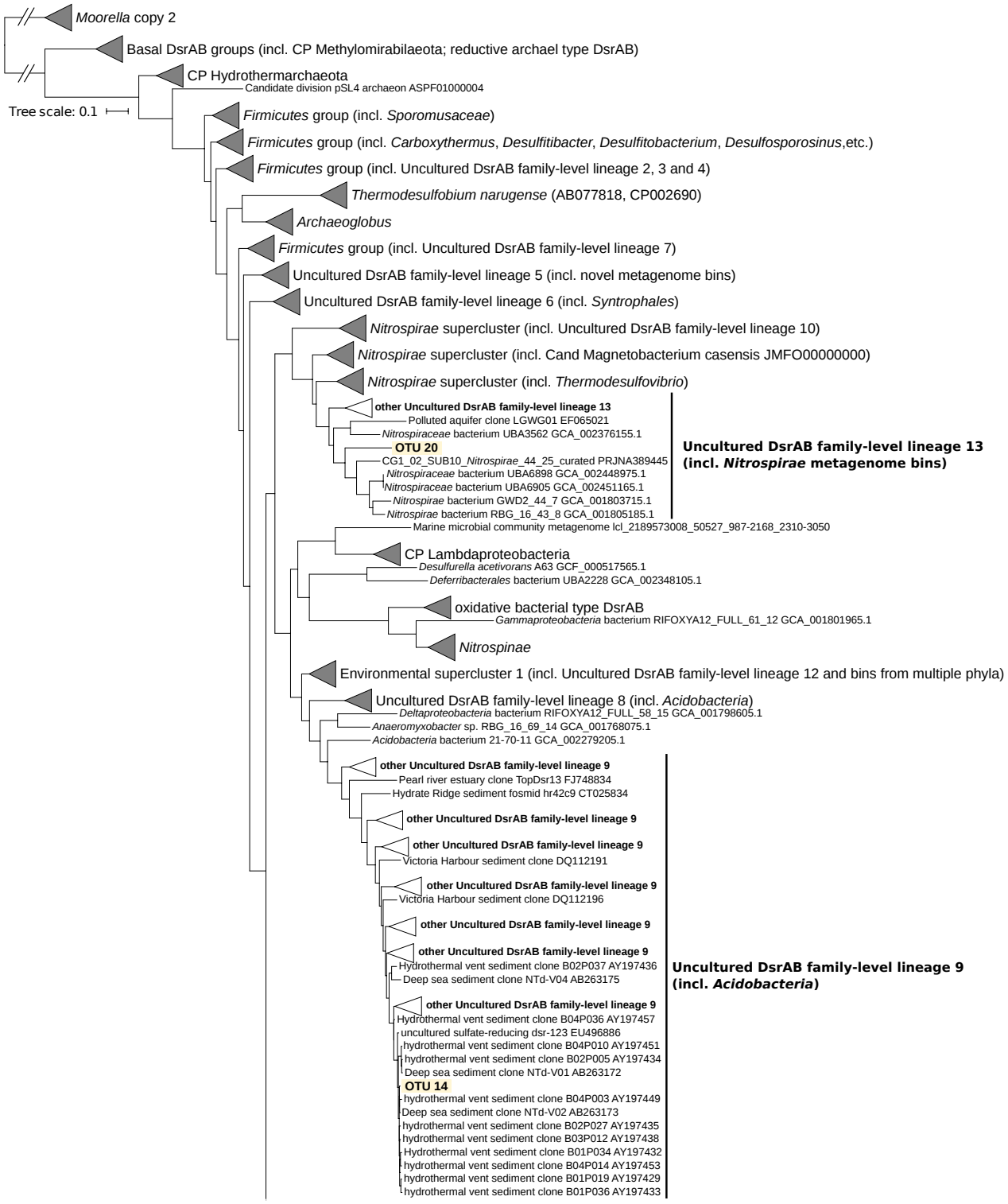
Moorella copy 2
Basal DsrAB groups (incl. CP Methylomirabilaeota; reductive archael type DsrAB)
CP Hydrothermarchaeota
Candidate division pSL4 archaeon ASPF01000004
Tree scale: 0.1
Firmicutes group (incl. *Sporomusaceae*)
Firmicutes group (incl. *Carboxythermus*, *Desulfitibacter*, *Desulfitobacterium*, *Desulfosporosinus*,etc.)
Firmicutes group (incl. Uncultured DsrAB family-level lineage 2, 3 and 4)
Thermodesulfobium narugense (AB077818, CP002690)
Archaeoglobus
Firmicutes group (incl. Uncultured DsrAB family-level lineage 7)
Uncultured DsrAB family-level lineage 5 (incl. novel metagenome bins)
Uncultured DsrAB family-level lineage 6 (incl. *Syntrophales*)
Nitrospirae supercluster (incl. Uncultured DsrAB family-level lineage 10)
Nitrospirae supercluster (incl. Cand Magnetobacterium casensis JMFO00000000)
Nitrospirae supercluster (incl. *Thermodesulfovibrio*)
other Uncultured DsrAB family-level lineage 13
Polluted aquifer clone LGWG01 EF065021
Nitrospiraceae bacterium UBA3562 GCA_002376155.1
OTU 20
CG1_02_SUB10_*Nitrospirae*_44_25_curated PRJNA389445
Nitrospiraceae bacterium UBA6898 GCA_002448975.1
Nitrospiraceae bacterium UBA6905 GCA_002451165.1
Nitrospirae bacterium GWD2_44_7 GCA_001803715.1
Nitrospirae bacterium RBG_16_43_8 GCA_001805185.1
Uncultured DsrAB family-level lineage 13 (incl. *Nitrospirae* metagenome bins)
Marine microbial community metagenome lcl_2189573008_50527_987-2168_2310-3050
CP Lambdaproteobacteria
Desulfurella acetivorans A63 GCF_000517565.1
Deferribacterales bacterium UBA2228 GCA_002348105.1
oxidative bacterial type DsrAB
Gammaproteobacteria bacterium RIFOXYA12_FULL_61_12 GCA_001801965.1
Nitrospinae
Environmental supercluster 1 (incl. Uncultured DsrAB family-level lineage 12 and bins from multiple phyla)
Uncultured DsrAB family-level lineage 8 (incl. *Acidobacteria*)
Deltaproteobacteria bacterium RIFOXYA12_FULL_58_15 GCA_001798605.1
Anaeromyxobacter sp. RBG_16_69_14 GCA_001768075.1
Acidobacteria bacterium 21-70-11 GCA_002279205.1
other Uncultured DsrAB family-level lineage 9
Pearl river estuary clone TopDsr13 FJ748834
Hydrate Ridge sediment fosmid hr42c9 CT025834
other Uncultured DsrAB family-level lineage 9
other Uncultured DsrAB family-level lineage 9
Victoria Harbour sediment clone DQ112191
other Uncultured DsrAB family-level lineage 9
Victoria Harbour sediment clone DQ112196
other Uncultured DsrAB family-level lineage 9
other Uncultured DsrAB family-level lineage 9
Hydrothermal vent sediment clone B02P037 AY197436
Deep sea sediment clone NTd-V04 AB263175
other Uncultured DsrAB family-level lineage 9
Hydrothermal vent sediment clone B04P036 AY197457
uncultured sulfate-reducing dsr-123 EU496886
hydrothermal vent sediment clone B04P010 AY197451
hydrothermal vent sediment clone B02P005 AY197434
Deep sea sediment clone NTd-V01 AB263172
OTU 14
hydrothermal vent sediment clone B04P003 AY197449
Deep sea sediment clone NTd-V02 AB263173
hydrothermal vent sediment clone B02P027 AY197435
hydrothermal vent sediment clone B03P012 AY197438
Hydrothermal vent sediment clone B01P034 AY197432
hydrothermal vent sediment clone B04P014 AY197453
hydrothermal vent sediment clone B01P019 AY197429
hydrothermal vent sediment clone B01P036 AY197433
Uncultured DsrAB family-level lineage 9 (incl. *Acidobacteria*)

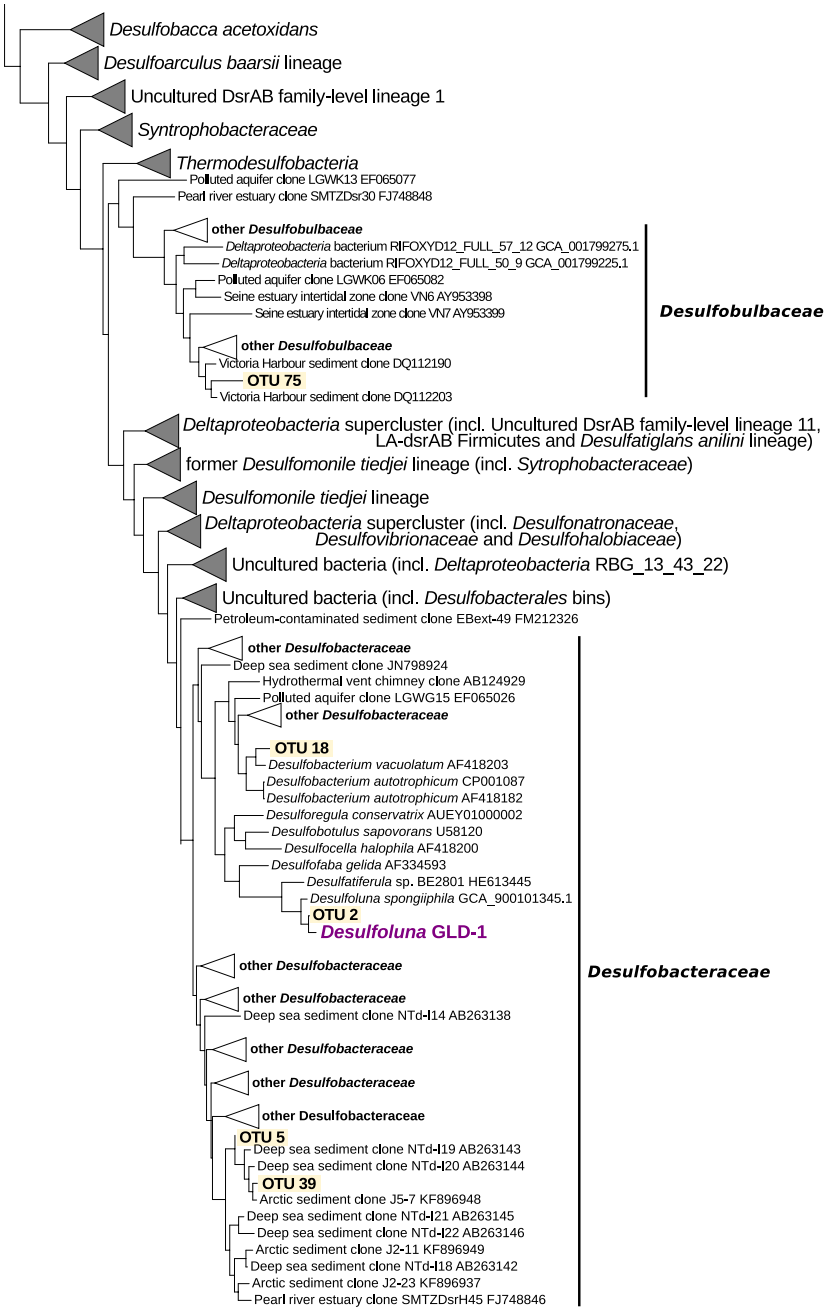

Supplementary Figure S4. Phylogenetic affiliation of *dsrB* OTU sequences. Tree was constructed with Fasttree (Price *et al.*, 2010) based on a DsrAB reference alignment (Pelikan *et al.*, in prep) and the DsrAB sequence from MAG *Desulfoluna* GLD_1, which was aligned using MAFFT (Katoh *et al.*, 2002). *dsrB* OTUs were aligned to the extended reference alignment with MAFFT (Katoh *et al.*, 2002), and then placed into the reference tree using the EPA algorithm (Berger *et al.*, 2011) in RAxML (Stamatakis, 2014). The tree was visualized in iTOL (Letunic and Bork, 2007).

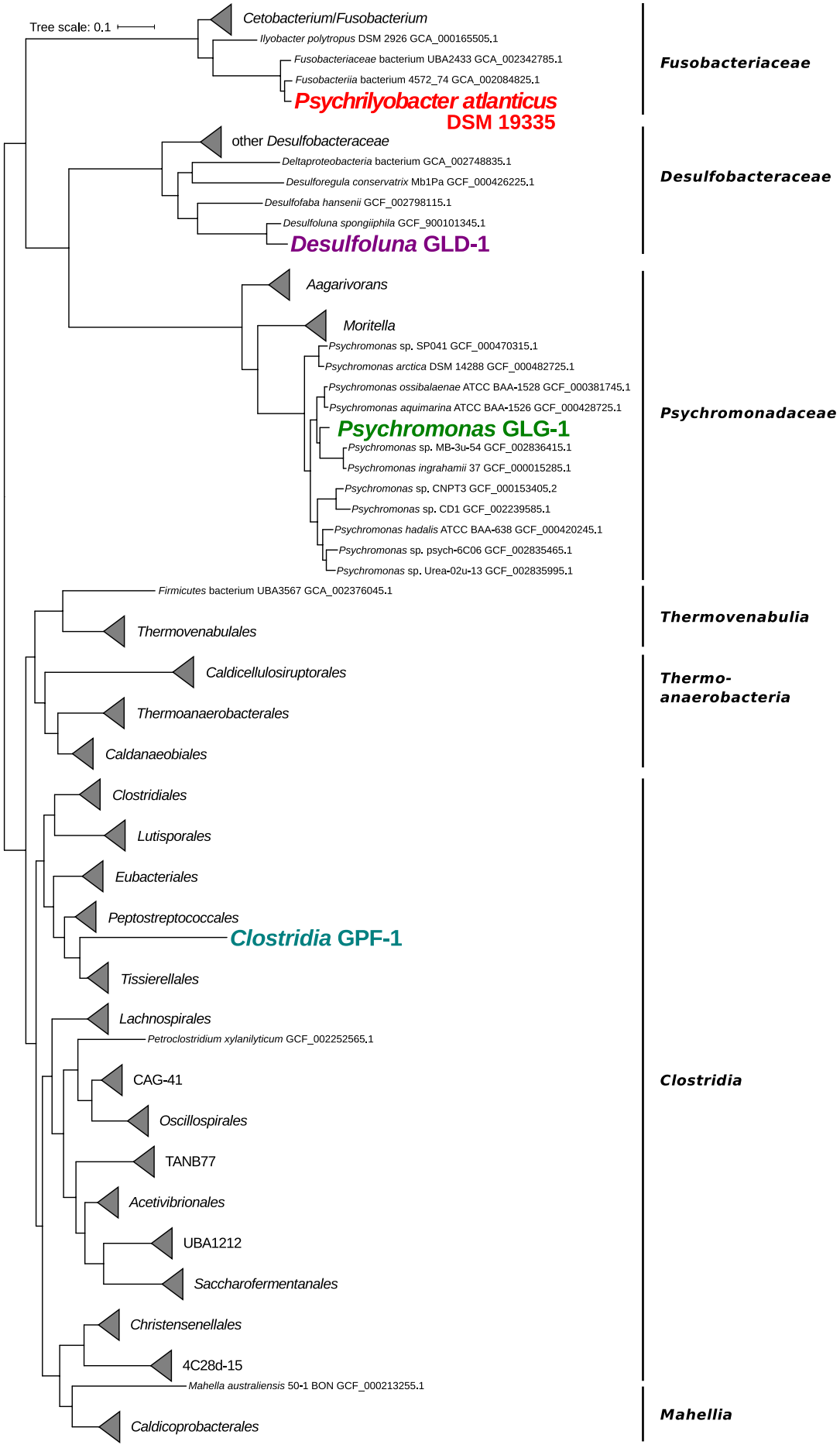

Supplementary Figure S5. Phylogenetic affiliation of metagenome assembled genomes (MAGs) and the genome of *Psychrilyobacter atlanticus*. Tree was constucted with FastTree (Price *et al.*, 2010) from the concatenated marker gene alignment provided by GTDB (Parks *et al.*, 2015). The tree was visualized in iTOL (Letunic and Bork, 2007).

Supplementary Table S1. Summary of MEROPS and ESTHER database description for peptidases and lipases, respectively.

Peptidases		
MEROPS ID	**MEROPS description summary**	**Selected**
A8	production of the bacterial cell wall	No
M1	some are cleaving AAs from small peptides	Yes
M3	Lactobacillus Oligoendopeptidase cleaves oligopeptides	Yes
M14	digestion of food and other functions	Yes
M20	conversion of proteins to free amino acids.	Yes
M24	removes N-terminal Methionine from protein	Yes
M28	alkaline phosphatase isozyme conversion	No
M29	catabolic peptidase in Streptococcus thermophilus	Yes
M42	used by Lactobacillus for nutrition on milk	Yes
M48	degradation of abnormal proteins	No
M50	regulated intermembrane proetolysis	No
S8	probably involved in nutrition	Yes
S12	synthesis and remodelling of bacterial cell walls	No
S15	degradation of casein	Yes
S24	regulatory stress response	No
S26	remove the signal peptides and facilitate secretion	No
Lipases		
ESTHER family	**ESTHER description summary**	**Selected**
6_AlphaBeta_hydrolase	not well characterized	No
Abhydrolase_7	acetyl-esterase_deacetylase or Dienelactone_hydrolase or xylan esterase	No
Bacterial_EstLip_FamX	Family of Bacterial lipolytic enzymes	Yes
Carb_B_Bacteria	carboxylesterase, type B	Yes
CarbLipBact_2	members of this group are esterases, lipases	Yes
Duf_1023	proteins of unknown function	No
Duf_3089	lipolytic enzyme family defined from isolation and characterization of two esterases from a metagenomic library	Yes
Duf_900	proteins of unknown function	No
Epoxide_hydrolase	conversion of epoxides to corresponding diols	No
GTSAGmotif	lipases from metagenomic library	Yes
Hormone-sensitive_lipase_like	esterase/lipase, family IV	Yes
Lipase_2	lipases	Yes
Lipase_3	lipases	Yes
Monoglyceridelipase_lysophospholip	has some homology to peptidases S33	No
NFM-deformylase	N-formylmaleamic acid to formic and maleamic acid	No
PGAP1	attachment to proteins factor 1	No

Supplementary Table S2. Significant enrichment of 16S rRNA gene OTUs in ^{13}C-fractions of DNA stable isotope gradients.

OTU	Taxonomy	base mean	log2-fold change	adjusted p-value	Incubation	Day
OTU_80	*Gammaproteobacteria*, *Vibrionaceae*	8.7	7.7	0.000	Proteins	10
OTU_80	*Gammaproteobacteria*, *Vibrionaceae*	8.7	6.7	0.002	Lipids	5
OTU_232	*Deltaproteobacteria*, *Desulfatiglans*	2.4	6.4	0.005	Proteins	10
OTU_4	*Gammaproteobacteria*, *Psychromonas*	936.5	5.5	0.000	Lipids	5
OTU_312	*Cyanobacteria*	1.9	5.2	0,034	Proteins	10
OTU_4	*Gammaproteobacteria*, *Psychromonas*	936.5	4.9	0.000	Lipids	10
OTU_4141	*Firmicutes*, *Defluviitaleaceae*	5.2	4.8	0.015	Lipids	10
OTU_183	*Deltaproteobacteria*, Sva0485	4.2	4.8	0.003	Proteins	10
OTU_184	Bacteroidetes, *Prolixibacter*	1.4	4.5	0.083	Proteins	10
OTU_123	*Marinimicrobia*	4.3	4.5	0.007	Proteins	10
OTU_4	*Gammaproteobacteria*, *Psychromonas*	936.5	4.5	0.000	Proteins	5
OTU_80	*Gammaproteobacteria*, *Vibrionaceae*	8.7	4.3	0.015	Lipids	10
OTU_124	*Bacteroidetes*, BD2-2	3.6	3.7	0.055	Proteins	10
OTU_285	*Gammaproteobacteria*, JTB255	2.7	3.6	0.083	Proteins	10
OTU_13310	*Deltaproteobacteria*, *Desulfofrigus*	5.4	3.5	0.072	Lipids	10
OTU_4719	*Deltaproteobacteria*, NB1-J	3.1	3.3	0.098	Proteins	10
OTU_54	*Gammaproteobacteria*, *Vibrionaceae*	9.1	3.2	0.030	Proteins	5
OTU_128	*Gammaproteobacteria*, Sva0071	4.1	3.1	0.045	Proteins	10
OTU_1	*Firmicutes*, JTB215	967.1	3.0	0.018	Proteins	5
OTU_202	*Firmicutes*, *Clostridiales*	2.1	3.0	0.098	Proteins	10
OTU_205	*Gammaproteobacteria*, *Thiotrichaceae*	3.2	3.0	0.083	Proteins	10
OTU_4050	*Firmicutes*, *Fusibacter*	25.8	3.0	0.001	Proteins	10
OTU_4	*Gammaproteobacteria*, *Psychromonas*	936.5	2.8	0.009	Proteins	10
OTU_1	*Firmicutes*, JTB215	967.1	2.8	0.036	Lipids	10
OTU_38	*Firmicutes*, *Clostridiales*	11.2	2.6	0.006	Proteins	5
OTU_19	*Deltaproteobacteria*, SEEP-SRB1	22.5	2.1	0.009	Proteins	10
OTU_892	*Deltaproteobacteria*, *Desulfobulbaceae*	11.0	2.1	0.098	Proteins	10
OTU_5	*Fusobacteria*, *Psychrilyobacter*	297.5	2.0	0.005	Proteins	5
OTU_36	*Deltaproteobacteria*, *Desulfobulbaceae*	16.0	2.0	0.068	Proteins	10
OTU_44	*Deltaproteobacteria*, *Desulfatiglans*	16.5	1.8	0.098	Proteins	10
OTU_67	*Deltaproteobacteria*, *Desulfoconvexum*	19.0	1.7	0.055	Proteins	10
OTU_2	*Deltaproteobacteria*, *Desulfofrigus*	699.6	1.3	0.043	Proteins	10
OTU_5	*Fusobacteria*, *Psychrilyobacter*	297.5	1.3	0.055	Proteins	10

Supplementary Table S3. Significant enrichment of *dsrB* OTUs in ^{13}C-fractions of DNA stable isotope gradients.

OTU	Taxonomy	base mean	log2-fold change	adjusted p-value	Incubation	Day
OTU_14	Uncultured DsrAB lineage 9 (incl. *Acidobacteria*)	137.1	4.7	0.000	Proteins	10
OTU_20	Uncultured DsrAB lineage 13 (incl. *Nitrospirae*)	6.0	4.3	0.007	Proteins	10
OTU_18	*Deltaproteobacteria*, *Desulfobacteraceae*	50.1	3.3	0.001	Lipids	10
OTU_39	*Deltaproteobacteria*, *Desulfobacteraceae*	14.8	3.2	0.019	Proteins	10
OTU_2	*Deltaproteobacteria*, *Desulfobacteraceae*	340.7	2.4	0.001	Lipids	10
OTU_75	*Deltaproteobacteria*, *Desulfobulbaceae*	9.5	2.4	0.077	Proteins	10
OTU_5	*Deltaproteobacteria*, *Desulfobacteraceae*	27.7	2.3	0.082	Proteins	10

Supplementary Table S4. Genome statistics of selected metagenome bins. Comp, CheckM completeness. Cont, CheckM contaminaton. SH, CheckM strain heterogeneity.

Bin	GTDB classification	Closest relative [ANI (% aligned) / AAI (% aligned)]	Comp	Cont	SH
Psychromonas GLG-1	g__Psychromonas	*Psychromonas aquimarina* ATCC BAA-1526 GCF_000381745.1 [80.7 (41.8) / 80.73 (66.28)]	97.39	0.81	50
Tissierellales GPF-1	o__Tissierellales	*Caloranaerobacter azorensis* DSM 13643 GCA_900129995.1 [- / 53.39 (37)]	99.07	0.7	0
Desulfoluna GLD-1	g__Desulfoluna	*Desulfoluna spongiiphila* GCA_900101345.1 [79.42 (39.41) / 76.93 (68.72)]	94.95	1.36	0

Supplementary Table S5. Annotation of MAGs and the genome of *Psychrilyobacter atlanticus*.

	Psychrilyobacter atlanticus	***Psychromonas* GLG-1**	***Desulfoluna* GLD-1**	***Tissierellales* GPF-1**
Extracellular peptidases				
M3	K337_v1_10834	-	-	-
M20	-	-	-	FUSI_v1_490026
M24	K337_v1_10582	-	-	FUSI_v1_750006
S8	-	-	-	FUSI_v1_960008
Intracellular peptidases				
M1	K337_v1_20320	PSYM_v1_1690003	DESP_v1_990015	-
M3	K337_v1_10060 K337_v1_10959	PSYM_v1_200017	DESP_v1_1000010	FUSI_v1_620036
M14	-	-	-	FUSI_v1_430016
M20	K337_v1_11550 K337_v1_12047 K337_v1_12179 K337_v1_20729 K337_v1_20883 K337_v1_20919 K337_v1_10663 K337_v1_10999	PSYM_v1_1880004 PSYM_v1_770006	DESP_v1_1930005 DESP_v1_450039 DESP_v1_950012 DESP_v1_370017	FUSI_v1_10038 FUSI_v1_100004 FUSI_v1_110018 FUSI_v1_230059 FUSI_v1_350001 FUSI_v1_480007 FUSI_v1_480008 FUSI_v1_520043 FUSI_v1_690003 FUSI_v1_810064 FUSI_v1_1010016 FUSI_v1_1200040 FUSI_v1_90003 FUSI_v1_490033 FUSI_v1_840169 FUSI_v1_1200040
M24	K337_v1_10205 K337_v1_30031 K337_v1_11495 K337_v1_20327	PSYM_v1_40024 PSYM_v1_190014	DESP_v1_210001 DESP_v1_670013	FUSI_v1_640120 FUSI_v1_940096
M29	K337_v1_10108	-	-	FUSI_v1_670015
M42	K337_v1_11926 K337_v1_20353 K337_v1_20380 K337_v1_20685 K337_v1_20968 K337_v1_20994	-	-	FUSI_v1_720007 FUSI_v1_640071 FUSI_v1_640072 FUSI_v1_640073 FUSI_v1_900026
S15	-	PSYM_v1_250021	DESP_v1_550012	-
Extracellular lipases				
Carboxylesterase, type B (carboxylesterase)	-	PSYM_v1_1870005	-	-
Bacterial_EstLip_FamX (esterase / lipase)	-	-	-	FUSI_v1_10055
Membrane lipases				
Carboxylesterase, type B (carboxylesterase)	-	-	-	FUSI_v1_1090001
Bacterial_EstLip_FamX (esterase / lipase)	-	-	-	FUSI_v1_840070
Intracellular lipases				
Carboxylesterase, type B (carboxylesterase)	-	PSYM_v1_2290005	DESP_v1_250018	

Hormone-sensitive_lipase_like	-	-	-	FUSI_v1_1110043 FUSI_v1_1220006
Lipase_3 (lipase)	-	-	DESP_v1_1460001	-
CarbLipBact_2 (carboxylesterase)	-	-	DESP_v1_330004 DESP_v1_170009	-
Extracellular glycoside hydrolases				
GH 1	-	PSYM_v1_2060004 PSYM_v1_540012	-	-
GH 3	K337_v1_11729	PSYM_v1_1230007 PSYM_v1_2870002	-	-
GH 5	-	-	-	-
GH 9	-	-	DESP_v1_770006	-
GH 13	-	PSYM_v1_20031 PSYM_v1_270004 PSYM_v1_1260002 PSYM_v1_1400003 PSYM_v1_2970001 PSYM_v1_720010	-	FUSI_v1_1250081
GH 15	-	-	-	-
GH 16	-	PSYM_v1_700008	-	-
GH 17	-	PSYM_v1_700006	-	-
GH 18	-	PSYM_v1_1680004	-	-
GH 20	-	-	-	-
GH 26	-	-	-	FUSI_v1_320001
GH 31	-	-	-	-
GH 81	-	PSYM_v1_700005	-	-
Peptide, amino acid transporters				
peptide ABC transporter solute-binding protein	K337_v1_11982 K337_v1_20616 K337_v1_20977 K337_v1_21084 K337_v1_10066 K337_v1_10067 K337_v1_10987 K337_v1_11888 K337_v1_10949	PSYM_v1_160012 PSYM_v1_1890004 PSYM_v1_2570005	DESP_v1_390002 DESP_v1_950007 DESP_v1_1230003 DESP_v1_1230007 ESP_v1_2060002	FUSI_v1_30041 FUSI_v1_30042 FUSI_v1_30043 FUSI_v1_350009 FUSI_v1_430021 FUSI_v1_690012 FUSI_v1_640053 FUSI_v1_900024 FUSI_v1_1230026
peptide ABC transporter permease	K337_v1_11985 K337_v1_11986 K337_v1_20617 K337_v1_20618 K337_v1_20981 K337_v1_20982 K337_v1_21082 K337_v1_21083 K337_v1_10064 K337_v1_10065 K337_v1_10988 K337_v1_10989 K337_v1_10947 K337_v1_10948	PSYM_v1_160014 PSYM_v1_160013 PSYM_v1_1890002 PSYM_v1_1890003 PSYM_v1_2570003 PSYM_v1_2570004	DESP_v1_950008 DESP_v1_950009 DESP_v1_1230004 DESP_v1_1230005 DESP_v1_190003 DESP_v1_190004 DESP_v1_178000 DESP_v1_2060001 DESP_v1_1780002	FUSI_v1_30046 FUSI_v1_30047 FUSI_v1_350007 FUSI_v1_350008 FUSI_v1_430017 FUSI_v1_430018 FUSI_v1_490040 FUSI_v1_490041 FUSI_v1_690010 FUSI_v1_690011 FUSI_v1_640051 FUSI_v1_640052 FUSI_v1_900022 FUSI_v1_900023
peptide ABC transporter ATP-binding protein	K337_v1_11983 K337_v1_11984 K337_v1_20619 K337_v1_20620 K337_v1_20978 K337_v1_20979 K337_v1_21080	PSYM_v1_160011 PSYM_v1_1890001 PSYM_v1_2570002	DESP_v1_390001 DESP_v1_950010 DESP_v1_950011 DESP_v1_1230006 DESP_v1_190006 DESP_v1_190007 DESP_v1_190005	FUSI_v1_30044 FUSI_v1_30045 FUSI_v1_100008 FUSI_v1_350005 FUSI_v1_350006 FUSI_v1_430019 FUSI_v1_430020

	K337_v1_21081 K337_v1_10062 K337_v1_10063 K337_v1_10990 K337_v1_10991 K337_v1_10945 K337_v1_10946		DESP_v1_1780003 DESP_v1_1780004	FUSI_v1_490038 FUSI_v1_490039 FUSI_v1_490042 FUSI_v1_690008 FUSI_v1_690009 FUSI_v1_640049 FUSI_v1_640050 FUSI_v1_900020 FUSI_v1_900021
proton-dependent oligopeptide transporter	K337_v1_11684 K337_v1_11558 K337_v1_20326 K337_v1_10621	-	-	-
oligopeptide transporter, OPT superfamily	K337_v1_12103	-	-	-
(branched-chain) amino acid ABC transporter substrate-binding protein	K337_v1_11898 K337_v1_11901 K337_v1_11933 K337_v1_20143 K337_v1_10045 K337_v1_10750 K337_v1_10972 K337_v1_10099 K337_v1_10358	PSYM_v1_920003 PSYM_v1_100037 PSYM_v1_1070010 PSYM_v1_1780001 PSYM_v1_2250004 PSYM_v1_1030041 PSYM_v1_570012	DESP_v1_460004 DESP_v1_200032 DESP_v1_1650008 DESP_v1_2270001 DESP_v1_990022 DESP_v1_1440005 DESP_v1_130006 DESP_v1_170002 DESP_v1_170021 DESP_v1_270015	FUSI_v1_30075 FUSI_v1_120029 FUSI_v1_410010 FUSI_v1_450023 FUSI_v1_560002 FUSI_v1_840088 FUSI_v1_1010014 FUSI_v1_1200070 FUSI_v1_1200071
(branched-chain) amino acid ABC transporter permease	K337_v1_11905 K337_v1_11932 K337_v1_20142 K337_v1_10042 K337_v1_10043 K337_v1_10749 K337_v1_10971 K337_v1_10100 K337_v1_10359	PSYM_v1_1780002 PSYM_v1_1780003 PSYM_v1_2250005	DESP_v1_2270002 DESP_v1_1240011 DESP_v1_1440006 DESP_v1_130005 DESP_v1_170002 DESP_v1_270016	FUSI_v1_30074 FUSI_v1_120030 FUSI_v1_120033 FUSI_v1_410006 FUSI_v1_410007 FUSI_v1_450020 FUSI_v1_450021 FUSI_v1_560003 FUSI_v1_560004 FUSI_v1_840085 FUSI_v1_840086 FUSI_v1_1010013 FUSI_v1_1200072 FUSI_v1_1200073
(branched-chain) amino acid ABC transporter ATP-binding protein	K337_v1_11904 K337_v1_11931 K337_v1_20141 K337_v1_10044 K337_v1_10748 K337_v1_10970 K337_v1_10101 K337_v1_10360	PSYM_v1_3310003 PSYM_v1_2250006	DESP_v1_1440007 DESP_v1_130004 DESP_v1_170021 DESP_v1_270017	FUSI_v1_30073 FUSI_v1_120031 FUSI_v1_410008 FUSI_v1_410009 FUSI_v1_450022 FUSI_v1_560005 FUSI_v1_560006 FUSI_v1_840087 FUSI_v1_1010012 FUSI_v1_1200074 FUSI_v1_1200075
amino acid transporter (not ABC-type)	K337_v1_10033 K337_v1_10196 K337_v1_10219 K337_v1_10420 K337_v1_10462 K337_v1_10880 K337_v1_11085 K337_v1_11091 K337_v1_11117 K337_v1_11120 K337_v1_11272 K337_v1_11297 K337_v1_11822 K337_v1_11837 K337_v1_11930 K337_v1_12087 K337_v1_12145 K337_v1_20015 K337_v1_20017 K337_v1_20113 K337_v1_20190	PSYM_v1_1090001 PSYM_v1_1090002 PSYM_v1_112009 PSYM_v1_1120010 PSYM_v1_920006 PSYM_v1_1000001 PSYM_v1_1770003 PSYM_v1_2690005 PSYM_v1_3290005 PSYM_v1_470002 PSYM_v1_500008	DESP_v1_20048 DESP_v1_550024 DESP_v1_140024 DESP_v1_190021 DESP_v1_200033	FUSI_v1_800082 FUSI_v1_30079 FUSI_v1_90002 FUSI_v1_500003 FUSI_v1_430065 FUSI_v1_540090 FUSI_v1_430069 FUSI_v1_800083 FUSI_v1_1110033 FUSI_v1_1200047

	K337_v1_20319 K337_v1_20640 K337_v1_20641 K337_v1_20646 K337_v1_20680 K337_v1_20783 K337_v1_21020			
Fatty acid transporters				
short-chain fatty acid transporter	K337_v1_10807	-	-	-
long-chain fatty acid transporter	-	PSYM_v1_3160003 PSYM_v1_240004	DESP_v1_1780005	-
lipid carrier protein	-	PSYM_v1_1250003	-	-
Glutamine degradation to glutamate				
glutaminase (EC 3.5.1.2) / glutamate synthase (NADH) (EC 1.4.1.13)	K337_v1_12167 K337_v1_20289 K337_v1_11291 K337_v1_20098 K337_v1_11119	PSYM_v1_890008 PSYM_v1_60010 PSYM_v1_60010 PSYM_v1_60011 PSYM_v1_60011	DESP_v1_90044 DESP_v1_100036 DESP_v1_100037 DESP_v1_100038 DESP_v1_170010 DESP_v1_950005	FUSI_v1_60019 FUSI_v1_430050 FUSI_v1_430103 FUSI_v1_640141 FUSI_v1_840028
Histidine degradation to glutamate				
histidin ammonia lyase (EC 4.3.1.3)	K337_v1_20957	PSYM_v1_80008	-	FUSI_v1_460027
urocanate hydratase (EC 4.2.1.49)	K337_v1_20351	-	-	FUSI_v1_640043
imidazolonepropionase (EC 3.5.2.7)	K337_v1_20956	-	DESP_v1_850010	FUSI_v1_640040 FUSI_v1_680002 FUSI_v1_350003
formimidoylglutamase (EC 3.5.3.8)	K337_v1_20958	-	-	-
Glutamate degradation via methylaspartate pathway to pyruvate				
methylaspartate mutase, mutE (EC 5.4.99.1)	K337_v1_11676 K337_v1_11678	-	-	FUSI_v1_940031 FUSI_v1_940032
methylaspartate ammonia-lyase (EC 4.3.1.2)	K337_v1_11673	-	-	-
2-methylmalate dehydratase (EC 4.2.1.34)	-	-	-	-
citramalate lyase (EC 4.1.3.22)	-	-	-	-
Glutmate degradation via hydroxyglutarate pathway to butyrate				
glutamate / leucine dehydrogenase (EC 1.4.1.2, EC 1.4.1.3, EC 1.4.1.4)	K337_v1_11103 K337_v1_11104	PSYM_v1_60003 PSYM_v1_2910003	DESP_v1_1130001 DESP_v1_1890001	FUSI_v1_10079
2-hydroxyglutarate dehydrogenase (EC 1.1.99.2)	K337_v1_11115	-	-	FUSI_v1_10080
glutaconate CoA-transferase (EC 2.8.3.12)	-	-	-	-
2-hydroxyglutaryl CoA dehydratase (EC 4.2.1.-)	K337_v1_21025 K337_v1_11508 K337_v1_11511	-	-	-
glutaconyl-CoA decarboxylase subunit delta (EC 4.1.1.70)	K337_v1_20059	-	-	-
glutaconyl-CoA decarboxylase subunit gamma (EC 4.1.1.70)	K337_v1_20060	-	-	FUSI_v1_940037
glutaconyl-CoA decarboxylase subunit beta (EC 4.1.1.70)	K337_v1_20061	-	-	FUSI_v1_940038

butyryl-CoA dehydrogenase (EC 1.3.8.1)	K337_v1_30044	-	-	FUSI_v1_410001
butyryl coenzyme A transferase, alpha subunit (EC 2.8.3.8)	K337_v1_10805	-	-	-
butyryl coenzyme A transferase, beta subunit (EC 2.8.3.8)	K337_v1_10806	-	-	-
Asparagin degradation to aspartate				
asparaginase (EC 3.5.1.1)	K337_v1_20898	PSYM_v1_100035 PSYM_v1_100036	DESP_v1_1280014	FUSI_v1_280010
L-Homocysteine degradation to cysteine and L-cysteine degradation to pyruvate				
cystathionine β-synthase (EC 4.2.1.22)	-	PSYM_v1_2510003	-	FUSI_v1_150018 FUSI_v1_1110062
cystathionine gamma-lyase (EC 4.4.1.1) / cysteine synthase (EC 2.5.1.47)	K337_v1_11683 K337_v1_20987	PSYM_v1_660011 PSYM_v1_410001	DESP_v1_220021	FUSI_v1_460004
Tryptophane degradation to pyruvate				
tryptophanase / L-cysteine desulfhydrase, PLP-dependent (EC 4.1.99.1)	K337_v1_20947	-	-	-
L-Serine degradation to pyruvate / Threonine degradation (I) to 2-oxobutanoate				
L-serine ammonia-lyase (EC 4.3.1.17) / threonine ammonia-lyase (EC 4.3.1.19)	K337_v1_10253 K337_v1_11287	PSYM_v1_590011 PSYM_v1_120009	DESP_v1_1300002 DESP_v1_510015	FUSI_v1_60011 FUSI_v1_630018 FUSI_v1_630019
Alanine degradation to pyruvate				
alanine dehydrogenase (EC 1.4.1.1)	K337_v1_11051 K337_v1_11052	PSYM_v1_480006	DESP_v1_20046	-
Methionine degradation to 2-oxobutanoate and methanethiol				
methionine gamma-lyase (EC 4.4.1.11)	K337_v1_10331 K337_v1_11588 K337_v1_11915	PSYM_v1_20036	-	FUSI_v1_220005 FUSI_v1_560010 FUSI_v1_690004
Threonine degradation (II) to glycine and acetyl-CoA				
L-threoninie 3-dehydrogenase (EC 1.1.1.103)	-	PSYM_v1_2590001	DESP_v1_180022	FUSI_v1_560008
glycine C-acetyltransferase (EC 2.3.1.29)	-	PSYM_v1_2590002	DESP_v1_180021	FUSI_v1_520059
Threonine degradation (IV) to glycine and acetyl-CoA				
low specificity L-threonine aldolase (EC 4.1.2.5)	K337_v1_11380	-	DESP_v1_2820002 DESP_v1_2820003	FUSI_v1_190001 FUSI_v1_800055 FUSI_v1_1050006
iron-type aldehyde-alcohol dehydrogenase (NAD^+) (EC 1.2.1.10/EC 1.1.1.1)	K337_v1_20115	-	DESP_v1_470013 DESP_v1_680010 DESP_v1_910009 DESP_v1_1710010 DESP_v1_20005	FUSI_v1_540069 FUSI_v1_670074
Arginine degradation (III) to putrescine				
arginine decarboxylase (EC 4.1.1.19)	K337_v1_12041	-	-	FUSI_v1_1250057
agmatinase (EC 3.5.3.11)	K337_v1_12038	-	-	-

Arginine degradation (V) to L-ornithine and CO_2				
arginine deaminase (EC 2.5.3.6)	-	-	-	FUSI_v1_270051
ornithine carbomyltransferase (EC 2.1.3.3)	K337_v1_11897	PSYM_v1_210021	DESP_v1_880023	FUSI_v1_270052 FUSI_v1_1110063
carbamate kinase (EC 2.7.2.2)	-	PSYM_v1_500009	-	FUSI_v1_420066 FUSI_v1_840014
Lysine degradation to butyrate and acetate				
lysine 2,3-aminomutase (EC 5.4.3.2)	K337_v1_10812	PSYM_v1_780016	DESP_v1_1120011 DESP_v1_10005 DESP_v1_280028	-
lysine 5,6-aminomutase (EC 5.4.3.3)	K337_v1_10808 K337_v1_10809	-	-	-
L-erythro-3,5-diaminohexano ate dehydrogenase (EC 1.4.1.11)	K337_v1_10813	-	-	-
3-keto-5-aminohexanoate cleavage enzyme	K337_v1_10814	-	-	-
3-aminobutyryl-CoA ammonia-lyase (EC 4.3.1.14)	K337_v1_10815	-	-	-
acyl-CoA dehydrogenase (EC 1.3.8.1)	K337_v1_30044	-	DESP_v1_1630011 DESP_v1_1600001 DESP_v1_30013	-
butyrate—acetoacetate CoA-transferase (EC 2.8.3.9)	-	-	-	-
acetyl-CoA acetyltransferase (EC 2.3.1.9)	K337_v1_30048	-	DESP_v1_490008 DESP_v1_1000008 DESP_v1_2710001	-
Glycine cleavage complex				
glycine dehydrogenase (decarboxylating) (EC 1.4.4.2)	K337_v1_20307 K337_v1_20308 K337_v1_20310	PSYM_v1_420003	DESP_v1_20040 DESP_v1_20041 DESP_v1_20042	FUSI_v1_650007 FUSI_v1_650008 FUSI_v1_650009 FUSI_v1_650010
aminomethyltransferase (EC 2.1.2.10)	K337_v1_20310	PSYM_v1_420003	DESP_v1_20042 DESP_v1_20043	FUSI_v1_650007 FUSI_v1_650008 FUSI_v1_650009 FUSI_v1_650010
dihydrolipoyl dehydrogenase (EC 1.8.1.4)	K337_v1_11268 K337_v1_20310	PSYM_v1_420003	DESP_v1_20042 DESP_v1_20045 DESP_v1_860012	FUSI_v1_650006 FUSI_v1_650007 FUSI_v1_650008
branched-chain α-keto acid dehydrogenase complex				
2-keto-isovalerate dehydrogenase (EC 1.2.4.4)	-	-	-	FUSI_v1_810055
dihydrolipoyllysine-residue (EC 2.3.1.168)	-	-	-	FUSI_v1_810055
dihydrolipoyl dehydrogenase (EC 1.8.1.4)	-	-	-	FUSI_v1_650006 FUSI_v1_1010005 FUSI_v1_1170018 FUSI_v1_810055
Aminotransferases				
aminotransferase class I and II	K337_v1_10796	-	-	FUSI_v1_410019 FUSI_v1_890014
aminotransferase class III	-	-	-	FUSI_v1_640091
aromatic acid aminotransferase (EC 2.6.1.57)	-	-	-	FUSI_v1_860012 FUSI_v1_10026
aspartate aminotransferase (EC 2.6.1.1)	K337_v1_12185	PSYM_v1_1700002 PSYM_v1_1060009	DESP_v1_120019	FUSI_v1_1110051 FUSI_v1_20102

				FUSI_v1_220004 FUSI_v1_20114 FUSI_v1_110019 FUSI_v1_190006
branched-chain amino transferase (EC:2.6.1.42)	K337_v1_11732 K337_v1_20081	-	DESP_v1_1080001	FUSI_v1_840093 FUSI_v1_620044
histidinol-phosphate aminotransferase (EC 2.6.1.9)	-	PSYM_v1_3080002 PSYM_v1_1160007	DESP_v1_1210008	FUSI_v1_360042
alanine transaminase (EC 2.6.1.2)	-	PSYM_v1_760004	-	-
alanine---glyoxylate transaminase (EC 2.6.1.44)	K337_v1_20164	-	-	-
acetylornithine aminotransferase (EC 2.6.1.11)	-	PSYM_v1_80040	DESP_v1_880024	FUSI_v1_10046 FUSI_v1_30035
Beta-oxidation of long-chain fatty acids				
acyl-CoA synthetase (EC 6.2.1.3 / EC 6.2.1.-)	K337_v1_10867	PSYM_v1_3630002 PSYM_v1_2450001 PSYM_v1_410016 PSYM_v1_2980005	DESP_v1_270013 DESP_v1_270014 DESP_v1_450036 DESP_v1_2370003 DESP_v1_670010	-
acyl-CoA dehydrogenase (EC 1.3.8.-)	-	PSYM_v1_1300009	DESP_v1_30013 DESP_v1_1600001 DESP_v1_1630011	FUSI_v1_410001
fused enoyl-CoA hydratase/isomerase 3-hydroxyacyl-CoA dehydrogenase (EC 4.2.1.17, EC 5.3.3.8, EC 5.1.2.3, EC 1.1.1.35)	-	PSYM_v1_3780002	-	-
enoyl-CoA hydratase/isomerase (EC 4.2.1.17)	-	PSYM_v1_2230002	DESP_v1_280008 DESP_v1_290019 DESP_v1_620004	-
3-hydroxyacyl-CoA dehydrogenase (EC 1.1.1.35)	-	-	DESP_v1_2710002 DESP_v1_500017	-
acyl-CoA thiolase (acetyl-CoA transferase) (EC 2.3.1.16)	-	PSYM_v1_3630003 PSYM_v1_3780001	DESP_v1_500016	-
Glycerol degradation				
glycerol-3-phosphate transporter	K337_v1_10282	-	-	FUSI_v1_10096
glycerol facilitator	K337_v1_10202	-	-	FUSI_v1_810044
glycerol kinase (sn-glycerol-3-phosphate generating) (EC 2.7.1.30)	K337_v1_10203	-	DESP_v1_1420006	FUSI_v1_810043
glycerol-3-phosphate dehydrogenase (EC 1.1.5.3)	K337_v1_11183 K337_v1_12015	-	DESP_v1_1240008	FUSI_v1_520017 FUSI_v1_960006
Glycolysis	present	present	present	present
Lactate degradation to pyruvate (reversible except for LUD-type L-lactate dehydrogenase)				
L-lactate permease, LutP and LctP	K337_v1_21046	-	DESP_v1_620009 DESP_v1_2490001	FUSI_v1_1110024
L-lactate, D-lactate, and/or glycolate dehydrogenase, GlcD	K337_v1_21047	-	DESP_v1_620008 DESP_v1_70033 DESP_v1_450018	FUSI_v1_430010 FUSI_v1_1110021
L-lactate, D-lactate, and/or glycolate dehydrogenase, GlcF	-	-	DESP_v1_620007 DESP_v1_70046	-
D-lactate dehydrogenase (cytochrome) (EC 1.1.2.4)	-	-		FUSI_v1_1210024

L-lactate dehydrogenase (EC 1.1.1.27)	-	-	-	FUSI_v1_460018
D-lactate dehydrogenase (EC 1.1.1.28)	K337_v1_11115	PSYM_v1_50008	-	FUSI_v1_10080
L-lactate dehydrogenase (EC 1.1.2.3)	-	-	-	-
LUD-type L-lactate dehydrogenase, LutABC (EC 1.1.-.-)	-	-	DESP_v1_450001 DESP_v1_450002 DESP_v1_450003	-
Butyrate degradation to butyryl-CoA				
butyrate kinase (EC 2.7.2.7)	K337_v1_11804	-	DESP_v1_480015	FUSI_v1_1210033 FUSI_v1_520026 FUSI_v1_800012
phosphate butyryltransferase (EC 2.3.1.19)	K337_v1_11805	-	DESP_v1_480016	FUSI_v1_1210032 FUSI_v1_520025 FUSI_v1_800016
Butyrate degradation to butyryl-CoA				
butanoate CoA-transferase (EC 2.8.3.-)	-	-	DESP_v1_1500004	-
Formate degradation to CO_2 and H^+				
formate dehydrogenase accessory protein, FdhE	-	-	DESP_v1_2210006	-
formate dehydrogenase alpha subunit, FdhA	-	-	DESP_v1_2210007 DESP_v1_2210008	-
formate dehydrogenase beta subunit, FdhB	-	-	DESP_v1_2210009	-
iso-butyrate isomerization to butryl-CoA				
cob(I)alamin adenosyltransferase	K337_v1_20070	PSYM_v1_200016	DESP_v1_1080011 DESP_v1_300016	FUSI_v1_1080006
isobutyryl-CoA mutase, N-terminal domain subunit	-	-	-	FUSI_v1_940031
isobutyryl-CoA mutase, C-terminal domain subunit (cobalamin B12-binding domain protein)	-	-	-	FUSI_v1_940032
LAO/AO transport system ATPase, MeaB-like protein	-	-	-	FUSI_v1_940033
Propionate degradation to succinyl-CoA (reversible)			-	
propionyl-CoA carboxylase, gamma subunit (EC 6.4.1.3)	-	-	DESP_v1_1040006	FUSI_v1_940035
propionyl-CoA carboxylase, beta subunit (EC 6.4.1.3)	-	-	DESP_v1_1040008	FUSI_v1_940037
acetyl-CoA carboxylase, gamma subunit (EC 6.4.1.2) / propionyl-CoA carboxylase, alpha subunit (EC 6.4.1.3)	K337_v1_10646	-	-	FUSI_v1_520003 FUSI_v1_520004
acetyl-CoA carboxylase, beta subunit (EC 6.4.1.2) / propionyl-CoA carboxylase, gamma subunit (EC 6.4.1.3)	K337_v1_10913	-	-	FUSI_v1_520002
methylmalonyl-CoA epimerase (EC 5.1.99.1)	-	-	-	FUSI_v1_940034
methylmalonyl-CoA mutase accessory protein	-	-	-	FUSI_v1_940033
methylmalonyl-CoA mutase (EC 5.4.99.2)	-	-	-	FUSI_v1_940031 FUSI_v1_940032
TCA cycle				

citrate synthase (EC 2.3.3.1)	-	PSYM_v1_30012	DESP_v1_90043 DESP_v1_160029	FUSI_v1_800040
aconitate hydratase (EC 4.2.1.3)	-	PSYM_v1_2890003 PSYM_v1_1280001	DESP_v1_90042 DESP_v1_1190001 DESP_v1_3390001	FUSI_v1_800038
isocitrate dehydrogenase (NAD+) (EC 1.1.1.41) / isocitrate dehydrogenase (NADP+) (EC 1.1.1.42)	-	PSYM_v1_2270005	DESP_v1_2350002	FUSI_v1_800039
2-oxoglutarate decarboxylase, thiamin-requiring (EC 1.2.4.2) [2-oxoglutarate dehydrogenase complex]	-	PSYM_v1_30006	-	-
dihydrolipoamide succinyltransferase (EC 2.3.1.61) [2-oxoglutarate dehydrogenase complex]	-	PSYM_v1_30005	-	FUSI_v1_1170017
lipoamide dehydrogenase (EC 1.8.1.4) [2-oxoglutarate dehydrogenase complex]	K337_v1_11268	PSYM_v1_420003	DESP_v1_20045 DESP_v1_860012	FUSI_v1_1170018 FUSI_v1_1010005 FUSI_v1_650006
succinyl-CoA synthetase, alpha chain (EC 6.2.1.5)	-	PSYM_v1_30002 PSYM_v1_30003	DESP_v1_2040003	
succinyl-CoA synthetase, beta chain (EC 6.2.1.5)	-	PSYM_v1_30004	DESP_v1_2040005	
succinate dehydrogenase (EC 1.3.5.1)	-	PSYM_v1_30007 PSYM_v1_30008 PSYM_v1_30009 PSYM_v1_30010	DESP_v1_2040002 DESP_v1_1650002	FUSI_v1_1290010
fumarate hydratase class I (EC 4.2.1.2)	K337_v1_11158 K337_v1_11159 K337_v1_20911 K337_v1_20912	PSYM_v1_1700003	DESP_v1_1020008 DESP_v1_2260002	FUSI_v1_1250059 FUSI_v1_1250060
malate dehydrogenase (EC 1.1.1.37) / Malate dehydrogenase (oxaloacetate-decarboxylating) (NADP(+)) (EC 1.1.1.40)	-	PSYM_v1_570011 PSYM_v1_3810001	DESP_v1_230006	-
ferrodoxin oxidoreductases				
2-oxoglutarate ferredoxin oxidoreductase subunit alpha (EC 1.2.7.3) (KOR)	-	PSYM_v1_510008	DESP_v1_2130003 DEPS_v1_690022 DESP_v1_960009 DESP_v1_90046	FUSI_v1_520029 FUSI_v1_1210029 FUSI_v1_130004
2-oxoglutarate ferredoxin oxidoreductase subunit beta (EC 1.2.7.3) (KOR)	-	PSYM_v1_510009	DESP_v1_2130004 DESP_v1_690021 DESP_v1_960010	FUSI_v1_520030 FUSI_v1_1210028 FUSI_v1_130003
2-oxoglutarate ferredoxin oxidoreductase subunit gamma (EC 1.2.7.3) (KOR)	-	-	DESP_v1_2130005	FUSI_v1_520031 FUSI_v1_1210027 FUSI_v1_130002
2-oxoglutarate ferredoxin oxidoreductase subunit delta (EC 1.2.7.3) (KOR)	-	-	DESP_v1_2130002	FUSI_v1_520028 FUSI_v1_1210030
pyruvate/ketoisovalerate oxidoreductase, delta subunit, putative (EC 1.2.7.1/ EC 1.2.7.7) (POR/VOR)	K337_v1_10071	-	DESP_v1_1080004	FUSI_v1_10160 FUSI_v1_10121
pyruvate/ketoisovalerate oxidoreductase, alpha subunit (EC 1.2.7.1/ EC 1.2.7.7) (POR/VOR)	K337_v1_10072	PSYM_v1_2910001	DESP_v1_1080005	FUSI_v1_10161 FUSI_v1_10122
pyruvate/ketoisovalerate oxidoreductase, beta subunit (EC 1.2.7.1/ EC 1.2.7.7) (POR/VOR)	K337_v1_10073	-	DESP_v1_1080006	FUSI_v1_10162 FUSI_v1_10123
pyruvate/ketoisovalerate oxidoreductase, gamma	K337_v1_10074	PSYM_v1_2910002	DESP_v1_1080003	FUSI_v1_10159 FUSI_v1_10124

subunit(EC 1.2.7.1/ EC 1.2.7.7) (POR/VOR)				
tungsten-containing aldehyde:ferredoxin oxidoreductase (EC 1.2.7.5) (AOR)	K337_v1_10511	-	-	FUSI_v1_1110012
pyruvate-flavodoxin oxidoreductase (EC 1.2.7.-) (PFOR)	K337_v1_11862	PSYM_v1_2050003 PSYM_v1_2530001	-	FUSI_v1_120078
indolepyruvate:ferredoxin oxidoreductase (IOR) subunit α (EC 1.2.7.8)	-	-	DESP_v1_30060	FUSI_v1_800015
indolepyruvate:ferredoxin oxidoreductase (IOR) subunit β (EC 1.2.7.8)	-	-	DESP_v1_30062	FUSI_v1_800014
Oxobutanoate/pyruvate degradation to propionate/acetate				
2-ketobutyrate/pyruvate-formate lyase I (EC 2.3.1.54)	K337_v1_11221	PSYM_v1_2190001	DESP_v1_550004	FUSI_v1_480003
phosphate acetyltransferase (EC 2.3.1.8)	K337_v1_11864	PSYM_v1_120027	DESP_v1_960006 DESP_v1_1280029	FUSI_v1_640081
acetate kinase A and propionate kinase 2 (EC 2.7.2.1)	K337_v1_11863	PSYM_v1_120028	DESP_v1_1280030	FUSI_v1_320010
Pyruvate dehydrogenase complex, conversion of pyruvate to acetyl-CoA				
pyruvate dehydrogenase E1 component alpha subunit (EC 1.2.4.1)	K337_v1_11265	PSYM_v1_2320001 PSYM_v1_420001 PSYM_v1_1400001 PSYM_v1_3960001	-	FUSI_v1_810058
pyruvate dehydrogenase E1 component beta subunit (EC 1.2.4.1)	K337_v1_11266	PSYM_v1_2320002	-	FUSI_v1_810057
dihydrolipoyllysine-residue acetyltransferase (EC 2.3.1.12)	K337_v1_11267	PSYM_v1_2320003 PSYM_v1_420002	-	FUSI_v1_810056 FUSI_v1_1170017
dihydrolipoyl dehydrogenase (EC 1.8.1.4)	K337_v1_11268	PSYM_v1_420003	DESP_v1_20045 DESP_v1_860012	FUSI_v1_1170018 FUSI_v1_1010005 FUSI_v1_650006
Acetate production from acetyl-CoA or reverse				
acetyl-CoA synthetase bifunctional acetate—CoA / propionate—CoA ligase (AMP-forming) (EC 6.2.1.1/17)	-	PSYM_v1_1400002 PSYM_v1_450009	-	-
acetate—CoA ligase (ADP-forming) (EC 6.2.1.13)	-	-	-	-
pyruvate to oxalacetate				
pyruvate carboxylase (EC 6.4.1.1)	K337_v1_20163	-	-	FUSI_v1_1200032
Sulfur cycling genes				
adenylyl-sulfate reductase, AprB (EC 1.8.99.2)	-	-	DESP_v1_120032	-
adenylyl-sulfate reductase, AprA (EC 1.8.99.2)	-	-	DESP_v1_120031	-
quinone-interacting membrane-bound oxidoreductase complex, QmoA	-	-	DESP_v1_120030	-

quinone-interacting membrane-bound oxidoreductase complex, QmoB	-	-	DESP_v1_120029	-
quinone-interacting membrane-bound oxidoreductase complex, QmoC	-	-	DESP_v1_120028	-
sulfate adenylyltransferase, Sat (EC 2.7.7.4)	-	-	DESP_v1_120027	-
dissimilatory sulfite reductase, DsrA (EC 1.8.99.5)	-	-	DESP_v1_100003	-
dissimilatory sulfite reductase, DsrB (EC 1.8.99.5)	-	-	DESP_v1_100002	-
probable regulatory protein, DsrD	-	-	DESP_v1_100001	-
dissimilatory sulfite reductase, DsrC (EC 1.8.99.5)	-	-	DESP_v1_160016	-
putative component of dissimilatory sulfate reduction system, DsrT	-	-	DESP_v1_50034	-
sulfite reduction-associated membrane complex ([DsrC]-trisulfide reductase), DsrM (1.8.5.M1)	-	-	DESP_v1_50033	-
sulfite reduction-associated membrane complex ([DsrC]-trisulfide reductase), DsrK (1.8.5.M1)	-	-	DESP_v1_50032	-
sulfite reduction-associated membrane complex ([DsrC]-trisulfide reductase), DsrJ (1.8.5.M1)	-	-	DESP_v1_50031	-
sulfite reduction-associated membrane complex ([DsrC]-trisulfide reductase), DsrO (1.8.5.M1)	-	-	DESP_v1_50030	-
sulfite reduction-associated membrane complex ([DsrC]-trisulfide reductase), DsrP (1.8.5.M1)	-	-	DESP_v1_50029	-
probable siroheme amidase, DsrN (EC 6.3.5.M1)	-	-	DESP_v1_1190011	-
soluble inorganic pyrophosphatase (sPPase) (EC 3.6.1.1)	K337_v1_11979	PSYM_v1_310018	DESP_v1_30033	-
adenylate kinase (EC 2.7.4.3)	K337_v1_30030	PSYM_v1_440003	DESP_v1_1090008	FUSI_v1_940095
Anaerobic sulfite reductase, subunit A (EC 1.8.1.-)	K337_v1_20489 K337_v1_20742	-	-	-
Anaerobic sulfite reductase, subunit B (EC 1.8.1.-)	K337_v1_20488 K337_v1_20741	-	-	-
Anaerobic sulfite reductase, subunit C (EC 1.8.1.-)	K337_v1_20487 K337_v1_20740	-	-	-
Nitrate reduction to ammonium (DNRA)				
perimplasmic nitrate reductase, large subunit, NapA	-	PSYM_v1_295000 PSYM_v1_2740007	-	-
periplasmic nitrate reductase, electron transfer subunit, NapB	-	PSYM_v1_2740004	-	-
periplasmic nitrate reductase, cytochrome c-type, NapC	-	PSYM_v1_2740003	-	-
periplasmic nitrate reductase,	-	PSYM_v1_2950002	-	-

chaperone, NapD				
periplasmic nitrate reductase, ferredoxin-type protein, NapF	-	PSYM_v1_2950003	-	-
periplasmic nitrate reductase, ferredoxin-type protein, NapG	-	PSYM_v1_2740006	-	-
periplasmic nitrate reductase, ferredoxin-type protein, NapH	-	PSYM_v1_2740005	-	-
formate-dependent nitrite reductase, cytochrome c552, NrfA	-	-	-	-
formate-dependent nitrite reductase, cytochrome c-type protein, NrfB	-	-	-	-
formate-dependent nitrite reductase, 4Fe4S subunit, NrfC	-	PSYM_v1_150004	-	-
formate-dependent nitrite reductase, membrane subunit, NrfD	-	PSYM_v1_150005	-	-
Fumarate reduction				
fumarate reductase, flavoprotein subunit	-	PSYM_v1_1240008	-	-
fumarate reductase iron-sulfur subunit	-	PSYM_v1_1240007	-	-
fumarate reductase, subunit C	-	PSYM_v1_1240006	-	-
fumarate reductase, D subunit	-	PSYM_v1_1240005	-	-
Oxygen respiration				
cbb3-type cytochrome c oxidase (EC 1.9.3.1)	-	PSYM_v1_70013 PSYM_v1_70014 PSYM_v1_70015 PSYM_v1_70016	-	-
cytochrome bd–type oxidase	-	PSYM_v1_180033 PSYM_v1_180034	DESP_v1_4300221 DESP_v1_430022	-
cytochrome-c oxidase	-	-	DESP_v1_460009 DESP_v1_460010 DESP_v1_460011 DESP_v1_460012	-
Type I SS				
TolC	-	PSYM_v1_3060001	DESP_v1_360002	-
HlyD	-	PSYM_v1_3060002	-	-
HylB	-	PSYM_v1_3060003	-	-
Type II SS				
GspC	-	PSYM_v1_50014	DESP_v1_640009	-
GspD	K337_v1_10274	PSYM_v1_50015	DESP_v1_640008	-
GspE	-	PSYM_v1_50016	DESP_v1_640007	-
GspF	-	PSYM_v1_50017	DESP_v1_2030004	-
GspG	-	PSYM_v1_50018	DESP_v1_640017	-
GspH	-	PSYM_v1_50019	-	-
GspI	-	PSYM_v1_50020	DESP_v1_640015	-
GspJ	-	PSYM_v1_50022	DESP_v1_640014	-

GspK	-	PSYM_v1_50023	DESP_v1_640013	-
GspL	-	PSYM_v1_50024	DESP_v1_640012	-
GspM	-	PSYM_v1_50025	DESP_v1_640011	-
GspN	-	PSYM_v1_50026	DESP_v1_640010	-
Twin arginine translocation				
TatA	-	PSYM_v1_2920002	DESP_v1_130035	-
TatB	-	PSYM_v1_2920003	DESP_v1_400009	-
TatC	-	PSYM_v1_2920004	DESP_v1_400010	-
TatD	-	PSYM_v1_2920005	-	-
Sec pathway				
SecA	K337_v1_11974	PSYM_v1_530006	DESP_v1_610007	FUSI_v1_940046
SecB	-	PSYM_v1_30031	-	-
SecF	K337_v1_10344	PSYM_v1_1420009 PSYM_v1_2420001	DESP_v1_340009	FUSI_v1_180008
SecD	K337_v1_10343	PSYM_v1_1420010 PSYM_v1_2420002	DESP_v1_340010	FUSI_v1_180009
YajC	K337_v1_12023	PSYM_v1_2420003	DESP_v1_340011	FUSI_v1_180012
SecE	K337_v1_10236	PSYM_v1_230024	DESP_v1_930004	FUSI_v1_940061
SecG	K337_v1_10735	PSYM_v1_1410004	DESP_v1_1070001	FUSI_v1_690027
SecY	K337_v1_10010	PSYM_v1_110032	DESP_v1_350007	FUSI_v1_940094
YidC	K337_v1_10153	PSYM_v1_80033	DESP_v1_100022	FUSI_v1_230014
Ffh	K337_v1_10560	PSYM_v1_270001	DESP_v1_30048	FUSI_v1_320018
FstY	K337_v1_11865	PSYM_v1_940007	DESP_v1_20037	FUSI_v1_320016
Type IV SS				
VirB2	K337_v1_20573	-	-	-
VirB8	K337_v1_20574	-	-	-
VirB9	K337_v1_20575	-	-	-
VirB10	K337_v1_20576	-	-	-
VirD4	K337_v1_20580	-	-	-
VirB11	K337_v1_20582	-	-	-
VirB3	K337_v1_20583	-	-	-
VirB4	K337_v1_20584	-	-	-
VirB5	K337_v1_20585	-	-	-
VirB6	K337_v1_20586	-	-	-
VirB1	-	-	-	-
VirB7	-	-	-	-
Type V SS				

Type Va	K337_v1_10452 K337_v1_11022 K337_v1_20589	PSYM_v1_90026 PSYM_v1_2620003	-	-
Type Vb	K337_v1_11330	-	-	-
Type Vc	K337_v1_11400 K337_v1_117437K 337_v1_20001	-	-	-

References

Berger, S. A., Krompass, D., and Stamatakis, A. (2011) Performance, accuracy, and Web server for evolutionary placement of short sequence reads under maximum likelihood. *Syst. Biol.* **60**: 291–302.

Katoh, K., Misawa, K., Kuma, K.-I., and Miyata, T. (2002) MAFFT: a novel method for rapid multiple sequence alignment based on fast Fourier transform. *Nucleic Acids Res.* **30**: 3059–3066.

Letunic, I., and Bork, P. (2007) Interactive Tree Of Life (iTOL): an online tool for phylogenetic tree display and annotation. *Bioinformatics* **23**: 127–128.

Price, M. N., Dehal, P. S., and Arkin, A. P. (2010) FastTree 2 – Approximately Maximum-Likelihood Trees for Large Alignments. *PLoS One* **5**: e9490.

Pruesse, E., Peplies, J., and Glöckner, F. O. (2012) SINA: accurate high-throughput multiple sequence alignment of ribosomal RNA genes. *Bioinformatics* **28**: 1823–1829.

Quast, C., Pruesse, E., Yilmaz, P., Gerken, J., Schweer, T., Yarza, P., *et al.* (2013) The SILVA ribosomal RNA gene database project: improved data processing and web-based tools. *Nucleic Acids Res.* **41**: D590–6.

Stamatakis, A. (2014) RAxML version 8: a tool for phylogenetic analysis and post-analysis of large phylogenies. *Bioinformatics* **30**: 1312–1313.

Chapter 5

DNA-foraging bacteria in the seafloor

Kenneth Wasmund, **Claus Pelikan**, Margarete Watzka, Andreas Richter, Amy Noel, Casey R.J. Hubert, Thomas Rattei, Thilo Hofmann, Craig W. Herbold, and Alexander Loy

Reference:

bioRxiv 528695; doi: 10.1101/528695

Supplementary information available at:

https://www.biorxiv.org/content/10.1101/528695v1.supplementary-material

Author contributions:

K.W. and A.L. conceived and designed the study. A.N. and C.R.J.H were responsible for sample collection and processing. K.W. and C.P. performed the incubation experiments and molecular analyses. M.W. and A.R. performed gas chromatography analyses. T.H. performed sediment iron and manganese analyses. K.W., C.P. and C.W.H performed bioinformatic processing and analyses. K.W. analysed and interpreted the data. K.W. and A.L. wrote the manuscript with contributions from all authors.

DNA-foraging bacteria in the seafloor

Kenneth Wasmund[1,2]*, Claus Pelikan[1,2], Margarete Watzka[3], Andreas Richter[2,3], Amy Noel[4], Casey R.J. Hubert[4], Thomas Rattei[5], Thilo Hofmann[6], Craig W. Herbold[1], Alexander Loy[1,2]

[1]Division of Microbial Ecology, Department of Microbiology and Ecosystem Science, Research Network Chemistry meets Microbiology, University of Vienna, Vienna, Austria.
[2]Austrian Polar Research Institute, Vienna, Austria.
[3]Division of Terrestrial Ecosystem Research, Department of Microbiology and Ecosystem Science, Research Network Chemistry meets Microbiology, University of Vienna, Vienna, Austria.
[4]Geomicrobiology Group, Department of Biological Sciences, University of Calgary, Calgary, Canada.
[5]Division of Computational Systems Biology, Department of Microbiology and Ecosystem Science, Research Network Chemistry meets Microbiology, University of Vienna, Vienna, Austria.
[6]Department of Environmental Geosciences, University of Vienna, Vienna, Austria.

*Correspondence to wasmund@microbial-ecology.net

Abstract

Extracellular DNA is a major macromolecule in global element cycles, and is a particularly crucial phosphorus as well as nitrogen and carbon source for microorganisms in the seafloor. Nevertheless, the identities, ecophysiology and genetic features of key DNA-foraging microorganisms in marine sediments are completely unknown. Here we combined microcosm experiments, stable isotope probing and genome-centric metagenomics to study microbial catabolism of DNA and its sub-components in anoxic marine sediments. ^{13}C-DNA added to sediment microcosms was largely degraded within ten days and mineralised to $^{13}CO_2$. Stable isotope probing showed that diverse *Candidatus* Izemoplasma*, Lutibacter*, *Shewanella*, *Fusibacteraceae* and *Nitrincolaceae* incorporated DNA-derived ^{13}C-carbon. Genomes representative of the ^{13}C-labelled taxa were recovered and all encoded enzymatic repertoires for catabolism of DNA. Comparative genomics indicated that DNA can be digested by diverse members of the order *Candidatus* Izemoplasmatales (former *Tenericutes*), which appear to be specialised DNA-degraders that encode multiple extracellular nucleases. *Fusibacteraceae* lacked genes for extracellular nucleases but utilised various individual purine- and pyrimidine-based molecules, suggesting they 'cheated' on liberated sub-components of DNA. Close relatives of the DNA-degrading taxa are globally distributed in marine sediments, suggesting that these poorly understood taxa contribute widely to the key ecosystem function of degrading and recycling DNA in the seabed.

Introduction

Subsurface environments including marine sediments harbour the bulk of microbial biomass on Earth[1]. Nevertheless, the functional capabilities and ecological roles of most of the diversity of subsurface microorganisms remain completely unknown[2]. The vast majority of microorganisms inhabiting marine sediments are ultimately sustained by heterotrophic metabolisms. Heterotrophs are predominantly fuelled by organic matter derived from primary production in the overlying water column and/or from land-derived inputs[3, 4]. Heterotrophic metabolisms are sustained by direct involvement in the initial break-down and catabolism of organic molecules, or indirectly, via the use of by-products of such catabolism, e.g., low molecular weight degradation products or fermentation products[5]. Additionally, cell debris released after the death and lysis of organisms, as well as excreted exometabolites, supply organic molecules for the growth of microorganisms[6, 7]. These sources collectively provide an immense diversity of organic molecules[8, 9]. Many of these organics can be used as nutrient and energy sources to sustain expansive numbers of microorganisms of very diverse composition in marine sediments[10]. The identities of microorganisms that use different kinds of organic molecules in marine sediments, are however, largely unknown. This is despite the fact that such knowledge lies central to our fundamental understandings of how microorganisms control biogeochemical cycles. It is also important for our understandings of ecological niche differentiation among microorganisms that utilise different substrates, and how this ultimately influences the diversity and community structures of microorganisms in the seafloor.

In general, the most abundant of the various classes of organic molecules available for catabolism by microorganisms in marine sediments, and in most other environments, include proteins, lipids, carbohydrates and nucleic acids – the molecules that make-up most of the biomass of any cell or virus[11-13]. Of these, DNA is known to contribute substantially to oceanic and sedimentary biogeochemical cycles, acting as a significant source of carbon, nitrogen and phosphorus, and providing an energy source[14-16]. Estimates suggest 'bioavailable' DNA, i.e., DNA available for digestion by extracellular nucleases, supplies microbial communities of coastal and deep-sea sediments with 2-4% of their carbon requirements, 7-4% of their nitrogen requirements, and a remarkable 20-47% of their phosphorus requirements[14, 16]. Analyses of microbial 16S rRNA genes derived from extracellular- and intracellular-DNA pools in marine sediments showed that extracellular

DNA is rapidly turned-over in both shallow and deeper sediments (down to 10-12 meters)[17, 18].

Some microorganisms are capable of catabolizing DNA via concerted steps involving extracellular digestion[19], import systems[20], and catabolic breakdown of imported sub-components in the cytoplasm[21]. Degradation products of nucleic acids such as urea and ammonium, as well as CO_2 and acetate[22], are also important nutrients for other members of microbial communities. Nucleic acids might be especially important phosphorus sources in sediments rich in metal-oxides such as Fe(III)- or Mn(IV)-oxides, whereby strong sorption of phosphorus to the metal oxides can occur, thereby diminishing bioavailable pools of this crucial nutrient[23]. Despite the fact that nutrient-rich and ubiquitous DNA biomolecules are available in marine sediments, our knowledge of microorganisms that degrade and mineralise DNA remains poor[24].

In this study, we identified key-players that degrade and catabolise extracellular DNA in marine sediments. We hypothesized this abundant organic macromolecule might nourish and explain the presence of some of the commonly found taxonomic groups of microorganisms in marine sediments. To identify and study the ecophysiology of DNA-degrading microorganisms, we set-up microcosms with sediment from the Baffin Bay in between Canada and Greenland. Microcosms were either supplemented with ^{13}C-labelled DNA, or individual DNA sub-components, and incubated under cold, anoxic conditions. We then analysed biogeochemical parameters and the microbial communities over a time-series of weeks via DNA-based stable isotope probing (DNA-SIP) and 16S rRNA gene amplicon sequencing. We subsequently retrieved the genomes of DNA-degraders identified by SIP via metagenomics to examine them for encoded DNA-degrading enzymes and catabolic pathways for molecular sub-components of DNA. The combined results provided multiple lines of evidence for the ability to degrade DNA by diverse groups of poorly understood bacteria, thereby providing new insights into potential niche occupation and *in situ* functions of these bacteria in the seafloor.

Results

Microcosm experiments show mineralization of DNA under cold, anoxic conditions

Anoxic microcosms with slurries of marine sediments from the Baffin Bay, Greenland, were individually amended with ^{13}C-labelled or unlabelled genomic DNA from the archaeon *Halobacterium salinarum*, as well as the unlabelled nucleobases adenine, thymine, guanine and cytosine, and the nucleosides 2-deoxyadenosine and thymidine (Supp. Table 1). Complete mineralization of added DNA to CO_2 was confirmed by isotopic analysis of CO_2 in the headspace of the microcosms. This showed CO_2 became enriched in ^{13}C already at early time points (4 days), and that ^{13}C-CO_2 was produced over time (Supp. Fig. 1). Bacterial community analyses via amplicon sequencing of 16S rRNA genes from the microcosms revealed that the supplemented *Halobacterium* DNA was mostly depleted from approximately 1.3% to 0.1% from day 4 to day 10, respectively, and was only present in minor relative abundances (<0.1%) from day 13 and after (Supp. Fig. 2). Chemical analyses showed high concentrations of total manganese and iron that may support metal-reducing populations (Supporting information). Bacterial taxa related to known metal-reducing microorganisms[25] collectively dominated both starting sediments and sediments in microcosms during the incubations. Bacterial community compositions among microcosms treated with DNA and controls were similar over the time of the experiment (Supporting information, Supp. Fig. 3 and 4).

SIP identifies diverse taxa that incorporate ^{13}C-carbon from DNA

DNA-SIP identified bacterial taxa that incorporated ^{13}C-carbon from the added ^{13}C-DNA during replication and growth, and therefore must have either: i) catabolised the added DNA and/or sub-components of DNA, ii) salvaged nucleobases or nucleosides for incorporation during replication, or iii) utilised fermentation products released from catabolism of the added DNA. Numbers of bacterial 16S rRNA genes determined from qPCR analyses across all gradient density fractions revealed only slightly higher abundances of 16S rRNA genes in some 'heavy' density fractions ($\geq$1.725 g ml^{-1})[26] from incubations with ^{13}C-DNA compared to ^{12}C-DNA, from several time points, i.e., days 4, 10 and 13 (Supp. Fig. 5). Later time points showed no elevated 16S rRNA gene abundances in heavy fractions and therefore subsequent analyses focused on the first three time points, and thus, largely on the primary DNA degraders.

Amplicon sequencing of 16S rRNA genes across various $CsCl_2$ density gradients identified individual operational taxonomic units (OTUs) that displayed significantly increased relative abundances in multiple 'heavy' density fractions (>1.725 g ml^{-1}) from ^{13}C-DNA treatments versus similar densities from ^{12}C-DNA control treatments. We first identified individual OTUs that were significantly enriched at two or more time points. Further, we identified OTUs that were significantly enriched at only one time point but belonged to the same bacterial groups as those enriched at two time points. This identified 27 OTUs that belonged to five bacterial taxa (Fig. 1). The summed relative abundances of all OTUs from these groups were calculated across the different density gradients and showed significantly higher relative abundances of these taxa in 'heavy' fractions of the gradients (Supp. Fig. 6). OTUs related to the *Nitrincolaceae* did not collectively show higher relative abundances in heavy fractions from ^{13}C-DNA treatments, except for OTU 4994 (Supp. Fig. 6). Phylogenetic analyses of 16S rRNA genes from the labelled OTUs showed that they were affiliated with: i) the genus *Shewanella* (class *Gammaproteobacteria*); ii) the family *Fusibacteraceae* (phylum *Firmicutes*), iii) the genus *Candidatus* Izemoplasma (GTDB phylum *Firmicutes*, formerly phylum *Tenericutes*); iv) the genus *Lutibacter* (GTDB phylum *Bacteroidota*, formerly phylum *Bacteroidetes*); and v) the family *Nitrincolaceae* (GTDB, formerly *Oceanospirillaceae*) (class *Gammaproteobacteria*) (Fig. 1). The naming of the *Ca.* Izemoplasma (formely *Ca*. Izimaplasma) is described in further detail below. Examination of 16S rRNA gene sequences in publically available sequence databases showed that closely related sequences from these five groups are globally distributed in coastal and deep-sea sediments (Supporting information, Supp. Fig. 7).

Distinct responses of diverse bacteria to additions of DNA, nucleobases or nucleosides

Complementary to the SIP analyses, we also tracked the relative abundances of individual OTUs in response to additions of DNA, as well as additions of individual sub-components of DNA (Fig. 1 and Supp. Fig. 8), i.e., the nucleobases adenine, thymine, guanine and cytosine, and the nucleosides 2-deoxyadenosine and thymidine (Supp. Table 1). This was performed in order to obtain indications for growth in response to the addition of these substrates. Among the OTUs that were identified as incorporating ^{13}C-carbon from ^{13}C-DNA by SIP analyses, two *Ca.* Izemoplasmataceae OTUs (23 and 224) showed significant increases in relative abundances in microcosms with DNA additions versus no-substrate controls, over multiple time points (Supp. Fig. 8). For nucleobases, only 5 OTUs responded to the pyrimidines thymine or cytosine, while 14 OTUs responded to the purines

adenine or guanine (Fig. 1). Compared to thymine, to which only 2 OTUs responded, 11 different OTUs responded to thymidine. Interestingly, although no *Fusibacteraceae* OTUs became enriched in microcosms in response to additions of DNA only, numerous OTUs (n=9) from this group were enriched in response to purine-based nucleobases or nucleosides, especially those containing adenine moieties. Six of these *Fusibacteraceae* OTUs were determined to be ^{13}C-labelled in the SIP experiment. *Fusibacteraceae* OTUs were the only taxa enriched by 2-deoxyadenosine, whereby 8 different OTUs responded. For instance, *Fusibacteraceae* OTU 8 dominated communities amended with 2-deoxyadenosine at day 10, reaching approximately 37% in relative abundance, versus 1% in the no-substrate controls (Supp. Fig. 8). Four of the *Fusibacteraceae* OTUs that responded to 2-deoxyadenosine also responded to adenine. These four OTUs also showed higher responses to the sugar-containing nucleoside 2-deoxyadenosine than the corresponding nucleobase adenine. Apart from taxa that were also labelled in the SIP analyses, several OTUs of the family *Endozoicomonadaceae* (class *Gammaproteobacteria*) were noticeably enriched in a number of treatments in this study, i.e., by DNA, adenine, guanine and thymidine (Fig. 1 and Supp. Fig. 8).

Recovery of genomes of DNA-degrading taxa

Near complete (>90%) metagenome-assembled genomes (MAG) that were representative of the taxa labelled in the SIP experiments were recovered (Supp. Table 2). These MAGs together with other publically available genomes and MAGs from related bacteria[23, 27-31], were analysed by phylogenomics (Fig. 2) and for genes encoding enzymes required to catabolise DNA (Fig. 3 and Supp. Table 3). The *Ca.* Izemoplasma MAG contained a 16S rRNA gene sequence that was 100% identical to OTU 23, which was labelled in the SIP experiment. All other MAGs recovered here did not contain 16S rRNA gene sequences. The *Nitrincolaceae* MAG BB-4 was predicted to be 79% complete. This MAG may not be representative of the *Nitrincolaceae* OTU 4994 that was determined to be labelled in the SIP analyses, since that OTU was present in very low abundance (<0.03% in any microcosm) and was unlikely to have been assembled and binned by our sequencing effort. Phylogenomic analyses (Fig. 2) and average nucleotide identity (ANI) analyses (Supp. Table 2), revealed that all MAGs constituted novel species or genera within their respective phylogenetic groups. For the *Ca.* Izemoplasma MAG, we propose the species name *Ca.* Izemoplasma acidinucleici (see below for detailed descriptions and Supporting information).

Extracellular and cell wall associated nucleases encoded in DNA-degraders

A key determinant for the ability to utilise DNA as a nutrient and/or energy source is the ability for extracellular digestion of DNA polymers. Importantly, extracellular nucleases can also be differentiated from nucleases used for recycling nucleic acids in the cytoplasm[19]. Accordingly, we identified genes for extracellular nucleases in MAGs and/or related reference genomes of *Shewanella*, *Lutibacter*, *Nitrincolaceae* and *Ca.* Izemoplasma populations (Fig. 3 and Fig. 4). We did not, however, find any genes related to extracellular nucleases in the *Fusibacteraceae* MAG BB-3 or reference genomes. Strikingly, up to five extracellular nucleases were encoded in some of the marine *Ca.* Izemoplasmataceae (Fig. 3). Further, related MAGs from an undescribed *Ca.* Izemoplasmatales family UBA5603 (Fig. 2) and a related yet undescribed *Bacilli* family CAG-313 (Fig. 2), also harboured numerous copies of extracellular nuclease genes (Fig. 3). Encoded extracellular nucleases identified in our *Shewanella* MAG BB-2 are homologs to extracellular nucleases previously shown to be highly expressed when *Shewanella oneidensis* MR-1 was grown on DNA[23, 32].

To facilitate the import of DNA sub-components into cells, further deconstruction of nucleotides and nucleosides is necessary[5]. Interestingly, MAGs from the *Ca.* Izemoplasmataceae and *Ca*. Izemoplasmatales family UBA5603 harboured conspicuous genomic loci associated with multiple extracellular nuclease genes that encoded enzymes that may facilitate further digestion and import of nucleic acid components, i.e., additional 3'-5' nucleases, phosphohydrolases, ABC-transporters and phosphate transporters (Fig. 5). Sequence homology searches of the 'substrate-binding subunit' of the ABC-transporters against the IMG database[33] identified that the genomes of organisms with best hits also encoded nucleases or nucleosidases within the same genomic neighbourhood. This indicated that these are probable nucleoside or nucleobase transporters. Additionally, this loci encoded a large protein (1049 amino acids) (Fig. 5) that was noteworthy because it contained nucleic acid-binding, nuclease and 'lamin-tail' domains (Supp. Fig. 11 and see Supporting Results and Discussion).

The *Shewanella* MAG BB-2 recovered here encoded several nucleotidases previously shown to be critical for growth on extracellular DNA[23], i.e., excreted bifunctional 2',3' cyclic nucleotide 2' phosphodiesterase/3' nucleotidases and a putative UDP-sugar hydrolase protein with 5' nucleotidase domains (included under nucleotidases in Fig. 3). *Lutibacter* and *Shewanella* also harboured multiple copies of genes for 5'-nucleotidases that were predicted to the reside in their periplasms (Fig. 3 and Fig. 4). Similarly, *Fusibacteraceae* and *Ca.* Izemoplasmataceae genomes encoded 5'-nucleotidases that were predicted to be located in

their cell walls or extracellularly, respectively (Fig. 3 and Fig. 4). Dephosphorylation of nucleotides by nucleotidases is critical because cell membranes are impermeable to nucleotides due to negatively-charged phosphate groups[34, 35].

Catabolic pathways for sub-components of DNA

Once imported into the cytoplasm, purine- and pyrimidine-deoxyribonucleosides may be further broken-down, whereby the respective bases may then enter catabolic pathways or salvage pathways used for incorporation into newly synthesised nucleic acids. We identified two copies of predicted 'purine deoxyribonucleoside phosphorylases' in most genomes of putative DNA-degraders (Fig. 3). The two different copies presumably offer specificity to the two purine nucleobases adenine and guanine. Specific adenosine deaminases were also annotated in all genomes of putative DNA-degraders, except for any of the *Ca.* Izemoplasmataceae. The *Fusibacter* sp. 3D3 reference genome harbored multiple copies of adenosine deaminase genes. Genes for 'pyrimidine deoxyribonucleoside phosphorylases' were detected in most *Ca.* Izemoplasmataceae genomes and in the *Fusibacter* sp. 3D3 reference genome. All putative DNA-degrading taxa encoded cytidine deamidases. Although uracil-specific phosphorylases that are required for further processing of 2-deoxycytidine via 2-deoxyuracil could not be identified, it is possible that the pyrimidine-nucleoside phosphorylases can catalyse both due to their known bifunctionality for these structurally similar substrates[36]. All DNA-degraders identified in this study therefore have enzymes required to cleave nucleobases into the sugar and base components.

The potential to catabolise the purine bases adenine and guanine were indicated by several lines of evidence. Genes for deaminases specific for both purine bases were present in *Fusibacteraceae* and various *Ca.* Izemoplasmataceae genomes (Fig. 3). In *Lutibacter* spp., adenine deaminase genes could only be identified in two organisms in the NCBI database, while in *Shewanella* spp., only *S. halifaxensis* appeared to harbor this gene. Guanine deaminase genes were also present in numerous *Lutibacter* and *Nitrincolaceae*, and were only identified in one *Shewanella*, i.e., *S. algae*.

In MAGs of the marine *Ca.* Izemoplasmataceae and the sister family UBA5603 (order *Ca.* Izemoplasmatales), genes for the two purine-specific deaminases were often located in close vicinity to each other, and were distinctively located in the same genomic region as genes for xanthine dehydrogenases and their accessory proteins (Supp. Fig. 9). Xanthine

dehydrogenases are key enzymes required for conversions of purine bases to xanthine, which is a common intermediate of purine breakdown[37]. These genomic loci were highly similar in *Ca*. Izemoplasmatales and the genomes of some *Clostridium* species (Supp. Fig. 9), which are among the few biochemically characterised anaerobic purine-degraders[21, 37]. Genes for enzymes required for the further catabolism of xanthine could not be unambiguously identified, since most are not described and are only predicted to occur based on biochemical inferences[21]. Nevertheless, several enzymes predicted to have amidohydrolase and hydantoinase activities were also encoded between the xanthine dehydrogenase genes (Supp. Fig. 9). These possibly play a role in the cleavage of the heterocyclic rings, and thus, further catabolism of xanthine. Genes for any enzymes involved in purine catabolism were notably absent from any MAGs from the *Bacilli* family CAG-313 (Fig. 3).

Apart from indications for the dephosphorylation of pyrimidines described above, we were unable to identify genes for anaerobic catabolic degradation of pyrimidine bases. This was not possible because the enzymes involved in this process in anaerobic microorganisms have not been identified.

Importantly, all MAGs representative of taxa that became labelled in our SIP experiment had the potential to catabolise the 2-deoxy-D-ribose-phosphate sugar moiety that can be liberated from nucleosides. In this regard, we identified genes for enzymes for catabolism of 2-deoxy-D-ribose-phosphate to D-glyceraldehyde 3-phosphate, an intermediate of glycolysis, and acetaldehyde, in all our MAGs (Fig. 3 and Fig. 4). Genes for aldehyde-alcohol dehydrogenases that could convert acetaldehyde to acetyl-CoA, were present in most labelled groups except in *Lutibacter* and *Nitrincolaceae*, and were only present in some marine *Ca*. Izemoplasmataceae MAGs, i.e., *Ca*. Izemoplasma sp. ZiA1 and HR1. Genes for a protein microcompartment that was postulated to be used for catabolising the liberated aldehydes in *Ca*. Izemoplasma sp. HR2[27], were not found in any other *Ca*. Izemoplasma MAGs analysed here.

De novo biosynthetic pathways for nucleotides encoded in DNA-degrading taxa

We identified large complements of genes encoding enzymes involved in the complete *de novo* syntheses of nucleotides in the genomes of most *Ca*. Izemoplasma (Supp. Table 4) (see Supporting information for descriptions). All other DNA-degraders identified in this study belong to bacterial groups that do not require supplementation of nucleic acid building blocks to growth media[29, 38-40].

Proposal of the novel species *Ca.* Izemoplasma acidinucleici and amendment of the genus name *Ca.* Izimaplasma to *Ca.* Izemoplasma

Based on a combination of unique phylogeny (based on 16S rRNA genes and concatenated single copy marker proteins) and genomic similarity (ANI), as well as genome-based predictions of nucleic acid catabolism that are supported by SIP results, we propose a novel species name *Candidatus* Izemoplasma acidinucleici for the *Ca*. Izemoplasma MAG recovered in this study. We have revised the previously suggested genus name *Ca*. Izimaplasma[27] to *Candidatus* Izemoplasma (Bernhard Schink and Aharon Oren, personal communication) of the family *Izemoplasmataceae* and order *Izemoplasmatales*. We propose the MAG of *Candidatus* Izemoplasma acidinucleici as type material for this lineage, since it fulfils the properties outlined by Chuvochina *et. al.*[41], with the only exception being that it is contained within 191 contigs.

- *Ca*. Izemoplasma gen. nov. (I.ze.mo.plas'ma. Gr. n. Izema, that what settles, sediment; - o-, connecting vowel; Gr. neut. n. plasma, something that forms, N.L. neut. n. Izemoplasma, a formed structure from sediment) with *Ca*. Izemoplasma acidinucleici (a.ci.di.nu.cle'i.ci. N.L. n. acidum nucleicu m, nucleic acid; N.L. gen. n. acidinucleici, of nucleic acid, referring to).

Discussion

This study revealed the identities of key microbial players involved in the turn-over and recycling of extracellular DNA in anoxic marine sediments for the first time using culture-independent approaches. Since over 90% of the seafloor is permanently under 4°C[42], the cold conditions used in our microcosm experiments represent conditions covering most of the seafloor. This was reflected by the detection of relatives of the DNA-degrading taxa in various sediments around the world's oceans, suggesting that these DNA-degrading taxa may contribute to DNA turn-over and mineralization on a global scale. Such heterotrophic processes may also be especially important in future arctic systems, where increased primary production due to decreased ice-cover is expected to dramatically alter carbon cycles and possibly increase inputs of phyto-detrital organic matter to the seafloor[43].

Members of the *Ca.* Izemoplasmataceae particularly stood out in this study because they became highly labelled in the SIP analyses, significantly increased in relative abundances when DNA was added to sediments and harboured various genes strongly indicating that they could catabolically exploit various sub-components of DNA. Strikingly, some *Ca.* Izemoplasmataceae encoded up to five extracellular nucleases, providing a clear indication that they can digest environmental DNA. Some of the extracellular nuclease genes were directly co-localised with genes encoding enzymes for further digestion of DNA into oligonucleotides and nucleosides, as well as removal of phosphates from nucleotides, and for transport of liberated nucleobases and phosphate into the cells. Together, the genomic co-localisations of these genes suggested that such processes are carried out in a co-ordinated manner and are therefore important nutrient acquisition strategies for these organisms.

Up to now, little was known regarding the ecological or biogeochemical roles of *Ca.* Izemoplasmataceae in marine sediments. One recent study of MAGs derived from marine sediments hinted that *Ca.* Izemoplasmataceae may catabolise nucleotides and the sugar moiety of DNA, among other key features such as the ability to grow via fermentation of few simple sugars[27]. Our analyses expand the ecophysiological understanding of *Ca.* Izemoplasmataceae by showing that they actively participate in the primary degradation of extracellular DNA polymers in anoxic marine sediments. The genomic analyses also show that they are evolutionary adapted for DNA catabolism, since they have relatively small genomes and limited catabolic repertoire for organics other than DNA. We therefore propose that they may establish their primary niche in sediments via the use of DNA as a nutrient and energy source. We also show that DNA-degrading capabilities are present in the *Ca.* Izemoplasmatales family UBA5603, which appears to be a sister clade of the marine *Ca.* Izemoplasmataceae that is primarily derived from the terrestrial subsurface. Genomes of the UBA5603 family (order Izemoplasmatales) did, however, lack many genes for enzymes required for *de novo* nucleotide biosyntheses, suggesting that they may degrade DNA for either, or both, salvage and/or catabolic purposes.

The detection of ^{13}C-labelled *Shewanella* and *Lutibacter* in the SIP analyses served as a good indication that *bone fide* DNA-degrading bacteria were detected by our SIP approach. This is because *Shewanella* are known to grow by catabolising DNA as a sole nutrient and energy source *in vitro*[23]. Similarly, members of the genus *Lutibacter* have been shown to possess hydrolytic activity for DNA *in vitro*, although it has not been reported whether they can grow using DNA as a sole nutrient[39]. *Shewanella* and *Lutibacter* are known to be capable of catabolising various simple organic substrates *in vitro*, e.g., amino acids, carboxylates and

sugars[28, 44]. Our data shows that diverse representatives of the *Shewanella* and *Lutibacter* also degrade DNA within *in situ*-like conditions. It further shows that they effectively compete with other DNA-degraders for DNA-derived carbon within the context of a complex community. This therefore provides important confirmation that these functional properties are expressed *in situ* and that they may be important nutrient acquisition strategies for these bacteria in marine sediments.

Our SIP analyses also showed various OTUs from the family *Nitrincolaceae* sourced carbon from DNA. We identified an extracellular nuclease encoded only in the genome of the isolate *Neptunomonas phycophila*, and accordingly, other enzymes required for catabolism of DNA-subcomponents were sparsely encoded among so far sequenced genomes of this family. Together, this suggested that degradation of extracellular DNA is a specialised physiological feature of only some *Nitrincolaceae* members. Indeed, various members of *Nitrincolaceae* are known to be a relatively versatile in catabolic terms, whereby they are known to degrade various carbohydrates, alcohols, organic acids and complex polycyclic aromatic hydrocarbons[45]. Alternatively, the low abundance *Nitrincolaceae* detected in this study and that could not be sampled for genomically, may have distinct genomes that harbour more expansive gene complements for enabling DNA catabolism.

Bacteria affiliated with the family *Fusibacteraceae* were conspicuous for their strong responses to additions of individual purine-based nucleobases and nucleosides, while also being highly labelled in the SIP analyses. Intriguingly, we could not identify known extracellular nucleases in the *Fusibacteraceae* MAG BB-3 or in any close relatives, and they did not increase in relative abundances when DNA was added as substrate. Although unknown extracellular nucleases may exist, their absence was notable because most previously described extracellular nucleases of anaerobic bacteria are derived from related *Firmicutes*, such as *Bacillus* and *Staphylococcus* species[46, 47]. This led us to infer that the *Fusibacteraceae* indeed lack extracellular nucleases. Instead, we could identify genes for multiple 5'-nucleotidases that were predicted to be embedded on their cell walls, as well as multiple gene clusters predicted to encode specific nucleoside/nucleotide transporters. Further, in-line with observations from the microcosm experiments that showed strong responses of multiple *Fusibacteraceae* OTUs to 2-deoxyadenosine amendments in the microcosms, the *Fusibacter* sp. 3D3 reference genome harboured multiple copies of adenosine deaminase genes. This may enable extra production of this enzyme and therefore more efficient processing of these molecules to the sugar and base moieties, which could then be further catabolised. Together, this indicates that these organisms may be ‘cheaters’, i.e., they may

use sub-components of DNA liberated into the sedimentary environment by other DNA-degraders. *Fusibacter* isolates are generally known to be capable of utilizing various simple carbohydrates[48-50], but until now, no *Fusibacter* species or closely related bacteria have been reported to have any activity related to DNA degradation or the degradation of molecular sub-components of DNA.

Finally, our analyses showed that additions of different individual sub-components of DNA to microcosms invoked highly distinct shifts in 16S rRNA gene relative abundances of diverse bacterial taxa. Interestingly, the different responses also occurred among distinct yet related members of some phylogenetic clades. For instance, various OTUs from the *Fusibacteraceae* responded differently to several DNA sub-components, especially purine-based molecules. This shows how different sub-components of DNA have the potential to be partitioned among different microorganisms. Free DNA subcomponents could arise if they are liberated from the parent molecule, e.g., after extracellular digestion of DNA by nucleases excreted by other primary DNA-degraders. This may therefore open-up multiple niches for different taxa, and in doing so, promote microbial diversity. In relation to this, additions of purine-based molecules consistently elucidated greater responses and from more diverse taxa, compared to responses to pyrimidine-based molecules. This aligns with previous research in estuarine waters, which showed that purine additions to water samples elicited considerably stronger end-product (urea) production than pyrimidines[51]. Further, we noted that more OTUs responded to nucleosides than their respective nucleobases. This signifies that the sugar moiety was preferentially exploited by some bacteria for energy conservation, rather than the base. This was especially notable for the pyrimidine nucleoside thymidine, which stimulated responses from eleven different OTUs, in comparison thymine itself that elucidated responses from only two OTUs.

Conclusions

In this study, we provide complementary evidence supporting the involvement of diverse bacteria belonging to the *Lutibacter*, *Shewanella*, *Fusibacteraceae, Ca.* Izemoplasmataceae and *Nitrincolaceae* in the anaerobic degradation of DNA in marine sediments. The *Ca.* Izemoplasmataceae organisms are replete with genes for enzymatic machinery necessary to deconstruct DNA from the extracellular environment and to subsequently import and fully catabolise different molecular sub-components of DNA. These genes were often conspicuously co-localised in *Ca.* Izemoplasmataceae genomes, suggesting

they have evolved to be regulated and function in a co-ordinated manner. Bacteria related to the *Fusibacteraceae* appeared to be very efficient at degrading purine-based DNA sub-components, but not extracellular DNA. We therefore propose that they may have been 'DNA cheaters' that utilised sub-components of DNA liberated by other members of the community. This study also supports results from previous *in vitro* studies of *Shewanella* and *Lutibacter* that demonstrated DNA-degrading capabilities, and importantly, shows that these bacteria perform such activities under *in situ*-like conditions. Together, this study sheds new light on the functional properties of several bacterial groups that are widespread yet poorly understood in marine sediments. These bacteria may thus collectively contribute to the essential process of turning-over the copious quantities of extracellular DNA that are present in vast expanses of the seafloor.

Materials and Methods

Sediment sampling and microcosm set-ups

Marine sediments (0-30 cm) were collected from two locations in northern Baffin Bay (Station 'KANE-2B' 79°30.909 -70°50.819 and 'GL-111' 76°18.354 -73°13.180) using a box corer aboard the Canadian Coast Guard icebreaker CCGS *Amundsen*, in July 2014. Sediments were filled into 250 ml Schott bottles to exclude oxygen, sealed and maintained at 4°C or on ice during transport. Sediments from both sites were mixed together in equal volumes, and then amended with cold (4°C) anoxic artificial seawater (1:1 v/v) (detailed in Supporting information). Resulting sediment slurries were and homogenised thoroughly within an anoxic glove-box (containing approximately 88% nitrogen, 2% hydrogen, 10% CO_2). Approximately 30 ml of sediment slurry was added to 100 ml serum flasks, and these were sealed and crimped with 2 cm thick black butyl rubber stoppers. Sediment slurries and microcosms were placed on top of frozen ice-packs during all preparation or manipulation steps in the anoxic glove-box. Microcosms were maintained at 4°C during all subsequent incubations.

Microcosm incubation conditions and subsampling

Microcosms were pre-incubated for 4 days prior to substrate additions and this time point where substrates were added is herein referred to as day 0. Substrates were also added directly after subsampling at day 10. Purified ^{13}C-labelled or unlabelled DNA extracted from

Halobacterium salinarum (Supporting information), which is not present at detectable abundances in typical marine sediments, was added as substrate at concentrations of 36 µg ml^{-1}. This amount was added because it is similar to that of total bioavailable DNA previously measured in marine sediments[14]. The nucleobases and nucleosides adenine, guanine, cytosine, thymine, 2-deoxyadenosine and thymidine (Sigma Aldrich, >99% pure) were added individually to separate microcosms, each to final concentration of 100 µM. Parallel microcosms without added substrates were analysed as 'no-substrate' controls. All treatment series (Supp. Table 1) were performed in triplicate microcosms.

Initial samples for microbial community analyses were taken directly after preparation of the sediment slurry, and following substrate amendments subsamples were taken for microbial community profiling, SIP and metagenomics at days 0, 4, 10, 13, 24, and 31. For microbial community profiling via 16S rRNA gene amplicon sequencing, 100 µl from each microcosm was subsampled. Additional 1 ml subsamples were taken at each time point for chemical analyses. Subsamples were kept on ice-packs inside the anoxic glove-box during subsampling, and were then immediately snap-frozen on dry-ice outside the glove-box and subsequently stored at -80°C. All tubes for subsampling were introduced into the anoxic glove-box at least 1 hr prior to subsampling to remove traces of O_2. Headspace gas (15 ml) was subsampled from microcosms using N_2-flushed syringes fitted with needles and injected into pre-evacuated 12 ml glass exetainers (Labco, UK) that were sealed with butyl-rubber stoppers.

DNA extractions

DNA for 16S rRNA gene amplicon sequencing and for density gradient centrifugations was extracted from 100 µl of microcosm slurries using a combination of bead beating, a cetyltrimethylammonium bromide-containing buffer and phenol-chloroform extractions (detailed in Supporting information). DNA for metagenomic library preparation was purified from 100 µl of microcosm subsamples using a MoBio Ultra Pure Power Soil Kit (MoBio, USA) following the manufacturer's instructions.

Density gradient centrifugations and quantitative PCR analyses of fractions

DNA from triplicates of specific treatments and time points to be analysed by DNA-SIP were combined equally to a total of 500 ng and subject to ultracentrifugation in a $CsCl_2$

solution with a VTi-90 rotor for 72 hrs following standard protocols[52]. Gradients were collected by fractionation into approximately 20 separate fractions of 200 µl each. The densities of the collected fractions were measured using a refractometer (AR200; Reichert Analytical Instruments, USA) at 22°C. DNA was concentrated and purified by precipitation with polyethyleneglycol (MW=8000) and glycogen, and subsequently washed using methods previously described[52]. DNA was diluted 1:100 in ddH_2O to facilitate PCR amplification.

PCR and quantitative real-time PCR amplification of 16S rRNA genes

PCR amplifications of 16S rRNA genes from DNA extracted from microcosms and density gradient centrifugation fractions were performed using a two-step PCR barcoding approach[53]. This was done using primers that target most *Bacteria* (341F: 5'-CCTACGGGNGGCWGCAG-3' and 785R: 5'-GACTACHVGGGTATCTAATCC-3')[54]. Both primers included 'head' sequences to facilitate barcoding in the second-step PCR[53]. PCR conditions are detailed in the Supporting information. PCR products were purified using a ZR-96 DNA Clean-up Kit™ (Zymo Research, USA) and pooled to equimolar concentrations after quantification using the Quant-iT™ PicoGreen® dsDNA Assay Kit (ThermoFischer Scientific, Germany). Sequencing was performed by MicroSynth (Switzerland) on an Illumina MiSeq instrument using MiSeq Reagent Kit v3 chemistry with 300 bp paired-end read mode. Negative DNA extract controls (no added sediment) and PCR negative controls (no DNA template) were performed and sequenced in parallel (even if no PCR product was detected).

Quantitative real-time PCR assays for bacterial 16S rRNA genes from fractions collected from $CsCl_2$ gradients were analysed using real-time PCR assays targeting *Bacteria* using the primers 341F (5'-CCTACGGGAGGCAGCAG-3') and 534R (5'-ATTACCGCGGCTGCTGGCA-3') (see Supporting information for details).

Bioinformatic processing of 16S rRNA gene amplicon data and statistics

The bioinformatic processing of 16S rRNA gene amplicon data was performed as previously described[53]. Briefly, read pairs were first assembled as contigs using QIIME's join_paired_ends.py script[55]. Sequences were then screened for chimeras and clustered into species-level OTUs at 99% sequence similarity using the UPARSE pipeline (version 8.0.1623)[56]. This involved dereplication of sequences, removal of singletons, and

determination of OTU centroids using a 1% radius. OTU abundances were determined by mapping filtered sequences to OTU centroids using 99% identity. OTU sequences were subsequently classified using the Naïve Bayesian classifier[57], as implemented in mothur (version 1.33.0)[58]. A confidence cutoff of 50% was used for the classification with the SILVA 119 SSU NR99 database as taxonomic reference[59].

The IMNGS webserver[60] was used to identify the presence and relative abundances of sequences related to OTUs representative of the ^{13}C-labelled taxa identified by SIP, in different publically available Short Read Archive (SRA) datasets. Sequence identity cut-offs of ≥95% for *Shewanella*, *Ca*. Izemoplasma and *Fusibacteraceae* OTUs, and ≥97% identity to *Lutibacter* and *Nitrincolaceae* OTUs were used when querying the SRAs via IMNGS (Supp. Fig. 7). A minimum overlap of 100 bp was required between query and database sequences.

Statistical analyses of 16S rRNA gene amplicon sequencing data

All statistical analyses of 16S rRNA gene amplicon data were performed using the Rhea package (version 1.0.1-5)[61] as implemented in the R software environment (version 1.1.383). To detect OTUs enriched in relative abundances in the dense fractions of $CsCl_2$ density gradients from ^{13}C versus ^{12}C treatments, the 'Serial Group Comparisons' pipeline of Rhea was applied. Default parameters were used except for the following: abundance_cutoff <- 0.001, prevalence_cutoff <- 0.1; max_median_cutoff <-0.001; ReplaceZero = "NO". This pipeline used the Wilcoxon Signed Rank Sum Test for matched OTUs to test for significant differences in OTU relative abundances between two treatments, at each time point. Relative abundance data of OTUs from at least three heavy fractions (ranging from 1.726-1.742 g ml^{-1}) from ^{13}C-amended versus corresponding unamended (^{12}C) control treatments, for day 4, 10 and 13, were used as input (Supp. Table 5). Data values obtained from fractions of >1.742 g ml^{-1} were excluded, since preliminary examination of plots of OTU relative abundances across gradients revealed very few taxa were labelled to such an extent that they increased in relative abundances in those fractions. For day 4, a 'pseudo-replicate' consisting of an average value from the available two heavy fractions was produced to result in triplicates and thus facilitate the statistical analysis (Supp. Table 5). To identify OTUs that were enriched in relative abundances in the different microcosm treatments versus the no-substrate controls, for each time point, the 'Serial Group Comparisons' pipeline of Rhea was applied as described above, using data from triplicate microcosms. Only OTUs that were significantly enriched in relative abundances at two or more time points, in each treatment series, were reported.

For beta diversity analysis of microbial communities in microcosms, principal coordinate analysis (PCoA) was performed using a Bray-Curtis dissimilarity matrix (including relative abundances). The plots were constructed with the 'vegan' package (version 2.5-3) in R. To avoid biases related to differences among library depths, sequencing libraries were all subsampled to a number of reads smaller than the smallest library (1620 reads).

Metagenomic library preparation, sequencing and analyses

Metagenomic libraries were prepared for sequencing and indexed using the Nextera XT DNA Library Preparation Kit (Illumina, USA), following the manufacturer's instructions. Five samples were selected to facilitate differential coverage binning, i.e., i) the initial sediment slurry, ii) day 4, ^{12}C-DNA treatment, iii) day 13, ^{13}C-DNA treatment, iv) day 24, ^{12}C-DNA treatment, and v) day 31, ^{13}C-DNA treatment. DNA libraries were purified using magnetic beads via the Agencourt AMPure XP kit (Beckman-Coulter), and sequenced by the Vienna BioCenter Core Facilities GmbH (VBCF) on one lane of an Illumina HiSeq 2500 instrument using HiSeq V4 chemistry with 125 bp paired-end mode.

Raw sequences were trimmed to 100 bp, and each sample dataset was assembled separately using IDBA-UD (version, 1.1.1) using default parameters[62]. Assembled contigs >1000 bp were automatically binned into genome bins based on a combination of nucleotide coding frequencies and sequence assembly coverage using MetaBat2 using each present binning strategy (version 2.12.1)[63], MaxBin2 (version 2.2.4)[64] and CONCOCT (version 0.4.1)[65]. Coverage profiles for binning were acquired by mapping trimmed reads to assemblies using BWA[66] and SAMtools[67]. Additionally, the sample from the day 31 ^{13}C-DNA treatment was also assembled using MetaSpades (version 3.11.1)[68] and additionally binned with MetaBat, MaxBin and CONCOCT. Genome bins from each binning tool and from each respective assembly were aggregated using DasTool (version 1.1.0)[69]. All genome bins were finally dereplicated using dRep (version 1.4.3)[70], with the following options: all genomes were dereplicated using an average nucleotide identity of ≥98% was used in the secondary ANI comparison, and all genomes that were >50% complete and <10% contamination were kept. The completeness and degree of potential contamination of the genome bins were evaluated by CheckM (version 1.0.7)[71]. Gene calling and initial genome annotations were performed via RAST[72]. Putative functions of predicted proteins were also checked via BLASTP[73] against the NCBI-nr database and evaluated in relation to relevant literature. Predictions of subcellular locations of predicted proteins were performed using

PSORTb (version 3.0)[74], with settings appropriate for the predicted cell wall types of the respective organism. Biochemical inferences were primarily based on the MetaCyc database[75]. Gene synteny depictions were produced using EasyFig[76].

Phylogenetic and average nucleotide identity analyses

All phylogenetic analyses of 16S rRNA gene sequences were performed in ARB (version 6.0.6) using maximum likelihood algorithms[77] and the SILVA 132 SSU NR99 database[59]. Query sequences were first aligned to the SILVA alignment with the SINA aligner[78], then sequences were inserted into the global reference tree using the parsimony option. A selection of near-full length sequences of close relatives and cultivated relatives of the query sequences were then selected and used to construct trees *de novo* using RaxML[79], fastDNAmL[80] and PhyML[81] algorithms as implemented in ARB with default settings and the ARB bacterial 'Positional variability by parsimony' filter. A consensus tree was then created with those three trees and short amplicon sequences were inserted into the consensus trees via the parsimony option of ARB.

Phylogenomic analyses were conducted by using an alignment of concatenated protein sequences derived from 43 single copy marker genes retrieved from the CheckM analyses. A tree was first constructed using these protein alignments derived from the query genomes and 8203 representative genomes downloaded from the NCBI database (as of July 2018). The tree was constructed using default parameters using FastTree (version 2.1.10)[82]. Manually selected reference sequences that were taxonomically informative for query sequences were obtained, and a second smaller tree was reconstructed using FastTree using only the selected reference and query sequences.

Average nucleotide identity (ANI) for comparison of genome relatedness were determined using JSpeciesWS server[83], based on BLAST ('ANIb').

Taxonomic names

In addition to 16S rRNA-based SILVA taxonomies, we used the newly proposed names of the Genome Taxonomy Database (GTDB) (version 0.1.3) that is based on genome phylogeny[46].

Chemical measurements

Carbon isotope compositions of CO_2 ($\delta^{13}C$ values in permille relative to VPD) were analysed by a headspace gas sampler (Gas- Bench II, Thermo Fisher, Bremen, Germany) coupled to an isotope ratio mass spectrometer (Delta V Advantage, Thermo Fisher, Bremen, Germany). CO_2 reference gas was calibrated using ISO-TOP gas standards (Air Liquide) with a certified ^{13}C concentrations.

For total sediment iron and manganese, inductively coupled plasma optical emission spectrometry (ICP-OES) measurement was applied on a Perkin Elmer 5300 DV (Pekin Elmer Inc., Waltham, MA, USA) after total fusion of 0.1 gram oven dried sediment samples (1 g original sample dried 3 h at 105°C, loss of ignition 6 h at 600°C, followed by 6 h at 1,000°C, LOI approx.. 80%) with 0.9 g di-lithium tetraboarate (Spectromelt A10, Merck, Darmstadt, Germany) using a Linn Lifumat, 9 min. at 1,050 °C (Linn High Therm Gmbh, Eschenfelden, Germany). The fusion product was dissolved in 50 ml of 5 molar HNO_3 (Normapur, VWR, Germany, double sub-boiled, Berghof BSB-939-IR) with 150 ml deionized water (MilliQ, Merck-Millipore, Darmstadt, Germany), and further diluted to a total volume of 250 ml. External linear matrix matched calibration was applied using single element manganese and iron standards (Merck-Millipore, Darmstadt, Germany), including quality control with LKSD1 and LKSD 4 certified lake sediment standards (Natural Resources Canada, Ottawa, Canada).

Data availability

All sequence data was deposited under Genbank Bioproject PRJNA510104. PCR-derived 16S rRNA gene amplicon sequence data is available under accessions SAMN10603326-SAMN10603488. Metagenomic sequence read data is available under accessions SAMN10594394-SAMN10594398. Metagenome-assembled genomes are available under accessions SAMN10805732-SAMN10805736.

Acknowledgements

This work was supported by the Austrian Science Fund (FWF) grants P25111-B22 and P29246-B29 to A.L. and K.W., respectively. We thank the Vienna BioCenter Core Facilities for metagenomic sequencing. We thank Prof. Bernhard Schink and Prof. Aharon Oren for their recommendations for nomenclature proposed in this study. We thank Dr. Angela Witte for kindly providing us with the *Halobacterium salinarum* strain and Fátima C. Pereira for

performing the PCoA analysis. For sampling, funding from ArcticNet and assistance from the Canadian Coast Guard, captain and crew of the CCGS *Amundsen*, and chief scientist are gratefully acknowledged.

Author contributions

K.W. and A.L. conceived and designed the study. A.N. and C.R.J.H were responsible for sample collection and processing. K.W. and C.P. performed the incubation experiments and molecular analyses. M.W. and A.R. performed gas chromatography analyses. T.H. performed sediment iron and manganese analyses. K.W., C.P., T.R. and C.W.H performed bioinformatic processing and analyses. K.W. analysed and interpreted the data. K.W. and A.L. wrote the manuscript with contributions from all authors.

Competing interests

All authors have no competing interests.

Materials & Correspondence

Requests for materials and/or correspondence can be made to Kenneth Wasmund and/or Alexander Loy

References

1. Bar-On, Y.M., Phillips, R. & Milo, R. The biomass distribution on Earth. *Proc. Natl. Acad. Sci. USA* **115**, 6506-6511 (2018).
2. Lloyd, K.G., Steen, A.D., Ladau, J., Yin, J. & Crosby, L. Phylogenetically Novel Uncultured Microbial Cells Dominate Earth Microbiomes. *mSystems* **3**, e00055-00018 (2018).
3. Biddle, J.F. et al. Heterotrophic Archaea dominate sedimentary subsurface ecosystems off Peru. *Proc. Natl. Acad. Sci. USA* **103**, 3846-3851 (2006).
4. Arndt, S. et al. Quantifying the degradation of organic matter in marine sediments: A review and synthesis. *Earth-Sci. Rev.* **123**, 53-86 (2013).
5. Arnosti, C. Microbial Extracellular Enzymes and the Marine Carbon Cycle. *Annu. Rev. Mar. Sci.* **3**, 401-425 (2011).
6. Bradley, J.A., Amend, J.P. & LaRowe, D.E. Necromass as a Limited Source of Energy for Microorganisms in Marine Sediments. *J. Geophys. Res. Biogeosci.* **123**, 577-590 (2018).
7. Baran, R. et al. Exometabolite niche partitioning among sympatric soil bacteria. *Nat. Commun.* **6**, 8289 (2015).
8. Schmidt, F., Elvert, M., Koch, B.P., Witt, M. & Hinrichs, K.U. Molecular characterization of dissolved organic matter in pore water of continental shelf sediments. *Geochim. Cosmochim. Acta* **73**, 3337-3358 (2009).
9. Rossel, P.E., Bienhold, C., Boetius, A. & Dittmar, T. Dissolved organic matter in pore water of Arctic Ocean sediments: Environmental influence on molecular composition. *Org. Geochem.* **97**, 41-52 (2016).
10. Oni, O.E. et al. Microbial Communities and Organic Matter Composition in Surface and Subsurface Sediments of the Helgoland Mud Area, North Sea. *Front. Microbiol.* **6**, 1290 (2015).
11. Burdige, D.J. Preservation of Organic Matter in Marine Sediments: Controls, Mechanisms, and an Imbalance in Sediment Organic Carbon Budgets? *Chem. Rev.* **107**, 467-485 (2007).
12. Hedges, J.I. & Oades, J.M. Comparative organic geochemistries of soils and marine sediments. *Org. Geochem.* **27**, 319-361 (1997).
13. Danovaro, R., Dell'Anno, A. & Fabiano, M. Bioavailability of organic matter in the sediments of the Porcupine Abyssal Plain, northeastern Atlantic. *Mar. Ecol. Prog. Ser.* **220**, 25-32 (2001).
14. Dell'Anno, A. & Danovaro, R. Extracellular DNA plays a key role in deep-sea ecosystem functioning. *Science* **309**, 2179 (2005).
15. Jørgensen, N.O.G. & Jacobsen, C.S. Bacterial uptake and utilization of dissolved DNA. *Adv. Microb. Ecol.* **11**, 263-270 (1996).
16. Corinaldesi, C., Dell'Anno, A. & Danovaro, R. Early diagenesis and trophic role of extracellular DNA in different benthic ecosystems. *Limnol. Oceanogr.* **52**, 1710-1717 (2007).
17. Torti, A., Jørgensen, B.B. & Lever, M.A. Preservation of microbial DNA in marine sediments: Insights from extracellular DNA pools. *Environ. Microbiol.* **20**, 4526-4542 (2018).
18. Ramírez, G.A., Jørgensen, S.L., Zhao, R. & D'Hondt, S. Minimal Influence of Extracellular DNA on Molecular Surveys of Marine Sedimentary Communities. *Front. Microbiol.* **9** (2018).

19. Gödeke, J., Heun, M., Bubendorfer, S., Paul, K. & Thormann, K.M. Roles of two *Shewanella oneidensis* MR-1 extracellular endonucleases. *Appl. Environ. Microbiol.* **77**, 5342-5351 (2011).
20. Ye, J. & van den Berg, B. Crystal structure of the bacterial nucleoside transporter Tsx. *EMBO J.* **23**, 3187-3195 (2004).
21. Hartwich, K., Poehlein, A. & Daniel, R. The Purine-Utilizing Bacterium *Clostridium acidurici* 9a: A Genome-Guided Metabolic Reconsideration. *Plos One* **7**, e51662 (2012).
22. Vogels, G.D. & Van der Drift, C. Degradation of purines and pyrimidines by microorganisms. *Bacteriol. Rev.* **40**, 403-468 (1976).
23. Pinchuk, G.E. et al. Utilization of DNA as a sole source of phosphorus, carbon, and energy by *Shewanella* spp.: Ecological and physiological implications for dissimilatory metal reduction. *App. Environ. Microbiol.* **74**, 1198-1208 (2008).
24. Torti, A., Lever, M.A. & Jørgensen, B.B. Origin, dynamics, and implications of extracellular DNA pools in marine sediments. *Mar. Genomics* **24**, 185-196 (2015).
25. Vandieken, V. et al. Three manganese oxide-rich marine sediments harbor similar communities of acetate-oxidizing manganese-reducing bacteria. *ISME J.* **6**, 2078-2090 (2012).
26. Pepe-Ranney, C. et al. Non-cyanobacterial diazotrophs mediate dinitrogen fixation in biological soil crusts during early crust formation. *ISME J.* **10**, 287-298 (2016).
27. Skennerton, C.T. et al. Phylogenomic analysis of *Candidatus* 'Izimaplasma' species: free-living representatives from a *Tenericutes* clade found in methane seeps. *ISME J.* **10**, 2679-2692 (2016).
28. Wissuwa, J., Bauer, S.L., Steen, I.H. & Stokke, R. Complete genome sequence of *Lutibacter profundi* LP1(T) isolated from an Arctic deep-sea hydrothermal vent system. *Stand. Genomic Sci.* **12**, 5 (2017).
29. Serrano, A.E. et al. First draft genome sequence of a strain from the genus *Fusibacter* isolated from Salar de Ascotan in Northern Chile. *Stand. Genomic Sci.* **12**, 43 (2017).
30. Parks, D.H. et al. Recovery of nearly 8,000 metagenome-assembled genomes substantially expands the tree of life. *Nat. Microbiol.* **2**, 1533-1542 (2017).
31. Kim, S.-J. et al. Draft Genome Sequence of "*Candidatus* Izimaplasma sp." Strain ZiA1, Obtained from a Toluene-Degrading and Iron-Reducing Enrichment Culture. *Microbiol. Resour. Announc.* **7**, e00861-00818 (2018).
32. Heun, M., Binnenkade, L., Kreienbaum, M. & Thormann, K.M. Functional specificity of extracellular nucleases of *Shewanella oneidensis* MR-1. *Appl. Environ. Microbiol.* **78**, 4400-4411 (2012).
33. Chen, I.A. et al. IMG/M: integrated genome and metagenome comparative data analysis system. *Nucleic Acids Res.* **45**, D507-D516 (2017).
34. Bengis-Garber, C. & Kushner, D.J. Role of membrane-bound 5'-nucleotidase in nucleotide uptake by the moderate halophile Vibrio costicola. *J. Bacteriol.* **149**, 808-815 (1982).
35. Sakai, Y. et al. Properties of the membrane-bound 5'-nucleotidase and utilization of extracellular ATP in *Vibrio parahaemolyticus*. *J. Gen. Microbiol.* **133**, 2751-2757 (1987).
36. Leer, J.C., Hammer-Jespersen, K. & Schwartz, M. Uridine phosphorylase from *Escherichia coli.* Physical and chemical characterization. *Eur. J. Biochem.* **75**, 217-224 (1977).
37. Dürre, P. & Andreesen, J.R. Purine and Glycine Metabolism by Purinolytic *Clostridia*. *J. Bacteriol.* **154**, 192-199 (1983).
38. Serres, M.H. & Riley, M. Genomic analysis of carbon source metabolism of *Shewanella oneidensis* MR-1: Predictions versus experiments. *J. Bacteriol.* **188**, 4601-4609 (2006).

39. Choi, A., Yang, S.J. & Cho, J.C. *Lutibacter flavus* sp. nov., a marine bacterium isolated from a tidal flat sediment. *Int. J. Syst. Evol. Microbiol.* **63**, 946-951 (2013).
40. Wang, Z.J., Xie, Z.H., Wang, C., Du, Z.J. & Chen, G.J. *Motiliproteus sediminis* gen. nov., sp. nov., isolated from coastal sediment. *Antonie van Leeuwenhoek* **106**, 615-621 (2014).
41. Chuvochina, M. et al. The importance of designating type material for uncultured taxa. *Syst. Appl. Microbiol.* **Online early** (2018).
42. Levitus, S. & Boyer, T. in World Ocean Atlas, Vol. Vol. 4 (US Department of Commerce, Washington, DC; 1994).
43. Smetacek, V. & Nicol, S. Polar ocean ecosystems in a changing world. *Nature* **437**, 362–368 (2005).
44. Driscoll, M.E. et al. Identification Of Diverse Carbon Utilization Pathways In *Shewanella oneidensis* MR-1 Via Expression Profiling. *Genome Inform.* **18**, 287-298 (2007).
45. Diéguez, A.L., Pichon, P., Balboa, S., Magnesen, T. & Romalde, J.L. Complete characterization of new isolates of *Neptunomonas phycophila* leads to emend its description and opens possibilities of biotechnological applications. *MicrobiologyOpen* **6**, e00519 (2017).
46. Parks, D.H. et al. A standardized bacterial taxonomy based on genome phylogeny substantially revises the tree of life. *Nat. Biotechnol.* **36**, 996–1004 (2018).
47. Pediaditakis, M., Kaufenstein, M. & Graumann, P.L. *Bacillus subtilis* hlpB Encodes a Conserved Stand-Alone HNH Nuclease-Like Protein That Is Essential for Viability Unless the hlpB Deletion Is Accompanied by the Deletion of Genes Encoding the AddAB DNA Repair Complex. *J. Bacteriol.* **194**, 6184-6194 (2012).
48. Fadhlaoui, K. et al. *Fusibacter fontis* sp. nov., a sulfur-reducing, anaerobic bacterium isolated from a mesothermic Tunisian spring. *Int. J. Syst. Evol. Microbiol.* **65**, 3501-3506 (2015).
49. Ben Hania, W. et al. Fusibacter tunisiensis sp. nov., isolated from an anaerobic reactor used to treat olive-mill wastewater. *Int. J. Syst. Evol. Microbiol.* **62**, 1365-1368 (2012).
50. Ravot, G. et al. *Fusibacter paucivorans* gen. nov., sp. nov., an anaerobic, thiosulfate-reducing bacterium from an oil-producing well. *International journal of systematic bacteriology* **49**, 1141-1147 (1999).
51. Berg, B.M. & Jørgensen , N.O.G. Purine and pyrimidine metabolism by estuarine bacteria. *Aquat. Microb. Ecol.* **42**, 215-226 (2006).
52. Neufeld, J.D. et al. DNA stable-isotope probing. *Nat. Protoc.* **2**, 860-866 (2007).
53. Herbold, C.W. et al. A flexible and economical barcoding approach for highly multiplexed amplicon sequencing of diverse target genes. *Front. Microbiol.* **6**, 731 (2015).
54. Klindworth, A. et al. Evaluation of general 16S ribosomal RNA gene PCR primers for classical and next-generation sequencing-based diversity studies. *Nucleic acids research* **41**, e1 (2013).
55. Caporaso, J.G. et al. QIIME allows analysis of high-throughput community sequencing data. *Nat. Methods* **7**, 335-336 (2010).
56. Edgar, R.C. UPARSE: highly accurate OTU sequences from microbial amplicon reads. *Nat. Methods* **10**, 996-998 (2013).
57. Wang, Q., Garrity, G.M., Tiedje, J.M. & Cole, J.R. Naïve Bayesian classifier for rapid assignment of rRNA sequences into the new bacterial taxonomy. *Appl. Environ. Microbiol.* **73**, 5261-5267 (2007).
58. Schloss, P.D. et al. Introducing mothur: Open-Source, Platform-Independent, Community-Supported Software for Describing and Comparing Microbial Communities. *App. Environ. Microbiol.* **75**, 7537-7541 (2009).
59. Quast, C. et al. The SILVA ribosomal RNA gene database project: improved data processing and web-based tools. *Nucleic Acids Res.*. **41**, D590-596 (2013).

60. Lagkouvardos, I. et al. IMNGS: A comprehensive open resource of processed 16S rRNA microbial profiles for ecology and diversity studies. *Sci. Rep.* **6**, 33721 (2016).
61. Lagkouvardos, I., Fischer, S., Kumar, N. & Clavel, T. Rhea: a transparent and modular R pipeline for microbial profiling based on 16S rRNA gene amplicons. *Peerj* **5**, e2836 (2017).
62. Peng, Y., Leung, H.C., Yiu, S.M. & Chin, F.Y. IDBA-UD: a *de novo* assembler for single-cell and metagenomic sequencing data with highly uneven depth. *Bioinformatics* **28**, 1420-1428 (2012).
63. Kang, D.W.D., Froula, J., Egan, R. & Wang, Z. MetaBAT, an efficient tool for accurately reconstructing single genomes from complex microbial communities. *Peerj* **3**, e1165 (2015).
64. Wu, Y.-W., Simmons, B.A. & Singer, S.W. MaxBin 2.0: an automated binning algorithm to recover genomes from multiple metagenomic datasets. *Bioinformatics* **32**, 605-607 (2016).
65. Alneberg, J. et al. Binning metagenomic contigs by coverage and composition. *Nat. Methods* **11**, 1144-1146 (2014).
66. Li, H. & Durbin, R. Fast and accurate short read alignment with Burrows-Wheeler transform. *Bioinformatics* **25**, 1754-1760 (2009).
67. Li, H. et al. The Sequence Alignment/Map format and SAMtools. *Bioinformatics* **25**, 2078-2079 (2009).
68. Nurk, S., Meleshko, D., Korobeynikov, A. & Pevzner, P.A. metaSPAdes: a new versatile metagenomic assembler. *Genome research* **27**, 824-834 (2017).
69. Sieber, C.M.K. et al. Recovery of genomes from metagenomes via a dereplication, aggregation and scoring strategy. *Nat. Microbiol.* **3**, 836-843 (2018).
70. Olm, M.R., Brown, C.T., Brooks, B. & Banfield, J.F. dRep: a tool for fast and accurate genomic comparisons that enables improved genome recovery from metagenomes through de-replication. *ISME J.* **11**, 2864-2868 (2017).
71. Parks, D.H., Imelfort, M., Skennerton, C.T., Hugenholtz, P. & Tyson, G.W. CheckM: assessing the quality of microbial genomes recovered from isolates, single cells, and metagenomes. *Genome research* **25**, 1043-1055 (2015).
72. Aziz, R.K. et al. The RAST Server: rapid annotations using subsystems technology. *Bmc Genomics* **9**, 75 (2008).
73. Altschul, S.F. et al. Gapped BLAST and PSI-BLAST: a new generation of protein database search programs. *Nucleic Acids Res.*. **25**, 3389-3402 (1997).
74. Yu, N.Y. et al. PSORTb 3.0: improved protein subcellular localization prediction with refined localization subcategories and predictive capabilities for all prokaryotes. *Bioinformatics* **26**, 1608-1615 (2010).
75. Caspi, R. et al. The MetaCyc database of metabolic pathways and enzymes and the BioCyc collection of Pathway/Genome Databases. *Nucleic Acids Res.* **42**, D459-471 (2014).
76. Sullivan, M.J., Petty, N.K. & Beatson, S.A. Easyfig: a genome comparison visualizer. *Bioinformatics* **27**, 1009-1010 (2011).
77. Ludwig, W. et al. ARB: a software package environment for sequence data. *Nucleic Acids Res.*. **32**, 1363-1371 (2004).
78. Pruesse, E., Peplies, J. & Glöckner, F.O. SINA: accurate high-throughput multiple sequence alignment of ribosomal RNA genes. *Bioinformatics* **28**, 1823-1829 (2012).
79. Stamatakis, A. RAxML version 8: a tool for phylogenetic analysis and post-analysis of large phylogenies. *Bioinformatics* **30**, 1312-1313 (2014).
80. Olsen, G.J., Matsuda, H., Hagstrom, R. & Overbeek, R. fastDNAmL: a tool for construction of phylogenetic trees of DNA sequences using maximum likelihood. *Comput. Appl. Biosci.* **10**, 41-48 (1994).
81. Guindon, S., Delsuc, F., Dufayard, J.F. & Gascuel, O. Estimating maximum likelihood phylogenies with PhyML. *Methods Mol. Biol.* **537**, 113-137 (2009).

82. Price, M.N., Dehal, P.S. & Arkin, A.P. FastTree: computing large minimum evolution trees with profiles instead of a distance matrix. *Mol. Biol. Evol.* **26**, 1641-1650 (2009).
83. Richter, M., Rosselló-Mora, R., Oliver Glöckner, F. & Peplies, J. JSpeciesWS: a web server for prokaryotic species circumscription based on pairwise genome comparison. *Bioinformatics* **32**, 929-931 (2016).

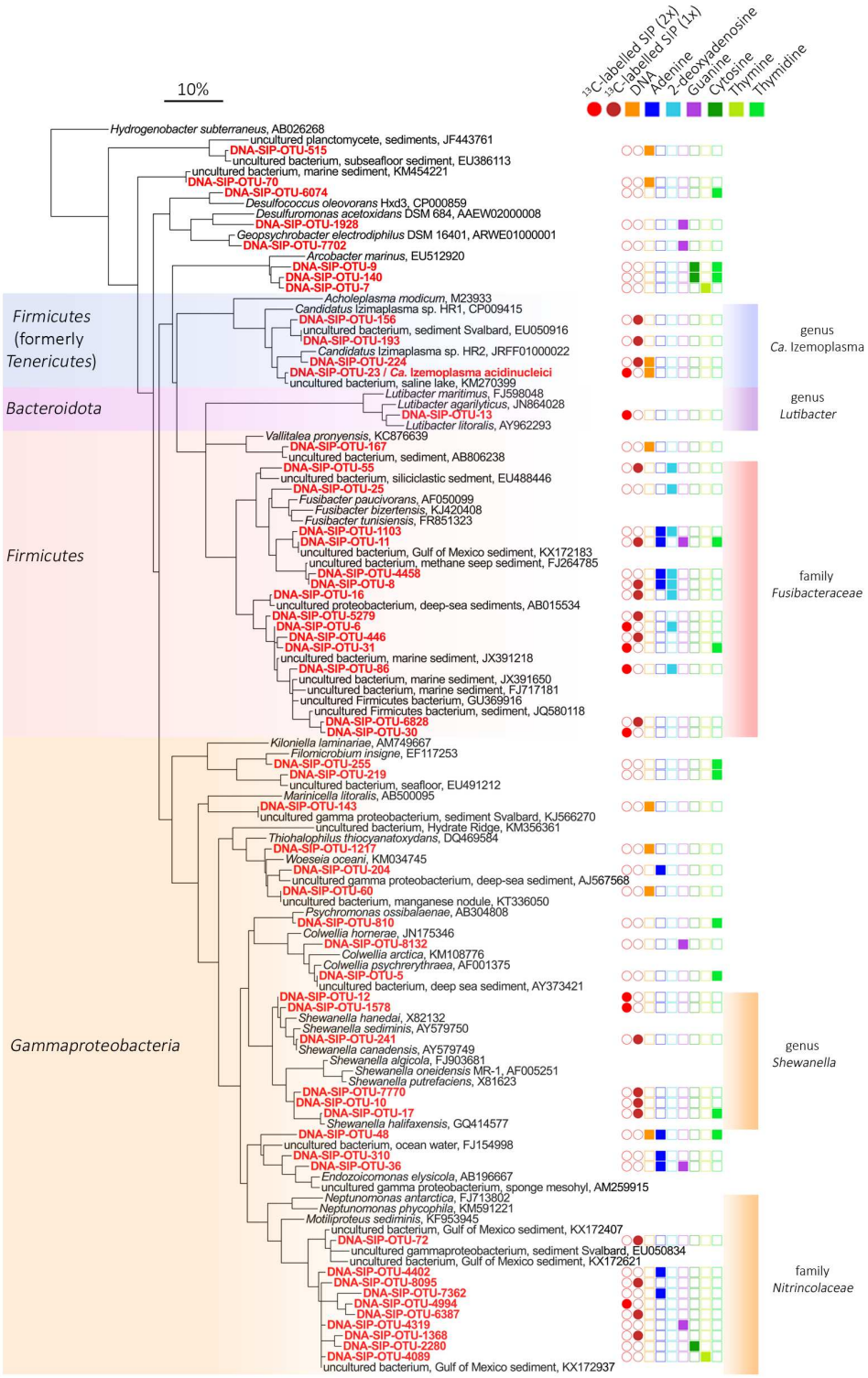

Fig. 1. Phylogeny of 16S rRNA OTUs determined to be enriched in ^{13}C in microcosms with ^{13}C-DNA as substrate and/or to have significantly increased in relative gene abundance in microcosms with unlabelled DNA or selected DNA sub-components. OTUs that were labelled at two points (2x) are indicated with bright red, while relatives that were labelled at one time point (1x) are indicated in dark red. 16S rRNA OTU sequences recovered in this study are highlighted in red and bold. Taxonomic groups that included DNA-degrading bacteria as determined by DNA-SIP analyses are highlighted by shaded colours. Genbank accessions are included for 16S rRNA gene reference sequences. The scale bar represents 10% sequence divergence.

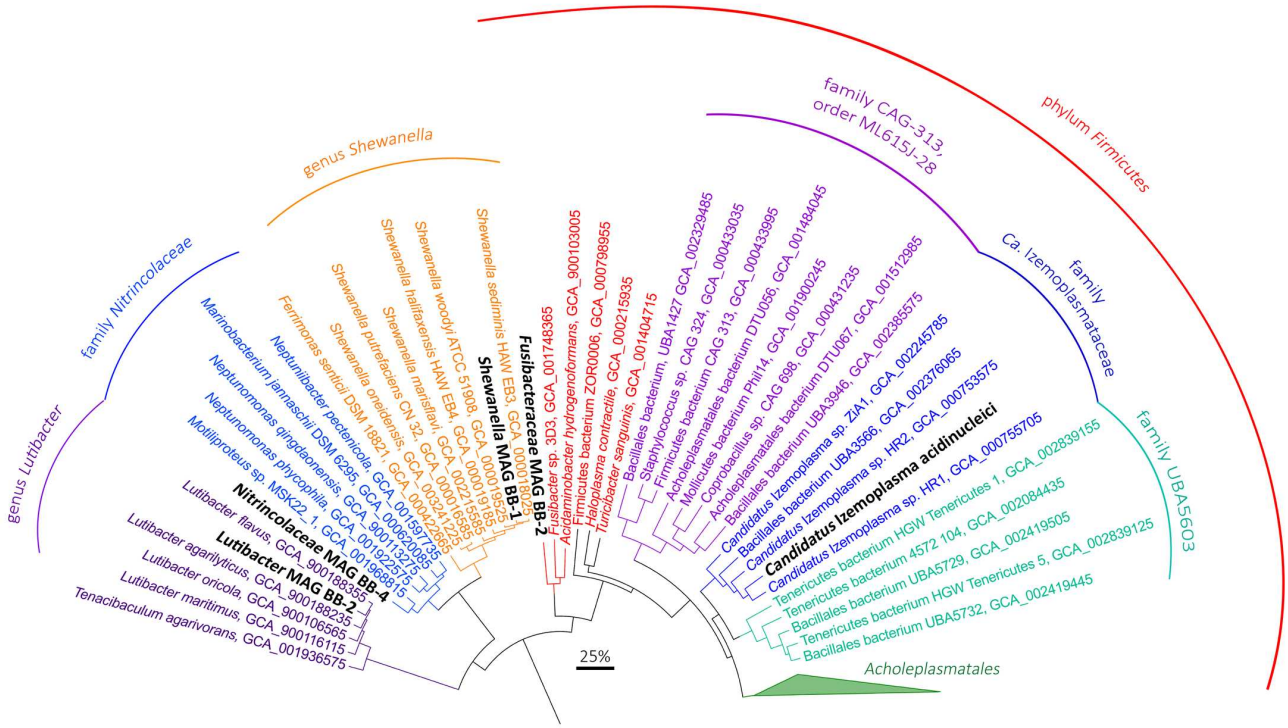

Fig. 2. Genome-based phylogeny using concatenated protein sequences derived from single copy marker genes retrieved from CheckM analyses. MAGs recovered in this study are highlighted in black and bold. The approximate maximum-likelihood tree was calculated using FastTree. The scale bar represents 25% sequence divergence.

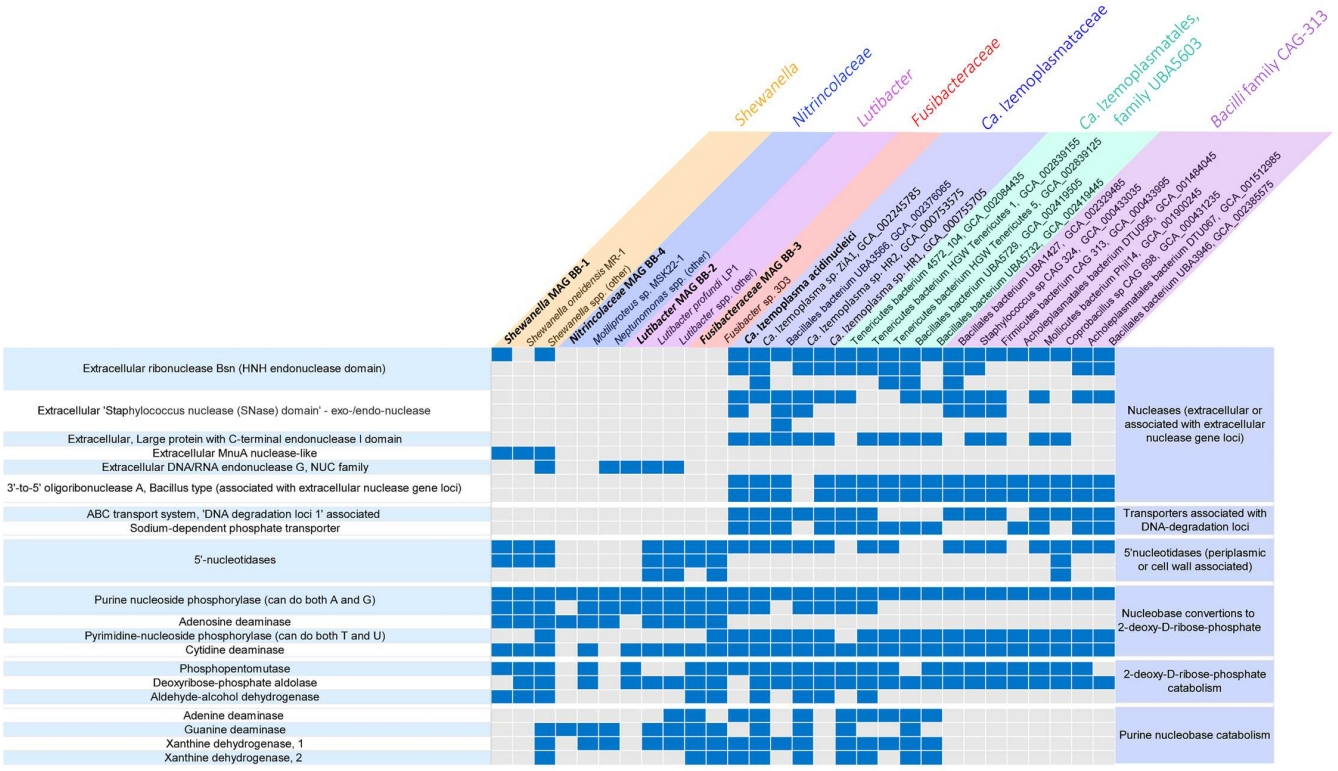

Fig. 3. Presence-absence of key genes for enzymes involved in DNA degradation, transport and catabolism of DNA sub-components in MAGs and genomes of selected isolates. A list of key annotations from MAGs identified in this study are listed in Supp. Table 3.

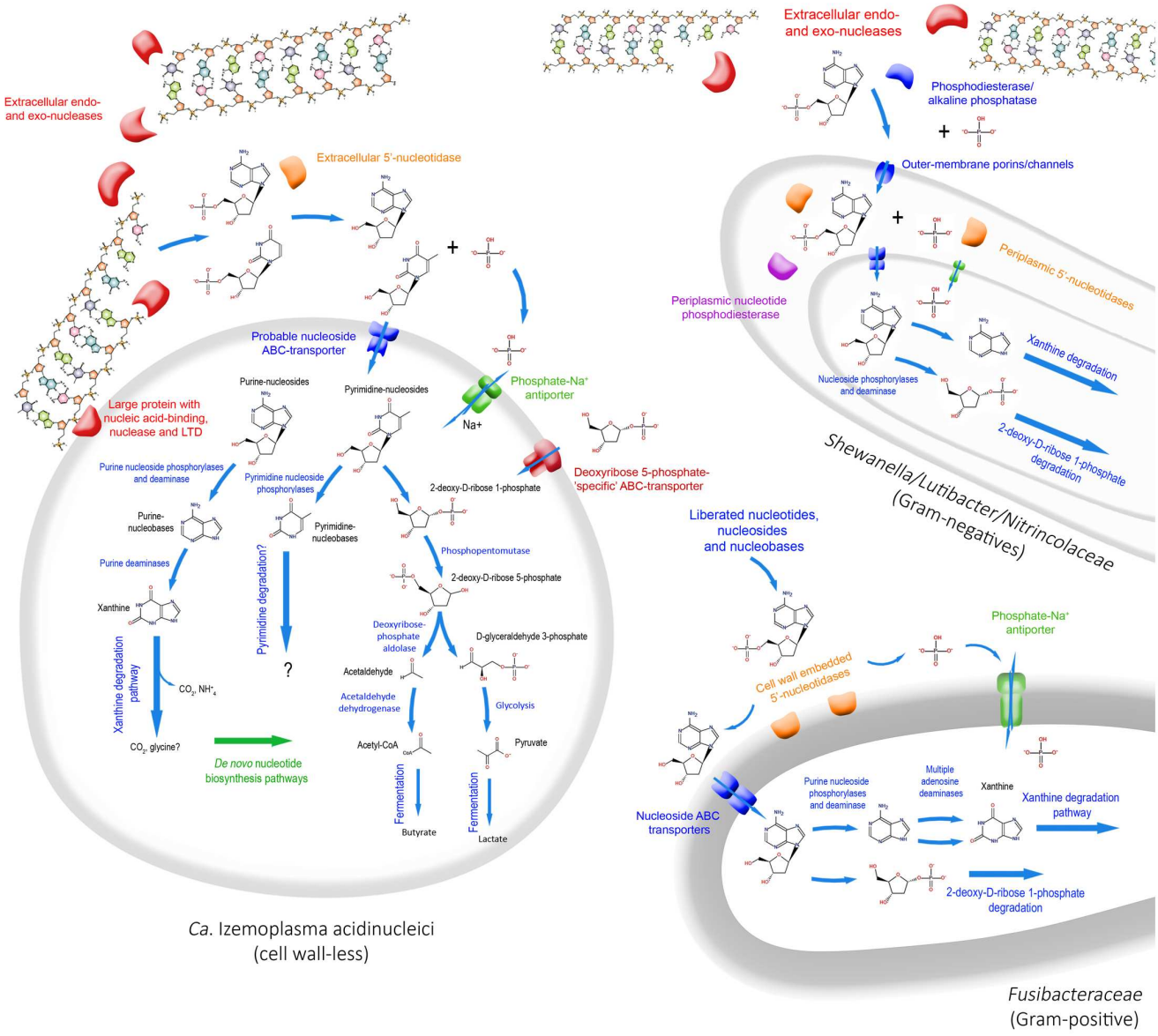

Fig. 4. Taxon-centric schematic depiction of key enzymes and other functional proteins related to DNA catabolism and transport annotated from MAGs and close relatives. More detailed pathways for catabolism of DNA sub-components are provided for *Ca.* Izemoplasma acidinucleici, and for clarity, simplified versions of these redundant pathways are provided as arrows for the other organisms. LTD = Lamin tail domain. DNA molecule structures were sourced and modified from Wikipedia, and are under the Creative Commons license.

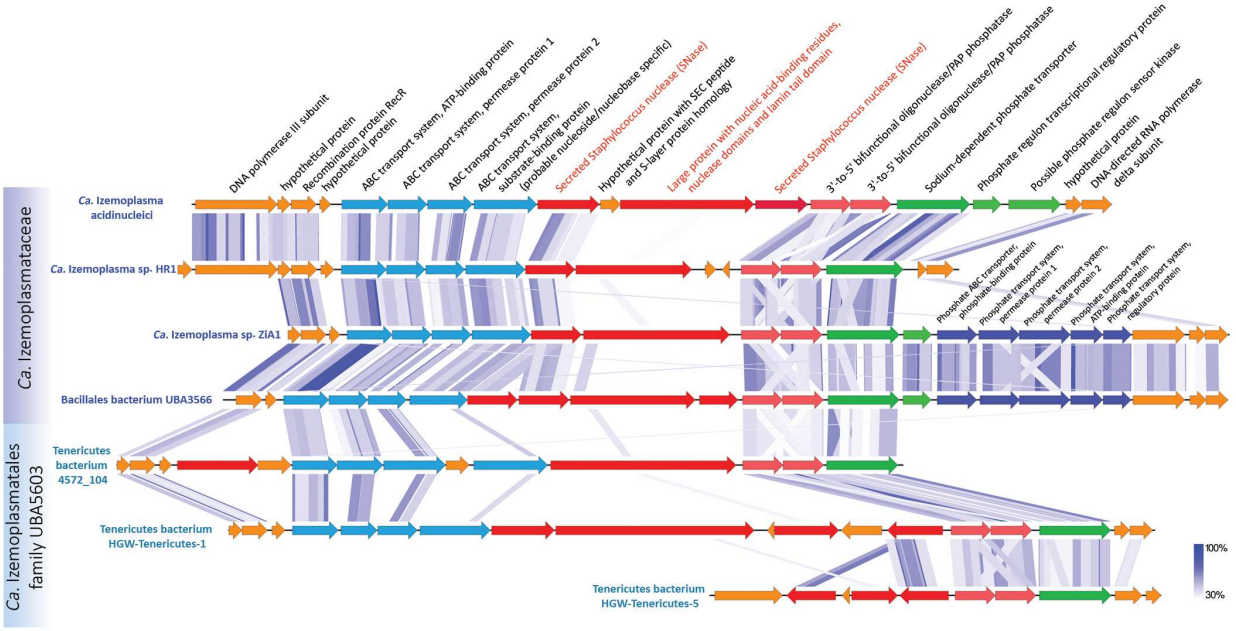

Fig 5. Gene arrangements of a putative 'DNA-degradation loci' in *Ca.* Izemoplasmatales MAGs. Shaded blue lines show regions with high sequence similarity and synteny as determined by tBLASTx using EasyFig. DNA-binding domains were predicted based on NCBI Conserved Domains (via BLASTP). Proteins predicted to be secreted are highlighted and labelled in red. Only scaffolds from MAGs with all or most genes present are included.

Concluding discussion

The aim of this thesis was to obtain a better understanding of the ecology and ecosystem function of sulfate-reducing microorganisms (SRM) and other key microorganisms that are involved in necromass degradation in arctic marine sediments. The investigations performed during this thesis employed next generation sequencing (NGS) to reveal community dynamics along environmental gradients and monitor the response of individual microorganisms in sediment microcosms supplemented with diverse stable isotope-labelled or unlabelled substrates. NGS of 16S rRNA genes to profile microbial communities has become routine in the field of microbial ecology (Franzosa *et al.*, 2015; Tremblay *et al.*, 2015; Parada *et al.*, 2016). However, until recently, NGS studies targeting genes that code for defined metabolic functions, such as *dsrB* as a marker for sulfur dissimilating microorganisms, were still rare mainly due to a lack of taxonomically classified reference databases and established workflows for sequence processing and analysis. The earlier introduction of a comprehensive DsrAB reference database was an important advancement for investigations of SRM diversity, distribution and ecosystem function (Müller *et al.*, 2015). The work presented in this thesis built upon the developed reference database and led to the development of a NGS sequencing and analysis pipeline for reductive bacterial-type *dsrA* and *dsrB* amplicons (Chapter 1). The Illumina Miseq system that was utilized provided 300 bp paired-end reads. Therefore, it was possible to merge overlapping *dsrB* sequencing reads (amplicon length: ~330 bp), whereas non-overlapping *dsrA* reads (amplicon length: ~730 bp) had to be rigorously filtered and combined into scaffolds (Herbold *et al.*, 2016). These differences in sequence processing resulted in significantly more *dsrB* amplicon data. Therefore, NGS-based SRM diversity analyses presented in Chapter 2 and 4 of this thesis were performed with *dsrB* as a target.

The whole pipeline of *dsrA* and *dsrB* amplicon generation and sequencing, as well as sequence processing and classification, was precisely evaluated with two complex mock communities. This enabled detailed investigations of errors that accumulated during amplicon generation and sequencing (Schirmer *et al.*, 2015; Herbold *et al.*, 2016). Notably, the mock communities consisted of 45 and 90 known *dsrAB* sequences from environmental clones. These were representative for a large part of the known diversity of reductive bacterial-type DsrAB and were amended in different quantities to mimic the uneven relative abundance distribution of a natural microbial community. The evaluations indicated that increased numbers of PCR cycles in the first amplification of *dsrA* and *dsrB*, i.e., during the two-step barcoding procedure (Herbold *et al.*, 2016), resulted in inadequate recovery of the mock community composition. Initial amplification of *dsrA* and *dsrB* was performed with highly degenerate primers, which are known to selectively amplify individual gene variants contained in PCR templates (Polz

and Cavanaugh, 1998). Therefore, it was concluded that the number of PCR-cycles during initial amplification of *dsrA* and *dsrB* should be kept as low as possible. Furthermore, *in silico* testing revealed that evolutionary placement of *dsrA* and *dsrB* sequences into the DsrAB reference phylogeny is a very valuable approach to accurately classify novel SRM, i.e., less than 80 % nucleic acid sequence similarity to any sequence in the reference database. Highly accurate classification in particular of taxa that are poorly represented in the reference taxonomy, is a key feature of the evolutionary placement algorithm (Berger *et al.*, 2011). This algorithm was recently also implemented into a combined classification approach for *nifH* NGS data (Angel *et al.*, 2018). The developed *dsrB* NGS pipeline was subsequently used to investigate the distribution and function of SRM in arctic marine sediments in Chapters 2 and 4 of this thesis. Furthermore, the approach presented in Chapter 1 was utilized to investigate acetate and propionate degrading *Syntrophobacteraceae* in rice paddy soils (Liu and Conrad, 2017; Liu *et al.*, 2018) and to reveal the effect of SRM community composition on sulfur isotope fractionation (Colangelo *et al.*, submitted).

The microbial reduction of sulfate is a key driver of the sulfur cycle in marine sediments (Froelich *et al.*, 1979; Bowles *et al.*, 2014). In shelf sediments in which SRM are responsible for about 50 % of total carbon mineralization (Jørgensen, 1982), organic matter-degrading microorganisms are most active in shallow sediment layers, where concentrations of sulfate and the supply of labile organic matter are highest (Røy *et al.*, 2012; Flury *et al.*, 2016). By combining *dsrB* and 16S rRNA amplicon sequence analyses, it was revealed that in sediments influenced by glacier run-off surface dwelling microbial communities were also found in deeper sediment layers (Chapter 2). This was most likely explained by rapid burial of surface-derived microbial communities under high amounts of inorganic material. These buried microbial assemblages remained active throughout the depth of the sediment cores, as indicated by high sulfate reduction rates six meters below the seafloor. The activity of SRM in deep glacier-proximal sediments required concurrently high activities of hydrolyzers and fermenters to sustain them (Arndt *et al.*, 2013), but it remained unclear which sources of organic matter were available for these heterotrophic microorganisms. Terrestrial organic matter, which was found in higher proportions in glacier-influenced sediments (Chapter 2), is very refractory and was thus less likely to be available for microbial degradation (Burdige, 2007; Wehrmann *et al.*, 2014). Furthermore, glacier-influenced sediments contained overall very low concentrations of total organic matter (Chapter 2), possibly because finer particles from glacial runoff caused high water turbidity, which resulted in reduced pelagic primary production (Etherington *et al.*, 2007). On the contrary, nutrient concentrations are elevated in glacier-influenced waters and grazing by zooplankton is reduced (J. M. Wçslawski and Legezytńska, 1998; Wadham *et al.*, 2013), thus promoting production. Therefore, it was hypothesized that glacier-influenced sediments receive low amounts of fresh and thus very reactive organic matter that is highly diluted and buried

rapidly with inorganic material (Bourgeois *et al.*, 2016). Similarly, low proportions of highly reactive organic matter might sustain the energy and carbon demands of microbial communities in deep glacier-influenced sediments investigated in Chapter 2.

A large part of the deeply buried sediment microbiota in glacier-influenced sediments were likely involved in sulfur cycling (Chapter 2). The most prevalent *dsrB*-harbouring microorganisms were *Deltaproteobacteria*. Furthermore, many of the *dsrB* OTUs were affiliated with the uncultured DsrAB family-level lineage 9 and an unclassified DsrAB cluster within the Environmental supercluster 1. These two enigmatic groups of DsrAB-harbouring microorganisms were recently linked to metagenome-derived genomes (MAGs) of the phyla *Acidobacteria* and *Chloroflexi*/*Planctomycetes*, respectively (Wasmund *et al.*, 2016; Anantharaman *et al.*, 2018). Representatives of these previously uncharacterized DsrAB lineages might contribute to sulfate reduction *in situ*, but might as well utilize the dissimilatory sulfate reduction pathway in reverse to oxidize sulfur, as suggested for *Acidobacteria* in wetlands (Hausmann et al., 2018).

Up to 95 % of the sulfide that is produced by SRM in marine sediments is eventually re-oxidized (Jørgensen, 1982; Canfield, 1989) by a combination of chemical and microbiological processes (Jørgensen and Nelson, 2004). Re-oxidation of sulfide was apparent in the investigated sediments, because sulfate reduction rates were high but sulfate was not depleted and sulfide never accumulated (Chapter 2). Chemical sulfide oxidation in glacier-influenced sediments was likely mediated by Fe(III) or Mn(IV) derived from glacial run-off, which likely resulted in the production of sulfur cycle intermediates such as S^0, polysulfides, SO_3^{2-} and $S_2O_3^2$ (Wehrmann *et al.*, 2017). Furthermore, glacier-influenced sediments harboured microbial taxa that comprised known sulfur-oxidizers (Chapter 2), i.e., candidate genus PHOS-HE36 (phylum *Ignavibacteriae*) (Koenig *et al.*, 2005), the *Woeseiaceae*/JTB255 sediment group (*Gammaproteobacteria*) (Dyksma *et al.*, 2016; Mußmann *et al.*, 2017), the *Rhodobacteriaceae* (*Alphaproteobacteria*) (Lenk *et al.*, 2012; Thrash *et al.*, 2017) and the genus *Sulforovum* (phylum *Campylobacterota*) (Inagaki, 2004). These putative sulfur-oxidizing microorganisms might have utilized chemically produced sulfur cycle intermediates as electron donors (Ghosh and Dam, 2009; Pjevac *et al.*, 2014; Dahl, 2017), but it remained unclear which electron acceptors were used for energy conservation. Oxygen and nitrate were presumably depleted within the first centimeters (Froelich *et al.*, 1979), but Mn(IV), which is found at elevated concentrations in glacier-influenced sediments (Wehrmann *et al.*, 2014), might have been used as an electron acceptor during the oxidation of elemental sulfur (Lovley and Phillips, 1994). Since the concentration of Mn(IV) was not determined in Chapter 2, its contribution to biotic sulfur-oxidation remains unknown. In contrast, the availability of Fe(III) in the investigated sediments was indicated by high concentrations of ferrous iron (Fe^{2+}) (Chapter 2), which was likely the product of biological iron reduction (Lovley *et al.*, 2004). Fe(III) might serve as electron acceptor during biological sulfur oxidation, but experimental evidence for this oxidation-reduction reaction is not available. Alternatively,

chemically produced sulfur cycle intermediates could have been disproportionated to sulfate and sulfide (Krämer and Cypionka, 1989; Thamdrup *et al.*, 1993; Finster *et al.*, 1998; Riedinger *et al.*, 2017). The majority of described sulfur disproportionators are, however, affiliated with the class *Deltaproteobacteria* (Wasmund et al., 2017). Hence, sulfur disproportionation is unlikely to explain high abundances of taxa affiliated to typical sulfur-oxidizing microorganisms in glacier-influenced sediments investigated in Chapter 2.

In contrast to glacier-influenced sediments in which sulfate reduction rates and concentrations of sulfate remained high to a depth of six meters below the seafloor, sediments from the continental shelf of Greenland displayed clear chemical gradients with increasing depth, i.e., the pore water concentration of sulfate decreased whereas the concentration of methane increased. These gradual changes in pore water chemistry strongly affected microbial community composition (Chapter 2), i.e., taxa that were affiliated with typical subsurface fermenters and acetogens increased their relative abundances with increasing depth, which suggested a switch away from a respiration-based metabolism to fermentation and acetogenesis. Pore water analyses from the same sediment cores showed that sulfate was only depleted at the very bottom of the core from shelf sediments and that all VFAs were always mineralized to CO_2 (Glombitza *et al.*, 2015). This means that respiration-based metabolisms also dominated in the energy limited subsurface. Therefore, depth-related microbial community changes were less likely explained by changing dominant metabolisms but rather by a selection for microorganisms that are adapted to conserving energy from very low amounts available energy (Petro *et al.*, 2017).

Marine sediments can be very dynamic and complex systems, both on a temporal and spatial scale, which can complicate *in situ* investigations of organic matter degradation processes and the involved microorganisms (Cravo-Laureau and Duran, 2014). Unsteady conditions in arctic marine sediments are mainly related to yearly light and temperature fluctuations, which lead to episodic organic matter inputs during a few blooming events in summer (Hebbeln and Wefer, 1991; Sørensen *et al.*, 2015). Microcosms experiments can reduce this environmental complexity, since stable incubation conditions can be maintained (Cravo-Laureau and Duran, 2014). To further investigate the taxa involved in sediment organic matter processing, sediment microcosms were amended with defined amounts of ^{13}C-labelled substrates, which enabled investigations of ^{13}C-carbon flow, e.g., into individual members of the microbial food web. In this thesis, microcosm experiments were performed with cyanobacterial necromass (Chapter 3), proteins, lipids and DNA (Chapter 4 and 5), as well as with acetate (Chapter 3), which together represented i) bulk organic matter, ii) some of the most abundant cellular macromolecules in marine sediments (Dell'Anno, 2005; Arndt *et al.*, 2013), and iii) the most important fermentation product acetate (Finke *et al.*, 2007), respectively.

Species-level 16S rRNA-OTUs of the taxa *Psychrilyobacter*, *Psychromonas*, *Marinifilum*, *Colwellia*, *Marinilabiaceae* and *Clostridiales* responded most strongly in incubations of a sulfidic Arctic (Svalbard) sediment sample with whole spirulina cell extract and thus represented the main hydrolzers and fermenters of cyanobacterial necromass (Chapter 3). *Psychrilyobacter*, *Psychromonas*, *Marinifilum* and *Clostridiales* increased in relative 16S rRNA gene abundance and also incorporated ^{13}C-carbon into their biomass, whereas *Colwellia* and *Marinilabiaceae* only increased in relative 16S rRNA transcript abundances. These analyses thus revealed different ecological strategies to cope with episodic supplies of organic matter that can occur in arctic marine sediments (Hebbeln and Wefer, 1991). Microorganisms either responded to substrate supply by high abundance increases (Teira *et al.*, 2007; Newton *et al.*, 2013), which might explain low initial abundances and fast growth of several hydrolzers and fermenters identified in this thesis, or by non-growth activity (Hausmann *et al.*, 2016, 2019). The latter ecological strategy is not well understood, but might be explained by lack of certain nutrients, or stress response, e.g., due to inadequate salinity or oxygen concentrations, which deviates ATP away from growth (Hausmann *et al.*, 2019).

The majority of hydrolzers and fermenters of cyanobacterial necromass were also discovered in incubations with individual macromolecules, which enabled an assignment of functional roles to specific microbial community members. *Psychrilyobacter* took-up much of the ^{13}C-carbon from the added proteins and was thus likely involved in protein degradation (Figure 6). However, although the genome of *Psychrilyobacter* encoded metabolic routes for amino acid catabolism, it did not encode a conventional secretion system for peptidases. This indicated that *Psychrilyobacter* species might be ‘cheaters’ (Velicer, 2003), i.e., depend on other hydrolyzers that liberate peptides and amino acids from proteins. This strategy could be widespread among *Fusobacteria*, since representatives of this phylum are generally not known to secrete extracellular enzymes (Kapatral *et al.*, 2003). Different subspecies of *Psychromonas* (16S rRNA sequence identity higher than 99 %) preferred either proteins or lipids as substrates. The metabolic versatility of this genus might explain its environmental success and the positive correlations of representative of this genus to phytodetritus inputs into marine sediments (Bienhold *et al.*, 2011). The MAG of a lipid-degrading *Psychromonas* strain encoded genes for a secreted esterase, an uptake mechanisms for long-chain fatty acids and the catabolism of fatty acids via beta-oxidation. The metabolic potential of protein-degrading *Psychromonas* strains remains to be investigated. The species-level *Clostridia* 16S rRNA-OTUs identified in Chapter 3 were all related to the family *Fusibacteraceae*. Other representatives of this family were involved in protein (Chapter 4) and DNA (Chapter 5) degradation (Figure 6). No MAGs from protein-degrading *Fusibacteraceae* were recovered, but the analyses presented in Chapter 5 indicated that DNA-degrading *Fusibacteraceae* might feed on nucleosides liberated by other primary degraders of high-molecular-weight DNA. *Marinifilum* and *Marinilabiaceae* were not identified in the

incubations with individual macromolecules, which might have been explained by their substrate preferences for carbohydrates (Na *et al.*, 2009; Ruvira *et al.*, 2013; Liu *et al.*, 2014). Even though *Colwellia* spp. can ferment amino acids (Techtmann *et al.*, 2016), they were not labelled in protein-amended incubations.

The incubations with specific macromolecules also revealed hydrolyzers and fermenters that were not found in incubations with cyanobacterial necromass, i.e., *Ca.* Izemoplasmatales, *Clostridia* (JTB215), *Lutibacter*, *Nitrincolaceae*, *Photobacterium, Shewanella* and *Vibrio* (Figure 6). The MAGs from the clostridial JTB215 sediment group and the candidate order *Ca.* Izemoplasmatales provided first insights into the roles of these enigmatic bacteria in arctic marine sediments. *Clostridia* (JTB215) incorporated ^{13}C-carbon in protein and lipid amended incubations and a related MAG encoded an array of extracellular peptidases, esterases and lipases (Figure 6). Further analyses indicated a substrate preference of these microorganisms for branched chain amino acids and glycerol. Additionally, *Clostridia* (JTB215) were inhibited by molybdate. Since sulfur metabolism genes were not identified in the genome of this bacterium, *Clostridia* (JTB215) might heavily depend on SRM to keep fermentation products at low concentration (McInerney *et al.*, 2008). *Ca.* Izemoplasmatales are likely specialised on DNA degradation in marine sediments (Figure 6), possibly on a global scale (Chapter 5). Representatives of the clostridial JTB215 sediment group and the candidate order *Ca.* Izemoplasmatales likely liberated oligomers and monomers from macromolecules in the incubations performed in this thesis with a diverse array of hydrolases (Figure 6). These *Firmutes* might release comparably higher amounts of hydrolases because these enzymes only have to cross one membrane, i.e., via the SEC pathway (van Wely *et al.*, 2001). Other MAGs recovered from DNA-supplemented microcosms were related to the genera *Lutibacter* and *Shewanella*, which confirmed the ability of these groups to degrade DNA under *in situ*-like conditions (Choi and Cho, 2006; Pinchuk *et al.*, 2008). Furthermore, the ^{13}C-enrichment of *Photobacterium* and *Vibrio* species in protein and lipid amended incubations, respectively, was in agreement with the physiological capabilities of closely related isolates (Wang *et al.*, 2011; Zhang *et al.*, 2015; Li *et al.*, 2017). The role of *Nitrincolaceae*, which incorporated ^{13}C-carbon during DNA degradation remains, however, elusive because no MAGs from this group were obtained and isolated members of *Nitrincolaceae* are known to degrade carbohydrates, alcohols, organic acids and complex polycyclic aromatic hydrocarbons but not DNA, nucleotides, or nucleosides (Diéguez *et al.*, 2017).

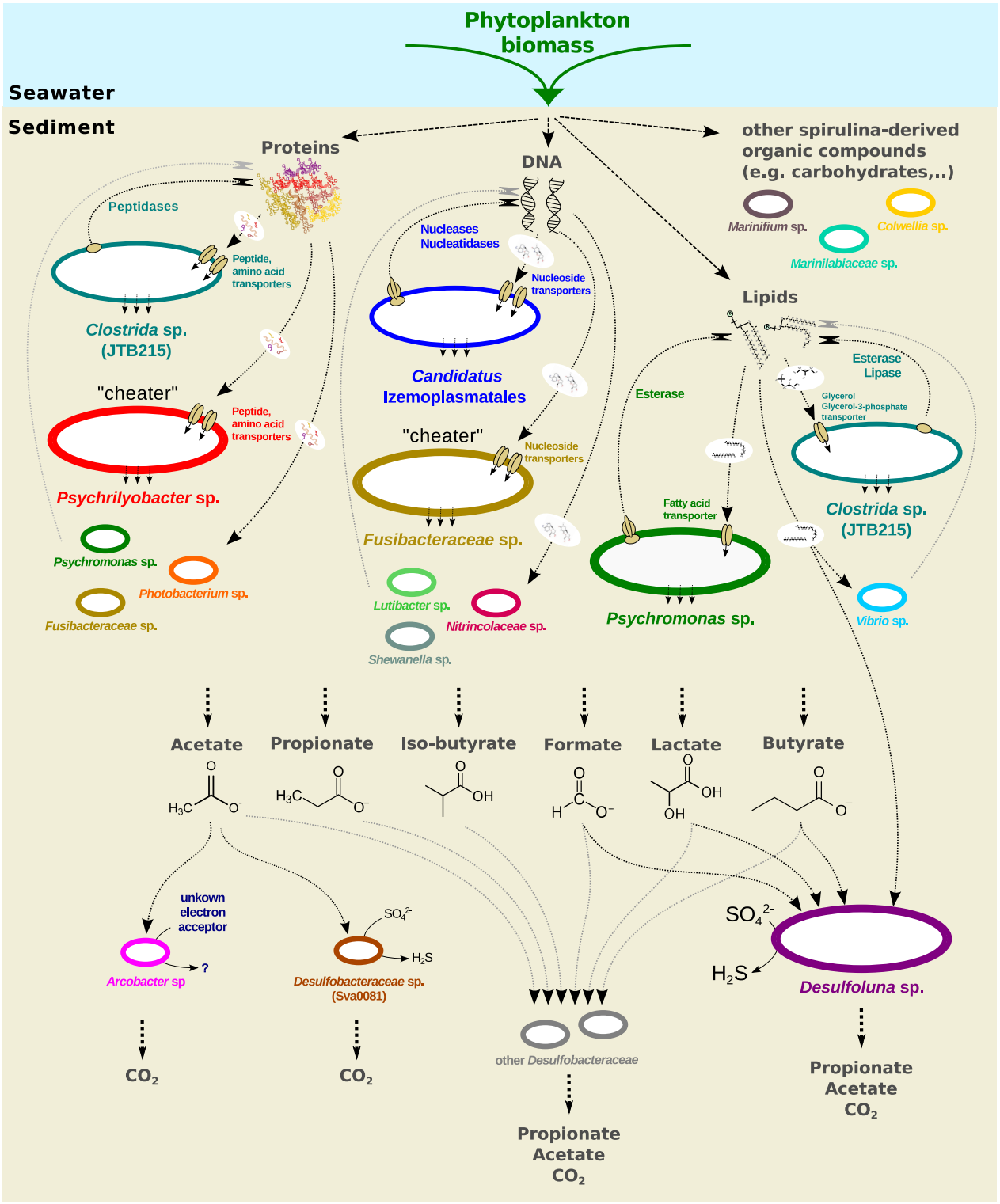

Figure 6. Identity and function of key organic matter degraders in anaerobic arctic marine sediments. The model summarizes the results from Chapters 3-5 of this thesis. Phytoplankton biomass from pelagic primary production settles to the seafloor and is degraded by a complex consortium of hydrolyzers and fermenters, which hydrolyze macromolecules extracellularly and liberate oligomers and monomers. These macromolecule subcomponents are incorporated and subsequently fermented to volatile fatty acids and lactate, which serve sulfate reducing microorganisms and other terminal mineralizers as substrates. Large cells indicate microorganisms that were represented by metagenome assembled genomes (MAGs), which enabled a detailed analysis of the metabolic capabilities of the respective microorganism. Exceptions are cells labelled as *Lutibacter* and *Shewanella* sp., since isolated representatives of these genera are described DNA degraders. Small cells indicate microorganisms that were only represented by OTU sequences. The metabolic capabilities of these microorganisms were inferred from differential relative abundance between incubation treatments, chemical analyses and ^{13}C-substrate incorporation.

Even though proteolysis was proposed to be an important trait of some sediment *Archaea* affiliated with the phylum *Bathyarchaeota* (Lloyd et al., 2013), none of the organic matter hydrolyzers and fermenters identified in this thesis were affiliated with the domain *Archaea*. Whole community investigations showed that overall abundance of *Archaea* was low and *Bathyarchaeota* abundance never reached >1% of the microbial community at any station/depth (Chapter 2). This was despite the utilization of universal 16S rRNA primers, i.e., U519F and 802R (Klindworth *et al.*, 2013), which cover 68.6 % of all *Bathyarchaeota*. Low *Bathyarchaeota* abundances might still reflect a bias of the utilized 16S rRNA gene primers against the representatives of this phylum in the sediments investigated in this thesis. Nonetheless, screening of a *Bathyarchaeota* MAG that was recovered from protein amended incubations did not reveal any extracellular peptidases (data not shown). Together, this data indicated that *Bathyarchaeota* played a minor role during protein degradation in the sediment microcosm incubations performed in Chapter 4. *Bathyarchaeota*, which are known to be 'deep' sediment specialists that persist under low energy conditions (Starnawski *et al.*, 2017), may be adapted for 'slow' protein degradation under low energy conditions, and therefore may have been missed by relatively short incubation experiments.

Hydrolysis and fermentation of added macromolecules lead to the development of volatile fatty acids (VFAs) and lactate (Figure 6), as well as other fermentation products that were not specifically analyzed in this thesis, e.g., ethanol, H_2 and CO_2. Reduced compounds such as VFAs are considered primary substrates for SRM in marine sediments (Arndt *et al.*, 2013). In microcosm incubations in which sulfate reduction was inhibited by molybdate, VFAs and lactate accumulated (Chapter 3 and 4), which confirmed the immediate control that SRM activity exerts on the concentration of these compounds (Finke *et al.*, 2007). Interestingly, the dynamics of VFA accumulation differed greatly between the incubations amended with whole spirulina cell extract and incubations amended with proteins and lipids. In molybdate-inhibited incubations amended with whole spirulina cell extract, lactate and all measured VFAs, including acetate and propionate, accumulated (Chapter 3). In contrast, in molybdate-inhibited incubations amended with protein and lipids, concentrations of propionate and acetate were lowest and only formate, butyrate, iso-butyrate and lactate accumulated over time (Chapter 4). This was surprising, because sulfate-reduction inhibition experiments with marine sediments usually result in high accumulations of acetate, which lead to the perception that acetate is among the most important electron acceptors for SRM (Fukui *et al.*, 1997; Finke *et al.*, 2007). The major difference between the two incubation experiments performed in Chapter 3 and 4 was the geographic location of the utilized sediments, i.e., Svalbard and Greenland, respectively. These results thus indicated an unusual physiology of the most responsive SRM from arctic marine sediments from Greenland, which has to be further investigated. Alternatively, it could signify that other terminal oxidizing guilds

were present in the Greenland sediments that may have used other electron acceptors, e.g., metal oxides.

Complementary incubations of sediment from Svalbard with acetate confirmed that SRM related to *Desulfobacteraceae* (Sva0081) became very active and thus likely utilized acetate to drive respiration (Chapter 3; Figure 6). Intriguingly, cellular activity of *Desulfobacteraceae* (Sva0081), as indicated by increases in relative 16S rRNA transcript abundance, did not result in overall population growth. Accordingly, incorporation of ^{13}C-carbon into *Desulfobacteraceae* (Sva0081) biomass was very low. This indicated that dominant SRM in arctic marine sediments from Svalbard might use energy conserved from acetate oxidation mainly for cellular maintenance (Rabus *et al.*, 2013), and thereby retain stable population sizes (Robador *et al.*, 2009). Investigation of ^{13}C-carbon incorporation in Chapter 3 employed stable isotope labeling in combination with catalyzed reporter deposition fluorescence *in situ* hybridization (CARD-FISH) and Raman microspectroscopy. This approach might not have been sensitive enough to detect acetate incorporation, since incubation experiments with acetate in tidal-flat sediments, which relied on radioactive labelling in combination with CARD-FISH and flow-sorting, revealed that similar *Desulfobacteraceae* incorporated high amounts of acetate (Dyksma *et al.*, 2018). In contrast to SRM, *Arcobacter* species responded with particularly high relative abundance increases in acetate-amended arctic sediment microcosms (Chapter 3). *Arcobacter* might utilize manganese, iron or nitrate as electron acceptors (Thamdrup *et al.*, 2000; Vandieken *et al.*, 2012; Canion *et al.*, 2013; Vandieken and Thamdrup, 2013), which likely enabled higher energy yields than the use of sulfate (Froelich *et al.*, 1979; LaRowe and Amend, 2014), and thus lead to population growth during acetate oxidation. The dominant SRM in protein and lipid amended microcosms, i.e., *Desulfoluna*, increased their population size during substrate incubations, as indicated by relative 16S rRNA gene abundance increase. Formate, lactate and butyrate constituted major substrates for the SRM in protein and lipid amended microcosms, with potential contributions from long-chain fatty acids (Figure 6). Besides the two SRM populations discussed above, the analyses presented in this thesis also identified other *Deltaproteobacteria*-related microorganisms that likely contributed to organic matter mineralization in arctic marine sediment microcosms (Figure 6).

Future research

The investigations performed in this thesis revealed links between microbial species and specific ecological functions in arctic marine sediments and enabled the proposal of metabolic pathways for the degradation of specific macromolecules. However, further investigations will have to confirm that the proposed pathways for extracellular macromolecule degradation, as well as for transport and intracellular degradation of oligomers and monomers are indeed transcribed and translated under experimental and/or *in situ* conditions. Furthermore, by monitoring macromolecule degradation using fluorescently labelled substrates (Arnosti, 2003) and analyzing concentrations of liberated oligomers and monomers, novel insights about the synchronization of individual steps of the organic matter degradation cascade could be obtained. Further research will also require to investigate the activity of identified microorganisms *in situ*, e.g., following a phytoplankton blooming event in summer. Metabolic activity of the identified microorganisms and their extracellular peptidases, lipases, esterases and nucleases could be tested via enzyme assays or metatranscriptomics (Lloyd *et al.*, 2013; Zinke *et al.*, 2018). Similar investigations might also reveal the *in situ* activity of primary hydrolyzers in glacier-influenced sediments investigated in Chapter 2, with potential implementations for suggested long-term carbon storage in fjord sediments (Smith *et al.*, 2015). If novel laboratory incubations are performed, the incubation conditions could be modified to specifically target *Archaea*. Representatives of this domain were not identified in protein incubations performed in Chapter 4 of this thesis, which was despite the fact that many sediment *Archaea* have the metabolic capacities for peptide and amino acid degradation (Lloyd *et al.*, 2013; Lazar *et al.*, 2016, 2017; Seitz *et al.*, 2016; Marshall *et al.*, 2017). Incubations with low substrate concentrations maintained for several month or even years might reveal protoelytic activities of some of these archaeal lineages, which constitute inhabitants of the energy limited sediment subsurface (Petro *et al.*, 2017; Starnawski *et al.*, 2017).

The ecological and physiological interpretations of microorganisms in glacier-influenced sediments were purely based on 16S rRNA and *dsrB* amplicon sequencing data in combination with chemical and physical analyses. Further investigation of the microbial community that thrives in glacier-influenced sediments in the Godthåbsfjord in Greenland thus should employ more advanced analyses, e.g., metagenomics and metatranscriptomics. Thereby, the metabolic potential and activity of microorganisms in glacier-influenced sediments could be investigated more accurately. *In situ* analyses across sediment depth at the 4 sampling stations investigated in Chapter 2 or laboratory incubations with different sulfur compounds could for example give novel insights into the ecology of SRM from uncultured DsrAB clades. This might reveal the physiological capabilities of representatives of the uncultured DsrAB family-level lineage 9,

which constituted up to 25 % of the total *dsrB* abundance in glacier-influenced sediments and were recently linked to the phylum *Acidobacteria* (Anantharaman et al., 2018). Furthermore, many *dsrB* sequences that were highly abundant in glacier-influenced sediments belonged to DsrAB clades of completely unknown phylogenetic affiliation, i.e., representatives of the uncultured DsrAB family-level lineage 3, 4 and 7, as well as of uncultured bacteria from the *Nitrospira* supercluster. Novel MAGs from glacier-influenced sediments might reveal the identity of some of these enigmatic clades. Furthermore, investigating the genomic potential of putative sulfur-oxidizers in combination with physiological analyses could reveal the contribution of these microorganisms to sulfur cycling in glacier-influenced marine sediments.

References

Anantharaman, K., Hausmann, B., Jungbluth, S.P., Kantor, R.S., Lavy, A., Warren, L.A., et al. (2018) Expanded diversity of microbial groups that shape the dissimilatory sulfur cycle. *ISME J.* **12**: 1715–1728.

Angel, R., Nepel, M., Panhölzl, C., Schmidt, H., Herbold, C.W., Eichorst, S.A., and Woebken, D. (2018) Evaluation of Primers Targeting the Diazotroph Functional Gene and Development of NifMAP – A Bioinformatics Pipeline for Analyzing nifH Amplicon Data. *Front. Microbiol.* **9**: 703.

Arndt, S., Jørgensen, B.B., LaRowe, D.E., Middelburg, J.J., Pancost, R.D., and Regnier, P. (2013) Quantifying the degradation of organic matter in marine sediments: A review and synthesis. *Earth-Sci. Rev.* **123**: 53–86.

Arnosti, C. (2003) Fluorescent derivatization of polysaccharides and carbohydrate-containing biopolymers for measurement of enzyme activities in complex media. *J. Chromatogr. B Analyt. Technol. Biomed. Life Sci.* **793**: 181–191.

Berger, S.A., Krompass, D., and Stamatakis, A. (2011) Performance, accuracy, and Web server for evolutionary placement of short sequence reads under maximum likelihood. *Syst. Biol.* **60**: 291–302.

Bienhold, C., Boetius, A., and Ramette, A. (2011) The energy–diversity relationship of complex bacterial communities in Arctic deep-sea sediments. *ISME J.* **6**: 724–732.

Bourgeois, S., Kerhervé, P., Calleja, M.L., Many, G., and Morata, N. (2016) Glacier inputs influence organic matter composition and prokaryotic distribution in a high Arctic fjord (Kongsfjorden, Svalbard). *J. Mar. Syst.* **164**: 112–127.

Bowles, M.W., Mogollón, J.M., Kasten, S., Zabel, M., and Hinrichs, K.-U. (2014) Global rates of marine sulfate reduction and implications for sub-sea-floor metabolic activities. *Science* **344**: 889–891.

Burdige, D.J. (2007) Preservation of organic matter in marine sediments: controls, mechanisms, and an imbalance in sediment organic carbon budgets? *Chem. Rev.* **107**: 467–485.

Canfield, D.E. (1989) Reactive iron in marine sediments. *Geochim. Cosmochim. Acta* **53**: 619–632.

Canion, A., Prakash, O., Green, S.J., Jahnke, L., Kuypers, M.M.M., and Kostka, J.E. (2013) Isolation and physiological characterization of psychrophilic denitrifying bacteria from permanently cold Arctic fjord sediments (Svalbard, Norway). *Environ. Microbiol.* **15**: 1606–1618.

Choi, D.H. and Cho, B.C. (2006) Lutibacter litoralis gen. nov., sp. nov., a marine bacterium of the family Flavobacteriaceae isolated from tidal flat sediment. *Int. J. Syst. Evol. Microbiol.* **56**: 771–776.

Cravo-Laureau, C. and Duran, R. (2014) Marine coastal sediments microbial hydrocarbon degradation processes: contribution of experimental ecology in the omics'era. *Front. Microbiol.* **5**: 39.

Dahl, C. (2017) Sulfur Metabolism in Phototrophic Bacteria. In, *Modern Topics in the Phototrophic Prokaryotes*., pp. 27–66.

Dell'Anno, A. (2005) Extracellular DNA Plays a Key Role in Deep-Sea Ecosystem Functioning. *Science* **309**: 2179–2179.

Diéguez, A.L., Pichon, P., Balboa, S., Magnesen, T., and Romalde, J.L. (2017) Complete characterization of new isolates of Neptunomonas phycophila leads to emend its description and opens possibilities of biotechnological applications. *Microbiologyopen* **6**: e00519.

Dyksma, S., Bischof, K., Fuchs, B.M., Hoffmann, K., Meier, D., Meyerdierks, A., et al. (2016) Ubiquitous Gammaproteobacteria dominate dark carbon fixation in coastal sediments. *ISME J.* **10**: 1939–1953.

Dyksma, S., Lenk, S., Sawicka, J.E., and Mußmann, M. (2018) Uncultured and Account for Major Acetate Assimilation in a Coastal Marine Sediment. *Front. Microbiol.* **9**: 3124.

Etherington, L.L., Hooge, P.N., Hooge, E.R., and Hill, D.F. (2007) Oceanography of Glacier Bay, Alaska: Implications for biological patterns in a glacial fjord estuary. *Estuaries Coasts* **30**: 927–944.

Finke, N., Vandieken, V., and Jørgensen, B.B. (2007) Acetate, lactate, propionate, and isobutyrate as electron donors for iron and sulfate reduction in Arctic marine sediments, Svalbard. *FEMS Microbiol. Ecol.* **59**: 10–22.

Finster, K., Liesack, W., and Thamdrup, B. (1998) Elemental sulfur and thiosulfate disproportionation by Desulfocapsa sulfoexigens sp. nov., a new anaerobic bacterium isolated from marine surface sediment. *Appl. Environ. Microbiol* **64**: 119–125.

Flury, S., Røy, H., Dale, A.W., Fossing, H., Tóth, Z., Spiess, V., et al. (2016) Controls on subsurface methane fluxes and shallow gas formation in Baltic Sea sediment (Aarhus Bay, Denmark). *Geochim. Cosmochim. Acta* **188**: 297–309.

Franzosa, E.A., Hsu, T., Sirota-Madi, A., Shafquat, A., Abu-Ali, G., Morgan, X.C., and Huttenhower, C. (2015) Sequencing and beyond: integrating molecular “omics” for microbial community profiling. *Nat. Rev. Microbiol.* **13**: 360–372.

Froelich, P.N., Klinkhammer, G.P., Bender, M.L., Luedtke, N.A., Heath, G.R., Cullen, D., et al. (1979) Early oxidation of organic matter in pelagic sediments of the eastern equatorial Atlantic: suboxic diagenesis. *Geochim. Cosmochim. Acta* **43**: 1075–1090.

Fukui, M., Suh, J., Yonezawa, Y., and Urushigawa, Y. (1997) Major substrates for microbial sulfate reduction in the sediments of Ise Bay, Japan. *Ecological Research* **12**: 201–209.

Ghosh, W. and Dam, B. (2009) Biochemistry and molecular biology of lithotrophic sulfur oxidation by taxonomically and ecologically diverse bacteria and archaea. *FEMS Microbiol. Rev.* **33**: 999–1043.

Glombitza, C., Jaussi, M., Røy, H., Seidenkrantz, M.-S., Lomstein, B.A., and Jørgensen, B.B. (2015) Formate, acetate, and propionate as substrates for sulfate reduction in sub-arctic sediments of Southwest Greenland. *Front. Microbiol.* **6**: 846.

Hausmann, B., Knorr, K.-H., Schreck, K., Tringe, S.G., Glavina Del Rio, T., Loy, A., and Pester, M. (2016) Consortia of low-abundance bacteria drive sulfate reduction-dependent degradation of fermentation products in peat soil microcosms. *ISME J.* **10**: 2365–2375.

Hausmann, B., Pelikan, C., Herbold, C.W., Köstlbacher, S., Albertsen, M., Eichorst, S.A., et al. (2018) Peatland Acidobacteria with a dissimilatory sulfur metabolism. *ISME J.* **12**: 1729–1742.

Hausmann, B., Pelikan, C., Rattei, T., Loy, A., and Pester, M. (2019) Long-Term Transcriptional Activity at Zero Growth of a Cosmopolitan Rare Biosphere Member. *MBio* **10**: e02189–18.

Hebbeln, D. and Wefer, G. (1991) Effects of ice coverage and ice-rafted material on sedimentation in the Fram Strait. *Nature* **350**: 409–411.

Herbold, C.W., Pelikan, C., Kuzyk, O., Hausmann, B., Angel, R., Berry, D., and Loy, A. (2016) Corrigendum: A flexible and economical barcoding approach for highly multiplexed amplicon sequencing of diverse target genes. *Front. Microbiol.* **7**: 870.

Hernsdorf, A.W., Amano, Y., Miyakawa, K., Ise, K., Suzuki, Y., Anantharaman, K., et al. (2017) Potential for microbial H2 and metal transformations associated with novel bacteria and archaea in deep terrestrial subsurface sediments. *ISME J.* **11**: 1915–1929.

Inagaki, F. (2004) Sulfurovum lithotrophicum gen. nov., sp. nov., a novel sulfur-oxidizing chemolithoautotroph within the -Proteobacteria isolated from Okinawa Trough hydrothermal sediments. *Int. J. Syst. Evol. Microbiol.* **54**: 1477–1482.

J. M. Wçslawski, W. and Legezytńska, J. (1998) Glaciers caused zooplankton mortality? *J. Plankton Res.* **20**: 1233–1240.

Jørgensen, B.B. (1982) Mineralization of organic matter in the sea bed—the role of sulphate reduction. *Nature* **296**: 643–645.

Jørgensen, B.B. and Nelson, D.C. (2004) Sulfide oxidation in marine sediments: Geochemistry meets microbiology. In, *Special Paper 379: Sulfur Biogeochemistry - Past and Present*., pp. 63–81.

Kapatral, V., Ivanova, N., Anderson, I., Reznik, G., Bhattacharyya, A., Gardner, W.L., et al. (2003) Genome analysis of F. nucleatum sub spp vincentii and its comparison with the genome of F. nucleatum ATCC 25586. *Genome Res.* **13**: 1180–1189.

Klindworth, A., Pruesse, E., Schweer, T., Peplies, J., Quast, C., Horn, M., and Glöckner, F.O. (2013) Evaluation of general 16S ribosomal RNA gene PCR primers for classical and next-generation sequencing-based diversity studies. *Nucleic Acids Res.* **41**: e1.

Koenig, A., Zhang, T., Liu, L.-H., and Fang, H.H.P. (2005) Microbial community and biochemistry process in autosulfurotrophic denitrifying biofilm. *Chemosphere* **58**: 1041–1047.

Krämer, M. and Cypionka, H. (1989) Sulfate formation via ATP sulfurylase in thiosulfate- and sulfite-disproportionating bacteria. *Arch. Microbiol.* **151**: 232–237.

LaRowe, D. and Amend, J. (2014) Energetic constraints on life in marine deep sediments. In, Kallmeyer J And Wagner (ed), *Microbial Life of the Deep Biosphere.*, 1. De Gruyter, Berlin, pp. 279–302.

Lazar, C.S., Baker, B.J., Seitz, K., Hyde, A.S., Dick, G.J., Hinrichs, K.-U., and Teske, A.P. (2016) Genomic evidence for distinct carbon substrate preferences and ecological niches of Bathyarchaeota in estuarine sediments. *Environ. Microbiol.* **18**: 1200–1211.

Lazar, C.S., Baker, B.J., Seitz, K.W., and Teske, A.P. (2017) Genomic reconstruction of multiple lineages of uncultured benthic archaea suggests distinct biogeochemical roles and ecological niches. *ISME J.* **11**: 1058.

Lenk, S., Moraru, C., Hahnke, S., Arnds, J., Richter, M., Kube, M., et al. (2012) Roseobacter clade bacteria are abundant in coastal sediments and encode a novel combination of sulfur oxidation genes. *ISME J.* **6**: 2178–2187.

Liu, P. and Conrad, R. (2017) Syntrophobacteraceae-affiliated species are major propionate-degrading sulfate reducers in paddy soil. *Environ. Microbiol.* **19**: 1669–1686.

Liu, P., Pommerenke, B., and Conrad, R. (2018) Identification of Syntrophobacteraceae as major acetate-degrading sulfate reducing bacteria in Italian paddy soil. *Environ. Microbiol.* **20**: 337–354.

Liu, Q.-Q., Wang, Y., Li, J., Du, Z.-J., and Chen, G.-J. (2014) Saccharicrinis carchari sp. nov., isolated from a shark, and emended descriptions of the genus Saccharicrinis and Saccharicrinis fermentans. *Int. J. Syst. Evol. Microbiol.* **64**: 2204–2209.

Li, Y., Zhou, M., Wang, F., Wang, E.T., Du, Z., Wu, C., et al. (2017) Photobacterium proteolyticum sp. nov., a protease-producing bacterium isolated from ocean sediments of Laizhou Bay. *Int. J. Syst. Evol. Microbiol.* **67**: 1835–1840.

Lloyd, K.G., Schreiber, L., Petersen, D.G., Kjeldsen, K.U., Lever, M.A., Steen, A.D., et al. (2013) Predominant archaea in marine sediments degrade detrital proteins. *Nature* **496**: 215–218.

Lovley, D.R., Holmes, D.E., and Nevin, K.P. (2004) Dissimilatory Fe(III) and Mn(IV) Reduction. In, Advances in Microbial Physiology. Elsevier, pp. 219–286.

Marshall, I.P.G., Starnawski, P., Cupit, C., Fernández Cáceres, E., Ettema, T.J.G., Schramm, A., and Kjeldsen, K.U. (2017) The novel bacterial phylum Calditrichaeota is diverse, widespread and abundant in marine sediments and has the capacity to degrade detrital proteins. *Environ. Microbiol. Rep.* **9**: 397–403.

McInerney, M.J., Struchtemeyer, C.G., Sieber, J., Mouttaki, H., Stams, A.J.M., Schink, B., et al. (2008) Physiology, Ecology, Phylogeny, and Genomics of Microorganisms Capable of Syntrophic Metabolism. *Ann. N. Y. Acad. Sci.* **1125**: 58–72.

Müller, A.L., Kjeldsen, K.U., Rattei, T., Pester, M., and Loy, A. (2015) Phylogenetic and environmental diversity of DsrAB-type dissimilatory (bi)sulfite reductases. *ISME J.* **9**: 1152–1165.

Mußmann, M., Pjevac, P., Krüger, K., and Dyksma, S. (2017) Genomic repertoire of the Woeseiaceae/JTB255, cosmopolitan and abundant core members of microbial communities in marine sediments. *ISME J.* **11**: 1276–1281.

Na, H., Kim, S., Moon, E.Y., and Chun, J. (2009) Marinifilum fragile gen. nov., sp. nov., isolated from tidal flat

sediment. *Int. J. Syst. Evol. Microbiol.* **59**: 2241–2246.

Nealson, K.H. and Saffarini, D. (1994) Iron and manganese in anaerobic respiration: environmental significance, physiology, and regulation. *Annu. Rev. Microbiol.* **48**: 311–343.

Newton, R.J., Huse, S.M., Morrison, H.G., Peake, C.S., Sogin, M.L., and McLellan, S.L. (2013) Shifts in the microbial community composition of Gulf Coast beaches following beach oiling. *PLoS One* **8**: e74265.

Parada, A.E., Needham, D.M., and Fuhrman, J.A. (2016) Every base matters: assessing small subunit rRNA primers for marine microbiomes with mock communities, time series and global field samples. *Environ. Microbiol.* **18**: 1403–1414.

Petro, C., Starnawski, P., Schramm, A., and Kjeldsen, K.U. (2017) Microbial community assembly in marine sediments. *Aquat. Microb. Ecol.* **79**: 177–195.

Pinchuk, G.E., Ammons, C., Culley, D.E., Li, S.-M.W., McLean, J.S., Romine, M.F., et al. (2008) Utilization of DNA as a sole source of phosphorus, carbon, and energy by Shewanella spp.: ecological and physiological implications for dissimilatory metal reduction. *Appl. Environ. Microbiol.* **74**: 1198–1208.

Pjevac, P., Kamyshny, A., Jr, Dyksma, S., and Mussmann, M. (2014) Microbial consumption of zero-valence sulfur in marine benthic habitats. *Environ. Microbiol.* **16**: 3416–3430.

Polz, M.F. and Cavanaugh, C.M. (1998) Bias in template-to-product ratios in multitemplate PCR. *Appl. Environ. Microbiol.* **64**: 3724–3730.

Rabus, R., Hansen, T.A., and Widdel, F. (2013) Dissimilatory Sulfate- and Sulfur-Reducing Prokaryotes. In, *The Prokaryotes*., pp. 309–404.

Riedinger, N., Brunner, B., Krastel, S., Arnold, G.L., Wehrmann, L.M., Formolo, M.J., et al. (2017) Sulfur Cycling in an Iron Oxide-Dominated, Dynamic Marine Depositional System: The Argentine Continental Margin. *Front Earth Sci. Chin.* **5**: 33.

Robador, A., Brüchert, V., and Jørgensen, B.B. (2009) The impact of temperature change on the activity and community composition of sulfate-reducing bacteria in arctic versus temperate marine sediments. *Environ. Microbiol.* **11**: 1692–1703.

Røy, H., Kallmeyer, J., Adhikari, R.R., Pockalny, R., Jørgensen, B.B., and D'Hondt, S. (2012) Aerobic microbial respiration in 86-million-year-old deep-sea red clay. *Science* **336**: 922–925.

Ruvira, M.A., Lucena, T., Pujalte, M.J., Arahal, D.R., and Macián, M.C. (2013) Marinifilum flexuosum sp. nov., a new Bacteroidetes isolated from coastal Mediterranean Sea water and emended description of the genus Marinifilum Na et al., 2009. *Syst. Appl. Microbiol.* **36**: 155–159.

Schirmer, M., Ijaz, U.Z., D'Amore, R., Hall, N., Sloan, W.T., and Quince, C. (2015) Insight into biases and sequencing errors for amplicon sequencing with the Illumina MiSeq platform. *Nucleic Acids Res.* **43**: e37.

Seitz, K.W., Lazar, C.S., Hinrichs, K.-U., Teske, A.P., and Baker, B.J. (2016) Genomic reconstruction of a novel, deeply branched sediment archaeal phylum with pathways for acetogenesis and sulfur reduction. *ISME J.* **10**: 1696–1705.

Smith, R.W., Bianchi, T.S., Allison, M., Savage, C., and Galy, V. (2015) High rates of organic carbon burial in fjord sediments globally. *Nature Geoscience* **8**: 450–453.

Sørensen, H.L., Meire, L., Juul-Pedersen, T., de Stigter, H.C., Meysman, F.J.R., Rysgaard, S., et al. (2015) Seasonal carbon cycling in a Greenlandic fjord: an integrated pelagic and benthic study. *Mar. Ecol. Prog. Ser.* **539**: 1–17.

Starnawski, P., Bataillon, T., Ettema, T.J.G., Jochum, L.M., Schreiber, L., Chen, X., et al. (2017) Microbial community assembly and evolution in subseafloor sediment. *Proc. Natl. Acad. Sci. U. S. A.* **114**: 2940–2945.

Techtmann, S.M., Fitzgerald, K.S., Stelling, S.C., Joyner, D.C., Uttukar, S.M., Harris, A.P., et al. (2016) Colwellia psychrerythraea Strains from Distant Deep Sea Basins Show Adaptation to Local Conditions. *Front. Environ. Sci. Eng. China* **4**: 33.

Teira, E., Lekunberri, I., Gasol, J.M., Nieto-Cid, M., Alvarez-Salgado, X.A., and Figueiras, F.G. (2007) Dynamics of the hydrocarbon-degrading Cycloclasticus bacteria during mesocosm-simulated oil spills. *Environ. Microbiol.* **9**: 2551–2562.

Thamdrup, B., Finster, K., Hansen, J.W., and Bak, F. (1993) Bacterial Disproportionation of Elemental Sulfur Coupled to Chemical Reduction of Iron or Manganese. *Appl. Environ. Microbiol.* **59**: 101.

Thamdrup, B., Rosselló-Mora, R., and Amann, R. (2000) Microbial manganese and sulfate reduction in Black Sea shelf sediments. *Appl. Environ. Microbiol.* **66**: 2888–2897.

Thrash, J.C., Cameron Thrash, J., Seitz, K.W., Baker, B.J., Temperton, B., Gillies, L.E., et al. (2017) Metabolic Roles of Uncultivated Bacterioplankton Lineages in the Northern Gulf of Mexico "Dead Zone." *MBio* **8**: e01017–17.

Tremblay, J., Singh, K., Fern, A., Kirton, E.S., He, S., Woyke, T., et al. (2015) Primer and platform effects on 16S rRNA tag sequencing. *Front. Microbiol.* **6**: 771.

Vandieken, V., Pester, M., Finke, N., Hyun, J.-H., Friedrich, M.W., Loy, A., and Thamdrup, B. (2012) Three manganese oxide-rich marine sediments harbor similar communities of acetate-oxidizing manganese-reducing bacteria. *ISME J.* **6**: 2078–2090.

Vandieken, V. and Thamdrup, B. (2013) Identification of acetate-oxidizing bacteria in a coastal marine surface sediment by RNA-stable isotope probing in anoxic slurries and intact cores. *FEMS Microbiol. Ecol.* **84**: 373–386.

Velicer, G.J. (2003) Social strife in the microbial world. *Trends Microbiol.* **11**: 330–337.

Wadham, J.L., De'ath, R., Monteiro, F.M., Tranter, M., Ridgwell, A., Raiswell, R., and Tulaczyk, S. (2013) The potential role of the Antarctic Ice Sheet in global biogeochemical cycles. *Earth and Environmental Science Transactions of the Royal Society of Edinburgh* **104**: 55–67.

Wang, H., Liu, J., Wang, Y., and Zhang, X.-H. (2011) Vibrio marisflavi sp. nov., isolated from seawater. *Int. J. Syst. Evol. Microbiol.* **61**: 568–573.

Wasmund, K., Cooper, M., Schreiber, L., Lloyd, K.G., Baker, B.J., Petersen, D.G., et al. (2016) Single-Cell Genome and Group-Specific dsrAB Sequencing Implicate Marine Members of the Class Dehalococcoidia (Phylum Chloroflexi) in Sulfur Cycling. *MBio* **7**: e00266–16.

Wasmund, K., Mußmann, M., and Loy, A. (2017) The life sulfuric: microbial ecology of sulfur cycling in marine sediments. *Environ. Microbiol. Rep.* **9**: 323–344.

Wehrmann, L.M., Formolo, M.J., Owens, J.D., Raiswell, R., Ferdelman, T.G., Riedinger, N., and Lyons, T.W. (2014) Iron and manganese speciation and cycling in glacially influenced high-latitude fjord sediments (West Spitsbergen, Svalbard): Evidence for a benthic recycling-transport mechanism. *Geochim. Cosmochim. Acta* **141**: 628–655.

Wehrmann, L.M., Riedinger, N., Brunner, B., Kamyshny, A., Hubert, C.R.J., Herbert, L.C., et al. (2017) Iron-controlled oxidative sulfur cycling recorded in the distribution and isotopic composition of sulfur species in glacially influenced fjord sediments of west Svalbard. *Chem. Geol.* **466**: 678–695.

van Wely, K.H.M., Swaving, J., Freudl, R., and Driessen, A.J.M. (2001) Translocation of proteins across the cell envelope of Gram-positive bacteria. *FEMS Microbiol. Rev.* **25**: 437–454.

Zhang, X.-Y., Han, X.-X., Chen, X.-L., Dang, H.-Y., Xie, B.-B., Qin, Q.-L., et al. (2015) Diversity of cultivable protease-producing bacteria in sediments of Jiaozhou Bay, China. *Front. Microbiol.* **6**: 1021.

Zinke, L.A., Glombitza, C., Bird, J.T., Røy, H., Jørgensen, B.B., Lloyd, K.G., et al. (2018) Microbial Organic Matter Degradation Potential in Baltic Sea Sediments Is Influenced by Depositional Conditions and In Situ Geochemistry. *Appl. Environ. Microbiol.* **85**: e02164–18.